Continuous Deposition of Carbon Nanotubes in an Arc-reactor and their Application in Field Emission Devices

---

A thesis submitted in partial fulfilment of the requirements

for the Degree of

Doctor of Philosophy in Chemical and Process Engineering

at the

University of Canterbury

by

Rahul K. Shastry

University of Canterbury

2007

Dedicated
To
My Parents

Acknowledgments

This thesis would not appear in its present form without the kind assistance and support of the following individuals;

I am indebted to my supervisor, Assoc Prof. John Abrahamson, for the guidance and support he has provided throughout the course of this research. His patience, despite my ignorance and spontaneity is greatly appreciated.

I would also like to express my gratitude to all the technical staff, especially to Peter Jones and Paul Tolson for building and realising all modifications to the continuous reactor, Gas sensor and the Luminescent tube, Bob Gordon for always organising and providing the required technical support in time, Tim for his help with the luminescent tube and Mike Lahood for his help with the gas sensor, Trevor Berry for his help with the video equipment and optics and finally to Glenn Wilson for making sure things arrived in time for carrying out this research. I would specially like to acknowledge the support of Neil Andrews from the Biological sciences SEM lab for teaching me to operate the SEM and Mike Flaws from the Department of Mechanical Engineering for his help with both the SEM and TEM.

I also wish to thank all my friends who made my stay in New Zealand so memorable. In no specific order, I wish to thank Thomas Querioux for creating a very competitive environment during the start of this research and being a great friend, all the Indian friends who never made me feel home sick, Hamdan Yusoff for his help with the research, John Gabites, Jack Rutherford for the talks about cricket, Kiwi lingo and everything else under the sun and specially to Abraham Beuger for his handy technical skills and all the discussions making our office a nice place to learn and work, besides teaching me to speak straight.

Finally, I am forever indebted to my parents and sister for their understanding, endless patience and encouragement when it was most required and to my beloved wife-Smitha for being the cause of this endeavour. I am also grateful to Harsha and Anoop for their unwavering support over the years.

Abstract

Carbon nanotubes have become one of the most important building blocks critical to nanotechnology. Carbon nanotubes have attracted the interests of many scientists since their discovery due to their remarkable properties and have been widely used for various applications. However, the bottle neck in nanotube research has been the lack of a cheap, continuous and fast nanotube production method.

This study concerns a reactor where nanotubes are continuously deposited on a carbon substrate using arc discharge at atmospheric pressure. This process appears to be the first to employ an arc discharge as the method for continuous mass deposition of nanotubes on a substrate. This nanotube deposition method eliminates the generic multistep process of nanotube deposition on substrates for its use in many applications. The effect of various parameters influencing growth and morphology of nanotubes on the substrate in the arc reactor (inter-electrode gap, atmosphere composition, current density, flushing, substrate type and speed and catalyst) have been systematically explored to optimise nanotube growth.

The field emission properties of the nanotube laden substrate are studied for use and applicability as electron emitters. The nanotube samples demonstrated superior emission properties, low turn-on field and excellent current stability when put into applications such as a luminescent tube and an ionisation sensor. Theoretical modelling of the behaviour of a single nanotube during field emission was performed using finite element analysis software (COMSOL 3.2) to understand the effect of nanotube length, diameter, and vacuum gap on an individual nanotube. The results reveal that resistive heating (temperature) limits the maximum current carried by an individual nanotube.

Furthermore, a new growth model is introduced to explain the formation of nanotubes from graphene fragments and nanocrystallites, due to polarisation of carbon species near the electrode surface suggesting that carbon vapour is unlikely to be responsible for nanotube growth.

TABLE OF CONTENTS

List of Figures

List of Tables

1.0 Introduction

1.1 Introduction:

The characteristic size of a system has a profound influence on its physical behaviour. With the recent leap in technology, it has become possible to manipulate and control substances at the nanometer level. The special properties of nano-sized substances can be used to create new materials and devices with fascinating functions. The properties of matter at the level of several atoms and molecules are governed by quantum physics laws enabling interesting properties connected to a large substance. The technology of downsizing processes and products to the nanometer level and the creation of new devices with greater functionality is coined “Nanotechnology”.

Nanotechnology constitutes an interdisciplinary field comprising several fields of basic sciences and stretches across a whole spectrum of fields, such as instrumentation technology, photonics, electronics, medicine, environmental and energy. Carbon nanotubes are one of the most important building blocks critical to nanotechnology. Nanotubes have attracted the interest of many scientists since their discovery due to their remarkable properties[1-3] and have been widely used for various applications[4-7].

1.2 Objective:

The mass production of nanotubes has been a bottleneck for nanotube research since its discovery, as the current methods employed are either too expensive or too laborious. Nanotubes are required to be anchored onto a substrate for their use in many applications ranging from flat panel displays, hydrogen storage systems and controlled drug delivery systems. The preparation of nanotubes for use in such systems usually requires a multi-step process, where nanotubes are produced in the first step, separated from other carbon forms in the second step and anchored onto a substrate in the last step. Many reports have been published describing the mass

production of nanotubes[8, 9] but very few have reported their growth on flexible substrate materials[10-12].

The conception of continuous deposition of carbon nanotubes arose from successful experiments by Mani and Hill in producing carbon nanotubes in a batch reactor, used by John Abrahamson and Peter Wiles in the late 1970s to observe carbon nanotubes. Subsequently, Siew and Keen[13] and Mani and Hill[14] working under John Abrahamson conceived and developed a reactor for the deposition of nanotubes on a continuously moving carbon substrate. Can Ulubay[15] commissioned the reactor to test the transferability of growth conditions from the batch reactor and Ray Archer[16] attempted a series of test runs to deposit nanotubes on the substrate. Finally, Thomas Querrioux[17] performed some modifications to the reactor besides attempting a series of runs to deposit nanotubes (sometimes), perhaps due to unexplored parameters.

The aim of this project is the study and optimisation of a single step continuous production[17] of nanotubes on a substrate using an arc discharge at atmospheric pressure. This process is the first to employ an arc discharge as the method for continuous mass deposition of nanotubes on a substrate. The objective of this work is also to investigate the effect of various parameters affecting the growth and morphology of nanotubes on the substrate. Finally, the field emission properties of the product will be studied for use and applicability as electron emitters. Theoretical modelling of the behaviour of a single nanotube during field emission will be performed using finite element analysis software to understand the effect of temperature on nanotube field emission.

The substrate surface temperature measurements were performed by Hamdan Yusoff as a part of his PhD theses in conjunction with my assistance in running the reactor. The initial design of the luminescent tube was inspired by the report of Bonard[18] and was performed by Sutida Marthosa[19]. The design of the ionization sensor was adapted from a luminescent tube design and was developed by Ryan Betty[20]. The help and nature of the contributions to this project by the above individuals has been acknowledged and mentioned in the relevant sections.

1.3 History:

Nanotubes are members of the “fullerene” family along with “buckyballs”, carbon molecules shaped like soccer balls. Carbon nanotubes were originally obtained as by-products of fullerenes accidentally discovered during radio astronomy studies. The mass production of fullerenes was begun by Krätschmer and Huffman in 1990 expanding the activity in this field[21]. The fullerene research gained importance with the discovery of high temperature superconductivity in fullerenes at critical temperatures above 30 K when doped with an alkali metal[22]. This led to increased interest in the search for new carbon forms and higher mass fullerenes and subsequent discovery of carbon nanotubes. Though the actual discovery of carbon nanotubes has been accredited to Sumio Ijima in 1991[23], various researchers reported similar findings of these tiny structures before him and were not recognised[24]. One such report was from John Abrahamson and Peter Wiles in 1979 at the University of Canterbury, New Zealand who reported finding hollow fibres of carbon on the anode surfaces after an arc discharge[25]. These fibres consisted of concentric layers of wrapped graphene with an interlayer spacing of .34 nm which later became known as nanotubes. Nanotube research has grown tremendously in the past few years with the subsequent discovery of single walled nanotubes in 1993[26, 27] and their useful properties. Various efforts to mass produce them are currently underway and are expected to open up a wide range of applications.

1.4 Fundamentals:

1.4.1 *Carbon Classification:*

Carbon is by far the most diverse and interesting element of all the elements known. The conventional forms of carbon widely known are graphite, diamond and amorphous carbon (as in carbon glass). New exotic forms of carbon like fullerenes, carbon nanotubes, and carbon nanofoam and diamond nanorods have also been synthesised. These carbon forms impart varied properties to carbon ranging from soft to hard, opaque to transparent, abrasive to smooth besides being inexpensive to costly. The synthesising techniques for these new carbon forms are established in the

laboratory but are not yet technologically feasible for mass production. However, they are readily gaining significance as an important form of carbon.

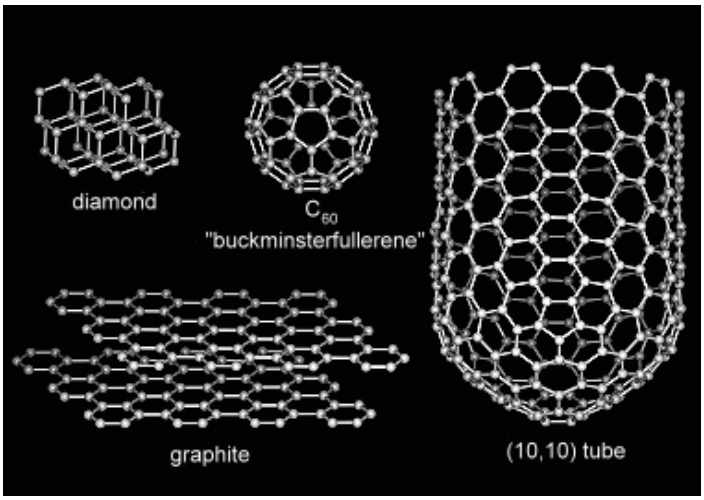

Fig.1. 1 Various forms of carbon.

1.4.2 *Carbon nanotubes:*

Carbon nanotubes are conceptually formed by rolling of layers of graphene into a seamless cylinder with closed ends. The ends of nanotubes are normally domed structures of six-membered rings, capped by a five-membered ring. Any tube with a nanoscale dimension is considered a nanotube, the most common being that made by carbon. Other non carbon nanotubes known are those made from silicon and boron nitrides. A distinction between nanotubes is made based on the number of enveloped layers. A single walled carbon nanotube (SWNT) is made of a single graphene layer and multi-walled carbon nanotubes (MWNT) consist of multiple graphene layers telescoped about one another.

1.4.2.1 Single walled carbon nanotubes (SWNT):

Single walled carbon nanotubes may be described as a single graphene sheet rolled into a cylinder. The ends of the tubes are terminated by spherical caps consisting of carbon hexagons and pentagons. They exhibit an axial symmetry and many of their

properties are dependent on their length- they are “pseudo one-dimensional”. The diameter of SWNTs varies from 0.4 nm - 8 nm [27-29] with lengths ranging from nanometers to many microns leading to very large aspect ratios. SWNTs require a catalyst for their growth and are expensive to produce. Different types of carbon nanotubes can be produced by rolling the graphene sheet in several ways. The three main types are armchair, zig-zag, and chiral. Armchair and zig-zag nanotubes have identical mirror images. A simple and common way of specifying nanotubes is by their chiral vector C_h. The chiral vector describes the way a graphene layer is rolled/twisted along the nanotube axis and is indicative of its size. SWNTs with different chiral vectors exhibit disparate properties such as electrical conductivity, mechanical strength and optical activity[28].

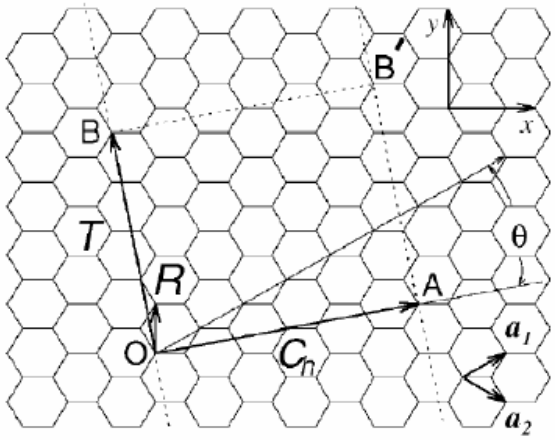

Fig.1. 2 Unrolled graphene sheet of a nanotube[28].

Fig 1.2 shows the flat hexagon lattices of a graphene sheet. A chiral vector $\boldsymbol{C}_h$ in an unrolled graphene sheet is defined as $n\boldsymbol{a}_1 + m\boldsymbol{a}_2$, where n and m are integers ($0 \leq |m| \leq n$), $\boldsymbol{a}_1$ and $\boldsymbol{a}_2$ are real space unit vectors of a hexagonal lattice as shown in Fig 1.2. OB is the direction of the nanotube axis and the vector OA is perpendicular to the tube axis.

Another important parameter is the chiral angle, which is the angle between C_h and $\hat{a}_1$. SWNTs are classified as zigzag, armchair and chiral (Fig 1.3) based on the chiral vector and chiral angle. The chiral angle and $\boldsymbol{C}_h$ of zigzag nanotubes is 0º and (n,0) and that of armchair nanotubes is 30º and (n,n). Chiral SWNTs have $\boldsymbol{C}_h$ = (n,m) where n is not equal to m, and a chiral angle which is greater than 0º and less than 30º.

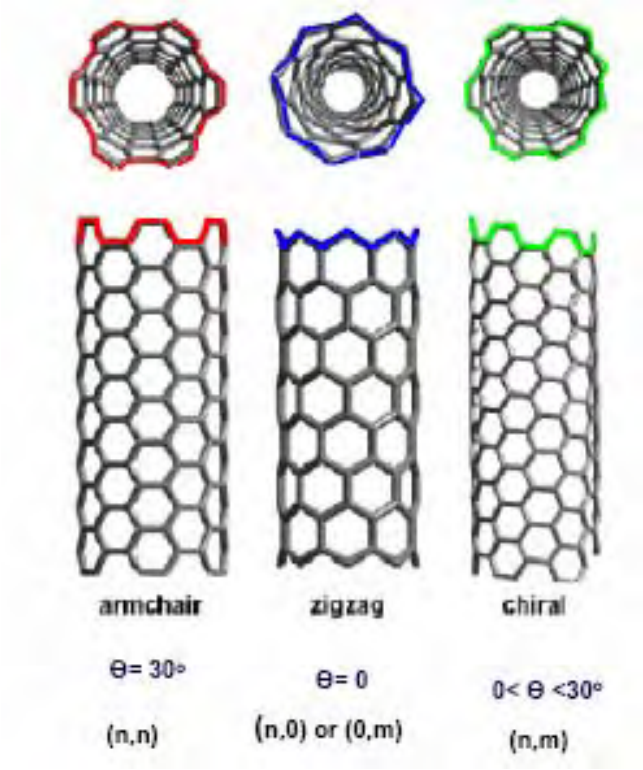

Fig.1. 3 Different nanotube structures[30].

The diameter of a carbon nanotube ‘d’ is given by

$d = L/\pi$

where L is the circumferential length of the nanotube given by

$L = |C| = \sqrt{C.C} = a\sqrt{n+m+nm}, \quad a = |a| = |a| = 2.49$ Å

Where lattice constant ‘a’ is the absolute value of the cell base vectors. Its value being higher than graphite due to a C-C bond length of 0.144 nm for carbon nanotubes compared with 0.142 nm for graphite.

1.4.2.2 Multi-walled carbon nanotubes:

The multi-walled carbon nanotubes were the first nanotube structure observed by early scientists[25] and by Iijima[23]. Multi-walled carbon nanotubes (MWNTs) consist of multiple concentrically nested carbon tubes as shown in Fig. 1.4 and are

made of multiple overlapping of graphene sheets. Their diameters range from a few nanometers to 40 nm or more depending on the number of concentric tubes. Multi-walled carbon nanotubes can be made easily and in large quantities compared to SWNTs, although they are likely to have more structural defects. There are two possible configurations for MWNTs depending on the way of wrapping graphene sheets as shown in the Fig. 1.4. A Swiss roll arrangement consists of graphene sheets rolled as scrolls and a “Russian doll’ like arrangement consists of concentric carbon tubes[15].

Energetic considerations show that the “scroll” like arrangement requires extra energy to maintain two edges at the beginning and at the end of the roll and are less likely to be stable[31]. Also the fact that most of the micrographs show an equal number of fringes on either side of the axis supports the “Russian doll” like arrangement for MWNTs. The scroll model also seems inconsistent as it requires reactive surfaces all along the length of the tube due to graphene layer arrangement which is unlikely from the observed experimental results.

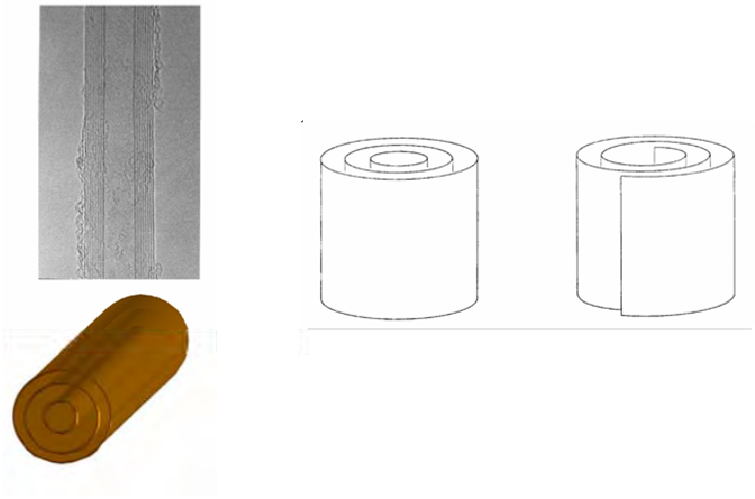

Fig.1. 4 Different possible arrangements for a multi-walled carbon nanotube[30].

1.4.3 *Other carbon nanoforms:*

1.4.3.1 Nanohorns:

Carbon nanohorns have the same graphitic carbon atom structure as normal carbon nanotubes produced without the use of a catalyst. Nanohorns are 2 to 3 nm in

diameter and 30 to 50 nm in length. The characteristic feature is that many nanohorns aggregate together to form a cluster with a diameter of about 20-100 nm, as shown in Fig. 1.5. Nanohorns have the potential to be a low cost material when compared to SWNT and exhibit superior adsorption properties[32]. Carbon nanohorns have for the first time (in 2002) cleared the United States Department of Energy threshold of commercial reality as methane gas storage material[33].[A criterion of 9 x 10^{-2} kg methane adsorbed per kg of nanohorn]

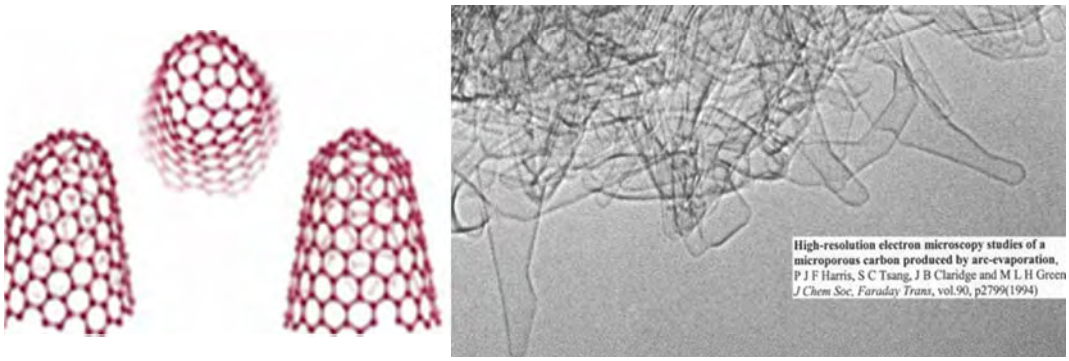

Fig.1. 5 Computer graphic[33] and TEM image of Carbon nanohorns[34].

1.4.3.2 Nanofibers:

Carbon nanofibres are often perceived as carbon nanotubes. Nanofibers summarise a large family of filamentous nanocarbons. Carbon nanofibers can be grown from gaseous hydrocarbons with the aid of metallic particles with size of 5-50 nm. They are amorphous in structure (Fig 1.6) and do not form a typical well ordered graphite molecular tubular structure at graphitisation temperatures of 2000 C[35]. Nanofibers have a low modulus and a moderate strength compared to nanotubes. They have a diameter range of 80-500 nm with a core diameter of 0.5-10 nm and with lengths of 5-40 cm.

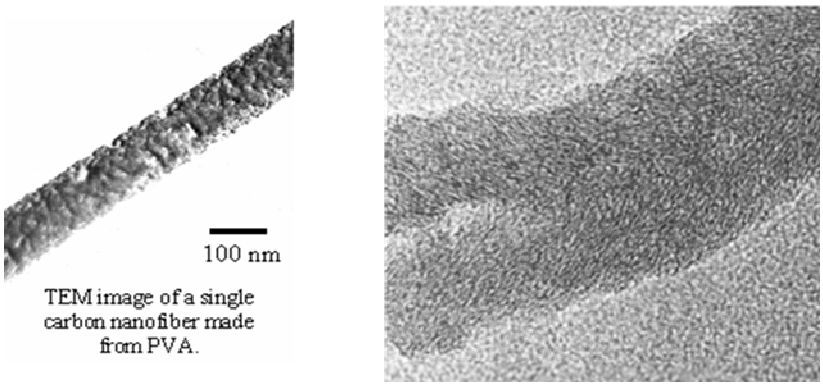

Fig.1. 6 TEM image of a carbon fibre showing its crystallinity[35].

1.4.3.3 Nanofoam:

Nanofoam consists of a low density cluster assembly of carbon atoms in the form of a three dimensional mist like web, as show in Fig. 1.7. It is considered as the fifth allotrope of carbon and is practically transparent in appearance and fairly brittle. Nanofoams are produced when a high energy laser is fired at a graphite or disordered solid carbon in an inert gas atmosphere[36]. An unusual property exhibited by carbon nanofoams is that of ferromagnetism as it is attracted to magnets like iron. Although this property vanishes after a few hours of nanofoam production it is preserved by cooling the nanofoam to temperatures of around -183 C. Nanofoams are expected to be very helpful for spintronic devices and in nanomedicine as sources of heat to destroy tumour cells and to enhance Magnetic Resonance Imaging (MRI)[37].

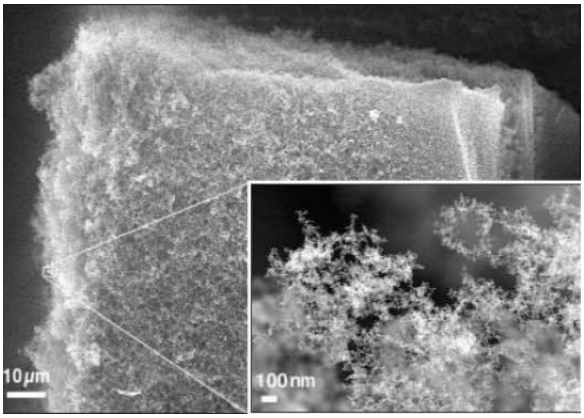

Fig.1. 7 TEM image of carbon nanofoam showing mist like carbon[38].

Apart from the previously mentioned carbon nanoforms, other forms like nanorods are promising for use in flexible solar cells[39], nano test-tubes which are nanotubes opened and filled with materials are useful for chemical reactions[40].

1.5 Methods of production:

Although carbon nanotubes have drawn significant attention from the scientific community, their large scale production has largely been missing. Different techniques and the current status for carbon nanotube synthesis are outlined in this section. The normal synthesis conditions for different methods are explained and a brief overview of the latest techniques and the possibilities of scaling up for large scale production are also explained.

Carbon nanotubes are generally produced by three main techniques namely arc discharge, laser ablation and chemical vapour deposition (CVD). There has been numerous techniques developed which are a hybrid of the above three basic methods in a quest to mass-produce them and to understand their growth process. All manufacturing techniques known so far produce nanotubes with a high degree of variability in their physical and electronic properties. The arc discharge process is more amenable for large scale production than CVD and is the interest of this thesis.

1.5.1 *Arc discharge:*

Arc discharge is the most common and easiest way to produce carbon nanotubes. The arc discharge method comprises striking a DC arc between two graphite electrodes generally separated by a small distance in a sealed chamber with an inert gas environment[25, 34], as shown in Fig. 1.8. The discharge vaporises one of the electrodes and results in the formation of a small rod shaped deposit on the other. It is possible to selectively grow nanotubes using arc discharge. A rod shaped deposit results in the formation of MWNTs between pure graphite electrodes, and SWNTs if the anode is filled with a metal catalyst such as Fe, Co, Ni, Y or Mo[26, 27]. However, this technique also results in the formation of other unwanted carbon forms, catalytic metal residues and massive production of soot. Purification step/steps are vital to separate nanotubes from these impurities before being manipulated for use in

specific applications[41]. The reproducibility of this method is also far from perfect, perhaps due to the extreme conditions of environment associated with its growth.

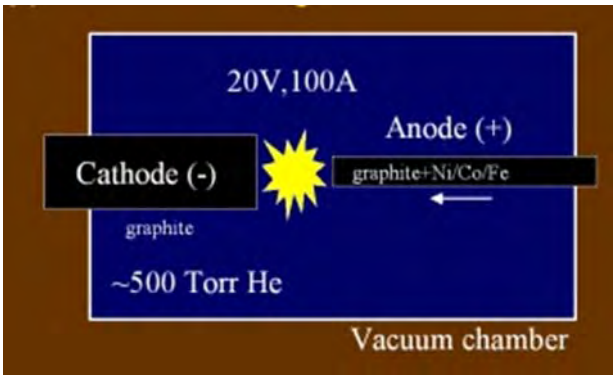

Fig.1. 8 Schematic of an arc discharge process.

Nanotube production by this method is influenced by a range of different parameters. Various research groups have tried to change and vary these parameters in an effort to mass produce nanotubes of good quality associated with fewer defects. The following parameters are found to have a huge impact in the way the carbon and catalyst molecules diffuse and cool which affects nanotube diameter and growth.

a) Reactor atmosphere:

The quantity as well as quality of nanotubes seems to improve when the discharge is performed in an inert atmosphere. Helium seems to present the most favourable conditions for good quality nanotubes up to a pressure limit of 66.7 kPa[42]. This pressure range is not found to be suitable for other inert gases. Experiments in argon (by itself) appear to have no major role in the growth process. For experiments with mixtures of the two gases, comparisons between the two inert gases indicate that the yield of nanotubes is higher in helium. The nanotube diameter decreases with increasing argon concentration[43]. Experiments under organic atmospheres[44, 45] vacuum[46], nitrogen[47], open air[48], hydrogen[49] or their combinations have also been carried out resulting in varying degree of success at various pressures[50] (from 50 mbar to 700 mbar).

b) Optical plasma control:

Another important parameter that influences the nanotube growth is the distance between the electrodes[51]. The plasma characteristics and vaporisation from the electrodes can be controlled by changing the inter-electrode gap. Most of the experiments have been performed at an arc gap of 1-2 mm and the effect of arc gap on nanotube growth at arc gaps above 2 mm has thus largely remained unexplored[52].

The arc current is another vital parameter that changes the plasma characteristics. Arc discharge is usually carried out under a current of 50-100 A with a 20 V drop across the electrodes. Other types of discharge like glow discharge[53], pulsed arc discharge[54] and arc discharges with lower current[55] have also been attempted in an effort to improve nanotube yield and quality.

c) Temperature control:

Nanotube growth may be strongly influenced by the electrode temperatures and hence is dependent on electrode diameters and cooling[56, 57]. The traditional arc discharge employs an anode diameter of 3-8 mm and a cathode diameter of around 5-16 mm. Nanotubes can also be grown on the anode surface by increasing its diameter apparently (but not measured) thereby lowering its surface temperature. The surface temperatures of the electrodes can also be controlled by cooling. It has been shown by research groups that the yield and quality of nanotubes increases when the electrodes are cooled[56, 58, 59].

d) Synthesis in liquid phase:

The problem in the conventional arc discharge process in an inert atmosphere is the duration of the arc discharge and the need to remove product from the reaction chamber periodically as it is formed. Carbon arcs have been very successful in producing carbon nanotubes under various liquid environments (Fig.1.9). The products from arc discharge in liquid environments settle down at the bottom and can be removed by filtration. Arc discharge under liquid environments is easily scalable for mass production and contains a large fraction of nanotubes with very few impurities[60]. The liquid medium acts as a heat sink and maintains the

necessary temperature gradients within the plasma favouring nanotube growth[45].

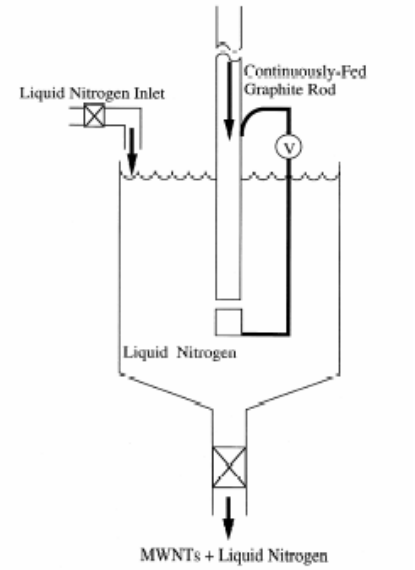

Fig.1. 9 Schematic of nanotube production under liquid nitrogen[47].

e) Other parameters:

The traditional arc discharge process has seen many changes attempted in a bid to control and alter various parameters to boost nanotube production and quality. Any variation to the arc discharge process is generally an effort to generate more plasma stability. A modified bowl-like cathode has been used to improve the oxidation resistance of nanotubes[61]. Efforts have been made to synthesise nanotubes in open air using a welding torch[48, 62] to allow easy escape of carbon soot. A magnetic field has been used to confine the plasma resulting in the production of defect-free highly pure (95%) nanotubes[63]. Plasma rotating arc discharge has been reported as an economical and possible way of mass producing nanotubes. In this method, the anode is rotated continuously resulting in a stable and increased plasma volume with higher temperatures[64]. A few other research groups have tried other modifications like gravity free arc discharge and have obtained some interesting results[65, 66].

1.5.2 *Laser ablation:*

Laser ablation uses a high power laser (usually Nd:YAG) to vaporise a graphite source loaded with a metal catalyst. This method is widely used for SWNT production and was first demonstrated by Smalley[67]. This method uses a quartz tube embedded in a furnace at 1200 C. The tube is maintained at a pressure of 500 Torr under a flow of inert gas. A pulsed or continuous laser is used to vaporise a graphite, pitch or carbonaceous feedstock placed inside the tube resulting in a hot expanding carbon vapour plume as shown in Fig. 1.10. The flowing inert gas takes away the carbon vapour to a cool zone outside the furnace where it condenses to form nanotubes held together by van der Waals forces[68]. A pure graphite target results in MWNT formation and SWNTs are formed if the target consists of graphite mixed with certain catalysts like Ni, Co, Fe and a mixture of different catalysts. Nanotubes produced by this method have a narrower size distribution than nanotubes produced from CVD and are also more structurally perfect.

The nanotube formation by this technique is similar to that by electric arc due to the similar reaction conditions and parameter requirements. The reproducibility and purity of the products formed are good, but scale up of this technique remains difficult and expensive due to the high cost of the laser[69].

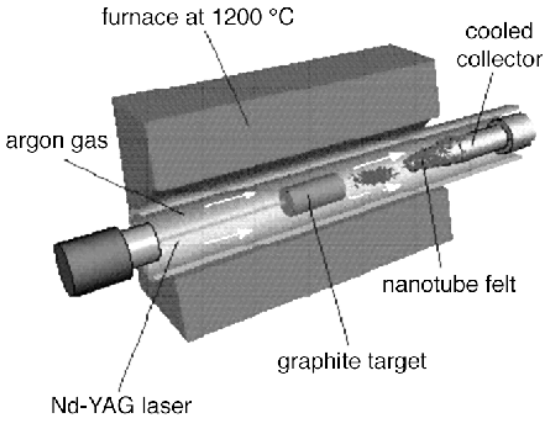

Fig.1. 10 Schematic of a laser ablation process[70].

1.5.3 *Chemical Vapor Deposition (CVD):*

Chemical vapour deposition is a process which transforms gaseous molecules called precursors into a solid material in the form of a thin film or powder on the surface of a substrate. An energy source is used to generate carbon precursors from a reactant carbon rich gas, in a reactor as shown in Fig. 1.11. These precursors are allowed to diffuse towards a heated substrate using a carrier gas and then adsorb on to the substrate surface. The precursor adsorbs until it saturates the surface forming a thin film. Gaseous reaction by products formed during the process is transported out of the reaction chamber due to the carrier gas flow. With the appropriate metal catalyst choice, one can preferentially grow single and multi-walled nanotubes. This process allows for extremely precise control of film thickness, uniformity and alignment on small areas[69].

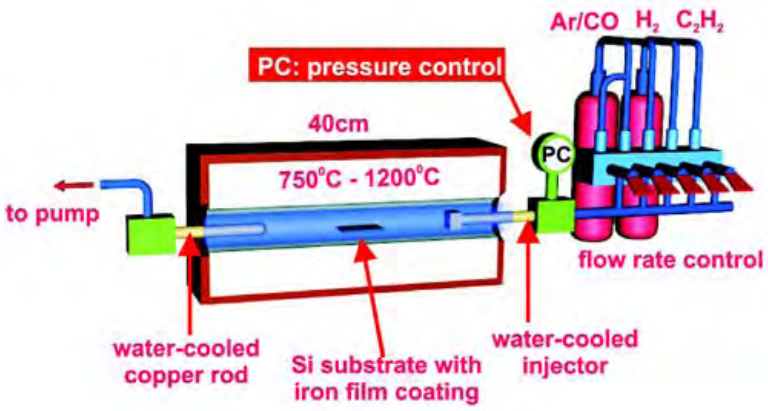

Fig.1. 11 Schematic of a Chemical Vapour Deposition (CVD) process[71].

CVD always requires a substrate preparation step before the actual synthesis. The desired transition metal catalyst is sputtered on to the substrate followed by an etching or annealing step to induce catalyst particle nucleation. The catalyst has a strong effect on the nanotube diameter, growth rate, wall thickness, morphology and microstructure. The synthesis temperature for nanotubes are usually in the range of 650-1500 C and a typical yield is about 30% weight. Nanotubes produced by CVD are structurally imperfect due to lower growth temperatures and various techniques have

been developed over the years to improve nanotube quality[69]. A number of CVD forms widely used by various research groups are as follows:

a) Plasma enhanced CVD: This process utilises plasma or a glow discharge to enhance the chemical reaction rate of the precursors and hence runs at significantly lower temperatures (> 450 C)[72, 73].
b) Thermal CVD: This process utilises a source of heat having sufficient temperature to pyrolise the gas source into its precursors. Its advantages are its simplicity, cheapness, high deposition rate and high flexibility with operating temperatures of around 800-1050 C[74, 75].
c) Laser assisted CVD: A medium power continuous laser source is impinged on the substrate to promote a localised chemical reaction enabling nanotube deposition[76]. It has got the advantage of deposition on thermally sensitive materials and has excellent step coverage.
d) Other techniques from the family of CVD used by research groups to successfully produce nanotubes are atmospheric chemical vapour deposition (APCVD)[77], low pressure chemical vapour deposition (LPCVD)[78], metal-organic chemical vapour deposition (MOCVD)[78], microwave plasma-assisted CVD (MPCVD)[79] and alcohol assisted CVD[80].

1.5.4 *Other production methods:*

New advances have been made in the synthesis of carbon nanotubes by some methods distinct from the more common methods explained above. They are as follows:

a) Electrolytic formation:

Carbon nanotubes are formed using ionic salts (LiCl, LiBr and $SnCl_2$) as electrolytes and carbon as electrodes. This method is unique as the graphite is not vaporised and condensed as in other methods. The apparatus uses an electrolyte-filled crucible acting as an anode and a cathode immersed in it at various depths as shown in Fig. 1.12 An external furnace heats the crucible till the electrolyte in it melts[81]. Nanotubes with a diameter of 10 nm are observed in the salts with the

wall structures depending on the electrolysis conditions. Salts which melt above 500 C were found to be suitable for nanotube production. Metals were found encapsulated inside the nanotube cavity when mixed electrolytes were used[82].

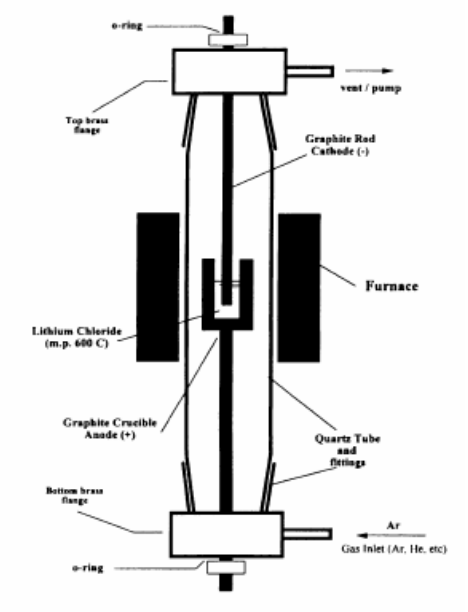

Fig.1. 12 Schematic of electrolytic formation of nanotubes[81].

b) Flame synthesis:

Flame synthesis of nanotubes is a novel technique based on diffusion flames. It presents the required conditions such as energy, carbon source and high enough temperature for nanotube growth[83]. The process consists of pyrolysing a carbon source (usually acetylene or ethylene) and a metal catalyst in an oxygen-fed flame. The flame is designed to have a flat temperature profile across its width. The carbon source decomposes into its precursors in the flame and gets nucleated by a substrate (wire or mesh) coated with a metal catalyst immersed in the flame. This enables nanotube growth, as depicted in Fig. 1.13. Nitrogen may be added to the substrate to reduce soot formation. The other way to minimise soot formation is to transport the nucleated carbon and catalyst particles away from the flame (by mixing with an inert gas) to a water-cooled surface, and aid nanotubes growth from deposited catalyst particles.

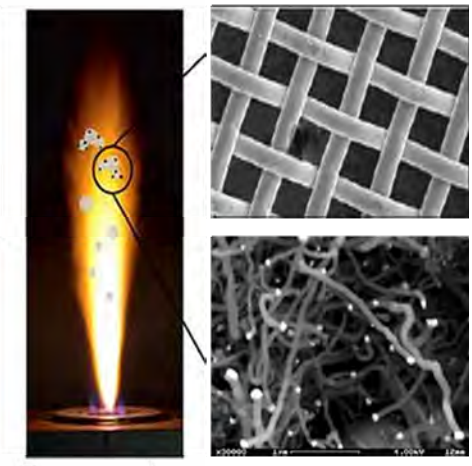

Fig.1. 13 Flame synthesis of carbon nanotubes[69].

1.6 Nanotube Purification:

Nanotubes are of high practical importance since they possess the desired characteristics for many specialised applications. Unfortunately, all the synthesis processes are associated with impurities such as metal catalyst particles, fullerene molecules, amorphous carbon and other carbon forms. Purification steps after carbon nanotube synthesis is usually needed in order to remove impurities for their application into useful devices.

So far there has been no universal single step purification technique that is capable of obtaining nanotubes with absolute purity and separation[69]. This is primarily due to the different synthesis methods that bring about varied levels and types of impurities requiring different purification procedures. The available purification techniques can be divided into two mainstreams, namely destructive separations and structure/size separations. The techniques that will be discussed under the above procedures are oxidation, annealing, microwave treatment, ultrasonication and micro-filtration.

1.6.1 *Oxidation:*

This method is most preferred to remove carbonaceous impurities rapidly and is based on the difference in reactivities between nanotubes, nanoparticles and metal impurities in oxidative environments. The sample to be purified can be heated at

varied temperatures in an atmosphere that can be oxygen[84], air[85] or in wet oxidising agents like H_2O_2 and/or H_2SO_4[86]. The yield and efficiency of this technique is highly influenced by factors like metal content, oxidation time, environment, temperature and the type of oxidising agent. Oxidation in the gas phase requires a precise control over oxidation time and temperature, as nanotubes are more likely to get oxidised and be destroyed easily with catalytic impurities. Purification using wet oxidising agents like acids and bases are preferred for nanotubes with high levels of metal impurities[69]. A proper selection of both the above mentioned methods is desirable to achieve greater efficiency and yields as acids can affect carbonaceous impurities (oxidation to carbon dioxide).

Though the procedure is simple and easy, absolute control of different factors is vital due to the risk of burning or oxidising 99 wt% of the sample. This method is useful for MWNT purification as SWNT appear to be damaged after purification by oxidative treatment[87]. The typical MWNT yield from this method is about 5-20% of the total slug formed from the conventional arc discharge process.

1.6.2 *Annealing:*

This method is a direct derivative of the technique used in the carbon fibre industry. High temperature annealing or graphitisation has been extensively performed in the Vapour Grown Carbon Fibre(VGCF) industry to remove defects from the carbon fibres[88, 89]. Graphitic carbon and other impurities get pyrolysed at graphitisation temperatures (upto 3000 C) resulting in the structural reorganisation of graphene layers.

This method consists of heating the nanotube sample in purged nitrogen or inert gas atmosphere at a constant rate of 10-20 C/min. Formational defects anneal at temperatures of around 1600 C and micro structural defects at 3000 C[90]. The metal impurities are melted when their melting temperatures are reached and they are removed from the nanotube ends by vaporisation. The interlayer spacing of nanotubes is also known to decrease for temperatures greater than 2200 C[90] but this decrease is not marked as in VGCF and requires a longer holding duration. The disadvantage of this method is that structural defects remain after high temperature annealing as side grafts and kinked tubes.

1.6.3 *Microwave purification:*

The Microwave purification has received huge importance due to its fast reaction time, low reaction temperatures and reliable control over varied forms of impurities. In this method, the nanotube samples are heated in a closed vessel filled with low volumes of an oxidising agent. (Ex: a strong acid or strong base)[91]. The pressure and temperature inside the vessel are controlled by altering the microwave power through a feedback system. Microwave heating causes vaporisation of the oxidising agent resulting in a vapour reflux in the closed vessel. The temperatures in the vessel rise above its boiling point leading to high oxidative environments. Amorphous carbon and metal impurities are dissolved due to oxidisation and pure nanotubes are left suspended in the solution. The reagent temperature and type are the only factors that control nanotube purity[92].

The advantage of this method is that purification occurs at relatively low temperatures (160-300 C) and in a shorter reaction time when compared to other destructive techniques. Table 1.1 lists a table for comparison of this technique with other methods described in literature and outlines its inherent advantages.

Comparisons of traditional purification methods and the new microwave-assisted purification method

	Temperature	Time	Reagent
Thermal purification	500–800°C	40–60min	O_2 or air
Chemical agent purification[a]	(1) Room temperature	(1) 1–3days	H_2O_2, HNO_3, HCl
	(2) Near boiling point	(2) 5–7h	H_2SO_4
Microwave-assisted purification	120–180°C	30min	HNO_3[a]

[a] The boiling points of H_2O_2, HNO_3, HCl, and H_2SO_4 solutions are 114°C, 122°C, 110°C, and 340°C, respectively.

Table 1. 1 Comparison of various purification methods for carbon nanotubes[92].

1.6.4 *Ultrasonication:*

This method involves immersing an ultrasonic probe into solvent containing nanotubes to impart vibrational energy to effect separation. High energy is dissipated within the solvent due to cavitations resulting in the dispersion

different nanoparticle agglomerates[93]. The initial size of the particles to be disordered is an important factor when using ultrasonics. The solvent molecules attack the surface of the nanotubes to break the network between them and the nanoparticles. The separation is highly dependent on the solvent, surfactant and the reagent used.

The stability and length of the dispersed nanotubes is affected by the choice of solvents[94]. The choice of solvent is so important that nanotubes with specific lengths (few hundred nm) can be obtained for a proper choice of solvent (alcohols or acids). The dispersed particles are known to be stable in some solvents but can also be destroyed or damaged for others[95]. Ultrasonication can also be used to impart defects on nanotube surface to facilitate functionalisation[96].

1.6.5 *Microfiltration:*

Microfiltration is a particle or size based separation technique which uses a membrane filter to trap the impurities in a nanotube sample in a low pressure or vacuum environment[97, 98]. The sample to be purified is suspended in a suitable aqueous surfactant to break up different impurities and to aid fractionation[99]. A solvent may also be used to disperse either the nanotube or the impurities and the insoluble components to be retained by the filter. It is then washed in a series of membranes (usually polycarbonate) with successive smaller pores to filter the impurities[100]. Microfiltration separation is inappropriate for nanotubes containing a higher percentage of soot since the soot particles can easily contaminate the membrane filter.

One of the main problems in microfiltration is the clogging of filter membranes and its inability to completely separate nanoparticles from nanotubes in a single step[101]. A careful selection of the suspension liquid and surfactant can bring a 90% wt/wt yield of nanotubes for a single step purification, as reported by various groups[102].

1.7 Conclusion:

Impurities like amorphous carbon, carbon nanoparticles, graphene fragments and metal catalysts are inherent in all synthesis methods. The separation of nanotubes according to their diameter and chirality is not viable at this time. A combination of the above techniques is absolutely vital to maximise the yield and purity of nanotubes. Care should be taken to choose the right technique and parameters to effect only the removal of impurities since most techniques have a destructive effect on nanotubes themselves.

1.8 Characterisation techniques:

The advent and progress of techniques to image and control matter at the nanoscale is a prerequisite for the advancement of nanotechnology. The limiting factor for utilising these materials in many applications is the development of appropriate strategies to successfully access the unique properties of the nanotubes. Characterisation methods should reveal one or many of the properties like nanotube size and type, surface defects, electronic characteristics, mechanical strength and thermal conductivity. A brief description of the most globally used characterisation techniques capable of revealing information at the nanoscale is discussed in this section:

1.8.1 *Electron microscopy:*

Electron microscopy of nanotubes comprises of the techniques of scanning electron microscopy (SEM) and transmission electron microscopy (TEM) for structural, electronic and property characterisation of nanotubes. Both techniques use a beam of highly energetic electrons to examine objects on a fine scale. This stream of electrons is focussed on the sample to be examined, thereby affecting the electron beam. These interactions are detected and transformed into an image, yielding information about the topography, morphology and composition[103] of nanotubes.

SEM is a quick method to analyse large areas of samples due to its ability to operate over a wide range of magnifications. SEM does not require laborious

sample preparation time and pre-treatment. The limitation of this method is its ability to reveal internal details and a lack of high resolution[104] beyond 5 nm. Sometimes the samples are gold coated when a higher resolution is desired.

Field emission SEM, commonly known as FESEM is a high resolution microscopy technique capable of achieving the highest resolution. FESEM produces clearer, less electrostatically distorted images with spatial resolution down to 1.5 nm and eliminates placing conducting coatings on insulating materials. This technique is also 3 to 6 times better than conventional SEM. HRTEM is a high resolution microscopy technique which reveals size, shape and arrangement of particles on the scale of atomic diameters. It works on the same principle as SEM but uses the transmitted electron beam from the sample to obtain the sample image. The main disadvantage is a small field view and the requirement of careful sample preparation with uniform thickness for electron transparency. TEM allows direct imaging of the layer planes and thus has an ability to look inside nanotubes and hence can reveal more details[105] than SEM.

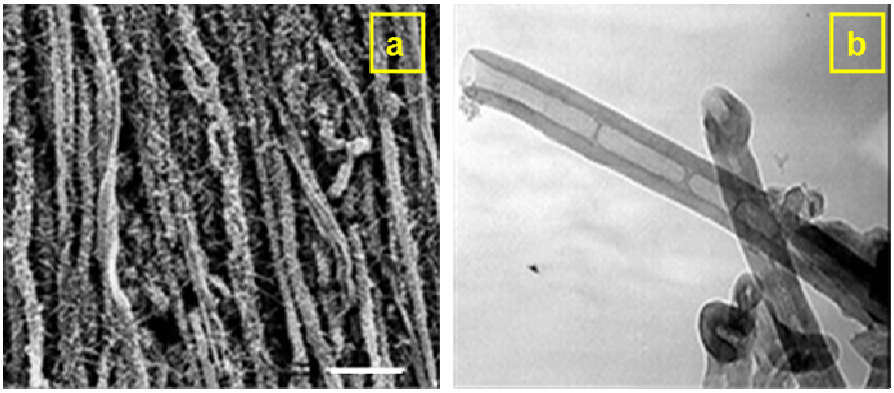

Fig.1. 14 Typical micrographs obtained from (a) SEM{scale bar = 20 µm} and (b) TEM.

1.8.2 *Atomic Force Microscopy (AFM):*

AFM is a type of scanned-proximity probe microscope which generally measures a local property like height, optical absorption or magnetism using a closely placed probe or tip. AFM operates by measuring attractive or repulsive forces between a sharp tip on a cantilever and a sample using contact or non contact mode. The tip is scanned over the sample causing a cantilever deflection due to van der Waals or other forces between the tip and the sample[106]. A laser beam is focussed on the top of cantilever which is reflected off onto an array of

photodiodes to reveal the details. An AFM can measure surface roughness with a nominal 5 nm lateral and 1 nm vertical resolution on all types of samples thereby yielding real space images down at the atomic scale[107]. AFM can operate in an ambient or in a liquid environment and can provide a true three dimensional surface profile.

1.8.3 *Raman spectroscopy:*

Raman spectroscopy is a very important technique in the study of the structure of matter by the scattering of laser light. A laser light is focussed on the surface of a sample resulting in the excitation (elastic and inelastic) of molecules in the sample which subsequently scatter light. This scattered portion of light is collected to produce a spectrum. Each material has a unique spectrum and acts as a fingerprint to identify materials[105].

Nanotubes (only SWNT and DWNT) have strong signals in two regions of the Raman spectral range. Graphite-like modes parallel to the aromatic plane are observed at around 1580 cm^{-1} with a defect mode between 1350 to 1380 cm^{-1} and a radial breathing mode at 140 and 220 cm^{-1}. These vibrational frequencies are related to the (n,m) indices of the nanotubes[105]. Raman spectroscopy is non destructive and requires no sample preparation. The other advantage is that Raman spectra can be obtained from very small samples or tiny areas directly on the surface of materials.

1.8.4 *Scanning Tunnelling Microscopy (STM):*

STM is an important characterisation tool which can simultaneously resolve the atomic structure and the density of states (DOS) of nanotubes. The basic principle of STM is based on the tunnelling current between a sharp metallic tip and a conducting sample. A small voltage is applied between the sample and the tip, resulting in a tunnelling current when the tip approaches the sample surface at a distance of approximately one nanometer[108]. The tip is mounted on a piezoelectric tube to map the movement of the tip which displays an image of the surface topography as shown in Fig. 1.15. The magnitude of the tunnelling current is extremely sensitive to the tip-sample gap, the local density of electronic states

of the sample and the local barrier height. A lateral resolution of 100 pm and a vertical resolution of 1 pm can be obtained under favourable conditions and hence individual atoms of a surface can be resolved and displayed[109]. This data can be used to predict the chirality of nanotubes and thus their electronic properties.

Although STM works well in air, as well as in liquids, an ultra high vacuum is desirable in order to avoid contamination of the samples. A very high rigidity of the STM cantilever is also desirable since the tunneling current exhibits an exponential dependence on the sample tip distance.

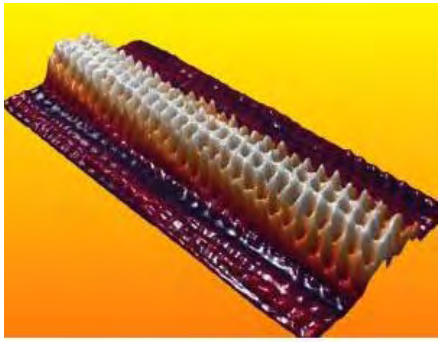

Fig.1. 15 Atomically resolved STM measurement of a carbon nanotube[110].

1.8.5 *Other techniques:*

A few other techniques like X-ray diffraction[111], Electron diffraction[112, 113] and Thermal Gravimetric Analysis (TGA)[114] are also commonly employed to characterise nanotubes. X-ray and electron diffraction works on the principle of scattering the source beam by crystals in the sample. Each type of technique is named after the source of the incident beam used. However, the scattering mechanism differs in different techniques. X-rays are scattered by the electron density cloud surrounding an atomic nucleus and electrons by the positive potential of the nucleus revealing characteristic diffraction patterns for different nanotubes. Electron radiation has significantly less penetrating power than the X-rays and hence requires a thin specimen, but has proven to be a reliable technique for determination of nanotube chirality[115]. The X-ray wavelength produced is of the same order of magnitude as the interatomic distances between atoms but can penetrate the sample more than electron radiation. Both diffraction techniques

can be used for statistical characterisation of nanotubes as they provide valuable information on interlayer spacing, structural strain, chirality and diameter distribution, as well as the number of layers for MWNTs[105].

Thermal gravimetric analysis is a simple analytical technique that measures the weight loss or gain of a material as a function of temperature. Since nanotubes have the highest resistance to oxidation of all the carbon forms, an idea of the purity of the sample can be obtained from TGA. Other forms of carbon possess less resistance to oxidation and burn out at lower temperatures than carbon nanotubes.

1.9 Nanotube analysis software:

Image analysis and data collection on nanotubes is of paramount importance to characterise nanotubes for their implementation in various practical devices. SIMAGIS® Nanotubes [116] is very useful software which provides consistent data on nanotubes density, SWNT rope thickness, alignment and particle dispersion. This automated analysis software performs a variety of tasks like counting the number of tubes, SWNT ropes and nanoparticles, besides measuring length, height, curvature and performing diameter analysis. This software analyses micrographs/images from the AFM, TEM and SEM to provide reliable information on different physical properties of nanotubes. This software has become an effective tool for data analysis in research and development of nanotube structures.

1.10 Nanotube properties:

The great variety of possible geometries for nanotubes provides a new dimension for interesting physical properties. Nanotubes have exceptional material properties such as electrical and thermal conductivity, strength, stiffness, and toughness. These special properties have generated a strong interest for their potential use in various applications. These special properties are discussed in detail in this section:

1.10.1 *Electronic properties:*

The electronic properties of nanotubes strongly depend on their chirality and diameter leading to either metallic or semi conducting nanotubes. As nanotubes possess macroscopic lengths when compared to their diameters, the number of allowed electronic states in the axial direction is large with a smaller number of states in the circumferential direction. This leads to quantum confinement of electrons along their axis causing ballistic electron transport enabling nanotubes to act as quantum wires[15]. Hence carbon nanotubes can carry high amounts of current upto 2 mA without dissipating energy and giving off heat.

Hamada[117] reported that about one-third of single walled nanotubes are metallic and the rest semi-conducting by calculating dispersion relationships for nanotubes with small diameters and chirality. Thus nanotubes conceivably combine the properties of metals and semi conductors leading to unique electronic properties and their use in nanoscale electronic devices. The mean free path for electron travel increases with nanotube diameter allowing more wave vectors in the circumferential direction. As the band gap in semi conducting nanotubes is inversely proportional to the tube diameter, the band gap becomes zero at large diameters making them exceptional ballistic conductors[28].

Another interesting property of nanotubes as investigated by Lemay[118] is their ability to suppress changes in the direction of electron transport, thus keeping the electrons moving persistently in one direction. As a result, nanotubes experience little or no resistance as there is little electron scattering, except at defects.

These unique electronic properties of nanotubes make them ideal candidates for use in electronic devices. Research has shown that nanotubes can be used as diodes when a metal-like nanotube is fused to a semi conducting one[119], as transistors when nanotubes were grown between metal islands on a silicon substrate[120, 121], as display units [122, 123], X-ray sources [124, 125], and ionisation gauges[126, 127] when used as electron emission sources.

1.10.2 *Mechanical properties:*

The mechanical properties of nanotubes are also highly dependent on their size, structure and topology. Since the C=C double bond is the strongest bond in nature, carbon nanotubes are widely regarded as the ultimate fiber for use in materials applications. The small diameter of nanotubes with their carbon-carbon sp^2 bonds and the high anisotropy of graphite have a remarkable effect on their mechanical properties. Nanotubes have high stability, strength and stiffness combined with low density and elastic deformability. Their high tensile strengths are well above 100 GPa, with a high bending strength of the order of 14-15 GPa and they have a measured Young's modulus of 1.4 TPa[28]. The strength of a material is intimately related to its structural imperfections and defects and nanotubes with its low density of defects exhibit strengths approaching their theoretical limit. The actual strengths in practical situations for MWNT are affected by the graphene layers sliding with respect to each other.

Evaluation of single nanotube properties is very taxing as it requires specially designed loading devices for experimentation. Most of the mechanical properties are based on computational simulations with an empirical methodology derived from studies on graphite[15].

Nanotubes exhibit interesting fracture and deformation behavior. Nanotubes are flattened, deformed and buckled as they deform and they can switch back into their normal morphological form with abrupt release of energy[128]. They can sustain large strains (up to 40%) without showing signs of fracture[129]. The other interesting behavior of nanotubes is the creation of Stone-Wales (pairs of 5-7 pentagon-heptagon) defects at high strains and the ability of these defects to move. This leads to their diameter reduction and introduces helicity in the region to where the defects move, inducing lattice orientation[130].

In conclusion, nanotubes seem to behave as ideal carbon fibers demonstrating outstanding mechanical properties such as high strength, extraordinary flexibility and resilience and are used in a wide range of products ranging from tennis racquets to spacecraft, super-composites, probe tips and aircraft body parts[131].

1.10.3 *Magnetic properties:*

Magnetic fields are found to have strong effects on the electronic structure and bulk properties of carbon nanotubes. Nanotubes exhibit both large diamagnetic and paramagnetic responses depending on the field direction, changes in Fermi energy, helicity and nanotube radius in weak fields[2]. The magnetic properties are sensitive to intrinsic layer defects and impurity atoms, and depend on the conditions of preparation. The basic electrical properties of semi-conducting nanotubes changes when they are placed in a magnetic field. This unique phenomenon is due to the shrinking of nanotube band gaps and due to the transfer of spin carried by electrons inside the magnetic field[132]. In stronger fields the band gap is predicted to disappear altogether with nanotubes to transform into metals. The average room temperature magnetisation in nanotubes is calculated to be 0.1 Bohr magnetons per carbon atom[133]. These properties were evaluated by placing solutions of nanotubes in strong magnetic fields of 45 T in strength and shining lasers on the samples. The amount of light emitted and absorbed by the samples was analysed to compute their magnetic properties.

This property of nanotubes leads to information on one dimensional magneto-excitons aiding researchers studying quantum computing, nonlinear optics and quantum optics[133].

1.10.4 *Chemical properties:*

The chemical properties of nanotubes are as equally exciting as their physical properties. Being considered as an allotrope of carbon, nanotubes possess the richness of carbon chemistry. Nanotubes are chemically inert along their surface if they have a perfect structure. The sites of preferential activity therefore are at their end caps and tips caused by curvature of the graphene sheets. Many of the chemical properties imparted to nanotubes are through functionalisation. Surfactants are used to modify the surface energy of nanotubes by attaching preferred chemical groups covalently and non-covalently. These groups then act as active sites enhancing the reactivity of nanotubes and promoting surface reactions[134]. Nanotubes caps are susceptible to oxidation and etching compared to its cylindrical surface, when exposed to oxidising atmospheres. The end caps of

nanotubes can be removed and then be filled with molecules and recapped[40]. Since many physical and chemical processes are initiated at the solid/gas or solid/liquid interface, nanotubes are considered prime materials for gas adsorption/storage and molecular filtration[135]. The unique physio-chemical properties of nanotubes like porosity, specific surface area, pore-size distribution and their ability to be semi conducting or metallic imparts a huge capability for adsorption of gases and vapours.

These interesting physio-chemical properties have rendered nanotubes to be used in a range of diverse applications such as multifunctional biological transporters for in situ drug delivery[136], DNA immobilization[137], electrodes for fuel cells[138], catalyst supports[139], nanoporous filters[135] and a range of other potential applications.

1.11 Nanotube applications:

The most exciting facet of carbon nanotubes is their remarkable potential for applications. Four broad areas namely composites, energy storage, molecular electronics are considered in this section.

1.11.1 *Energy storage:*

Carbonaceous materials have been traditionally used either as electrodes or as support materials for energy storage devices. Carbon nanotubes are of a great interest for electrochemical applications due to the high surface area, smooth surface topology and low resistivity of nanotubes. Nanotubes are hence expected to find various applications in the energy storage area ranging from hydrogen storage to lithium intercalation and supercapacitors through either adsorption or insertion mechanisms.

a) Hydrogen storage:

Nanotubes have generated considerable interest from both academia and industry due to various reports of extraordinary high and reversible hydrogen

adsorption[140-142]. Hydrogen systems are expected to address the energy issues of the world in the future due to its easy regeneration and the fact that its combustion product is water. Nanotubes have a high absorption capacity due to their high surface area and a liquid or gas can be stored inside them through a capillary effect[143]. A minimum storage requirement of 9 wt% hydrogen by 2015 and a volumetric density of 62 kg H_2/m^3 for fuel cells have been set by the Department of Energy as a threshold for economic purposes. However, experimental reports of high storage capacities by nanotubes (up to 14-20 wt %[142]) are so controversial that it is impossible to assess its application potential. A storage capacity in the range of ~4 wt% under moderate pressure and room temperature (obtained from experiments and calculations by numerous groups) is thought to be its absolute limit of adsorption[141]. Table 1.2 gives an overview of reported storage capacities of hydrogen in carbon nanotubes at room temperature. The results from nanotubes are quite disappointing due to the lack of a detailed understanding of the hydrogen storage mechanism. This is also due to the nature of hydrogen and the rigorous requirement of the experimental methods.

Material	Storage wt%	Temp (K)	Pressure (MPa)	Reference	Year
GNFs (tubular)	11.26	RT	11.35	Chambers	1998
CNFs	~10	RT	10.1	Fan	1999
Li/K-GNTs (SWNT)	~10	RT	8-12	Gupta	2000
GNFs	~10	RT	8-12	Gupta	2000
SWNT (lo purity)	5-10	273	0.04	Dillon	1997
SWNT (hi purity)	8.25	80	7.18	Ye	1999
CN nanobells	8	573	0.1	Bai	2001
Nano graphite	7.4	RT	1	Orimo	2000
SWNT (hi purity + Ti alloy)	6-7	~300-700	0.07	Dillon	2000
GNFs	6.5	RT	~12	Browning	2000
CNFs	~5	RT	10.1	Cheng	2000
MWNTs	~5	RT	~10	Zhu	2000
SWNT (hi purity + Ti alloy)	3.5-4.5	~300-600	0.07	Dillon	1999
SWNT (50% purity)	4.2	RT	10.1	Liu	1999
Li-MWNTs	~2.5	~473-673	0.1	Yang	2000
SWNT (50% purity)	~2	RT	echem	Nutzenadel	1999
K-MWNTs	~1.8	< 313	0.1	Yang	2000
(9,9) array	1.8	77	10	Wang	1999
MWNTs	< 1	RT	echem	Beguin	2000
CNF	0.1-0.7	RT	0.1-10.5	Poirier	2001
(9,9) array	0.5	RT	10	Wang	1999
SWNTs	~0.1	300-520	0.1	Hirscher	2000
Various	< 0.1	RT	3.5	Tibbets	2001
SWNT (+ Ti alloy)	0	RT	0.08	Hirscher	2001

Table 1. 2 Summary of various reported hydrogen storage for carbon nanotubes[144].

b) Lithium intercalation:

Nanotubes have shown promise for use as anode materials in lithium-ion power cells. Lithium batteries use the transfer of lithium between two electrodes (intercalation and de-intercalation) placed in an electrolyte to create a battery with the highest energy density. Nanotubes exhibit greater specific discharge capacity and energy due to their electro-negativity and their ability to accommodate more lithium ions per unit of carbon[145]. Nanotubes are also shown to possess both highly reversible and irreversible capacities. The intercalation of lithium into the structure of nanotubes is known to proceed through graphene walls via structural defects[146]. Although the exact location of Li ions in the intercalated nanotubes is still unknown, it is suggested that they reside in the interstitial sites between the layers[147]. The maximum reported reversible capacity for nanotubes is 1000 mA-hr/g compared to 372 mA-hr/g for graphite[148]. However nanotubes are still unsuitable for battery application due to the absence of a voltage plateau during discharge and a large hysterisis in voltage between charge and discharge[69].

c) Electrochemical supercapacitors:

Supercapacitors comprise of two electrodes separated by an electronically insulated material, which is ionically conducting in electrochemical devices. The capacitance depends on the separation between the charge on the electrodes and the counter charge in the electrolyte. Large capacitances result from electrodes made of nanotubes due to their high surface area and low resistivity. The performance of supercapacitors is judged in terms of its energy density. The energy density of supercapacitors is proportional to the surface area per unit volume of the electrode material. Nanotubes have the highest surface to volume ratio of all known carbon material (3000 m^2/g) as all their atoms are on their surface and hence make an ultimate material for supercapacitor electrodes[5], as shown in Fig. 1.16. Although the energy density of supercapacitors made from activated carbon is near their theoretical maximum, nanotubes have the advantage of having a lower resistance than activated carbon thus increasing its power density. The limiting factor is contacting nanotubes to the electrode polymer

backing and the ability to achieve that at low temperatures and with low costs against other materials[5].

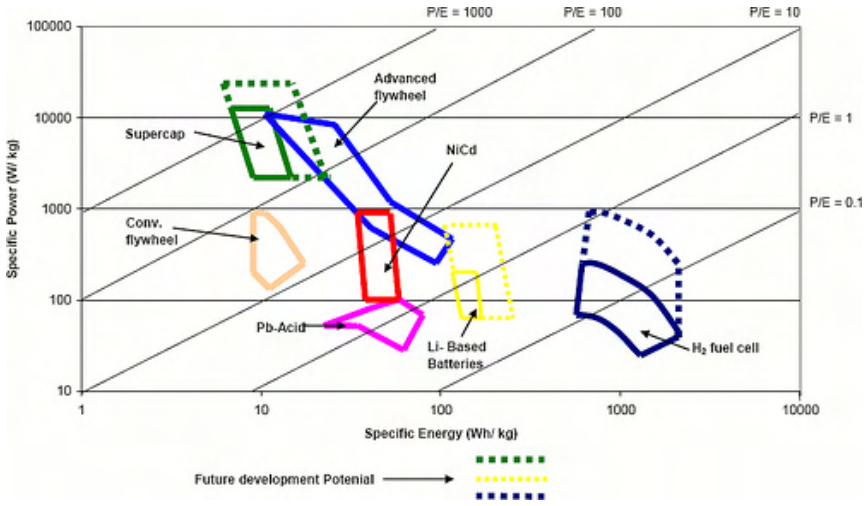

Fig.1. 16 Power density versus Energy density plot showing the highest energy density for fuel cells[5]

1.11.2 *Composite materials:*

Carbon nanotubes are ideal candidates for structural applications. Various applications for composites based on MWNTs and nanofibers are already commercialised. Carbon nanotubes based composites are reported to be six times stronger than the conventional carbon fibre composites[149]. The high modulus, low weight and high aspect ratio render nanotubes as promising fillers for a wide range of applications. The use of carbon nanotube reduces the “percolation threshold” of composites by imparting electronic conduction at lower loadings of nanotubes than larger conducting fillers[5]. Nanotube composites can also be used for shielding of electromagnetic interference (antishielding agents) due to its conductivity on airplane wings and fuselages. Nanotube composites can be transparent, if thin enough and have a huge advantage of being flexible and being compatible with polymer substrates[5]. CNT composites can be a viable alternative for transparent electronic conductors like Indium Tin Oxide (ITO) for the display market.

In addition nanotubes have attracted much interest as reinforcements for low weight structural composites. Their performance has been rather disappointing

due to uneven distribution and insufficient bonding across the nanotube/host interface[5]. This might be due to pull out by sliding of the different layers in MWNTs or tube shearing in SWNT ropes. The critical challenges lie in uniformly distributing nanotubes, sometimes achieved by breaking nanotubes into shorter segments or by having a superior nanotube-matrix adhesion for effective stress transfer[69]. Stronger bonds between nanotubes and the matrix can be achieved by functionalisation[150] or by using secondary bonds such as hydrogen bonding[151].

The most novel of the methods to produce nanotube composites is the ability to draw and spin nanotubes to indefinite lengths from a polymer solution (consisting of nanotubes) from a capillary orifice using an electric field[152]. The resulting fibre is post impregnated with epoxy to make a composite. This technology could have applications from textiles for bullet proof vests to super strong cables for "the space elevator".

1.11.3 *Nanotube electronics:*

Selected area deposition of nanotubes is possible with some nanotube preparation methods. Patterned deposition of nanotubes on the micro to nanoscale is a prerequisite for their application in molecular electronics, displays and actuators. Application of nanotubes as field emitters and the underlying theory will be discussed in more details in a later section.

The growth of the micro-electronics industry can only be sustained by the use of different materials, fabrication principles and device concepts to the existing ones. Carbon nanotubes can carry the highest current densities (10^{11} - 10^{14} A/mm^2) amongst all materials and hence are perfect candidates for electronic applications. Nanotubes have been successfully used in field effect transistors (FET) and have shown to have extremely good performance over silicon. The resulting figure of merit is 20 times better than the existing laboratory CMOS devices[5]. Nanotube FET intends to replace the existing source-drain channel structure with a nanotube. The transistors are fabricated either by lithographically fabricating

electrodes on a silicon substrate or by positioning nanotubes using an AFM[153] as shown in Fig. 1.17. Since the band gap of a nanotube depends on its chirality, it is possible to produce a diode by grafting a semi-conducting nanotube to a metallic one[119]. Nanotubes are poised to revolutionalise nano-electronics with their use in non-volatile memory for electromechanical relays[154], three-to four-terminal electronic devices[155] and nanotube transistors[156]. Nanotube transistors coupled together acts as a logical switch, which is the basic component of computers[157]. Carbon nanotubes show a large non-linear absorption of light due to its one dimensional band structure with singularities in the electronic density of states (Dos) and are also used in fast optical switches[158].

A significant problem of using nanotubes for electronic applications is the separation of a mixture containing both metallic and semi-conducting nanotubes. Control of position and direction during nanotube growth is also an issue as the size limit of molecular transistors is still determined by its contact dimensions[5].

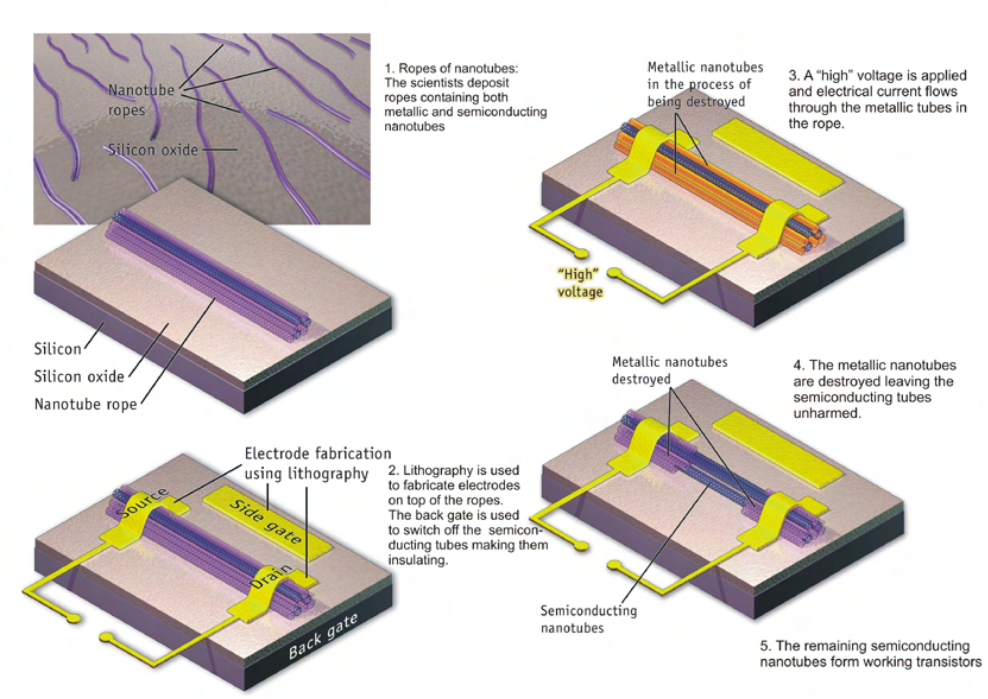

Fig.1. 17 Carbon nanotube electrode fabrication using lithography[153].

1.11.4 *Other applications:*

Various other applications of nanotubes have also been reported apart from the strongly researched areas mentioned previously. Some of the potential markets for the applications are enormous while others are pure science fiction. These applications include microscope (AFM) tips, drug delivery agents, templates, artificial muscles working on actuator principles, nano-gears, nano-test tubes, catalysis, dialysis filters and super strong ropes for a "space elevator".

Nanotubes are used as nanoprobes due to their bending abilities, conductivity and small dimensions. They are being used in an array of applications such as tips for AFM and STM[159-161], nanolithography[162] and nanoelectrodes for electrochemistry[163]. The high elasticity of nanotubes prevents them from breaking on contact with the substrate. Nanoprobes are reported to be suitable for imaging of biological molecules such as DNA[164] and for high resolution imaging[165]. Functionalised nanotubes have been reported for their use as probes for drug delivery, molecular recognition and chemically sensitive imaging. Organic molecules of comparable length scales seem to recognise helicity of nanotubes. Thus nanotubes are used for molecular recognition such as scaffolds for neuron regeneration and other biomedical applications[166].

Nanotubes suspended in electrolytes have been demonstrated to experience large strains when a small voltage is applied to one end. Thus nanotubes are used as actuators in artificial muscles[167] and in similar applications like micro-cantilevers[168]. Nanotubes have been reported to be used as templates to create nanowires of various compositions and structures. This property is due to its hollow cores and high aspect ratio which creates strong capillary forces inside them. The opening and filling of nanotubes is also used to perform interesting chemical reactions inside nanotube cavities enabling to act as nano-test tubes[169]. Nanotubes have also been reported to be used as templates for self-assembly of protein molecules[170]. Due to their high surface area and their ability to attach many chemical species to their side walls, nanotubes have also been reported to be used as catalyst supports[171].

Some applications of nanotubes have still remained in the realm of science fiction. The most popular is that of a nanotube rope strong enough to support an elevator

extending miles into space from earth. The notion that nanotubes can be produced inside the body by self replication (since all living organisms are made of carbon) and then be used to treat various diseases is another application considered as science fiction.

2.0 Field emission from carbon nanotubes

2.1 Introduction:

Vacuum microelectronics is a revolutionary technology using electron transport in vacuum after emission from microfabricated structures. Electron emission is defined as the discharge of free electrons caused by external energy transfer from the surface of a substance. Since the nucleus of an atom holds the free electrons together, an external energy is required to free the electrons from a surface consisting of a cluster of atoms. This external energy required by the electron to escape from a metal surface is known as the work function. The additional external energy required by the electron to overcome its work function can be imparted by various energy sources such as heat, light or electricity. Accordingly, electron emission from a surface of a metal can be grouped as follows:

1) Thermionic emission.
2) Photovoltaic emission.
3) Field emission.

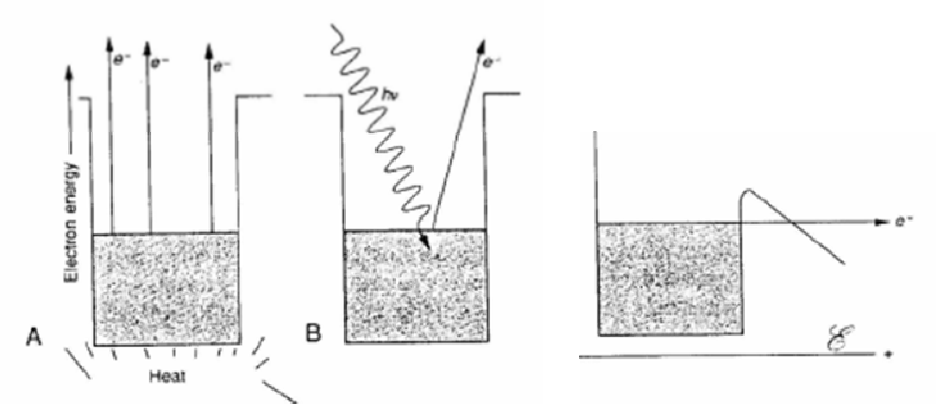

Fig.2. 1 Schematic of several types of emission. (a) Thermionic (b) Photovoltaic and (c) Field emission[172].

In thermionic emission, additional energy to the electron is imparted by raising its temperature. This causes an increase in the kinetic energy of electrons sufficient to overcome the work function resulting in electrons escaping from the metal surface, as

shown in Fig. 2.1. If the additional energy is transferred due to photons (beam of light) resulting in electron knockout from the metal surface, it is called photovoltaic emission. This type of emission is dependent on light intensity. Field emission occurs when the electrons are ejected from the surface of the metal due to a high electric field. Field emission occurs due to tunnelling of electrons through the potential barrier. This is caused by very sharp nanotube tips which enhance the applied energy. Field emission occurs at temperatures much lower than thermionic emission and hence is also known as cold cathode emission or auto electronic emission. All the above emission mechanisms seek to minimise the barrier to electron emission into vacuum by engineering the material properties (change in work function) or the physical geometry (changing field enhancement) of the emitting surface [173].

2.2 Emission types:

2.2.1 *Thermionic emission:*

Thermionic emission describes electron emission for situations where the cathode temperature is high and there is low relative field strength. As the temperature of the metal is increased, higher states in the metal surface become occupied by electrons which accumulate nearer to the Fermi level (ε_f) of the metal as shown in Fig. 2.2. At a high enough temperature, electrons gain sufficient kinetic energy to surmount the surface barrier and escape into the vacuum, resulting in thermionic emission.

Thermionic field emission follows the 'Richardson-Dushman' relationship[174] which relates the current density from a heated filament given by the following equation,

$$J(T) = AT^2\exp(-\phi/kT) \text{----------(2.1)}$$

A plot of log (J/T^2) versus 1/T yields a straight line and the work function (ϕ) of the emitter is obtained from the negative slope of the plot. The constant A can be measured in principle but is complicated in practice due to the need of knowing the emitting area independently since emission current is measured instead of the current density (J). The form of this equation can be derived readily from free

electron theory by considering the Fermi function, and integrating over all those electrons moving towards the surface whose 'perpendicular energy' is enough to overcome the emitter work function. In this calculation, the value of A when ignoring reflection at the surface by low energy electrons is $A= 4\pi mk^2e/h^3 = 120$ $A/cm^2/K^2$ [175]. Factors such as surface forces, material processes and surface roughness may cause this value to differ in actual solids. In addition to this, the probability of electrons reflected back from the surface to the metal instead of being emitted over the potential barrier may also change the value.

Thermionic emitters in the form of pointed wires or rods are used as electron sources in many electron optical devices such as oscilloscopes, TV and terminal displays, and both varieties of electron microscopes. A good thermionic emitter has to have a combination of a low work function and a high operating temperature. The most common thermionic emitter is tungsten which has a work function of 4.5 eV. Fundamental issues like robustness in practical environments and emission uniformity needs to be addressed and an intensive search for materials with better performance as thermionic emitters is still being pursued.

2.2.2 *Field emission:*

Field emission or cold cathode emission describes electron emission for situations where the field strength at the cathode is high and the temperature is low. When the electric field at the cathode is increased sufficiently, emission occurs due to quantum-mechanical tunnelling of electrons through the reduced height/distance of the triangular shaped barrier. At high field strengths of around 3 V/nm, the barrier width is of the order of 1 nm and electrons escape at a low (room) temperature by tunnelling. The probability of an electron tunnelling out is high if the barrier width 'w' is comparable to the de Broghlie wavelength (λ) of the electrons. Because the barrier width is smallest for the most energetic electrons, electrons close to the Fermi level tunnel out causing emission as shown in Fig. 2.2.

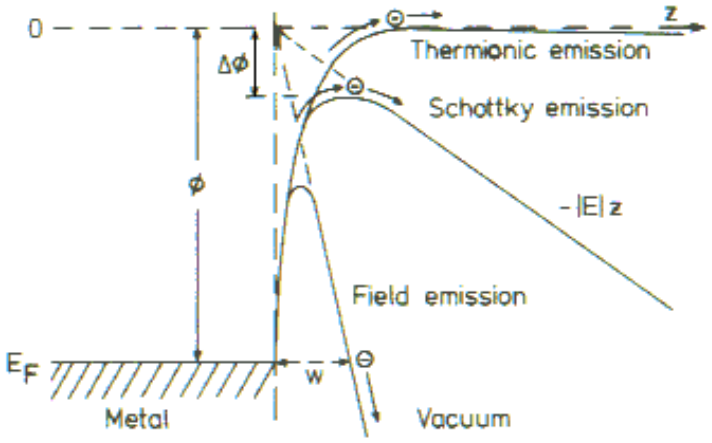

Fig.2. 2 Energy diagram showing the potential barrier for various types of emission and field emission due to tunnelling of electrons[176].

2.3 Theory of field emission:

The current density (J) of a material under the influence of a high electric field is given by the Fowler-Nordheim (F-N) equation[177]. The Fowler-Nordheim equation dictates that this current density is both a function of electrical field strength and the effective radius of the tip. The field (F) plays a similar role to the temperature in thermionic emission and the governing equation is derived from free electron theory by Fowler and Nordheim (Eq. 2.2). The current density (J) emitted by a cathode is given by the following equation:

$$J = A.\ F^2/Ø.\ \exp\left(-BØ^{3/2}/F\right) \text{----------} (2.2)$$

Where J (A/m^2) is the emission current density and Ø is the work function, A and B are constants derived from free electron theory, where $A= 6.2*10^{10}(\mu/Ø)^{0.5}/(\mu+Ø)$ A/m^2 and $B= 6.83 \times 10^9\ V^{0.5}/m$. 'μ' being the Fermi level potential (V) with respect to the bottom of the valence band. The electric field F is given by:

$$F = ßV_a/d \text{----------} (2.3)$$

Where ß is the field amplification factor which is a function of 'h/r' where 'h' is the height of the emission tip and 'r' the radius of curvature, V_a is the applied voltage and V/d is the voltage per unit distance across an electrode gap 'd'.

Experimentally, cold field emission requires a sharp tip with small radius 'r' and ultra high vacuum conditions. A voltage (V) is applied to the cathode and most of the field

is generated near the sharp tip. The field (F) generated at the apex of a sharp tip due to the applied voltage is also given by:

$$F = V/kr \quad \text{----------(2.4)}$$

Where 'V' is the applied potential for a known inter-electrode distance, 'r' is the apex radius and 'k' is a numerical constant which is related to the taper angle of the emitter. 'k' usually varies between 3-5 but is usually assigned a value of 5 for calculations. Field emitters typically operate with voltages between 1-5 kV and radii of around 100 nm. Therefore the tunnelling rate of electrons is also dependent on the shape and width of emitting structures.

A Fowler-Nordheim plot of log (I/V^2) versus 1/V gives a straight line due to the linear dependence of field on voltage and provides a characteristic check for the field emission mechanism. The current (I) is obtained by measuring the average current over entire emission area. The experimental data varies slightly from the model, both when the field emitter just begins to emit and at the high end of emission. As thermal excitation is not required, a field emission tip can operate at room temperature but a very good vacuum (lower pressures than 10^{-6} mbar) is mandatory for stable operation. Contamination of tips due to diffusion of adsorbed gases occurs often and a typical field emitter needs to be "flashed' (accomplished by joule heating) to obtain an emission from a clean surface. In-situ deposition of individual atoms on the tip is known to cause a jump in emitted current and/or a reduction in the work function. Thus the real nature of a field emission tip during use is somewhat shrouded in mystery.

The field emission principle has found extensive potential applications in new generations of flat-panel (computer, TV) displays, as a replacement for the traditional cathode-ray tubes.

2.3.1 Validity of F-N equation for sharp emitters:

The Fowler-Nordheim equation was derived based on the assumption that the surface of the emitter is planar, although the actual emitters are not literally planar. This assumption may be justified since the emission area on the surface of an emitter may be limited to such a small region at the apex of the emitter, that the area can be

regarded as planar[178]. As emitters get sharper (nanowire, nanotube), the F-N field emission formulae should be modified to consider the three dimensional geometry of the emitter. Various researchers have shown that field emission occurs at fields much lower than the value predicted by the F-N equation and that the equation (Eq. 2.2) leads to erroneous interpretation of the I-V data[179-181].

A review of the basic problem for field emission from sharp tips[182] reveals that for a radii of curvature $\geq$ 50 nm, the tunnelling electron sees essentially a 'flat' conducting surface within the distance $\leq$ 0.5 nm. The dependence of geometric and material parameters on field emission has been studied by various groups which show that energy distributions for non planar models are much wider than that predicted by the F-N planar model. Cutler et. al[182] deduced an equation for the current density of nanotube tips with non-planar geometries from the classical kinetic formulation theory, to give a current integral as follows:

$$J = A.\ F^2/Ø.\ \exp\left(-BØ^{3/2}/F - C/F^2\right) \text{ ---------- (2.5)}$$

Where A, B and C are constants related to the material properties and geometry of the emitter.

A plot of current density from Eq. 2.5 and the F-N equation as a function of external voltage is shown in Fig. 2.3. It is observed that the magnitude of current density for non planar models (hyperboloidal and conical tip geometry) does not increase as rapidly with the applied voltage but is significantly greater than that obtained from the F-N equation. But it is worth noting that as the field increases, the effect of geometry on the emission current is less pronounced as the tip becomes more "blunt" (flatter and physically not included in the model) and the current density approaches the value predicted by the F-N equation. Therefore the F-N equation is assumed to be valid for most field emission experiments although it underestimates the emitter area and overestimates the electric field.

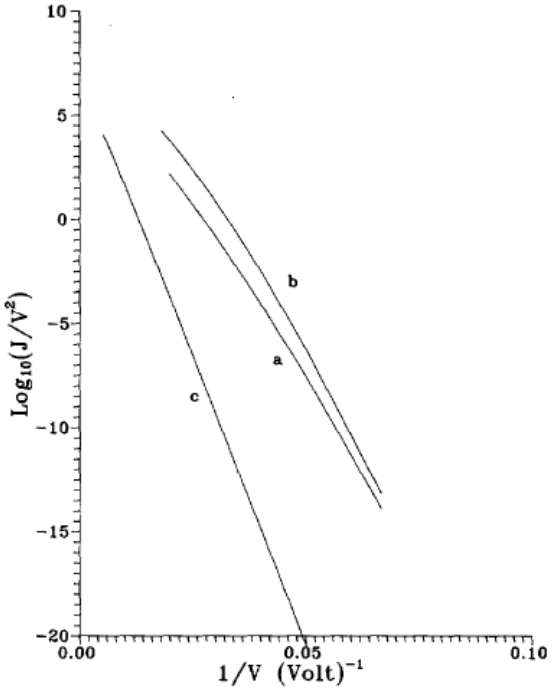

Fig.2. 3 Plot of log(J/ V^2) vs (1/V) for (a) hyperboloidal model with tip radius of 10 nm, (b) a conical tip model with half-angle of 70^0 and (c)a planar model from F-N equation[182].

2.3.2 Adsorbate effect on field emission:

The field emission property of a nanotube emitter that has been covered by an adsorbate has not been studied extensively. The nature of the emitter surface under high field is believed to be the driving force for adsorption. The surface atoms at the protrusions or defects on the emitter surface are always in a highly energetic state. The overall energy of the system is hence lowered by allowing atoms and molecules to combine with it, that is by adsorption[183]. The binding energy between the adsorbing atom and the emitter surface should be greater than the binding energy of the atoms themselves for adsorption to occur. The classical behaviour of adsorption and its effect on field emission is illustrated by studying the adsorption of an oxygen atom on molybdenum[184]. When oxygen molecules dissociatively adsorb as individual atoms onto the surface of molybdenum, the unoccupied orbital for an extra electron on the oxygen atom lies below the Fermi level and will reside on the Mo surface as O^- thus enhancing field emission.

The energy diagram for an electron on a clean cathode surface with a strong electric field is shown in Fig. 2.4. The schematic for an electron on a surface covered with

adsorbate such as oxygen is also indicated. The new electron state for O^- creates a barrier known as a Schottky barrier and provides a decreased thickness for the tunnelling electron. The adsorbed state (field + surface + atom) effectively lowers the work function creating an extra electronic state for the easy escape of the electron from the metal surface. This adsorbate coverage of the emitter surface strongly correlates to the field emission characteristics of all field emission cathodes.

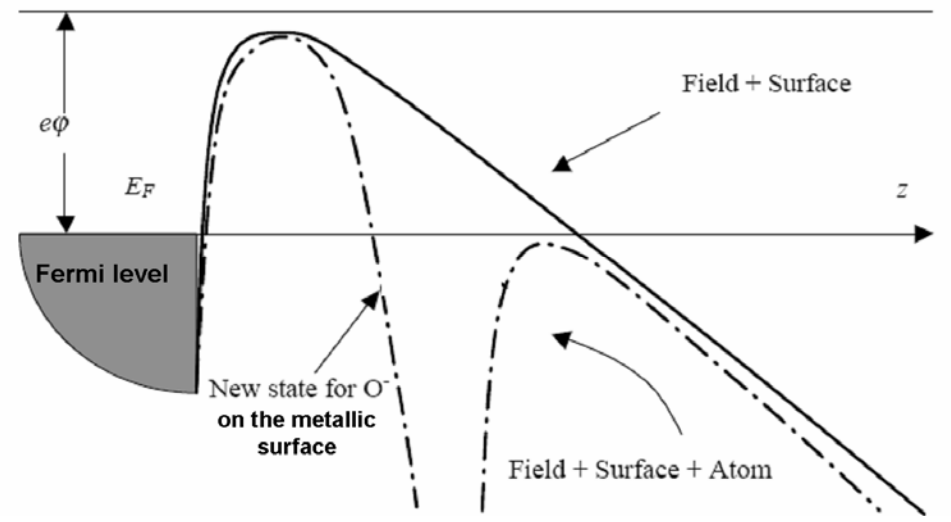

Fig.2. 4 Energy diagram for field emission with energy plotted as a function of distance from the metal surface 'z'. "Field + Surface" indicates the lowering of the potential barrier created by the applied field. "Field + Surface + Atom" indicates the potential seen by an electron residing on an adsorbate covered surface, with an extra electronic state for O^- existing below the Fermi energy[185].

It is expected that a strong bond (chemisorption) between the adsorbed atom and the emitter surface causes significant redistribution of the valence electron density leading to a change in work function. Accurate quantum-mechanical calculations of the electron density distribution between the adsorbed particle and the emitter surface are rather complicated and do not yet yield reliable values for the binding energy and for the dipole moment of adsorption. But a simple model characterises the change in work function to be equal to the dipole moment of the double layer formed by the positive ions and the induced negative charges on the surface[186]. The work function is strongly dependent on the coverage of the adsorbed atoms. The adsorbed layer is usually characterised, not by an absolute surface concentration, but by the relative coverage (Φ) where,

$$\Phi = N/N_{max} \text{---------- (2.6)}$$

where N_{max} is the greatest number of particles which can be arrayed on 1 cm of the surface, with dense packing. The value $\Phi = 1$ corresponds to a monolayer. As the density of the adsorbed ions increases, the positive potential of the adsorbed layer increases, and it becomes energetically more advantageous for the electrons to partially transfer through the adsorbed ions[186]. This leads to a decrease of the dipole moment per adatom, and also to an increase in the covalent components binding the surface layer to the substrate. Experimentally, it is found that the work function is a minimum when the coverage is close to or somewhat less than a monolayer[186].

If the coverage becomes greater than unity (or even before), the second layer begins to develop. In this case, bonding to the substrate becomes weak and the resulting work function approaches that of the adsorbate material leading to a decrease in emission current.

Although the theory is rather crude, field emission may occur in three different states, an initial adsorbate state where the work function is lowered facilitating easy extraction of electrons from the emitter surface[186], an intermediate stage where the emission is governed by the work function of the adsorbate (due to increase in its coverage) and a final stage where the adsorbed atoms are removed due to temperature increase caused by joule heating with the work function of the emitter governing field emission.

It is seen that several distinct effects are operative during field emission producing departures from the normal cold emission (F-N) law. These departures are associated with the nature of the surface barrier and/or due to the distortions of applied field near the emitter. The most pronounced cause of discrepancy leading to deviation from the F-N law[187] is from the irregularities at the atomic size (~0.3 nm). The secondary effect due to non uniformity or change of work function also leads to deviation from the F-N law and is important for coated (adsorbed) emitters.

2.4 Factors affecting field emission from carbon nanotubes:

Electron field emission from surfaces of conductive materials by strong electric fields is of great importance for fundamental and applied science. Carbon materials have

attracted huge interest as cold cathodes in vacuum electronic devices. Stable electron emission from various carbon materials like polycrystalline diamonds[188], diamond like films[189], carbon fibres[190], graphite powders[191] and other nanographitic crystallite materials have been demonstrated successfully. The main advantage of carbon materials for field emission is their strong covalent bonding which provides them with a high mechanical strength and chemical inertness for their operation as field emission cathodes. Carbon cathode materials can sustain the harsh conditions of residual ion bombardment and can operate effectively under high electric fields and vacuum. Despite the above properties, a rather weak interlayer bonding marks the destruction of parallel layers under high electric fields as observed in carbon fibres and graphite particles[7].

A carbon nanotube is a graphite sheet that is rolled into a cylinder of a few micrometers in length and a few nanometers in diameter where each carbon atom is bound to three others by a (covalent) sp^2 bond. The activation energy for surface migration is high and hence it can sustain extremely high fields needed for field emission[4]. The cylindrical surface prevents any layer from chipping off under the action of high electric field. Carbon nanotubes can also act as a semiconductor or metallic conductor depending on the exact arrangement of atoms along their axis. Therefore CNTs exhibit the right combinations of properties such as structural integrity, high aspect ratio, high thermal and electrical conductivity and chemical stability which make them an excellent choice for field emitters. Electron field emission from nanotubes was first demonstrated in 1995[192, 193] and has since been studied extensively. CNTs have a low turn-on field and exhibit high film current densities (10^{11} A/mm^2) due to their high aspect ratio providing optimum geometric field enhancement. Nanotubes exhibit an inverse relation to resistance when driven to high currents and do not suffer from electric field induced sharpening. Nanotubes are known to follow the F-N relationship wherein emission occurs from a conductive material under a strong field which is generated due to morphological features on its surface. Another approach assumes that emission occurs due to negative electron affinity (NEA) of diamond and diamond like species but this is ascertained to be only valid for carbon materials with sp^3 configuration[7].

Carbon nanotubes are used as electron sources in two types of set ups - namely as single and multiple-electron beam devices. Field emission from nanotubes as single electron beam devices will be covered in detail in a later chapter. The emphasis in this

section is on macroscopic carbon nanotubes cathodes (CNT films) and the factors affecting their emission characteristics. The most important parameter for field emission cathodes is their emission site density (ESD), which usually increases with applied field. Emission site density is the number of effective emitters per area of a specimen. The mode of electron source (cathode) preparation influences emission characteristics such as turn-on voltage, maximum current density obtained, emission stability and so on. The two main methods used for cathode preparation are as follows:

a) Printing the nanotube material as a paste using a binder[194-196].
b) Direct growth of nanotubes on a substrate using various forms of CVD[10, 197, 198].

The former method is easy for processing and is mainly used for nanotubes grown from arc discharge, but is limited in controlling various physical parameters affecting field emission. The problems associated are removal of residual binder, achieving good uniformity/density of nanotubes and aligning nanotubes perpendicular to the substrate. The second method is very effective for achieving selective growth and control of other parameters like length and distribution, but suffers from certain disadvantages. These are difficulties of uniform growth over large areas, reduced emission characteristics and substrate destruction at high growth temperatures. Several important parameters need to be considered to design and fabricate cathodes with optimised performances. Factors like the type of carbon nanotubes (MWNTs or SWNTs), their orientation, aspect ratio, areal density of nanotubes and nanotube interaction with the substrate are vital for a superior nanotube cathode. External factors like vacuum, design configuration (diode, triode) and adsorption also significantly affect the performance of a nanotube field emission system. The main factors affecting field emission from macroscopic nanotube cathodes are discussed in detail here under:

2.4.1 Length, screening and aspect ratio:

Carbon nanotubes are considered as one of the best electron-emitting materials due to high enhancement factors bestowed by its distinctive aspect ratio. The field enhancement is affected by the length, spacing, diameter and ultimately the areal

density of nanotubes. It is important to characterise the affect of length and spacing on field emission properties to obtain uniform field emission at low fields.

The areal density of nanotubes has a profound influence on the nanotube's overall emission behaviour as shown in Fig. 2.5, till a certain optimum number. The turn-on voltage is increased as the number density of nanotubes is increased[199, 200]. This increase in turn-on voltage is due to a decrease in enhancement factor resulting from decreased spacing between nanotubes of high density nanotubes, as shown in Fig. 2.6. However, the turn on voltage for low density nanotubes is significantly higher than for a sample with high density of nanotubes. The enhancement factors of carbon nanotube film can be approximated by the following equation[201]:

$$ß = ß_0[1-\exp(-2.3172s/l)] \quad \text{---------- (2.7)}$$

where

$$ß_0 = 1.2(l/r+2.15)^{0.9} \quad \text{---------- (2.8)}$$

where 's' is the spacing between the nanotubes, 'l' is the length of the nanotube, '$ß_0$' is the intrinsic enhancement of an individual nanotube and 'r' the radius of the nanotube.

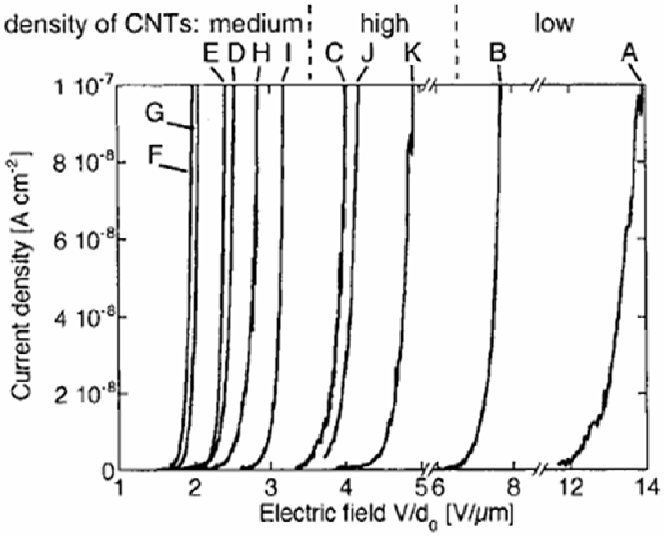

Fig.2. 5 Experimental values of turn-on voltage for nanotube films with different densities of CNTs[202].

It can be readily infered that as the number of emitters increase with decreasing intertube distance, screening effects become significant. This is shown by electrostatic calculations[203] leading to a decreased emission current density for increasing applied field.

The field emission is significantly affected by the height of nanotubes protruding from the substrate surface. It is often assumed that vertically oriented nanotubes are better emitters than random films, as the electrons are emitted from its tips. However, it is observed experimentally that the low field emission threshold is not virtually sensitive to nanotube orientation relative to the substrate surface. Low threshold fields are observed both when the nanotubes are oriented perpendicular to the surface, and when they virtually lie flat on the surface as films[204, 205]. However, results[206, 207] have shown a low threshold voltage and a high field enhancement for field emission from the side walls of MWNTs (when compared to their tips). Experimental results have shown an increasing threshold field for a decreasing tube height. This implies that higher current densities are associated with longer nanotubes[199]. Field penetration increases with an increase in tube height due to the corresponding increase in aspect ratio. Field screening affects dominate when the tube height is longer than the intertube spacing “s” (Fig. 2.6). Therefore high field emissions are obtained when tubes of high aspect ratio are separated at about an optimal inter-tube distance. This exact separation ratio [height (l) to spacing (s)] is still not conclusively agreed as various researchers have suggested different values[199, 208, 209].

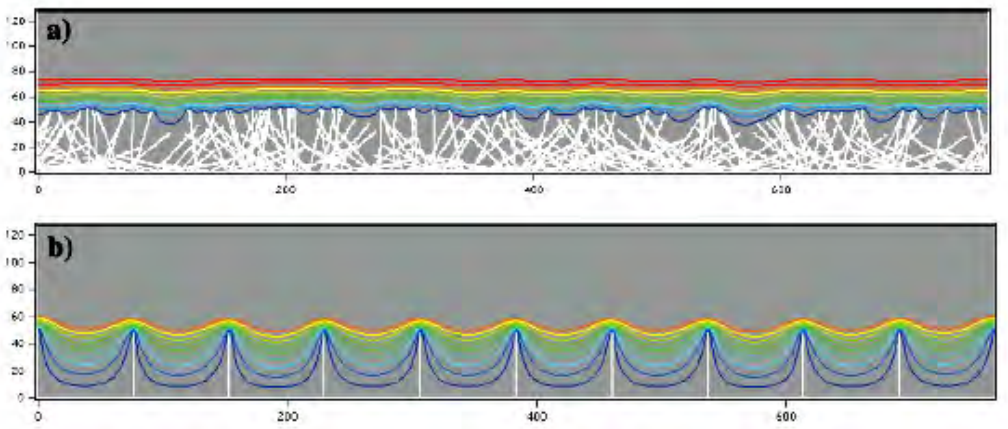

Fig.2. 6 Schematic showing (a) screening of equipotential lines leading to electric field screening and (b) CNTs spaced apart to minimise shielding [203].

The increase in length and inter-electrode spacing can reduce the threshold field for emission to a certain level. However, a reduction in nanotube diameter is necessary in order to decrease the threshold field further. Higher enhancement occurs for smaller diameter nanotubes due to the intrinsic dependence of the enhancement factor on radius (Eq. 2.8). It is not possible from the experimental results to correlate nanotube

diameter with field emission, as deposition of nanotubes for experimentation is still insufficiently controlled.

2.4.2 Temperature effect on field emission:

Extensive research in the area of carbon nanotubes as field emitters has focussed on nanotube films. With these multi-emitter systems, it becomes difficult to consider the effect of parameters like temperature and adsorption since it is impossible to exactly determine the number of nanotubes contributing to total emission current. Individual measurements on nanotubes provide a meaningful method to determine the physical mechanisms occurring during field emission and the reasons for emitter behaviour under various parameters. Nevertheless, this section provides a general overview of the temperature effect on the field emission behaviour from nanotube films.

Various researchers have provided evidence of joule heating occurring on individual nanotubes by performing electro-kinetic measurements[210-212]. Deviations from Fowler-Nordheim behaviour is observed on many occasions at high electric fields from carbon nanotube films. The experimental results also reveal that the non-linear behaviour of a Fowler-Nordheim curve during high electron emission is a result of strong ohmic heating, changing the nanotube tip temperatures. This temperature rise leads to increased emission current densities at high fields from nanotube cathodes, causing a decrease in the slope of the F-N plot. This significant higher electron emission is believed to be due to the onset of thermo-field emission[213].

The change in work function of nanotubes becomes significant when the nanotube temperature starts to rise. Tan[214] calculated the dependence of work function on temperature for a MWNT film grown on a silicon substrate and found significant reduction in the work function values above 373 K as shown in Fig. 2.7.

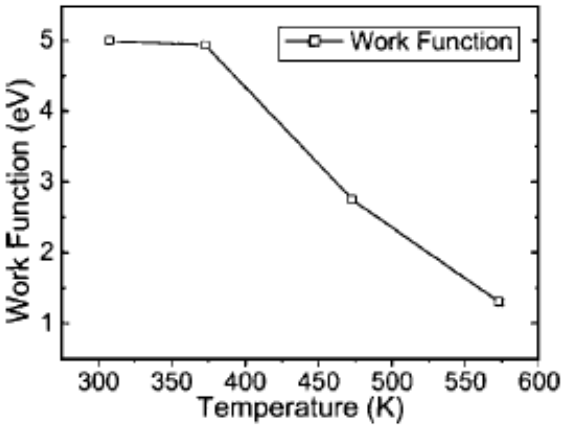

Fig.2. 7 Experimentally reported values of work function dependence on temperatures for a MWNT film[214].

However, the important factor to be considered is that the temperature (heating) controls the maximum capable current sustained by nanotubes. The electrons have to transit through a broader barrier at low temperatures as compared to at high temperatures where electrons can be removed easily. This leads to higher current densities and better field emission characteristics, as shown in the Fig. 2.8.

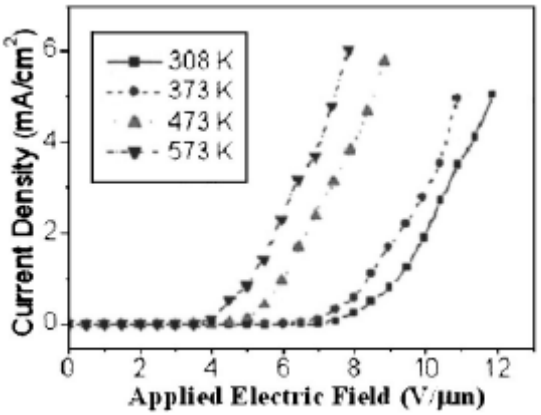

Fig.2. 8 Field emission characteristics of MWNT film at various substrate temperatures[214].

However, field assisted evaporation occurs to modify the nanotube leading to a reduction in length or destruction of the nanotube tip at high temperatures[211, 215]. It has been shown experimentally that tip temperatures as high as 2000 K are easily attained for currents in the microampere range[210, 212].

Local heating is also known to clean nanotube tips by removing adsorbates accumulated in a poor vacuum or during long term exposure to vacuum preventing re-

adsorption. Thus, field emission from clean nanotubes exhibits improved current stability due to thermal desorption. The joule heating mechanism is also believed to be responsible for light emission from nanotube samples, as reported by various groups[212, 216, 217]. This provides supporting evidence for the existence of high temperatures during field emission from nanotubes.

The above observations support the notion that current induced heating occurs in nanotubes and is partly responsible for high current densities from nanotubes. The dominating field emission mechanism will then be the thermal field mechanism, where emission current and current densities can be several orders of magnitude larger than cold field emission. The field emission characteristics like turn-on voltage and emission current densities are vastly improved at higher temperatures. The heating of nanotubes also permits desorption of adsorbates contributing to excellent current stability.

2.4.3 Effect of external atmosphere on nanotube field emission:

The key issue for the commercial viability of field emission cathodes are their operational stability. Carbon nanotubes are considered to be the perfect candidates for vacuum electronic applications, but there have been various reports of emitter failure during field emission. Alhough its intrinsic properties like surface morphology, work-function and aspect ratio influence field emission degradation, their failure has been largely attributed to various extrinsic factors. The field emission properties of carbon nanotubes are strongly influenced by extrinsic factors such as surrounding gas, pressure, degassed metal elements and impurities on the surface of the tip.

The existence of adsorbed species has a very strong influence on the emission properties of nanotubes[176, 185, 218]. The presence of gas species in nanotube samples is either due to a low level of vacuum or due to different gases present during its growth method. The field emission characteristics of nanotubes vary with the partial pressure of various gases/adsorbants and with the total pressure (vacuum) in the system. Exposure to various gases induces chemi- and physi-sorption on the surface of nanotube emitters[219]. Field emission from nanotubes is governed by gas adsorbates in the low voltage regime. High applied voltages induce local heating of nanotube tips causing desorption of adsorbates from the tip surface at a temperature

range of 600-800 K[220]. Surface modification due to adsorption of gas adsorbates induces variations in field emission characteristics during its operation. Field emission from nanotubes largely occurs in three regimes usually seen by a change in slope of the F-N equation. This three emission regimes are recognised as adsorption dominated, intermediate and intrinsic emission[221], where the intrinsic emission regime corresponds to emission from a clean nanotube surface.

Current “saturation” is observed in the adsorption dominated emission regime at the onset of adorbate desorption from the nanotube tip[222, 223]. A drop in current for higher voltages occurs due to further desorption of chemisorbed molecules resulting in loss of resonant enhanced tunnelling current in the intermediate regime. The emission behaviour of nanotube cathodes strongly varies for different gas adsorbate types. The adsorption of oxygen on nanotube tips causes etching and damage to the tip structure effecting a decrease in turn-on ratio and degradation in emission current[224]. Nitrogen adsorbates also exhibit a similar behaviour to oxygen. The similar tendencies of oxygen and nitrogen are attributed to their high electro-negativity which hinders electron emission by intensifying potential barriers[225]. Exposure to hydrogen is known to produce little or no change in emission current stability and is relatively stable over time[224]. Hydrogen also removes adsorbates from the nanotube surface, cleaning it by bombarding the surface with energetic hydrogen atoms. Adsorption of water molecules results in a rapid increase in emission current before exhibiting current saturation due to an adsorbate tunnelling state in water[226]. The field emission currents are found to be significantly increased with the adsorption of polar molecules and especially water. Polar molecules such as water get attracted to the nanotube tips with increasing applied field and form stable complexes at several degrees K above room temperature, enhancing field emission[227]. The magnitude of the dipole moment of an adsorbed molecule induces a reduction in the ionisation potential and in increase in the binding energy of adsorbates[218]. Thus lower turn-on voltages are obtained for molecules possessing higher dipole moments.

The other factors which could also induce field emission degradation are the degassed metal elements (from a phosphor layer) and residual catalyst metal impurities used for nanotube production[228]. The typical elements which get degassed from the

phosphor layer are Zn, Y and S. Zn interacts strongly with nanotube tips in spite of its low degassed amounts when compared to Y and S. It is presumed that Zn reacts chemically with the nanotube tip changing its sp^2 hybridised structure to a Zn-assisted sp^3 like bond[228]. It is also worth noting that the field emission characteristics of nanotube cathodes without the phosphor layer always show a better performance that the one with phosphor layer, as shown in Fig. 2.9.

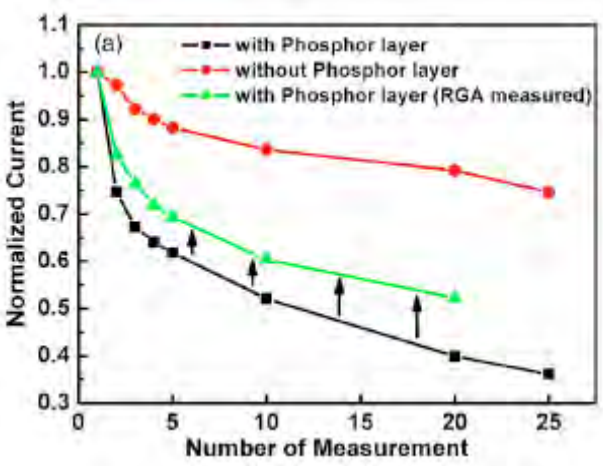

Fig.2. 9 Degradation behaviour of various panels with and without phosphor[228].

The field emission stability is significantly affected by the total pressure in the system (vacuum). Fig. 2.10 shows the dependence of emission current and degradation of MWNT film as a function of the total vacuum in the system. The emission current is shown to be more stable at high vacuum. A gradual degradation in emission characteristics is observed for all types of nanotubes as the system pressure is increased. However MWNTs are more stable than SWNTs and may have completely different degradation characteristics. Kim and co-workers[229] showed an increasing current density with time for MWNTs in the pressure range of 10^{-4} Torr in comparison to a decreased current density from SWNTs[229]. The decrease in emission current at low vacuum is attributed to the destruction of small diameter nanotubes either by ion bombardment or through tube-tube interactions/arcing, leading to low field amplification[230].

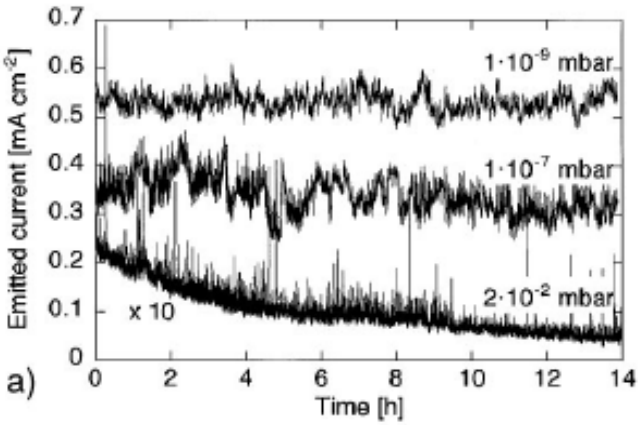

Fig.2. 10 Field emission degradation at various levels of vacuum for a MWNT film[230].

2.4.4 *Other factors affecting field emission from nanotube films:*

Other general factors which affect field emission from nanotube films are the inter-electrode gap, the type of nanotubes and the nature of their tips (open or closed). The average field (defined as E_{avg}=V/d where 'V' is the applied voltage and 'd' is the inter-electrode gap) necessary to obtain a certain emission current density decreases with the increase of the inter-electrode gap[231, 232], as shown in Fig. 2.11. This dependence is due to the variation of the field enhancement factor with distance. When the anode-cathode distance is small, the field enhancement decreases according to the relation ß = (h/r+2)*(1-h/d)[233], where 'h' is the height of nanotube. The field distribution around the tips of nanotubes is affected by the anode-cathode distance 'd' when the gap is small. When the distance is small, the field required to obtain a certain current density is large, as E_{avg} is also inversely dependent on the distance. The field at the tip at large gaps is determined by the curvature of the tip which is approximated to be V/r, where 'r' is the radius of curvature of the nanotube tip. The value of E approaches zero asymptotically for large 'd' thus requiring low voltages for small distances[231].

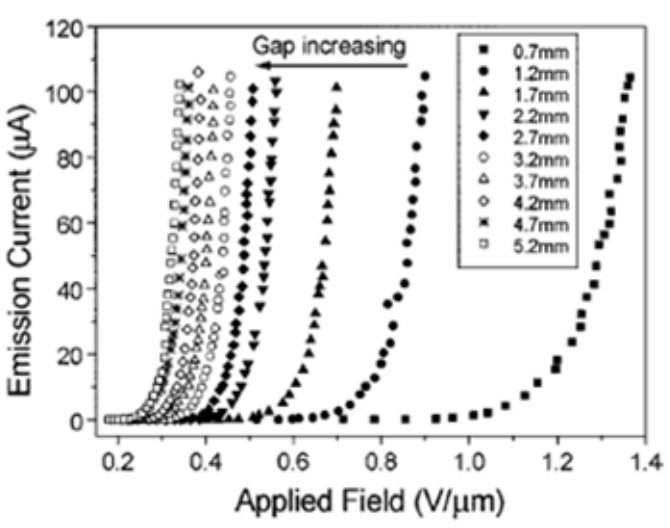

Fig.2. 11 Field emission curve of nanotubes for different inter-electrode gaps for NT films.

Comparison and interpretation of reported measurements of field emission properties of SWNTs and MWNTs is difficult because most groups use different experimental procedures, vary several parameters and/or give inadequate characterisation of samples. It is unclear so far whether the observed variations in field emission properties are due to the intrinsic properties of nanotubes, different preparation methods or both [3]. It is generally observed that the long term stability of SWNTs is inferior to MWNTs as shown in Fig. 2.12. A comparison between SWNTs and MWNTs at comparable chamber pressure and current density showed that the degradation factor was a factor of 10 faster for SWNTs[217, 234]. Their faster degradation is attributed to their single shell which makes them more susceptible to damage and degradation to ion bombardment unlike MWNTs, where their multiple shells stabilise their structure against harsh environments[205]. But on the other hand, the emission uniformity of SWNTs is more stable than MWNTs at higher current densities due to their higher degree of structural perfection. SWNTs possess a lower turn-on voltage due to their smaller diameter and hence a higher field amplification factor. However, results from various groups show that the emission threshold field of various types of nanotubes differ only by a factor of 2-3. The similarity between SWNTs and MWNTs is not surprising since SWNTs form close-packed bundles forming an effective bundle diameter of 10-100 nm which is comparable to typical diameters of MWNTs. Field emission from closed nanotube tips are shown to be always more efficient than that from open tips[4]. High field enhancements occur at closed tips due to their high curvature. Although an initial high enhancement is

observed for open tips due to the formation of sharp structures formed during tip opening, the enhancement factors decrease with the applied field due to their modification with time[235].

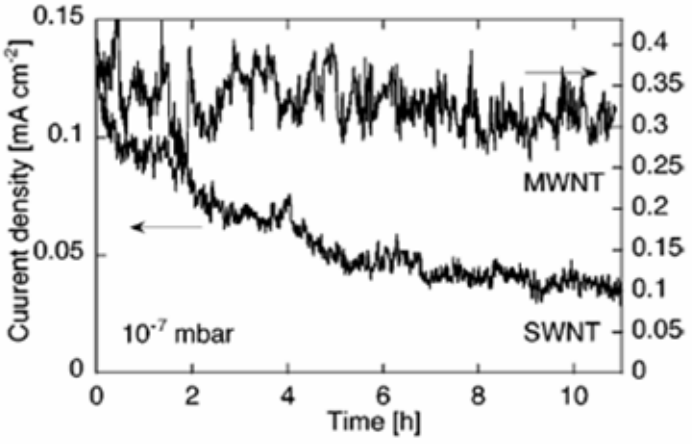

Fig.2. 12 Long term current stability of a SWNT and MWNT film at 10^{-7} mbar[234].

2.5 Application of carbon nanotubes as field emitters:

Since the initial report of field emission from carbon nanotubes [192, 193], several prototype devices and device concepts have been reported. Carbon nanotube electron sources exhibit superior properties such as low voltage operation, good emission stability, long lifetime, high brightness and low-energy spread[4]. The potential of carbon nanotubes as field emitters has been demonstrated in devices like field emission displays[122, 205, 236], X-ray tubes[237], gas ionisation sensors[238], microwave amplifiers[239], gas discharge tubes[240] and so on. The most promising of the above applications are the field emission display devices and high resolution electron beam instruments. A brief description and working mechanism of the above devices likely to be commercially available in the near future are discussed in the following sections.

2.5.1 *Field emission displays:*

The application area with the largest potential market for CNT electron sources is the flat panel field-emission display. Nanotubes are either grown on desired locations using CVD or nanotubes are mixed with an epoxy to form a paste and patterned on a

matrix of electrodes in a vacuum housing. The counter electrode is usually a conductive glass plate coated with phosphor. A potential of a few kilovolts is applied to the nanotube cathode to extract electrons which strike the phosphor layer causing excitation of the cathodoluminescent phosphor resulting in a generation of light. Different colours are obtained by using different fluorescent materials and images can be obtained by selectively addressing different positions of the nanotube matrix. High luminescence values twice more intense as that of conventional thermionic cathode ray tubes (CRTs) are easily attained for nanotube emitters operating under similar conditions. Various prototypes have been realised using nanotube emitters, a 4.5-inch three colour display[123, 241], a 9-inch full-colour display[123] and similar FED in diode configurations demonstrating high brightness at low applied fields[231].

A triode type design is desired for practical applications of nanotube FED since a diode type FED has a limitation of individual pixel control. A triode type device includes a closely spaced gate between the cathode and the anode. The electrons are extracted by applying a very low voltage on the gate. The emission current is controlled by maintaining a constant gate-to-cathode voltage. The gate also serves to converge the electron beam resulting in higher brightness and a sharper image from individual emitting sites. Several prototypes of this type have also been fabricated[242-244].

Fig. 2.13(a) shows the schematic of a field emission display unit and Fig. 2.13(b) shows the colour image produced by a 9 inch carbon nanotube based FED. Carbon nanotube based cathodes are also used as lighting elements. They possess the shape of the old vacuum tube and produce light by bombarding a phosphor coated surface with electrons. The configuration, called a “jumbotron lamp” is also available commercially. They are used as pixel elements for giant outdoor displays as they exhibit higher brightness and have a longer lifetime of about 8000 h[245]. There have also been efforts to realise lighting elements from nanotubes as an alternative to incandescent or fluorescent lamps. Although these tubes contain no mercury and yield higher brightness, the power needed is significantly higher than the commercial fluorescent tubes due to lack of efficient low voltage phosphors[18].

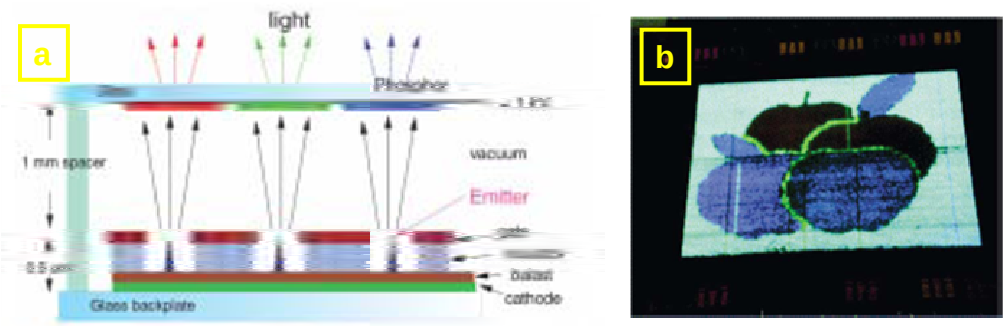

Fig.2. 13(a) Schematic of a triode type nanotube FED[5] and **(b)** a 9-inch nanotube based field emission display by Samsung[123].

Although the field emission device design looks simple, several problems are encountered in significantly improving pixel uniformity and device stability. Charging effects between the electrodes, maintaining a large voltage difference between them, display sealing and phosphor life time are among the few of the issues that are still unsorted. Tremendous progress has been made in the past few years and nanotube FEDs are expected to be a better alternative for commercial LCD and plasma displays in the near future.

2.5.2 *X-ray tubes:*

Carbon nanotube film cathodes have also been used as X-ray sources[124, 246]. X-rays are widely used in medical, diagnostic and industrial applications. A conventional X-ray tube consists of a thermionic cathode which emits electrons when heated to over 1000 C. These accelerated electrons hit a metal target emitting X-rays as shown in Fig. 2.14(a) for the case of nanotube film emitter. The old thermionic technology has several inherent limitations like a slow response time, short life time, large device size and low temporal resolution. The main advantage of a nanotube cathode is its ability to offer voltage controlled emission and its operation at room temperature.

Field emission X-ray sources based on thermionic emitters have been tested for diagnostic applications in the past, but have suffered from the need of a high extraction field and have short lifetimes[247, 248]. This type of application is very challenging as a film current density of at least 10 A/mm^2 is required for its operation. Yue[237] initially demonstrated that a nanotube based X-ray tube can generate

sufficient X-ray flux for imaging applications. Real X-ray imaging has been demonstrated since by various groups in both continuous and pulsed mode with temporal resolutions up to nanoseconds which is sufficient to image human extremities[125, 237]. {Fig 2.14(b)}

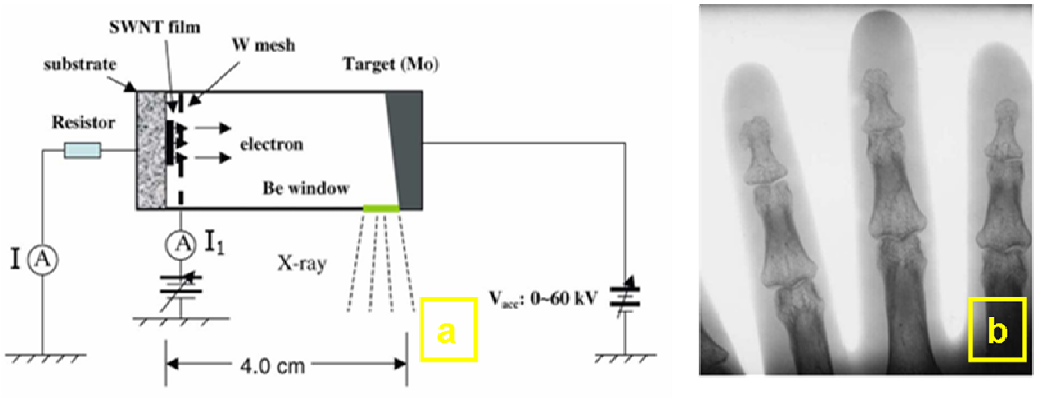

Fig.2. 14(a) Schematic representation of CNT based X-ray source and **(b)** an X-ray image of a human hand taken on a Polaroid film using the same[205].

Nanotube based X-ray sources are a clear alternative to conventional thermionic X-ray tubes. The benefit of a nanotube film cathode is its larger current density, its ability to operate at low vacuum levels and a better current stability. It also has the ability to produce focussed electron beams with a small energy spread and with a programmable pulse width and repetition rate[5, 205]. Thus a nanotube based cold cathode X-ray source can potentially lead to portable and miniature X-ray sources for various applications.

2.5.3 *Other Applications:*

Carbon nanotubes exhibit better field emission than other forms of carbon, diamond, diamond-like carbon and are a reliable alternative to thermionic emitters. A clear application of field emission from carbon nanotubes is as electron guns for scanning electron microscopes (SEMs) and transmission electron microscopes (TEMs)[249]. The conventional thermionic emitters used in these microscopes suffer from chromatic aberration, low brightness and a large energy spread. Electron sources from nanotubes exhibit higher brightness and a lower energy spread. A single MWNT is found to have a factor of 30 times higher brightness than the current emission source

and also has a small energy width of 0.25 eV. Their higher brightness improves spatial resolution and is an ideal source for point–projection microscopy[5]. The above properties facilitate their use in niche markets such as electron guns in which cost is not critical. Another use of carbon nanotubes as field emitters is in the area of power microwave amplifiers[203, 250]. Thermionic emitters are unsuitable for this type of application as it requires high current densities and a short cathode-gate distance. A prototype based on a SWNT cathode has been demonstrated to be able to reach the lower limit for operation in microwave tubes[251].

Another device in which nanotube cathodes show better performance is in a gas discharge tube used for over-voltage protection[240]. When the voltage between a nanotube cathode and a counter electrode reaches a threshold value for field emission, the emitted current induces a discharge in the inert-gas-filled inter-electrode gap, thereby preventing damage from a voltage surge of valuable circuitry in parallel with the discharge tube (such as telephone circuits).

Various groups have reported the use of carbon nanotubes as cathodes for gas ionisation sensors[126, 238]. These sensors work by fingerprinting the ionisation characteristics of various gases and work on the principle of Paschens law[252]. The breakdown voltages are reduced by several folds due to sharp tips of nanotubes, thereby enabling miniaturisation and battery powered operation. Nanotube sensors exhibit good sensitivity and selectivity and offer several practical advantages over commercial sensors[238]. Hence they may be used for a variety of applications, such as environmental monitoring, sensing in chemical processing plants, and gas detection[127] for counter-terrorism and in gas chromatographs. Nanotube cathodes are also employed in applications such as high precision thrusters for next generation space telescopes and in electrically driven mechanical resonators[253, 254].

2.6 Conclusion:

Carbon nanotubes are proven to be excellent field emitters providing a stable current at low applied fields and capable of operating in moderate vacuum. Despite the different growth techniques to deposit nanotubes on surfaces, it is hard to control and vary the density of nanotubes, their orientation and different physical factors affecting their field emission properties. There appears to be numerous gaps in understanding the role of adsorbates, the localised cap states, change in work function induced at higher temperatures, their degradation/destruction and several other phenomenon involved. Issues like incorporation of nanotubes in gated devices and the problem of contacts between nanotubes and their support also needs to be addressed. Further detailed studies, experiments and modelling are required to understand the physical and chemical state of nanotube emitters during field emission.
Several applications of nanotubes as field emitters have been proposed with applications like FEDs most likely to impact the commercial market in near future. The future growth of nanotube based field emission devices greatly relies on developing reproducible preparation methods at low cost and in better understanding the emission mechanism besides their electronic properties.

3.0 Experimental design and set-up

This section describes three different areas of experimentation. The first describes a brief history and development of the Canterbury continuous reactor. This first section also describes the evolution of the current continuous reactor set-up from the original batch reactor used by Peter Wiles and John Abrahamson[25] during their carbon nanotubes discovery. The second section describes the design, operation and testing of an ionisation sensor in which substrate-laden carbon nanotubes were used as a cathode. The third section gives a brief overview of the design of luminescent tubes and the challenges in realising these for operation.

3.1 Continuous reactor:

3.1.1 *Introduction:*

The objective of the current continuous reactor is to synthesise carbon nanotubes continuously in a single-step without the need for any pre- or post treatment. The idea of this continuous reactor was developed after successful experiments with the batch reactor by various students[13, 14] aimed at reproducing the results by Wiles and Abrahamson[25]. These experiments provided a better understanding of the optimal conditions required for nanotube formation. Juliana Chan designed the initial continuous reactor as a part of her undergraduate project. Based on the above results and experiments of their own in the batch reactor, Markus Leistner and Can Ulubay[15] performed a few modifications to the continuous reactor and also conducted a few runs. Although they were successful in producing nanotubes continuously, some of the parameters influencing arc discharge were not controlled and the results were thus not reproducible.

3.1.2 *Reactor description:*

The continuous reactor is a cylindrical brass reaction chamber with a wall thickness of 21 mm. The volume of the reactor is 1.3 L. Graphite rods of 8 mm diameter were used as electrodes and are fed by grooved wheels on a brass axle. Copper coils are soldered around the graphite electrodes to cool them and to aid the removal of heat generated by arc discharge. The high thickness of the wall imparts a high heat capacity to the reactor also assisting in additional heat removal from the chamber. Additional information about the reactor can be reviewed in the reports of Mani and Hill[14] and Siew and Keen[13]. Heat transfer calculations for the reactor can be found in the report of Siew and Keen. The electrodes in the reactor can be arranged either horizontally or perpendicularly with the anode position being fixed horizontally. Tension to the wheels is imparted by rubber O-rings and the entire feeding mechanism is encased in a Tufnol® insulating housing. The arc image is projected on a wall with the help of different observation ports housed in the reactor body and by using an appropriate lens as shown in the Fig. 3.1(a).

A carbon substrate cut into widths of 25 mm and lengths of around 1 m is passed through the reactor body (R) between the two electrodes. Originally this feed was via two knurled reels driven by a speed-controlled feeding motor (F) as shown in Fig. 3.1(b). An earthed deadweight (W) of approximately 200 g is connected at the end of the tape to keep it tensioned and to provide a uniform speed. The substrate (M) exits from the side of the reactor body through a water-cooled idling wheel inside the reactor body. Three additional gas inlet ports are housed in the reactor, one entering at the top lid to flush the reactor (C), a second (A) directing the gas to the anode and another a third near the product (tape) exit of the reactor placed close to the idling wheel to cool the substrate (M) as shown in the Fig. 3.1(b). The whole reactor system is placed under a evacuation enclosure with an additional port near the bottom end serving as an exit point for all gases. The reactor always operates at atmospheric pressure.

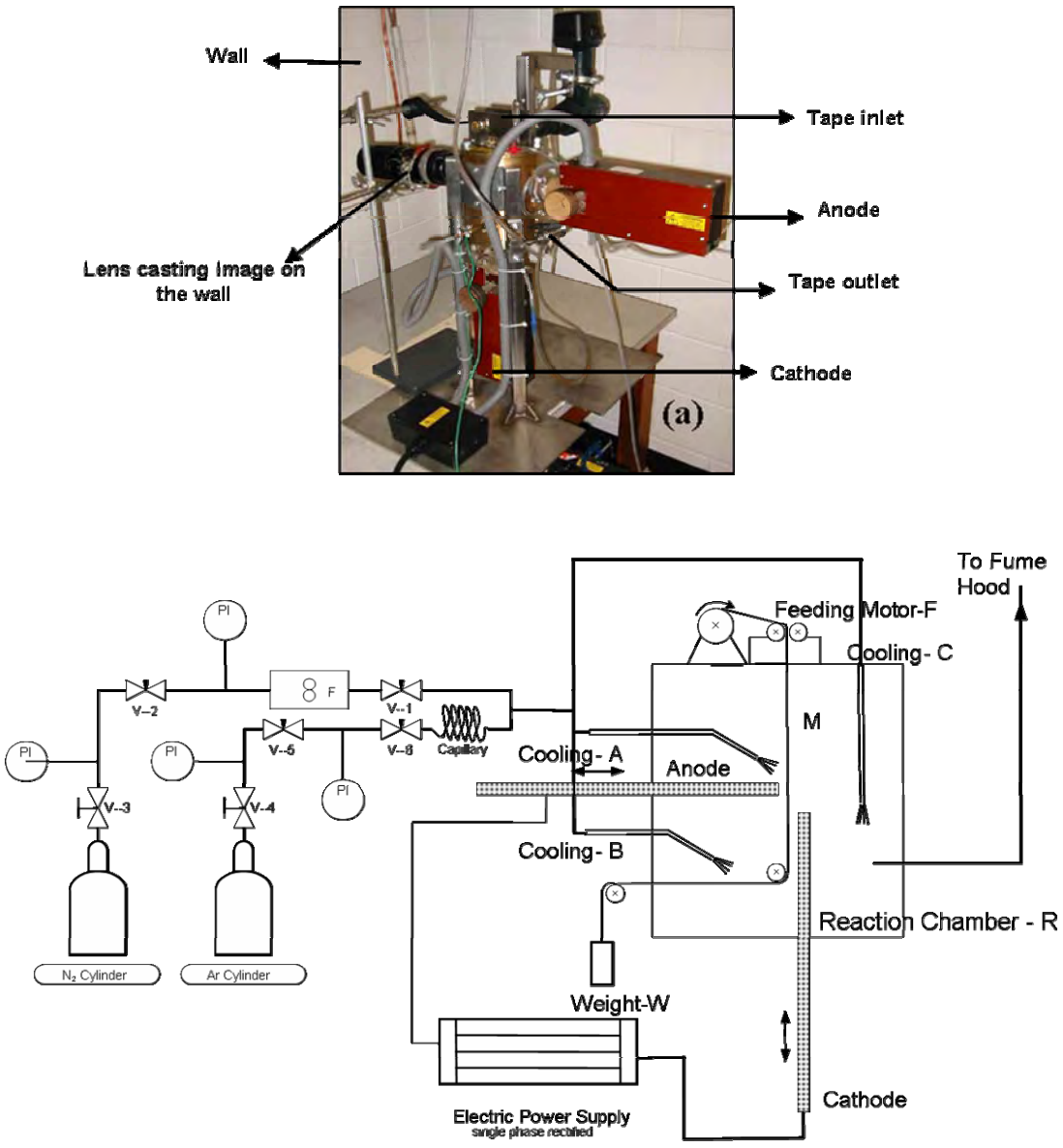

Fig.3. 1 (a) Continuous flow reactor[15] and (b) flow diagram of the continuous reactor.

3.1.3 *Modifications:*

The reactor was fully operational during the start of my study. Various modifications like installation of an additional gas inlet for cooling, cathode holders to accommodate a smaller diameter cathode and a speed-controlled motor were made by Ulubay[15] during his study. The reactor still had some inherent flaws in its design and further modifications were necessary for better ease of operation. Various modifications were made to the continuous reactor over the years of this study and are listed as follows.

3.1.3.1 Viewing ports:

The reactor body had small viewing ports on either side which made positioning the electrodes difficult when the reactor was closed. The projected image on the wall also did not clearly reveal the position of electrodes during arc discharge. The ports were hence enlarged and its profile was changed, as shown in Fig. 3.2 to obtain a clear image of the electrodes during arcing.

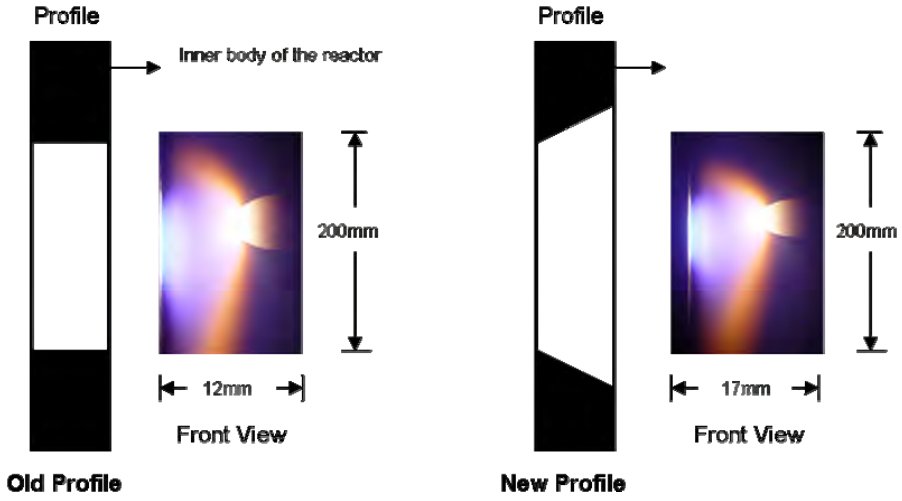

Fig.3. 2 Modifications performed on the view port.

3.1.3.2 Electrode arrangement:

The electrodes were oriented perpendicular to each other in the original set-up with a moving cathode and anode. This made striking the arcs difficult when the tape was in motion, as the tape would often sublimate during arc ignition bridging the electrodes. After a few initial runs with the above arrangement, the electrodes were oriented horizontally in line with each other for the ease of striking the arc and to obtain a better control over the inter electrode gap.

3.1.3.3 Anchoring graphite foils:

Carbon nanotube growth in arcs has been thought to be due to condensation of carbon vapour. Many authors have used various sources of carbon in an effort to improve the nanotube yield in arcs. An attempt was made to anchor graphite foils by sewing them to the substrate as shown in the Fig. 3.3. The foils (NGS Naturgraphit, 0.5 mm thickness) were cut into lengths of 40 mm and widths of 5 mm and were sewn on both sides of the tape using a cotton fibre (See Fig. 3.3).

The experiments were unsuccessful since the foils stuck between the knurled reels during tape motion. If successful, the foils usually fell down when exposed to the arc, due to burning of the cotton fibre. No nanotubes were observed in any of the burnt foils probably due to low residence times of the foils in the arc.

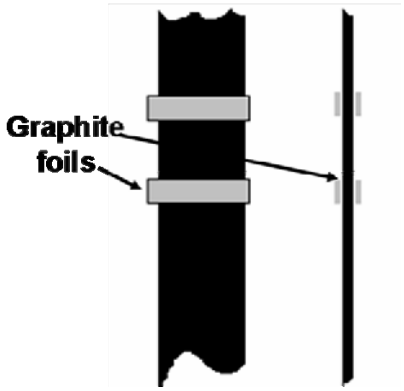

Fig.3. 3 Schematic of graphite foils anchored to a carbon substrate.

3.1.3.4 Electrode shape and size:

Chaney[255], while studying the properties of the low current carbon arc, noticed that the relationship between the current density and arc stability was very critical for a quiet and stable arc operation. This depended upon variables such as electrode arrangement, trim and its composition. They also observed that a minimum current density of 1.05 to 1.27 A/mm^2 seemed absolutely vital for arc stability. Many of the initial runs of our continuous reactor were performed with cathode and anode

diameters of 8 mm and with an arc current of 10 A. This corresponded to a cathodic and anodic current density of 0.198 A/mm^2. The arc always wandered on the anode and nanotubes were observed in very few runs. Another group working on nanotube production in arcs also observed that the nanotube yield increased with arc intensity, working up to 1.94 A/mm^2 on the cathode[256].

These reports led us to increase our cathodic current density in a quest to consistently produce nanotubes. Our power supply was capable of delivering a maximum of 20 A which when operated at its maximum capacity on an 8 mm diameter cathode corresponded to a current density of 0.397 A/mm^2. Therefore the cathode diameter was reduced to 3 mm diameter and the current was gradually increased starting from 14 A until the arc became unstable. A stable arc (just below starting to hiss) was obtained at 16 A which corresponded to a cathode current density of 2.26 A/mm^2 (well above that desired) and this was persisted with for future runs.

Various designs were attempted as shown in the Fig. 3.4(a-c) to find the best possible practical option of achieving a pointed cathode of 3 mm diameter. Finally the best design was to drill a hole of ~3 mm diameter for lengths of around 10 mm in an 8 mm diameter graphite electrode and to fix a 3 mm diameter graphite rod inside it. This helped us to easily replace the electrode after its consumption during the arc discharge.

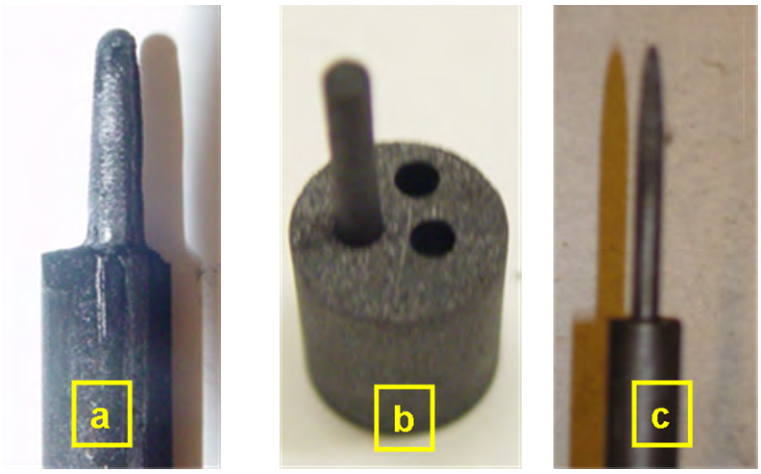

Fig.3. 4 Different versions of cathode, all having a point size of 3 mm, with type (c) used for all experiments.

The anode diameter was increased in an effort to increase the area of arc treatment on the tape. This was done by adding a graphite head of larger diameter to a graphite rod of 8 mm diameter (anode). Various sizes and types of anode were tested to obtain the largest arc treatment and/with a stable plasma. A graphite rod of 16 mm diameter capped to the anode was the best choice as we obtained an increase in the arc treated area from 8 mm (with an 8 mm diameter anode) to 14 mm.

A few runs were performed with the above anode design with some good results. The nanotube yield in an arc discharge has been reported to strongly depend on the cooling rate[56]. The anode design was changed again with an intention to provide additional cooling through the anode during arcing. A separate anode body was designed which consisted of a tungsten tube (length 40 mm and 8 mm diameter) fused to a stainless steel tubing (length 180 mm and 8 mm diameter). A graphite head capped the end of the tungsten tube inside the reactor. The other end of the stainless tube was attached via a flexible tube to a rotameter and the gas flow was as shown in Fig. 3.5.

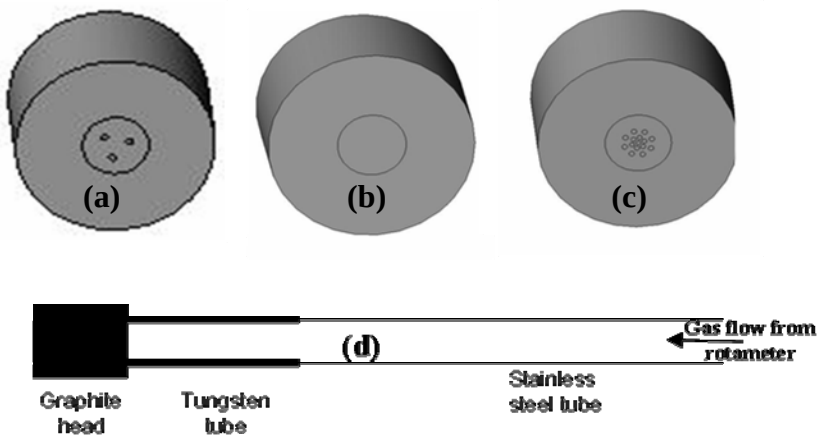

Fig.3. 5 Different designs of graphite anode head (a) three holed (b) porous graphite head (c) sixteen holed head and (d) anode tube design.

Three different designs of graphite heads were tested as show in the Fig. 3.5. The first design consisted of 3 holes (1 mm diameter), the second had porous graphite (5 mm length and 8 mm diameter) plugged near the centre of the graphite head and the third had 16 holes drilled near the centre. The velocity profiles at the surface of the tape due to a flow in the anode system were studied at room temperature using a Pitot tube.

The graphite head with holes resulted in localised flow profiles for different tape types due to tape texture. The velocity profile was fairly even for the porous graphite head and showed no uncovered areas and no uneven velocity peaks.

All our further experiments (unless specified) were performed with a cathode diameter of 3 mm diameter and a porous graphite anode head capped onto a system with a gas flow possible through its tubing whether or not a flushing gas flow was used.

3.1.3.5 Substrates:

Three different types {Fig. 3.6(a-c)} of carbon substrates were used in this study: A woven knitted tape {Fig. 3.6(a)}, a bidirectional tape {Fig. 3.6(b)} and a unidirectional tape {Fig. 3.6(c)}. The specifications of all the tapes used in this study are given in Appendix A.

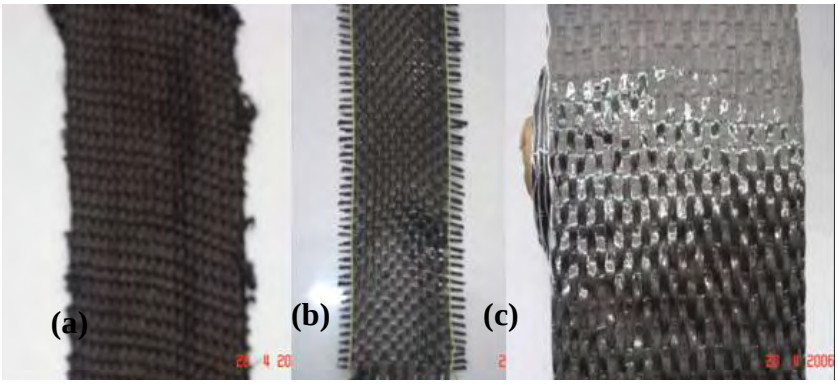

Fig.3. 6 Different types of carbon substrates **(a)** Woven tape **(b)** Bi-directional tape and **(c)** Uni-directional tape.

The **Woven tape** is manufactured by Carbonics Gmbh, in Germany under the trade name UVIS TR-3/2-22 {Fig. 3.6(a)}. The tape is a high purity knitted fabric with a specific weight of 770 g/mm^2 and a thickness of 2 mm. The Carbonics tapes are easier to handle and are much firmer than the other substrates. The tapes are cut into lengths of 1 m and widths of around 25 mm for their use in the reactor and used without any pre-treatment. Another set of the same tapes was also used for some of the final runs which had a weight of 470 g/mm^2 and a thickness of 1 mm.

The **Bi-directional tape** is manufactured by Sigmatex Limited, in UK under the trade name 200tex 3K {Fig. 3.6(b)}. This tape is also 99% pure with a specific weight of 200 g/mm^2 and a thickness of 0.4 mm. The tapes are sold wound on spools with widths of 25 mm and are cut into desired lengths for its use in the reactor. Among the impurities is an epoxy resin coating used with glass fibres to bond the edges of the carbon fibres to prevent them from fraying. These impurities were often removed by Joule heating (current 7 A and 160 V in air) prior to feeding them into the reactor.

The **Unidirectional tape** CU305 {Fig. 3.6(c)} is manufactured by Modulus in New Zealand and has a specific weight of 305 g/m^2 and is 97% pure. The remainder of 3% consisted of wool like glass fibre and glue stitches. These tapes were the most difficult to work with as they easily frayed and lost cohesion during pre-treatment due to the melting of the glue. This caused the loose fibres to bridge the gap between the electrodes during its motion and often led to a short.

3.1.3.6 Power supply:

Two different types of power supplies are used in this study. The commonly used power supply to the continuous reactor was a single phase rectified DC supply capable of delivering a current of 20 A. The second type of power supply was a three phase supply, originally used in the batch reactor (originally used in the previous acetylene arc reactor) and is capable of delivering 200 A. The circuit diagrams of both the test arrangements are provided in Appendix B. The single phase rectified power supply is smoothed by two large capacitor banks (of capacity 35 mF) minimising the current ripple and voltage ripple to 0.3 A and 0.4 V respectively as shown in Fig. 3.7(a). This filtered supply was used in all our experiments to find and to optimise various parameters affecting nanotube growth in the reactor.

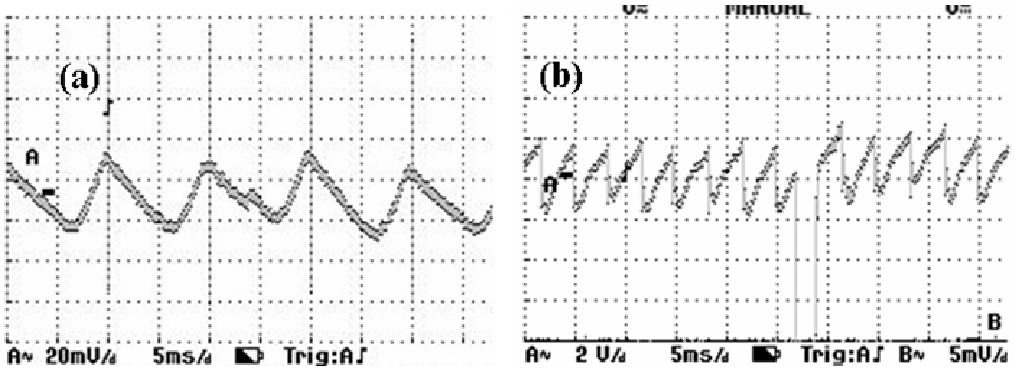

Fig.3. 7 Oscilloscope pictures showing the current ripple for (a) single phase power supply and (b) three phase power supply, both at 16 A. Note the 100 fold increase in scale for (b).

The three phase high power supply was used to find the effect of high currents on nanotube growth in our system. The voltage and current ripple of the system were tested in an effort to analyse the disappointing results with this supply. The measurement of these parameters confirmed a current ripple of 4 A and a voltage ripple of 17 V, as shown in the Fig. 3.7(b). Thus the three phase supply could not provide optimum conditions for nanotube growth.

3.1.3.7 Tape driving mechanism:

The biggest concern during the operation of the reactor was the uneven speed of the substrate. The selected cordless drill motor was too weak to feed the tape through the reactor at a constant speed. In order for the motor to solely determine the speed of the tape, the contact area between the tape and the knurled reels was increased by changing the tape positioning as shown in the Fig. 3.8. Though a fair degree of control on the tape was obtained, the edges of the bidirectional and unidirectional tapes often frayed due to its friction with the knurled reels, even before it encountered the arc.

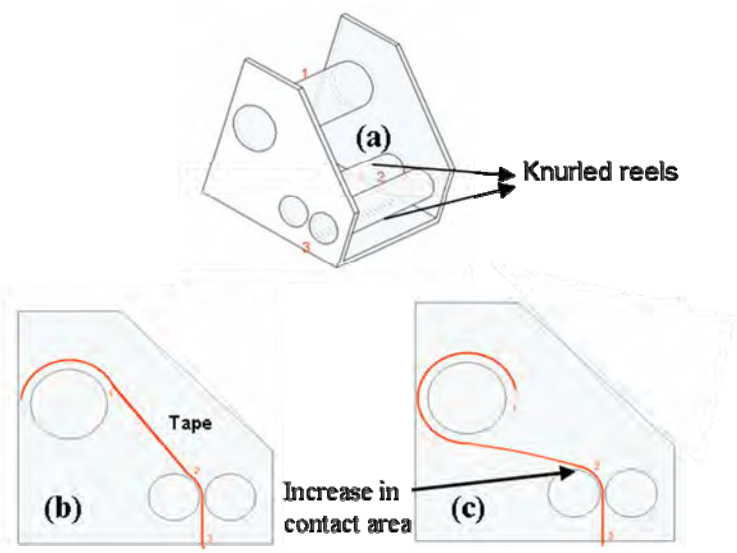

Fig.3. 8 (a) Tape driving mechanism with (b) previous arrangement and (c) the modified arrangement showing an increase in contact area[17].

A major modification was the selection of a completely new tape driving mechanism capable of varying the substrate speed from 0 to 5.2 mm/s. The system comprised a squirrel cage motor and gear box with a maximum output of 1370 rpm connected to a variable speed drive also capable of reversing the direction of the tape motion. The speed range of the motor when connected to the variable speed drive was in the range of 50 rpm-930 rpm. The motor was then connected to a reversible gear box (13.5:1 reduction) which delivers an output of 10 rpm-35 rpm. Two spools were designed to accommodate larger lengths of the tape for extended operations. These spools were driven by the gearbox and facilitate easy variation of tape speed in both directions. The moving tape was also supported by two dead weights to keep it taut. Further details and additional information on the selection, design and calculations on the tape driving mechanism can be reviewed in the report of Yusoff [2007 PhD theses to be submitted]. The calibration curve for tape velocities of different substrates can be found in Appendix C. The completed reactor setup with the new driving mechanism (Fig. 3.9) formed the basis for all our experiments in understanding nanotube growth.

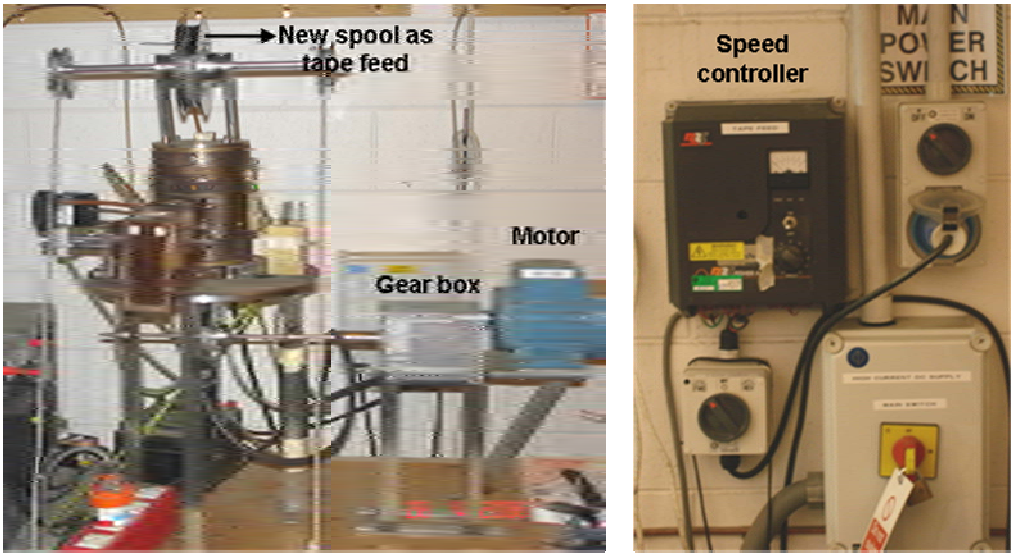

Fig.3. 9 Complete reactor set-up with the new driving mechanism.

3.1.4 *Reactor observation techniques:*

Apart from the different modifications performed on the reactor body, a few other minor changes had to be made to observe and control the arc process carefully. The imaging techniques involved the use of a high speed camera, a digital camera, a lens system and pyrometers. The arc treated tapes were observed using an SEM and the software Sigma Scam Pro 5.5 with the Mega Speed M550KV 8.0 was used to analyse the obtained micrographs.

3.1.4.1 Lens Support:

The arc side image is cast on the wall through a port using a lens and is used to monitor various arc parameters. This image allows us to determine the exact electrode locations and vary the inter electrode gap precisely, as shown in Fig. 3.10. The lens in the original system was fixed on a still support fixed to a retort stand. The stand had to be moved and adjusted during arc operation changing the focus for every run often yielding a bad image. A lens support was designed to house the lens permanently and to be able to slide along the optical axis between the arc and the wall, allowing instantaneous focus during the run. Another lens holder was also designed to accommodate different band filters which enable anode surface temperature

measurements through a pyrometer. Technical drawings and details about these supports can be found in the report of Yusoff.

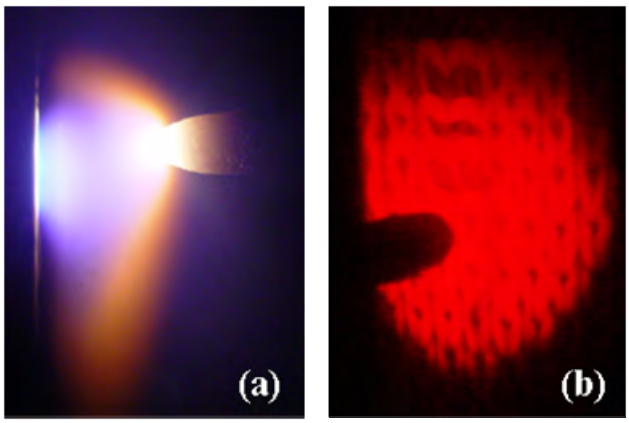

Fig.3. 10 (a) A typical arc image projected on the wall and **(b)** substrate surface as seen through the pyrometer (the cathode tip can also be seen from the side).

3.1.4.2 Electrode surface temperature measurement:

The frontal view of the anode (tape) through an observation port in the reactor body was used to analyse electrode temperatures. A lens holder in front of this observation port accommodated a neutral density filter (Roland ND1.0, 10% transmission) and then a narrow-band filter (Ealing electro-optics wavelength 670 nm, band width 665–675 nm) to observe the constant high intensity radiant source (anode). The electric arcs produces light with a high fraction of UV-light, similar to that of an arc welder and hence direct viewing was avoided for safety reasons. The pyrometer (OPTIX Ox 400) was placed in line with the above filters to analyse the temperature of the anode (moving substrate) during arc operation. The pyrometer operates with light filtered by its own filter to pass red at an average wavelength of 660 nm and has a temperature range of 2073-3073 K, and then the narrow band filter further restricts the red range. These filters together, lead to a new temperature range of 2460-4361 K for the pyrometer (OPTIX Ox 400). The optical pyrometer was calibrated to view the anode of a quiet arc operating at 16 A and assuming it was the anode surface temperature for a standard carbon arc (3800 K ± 5 K) [257]. A Sony digital camera (DSC-W1—5 Mega-pixels CCD sensor) was used in conjunction with the pyrometer to take pictures of the fibre substrate. The camera images of the substrate surface (taken

through the pyrometer) were then analysed for intensity using the image analysis software Sigma Scan Pro 5.0. The detailed procedure of estimating the substrate temperature and its calibration with respect to the radiance of a standard arc can be reviewed in the report of Yusoff [PhD theses-yet to be submitted].

3.1.4.3 Imaging and examining techniques:

All the samples were examined using a Scanning Electron Microscope (JEOL, JSM 6100 and LEICA660). The samples were prepared as follows;
Little strips of tape treated by the arc (see Fig. 3.11) were cut into various dimensions. The locations of the strips on the tape were labelled for reference. These strips were adhered to an SEM copper sample holder using double sided sticky carbon tape (Manufacturer: ProSciTech, Australia, Make: IA021). The samples were sometimes gold coated (thickness-1 nm) for better conductivity and resolution. Interesting spots in the sample were magnified and micrographs of these spots at different resolution were taken for analysis. The parameters of the SEM are specified in Appendix D.

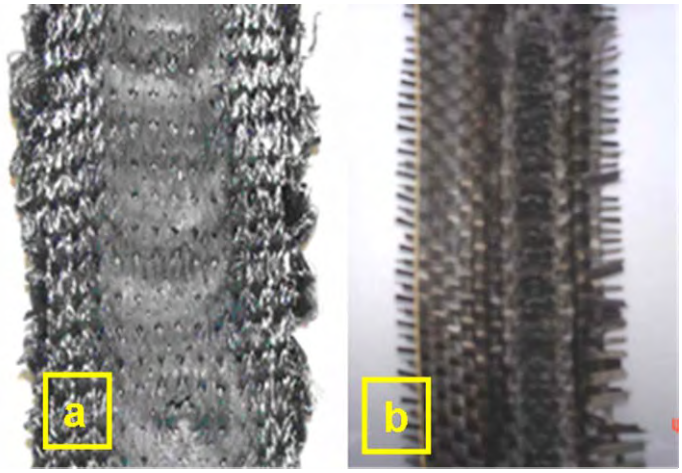

Fig.3. 11 Arc treated path on (a) Carbonics substrate and (b) Sigmatex substrate.

Sigma Scan® Pro 5.0 is a sophisticated image analysis application that allows one to capture, modify, enhance and measure digital images. Sigma Scan® Pro 5.0 was used to analyse the micrographs to obtain the mean diameter and length of nanotubes for all the samples. The scale bar in each micrograph was calibrated by converting the raw pixel co-ordinates into a specified measurement unit. The diameters and lengths of nanotubes in the micrographs were measured using the line measurement option,

which converted the pixel co-ordinates at different points into measurable units. These measurements were put in a worksheet for further analysis. The detailed procedure for the above measurements can be found in Sigma Scan® 5.0 user's guide.
The projected arc images on the wall were also captured using a digital camera. Apart from using a digital camera, a high speed camera (Manufacturer: Canadian Photonic Labs, Make: Mega Speed M550KV) was also used to capture arc images to study and observe the arc interaction with the substrate surface.

3.1.5 *Experimental Procedure:*

The steps below summarise a typical test run procedure:

- The tape is mounted on the spools tensioned by a dead weight at its end and is positioned to run between the electrodes.
- The anode is moved towards the tape until it is in contact with the tape.
- The cathode is generally positioned 4-5 mm away from the tape.
- The water valve is turned on to the cooling coils surrounding the electrodes.
- The reactor is flushed with appropriate gas mixtures for a period of about 5 minutes and all the cooling gas inlets are opened.
- The power supply is switched on to charge the capacitor banks and to engage the soft start circuit.
- The speed controller is switched on to set the tape speed to a known value.
- The arc is struck by moving the cathode to touch the tape and then is drawn away from the moving tape to maintain a known constant distance.
- A constant inter-electrode gap is maintained by observing the projected arc image on the wall.
- The power supply is switched off when the tape spool has very little tape left and the variable speed controller is switched off.
- The gas flow to the reactor is stopped and the cooling water is turned off after a period of about 10 minutes.
- The tapes are cut into small samples for examination under the electron microscope.

This continuous method of producing nanotubes on carbon fibres employs the substrate both as a carbon source and as an anode. The reactor always operates (unless specified otherwise) under atmospheric pressure with a current of ~16 A and ~70 V. The aim of this work was to investigate the effect of various physical parameters of the arc on nanotube occurrence, growth and substrate temperature. These varied parameters constitute the inter-electrode gap, substrate speed, gas environment, flushing and current density on the electrodes.

3.1.5.1 Inter-electrode gap:

Carbon nanotube production in arcs depends largely on arc-stability which in turn is related to the inter-electrode gap. The arc gap was varied from 1 mm to 8 mm at a certain tape speed observing the corresponding projected image on the wall. The tape speed was also adjusted so that the arc treatment on the tape was smooth and evenly distributed during a typical run. The arc strongly heated the tape which burnt a hole in it for any gap below 1 mm. Any attempts to increase the arc gap above 8 mm either doused the arc or led to large arc instabilities. Digital photographs of the substrate through the pyrometer were taken for each gap. The optical intensity of the photographs were analysed to calculate the substrate temperature corresponding to each gap. The samples from each gap were analysed using a SEM for nanotube occurrence. An optimal gap range was recognised at which nanotubes of considerable density and purity was obtained.

3.1.5.2 Substrate speed:

Once an optimal arc gap was recognised, the substrate speed was varied between 1 and 6 mm/s respectively using a Variable Speed Drive (VSD). The tape direction was also changed (upward and downward) to observe any changes in arc stability and distribution. Any increase in speed above 6 mm/s led to sheen like treatment on the tape and any speed below 1 mm/s led to substrate damage burning a hole in the tape. The substrate temperatures at each individual speed at the optimal gap were analysed via digital photographs. The samples at each corresponding speed were analysed in SEM to investigate the effect of tape speed on nanotube occurrence.

3.1.5.3 Reactor atmosphere:

Once an optimal gap and speed were identified, the gas flow (nitrogen, argon, helium or its mixture) through the porous anode {see Fig. 3.3(b)} was varied between 0 and 0.6 L/min. The reactor was always operated with a base flush flow rate of 10 L/min. An increase in anodic flow above 0.6 L/min led to huge instabilities in the arc, apparently due to the velocity of the opposing gas jet. The reactor atmosphere was changed by flushing the reactor with a gas mixture or by entirely replacing nitrogen with different gases. Inert gases like argon and helium delivered to a capillary at different pressures between 0-700 kPa corresponded to concentrations between 0-53500 ppm in the gas mixture. The substrate temperature at different concentrations was anlaysed to observe any changes to the optimal gap and tape speed, thereby on nanotube growth. Many runs were also performed without flushing any gas inside the reactor. The calibration curves (ID of the capillary – 1/16 inch) for the concentration of argon, helium and oxygen mixtures with nitrogen (10 L/min) are given in Appendix E.

It has been found that nanotube yields and production was increased when the arc reactors were operated in various carbon rich environments[44, 58]. A few runs were performed by using benzene as a carbon source in an effort to boost nanotube production. This was achieved by bubbling a nitrogen gas mixture through liquid benzene at room temperature. This allowed benzene concentrations to be varied between 0 and 15000 ppm. This benzene flow was sent through a port directed at the arc discharge, as shown in Fig. 3.12. The benzene concentration was controlled by varying the nitrogen gas flow using a rotameter. The bubbled gas mixture was analysed in a gas chromatograph (GC) to obtain the benzene concentrations at different flow rates. The calibration curve for benzene at different nitrogen flow rates is given in Appendix F.

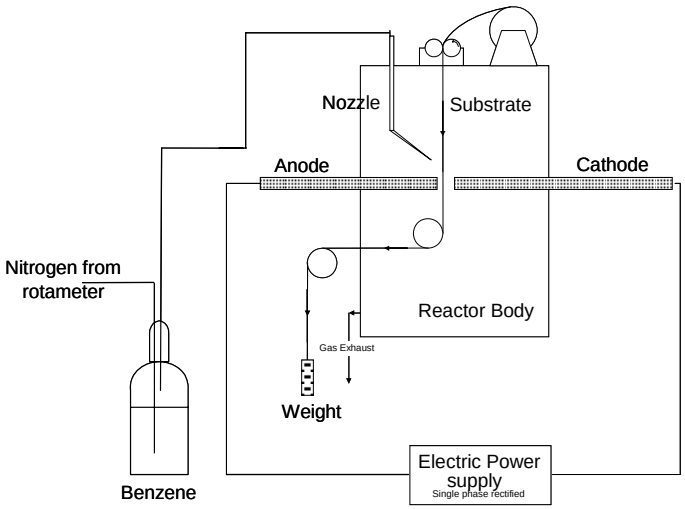

Fig.3. 12 Schematic representation of the reactor setup involving a hydrocarbon source (benzene).

3.1.5.4 Influence of catalyst:

3.1.5.4.1 Ferrofluid runs:

Carbon nanotubes can be preferentially fabricated on various substrates like silica, glass, alumina and carbon cloth by different techniques using different catalysts. Catalyst like Fe, Co, Ni and other transition metals and alloys act as seeds for nanotube growth by decomposing various hydrocarbon sources. Many groups have also reported nanotube growth employing catalysts on carbon materials using thermal CVD[258].

An effort to grow nanotubes was made by depositing an iron catalyst on our carbon substrate. The carbon substrate was dipped into a commercially available Ferrofluid solution (Manufacturer: Magnacol, Fe nanoparticles of ~10 nm diameter) diluted by using acetone. The number distribution of Fe nanoparticles on the carbon substrate was varied by changing the dilution rate. The nanoparticle-loaded substrate was dried at room temperature before it was fed through the reactor.

The effect of catalysts like iron, nickel and a mixture of iron-nickel on nanotube growth and occurrence in arcs were also explored. The concentrations (in wt % of the total substrate) were also changed in an effort to find the best catalyst/catalyst mixture for good quality nanotube occurrence on the substrate. A wet impregnation technique

was used to distribute/coat catalyst particles on the substrate. Further details about the sample preparation can be found in the report of Ostillinger[259]. The catalyst coated tapes were dried overnight in an oven maintained at a temperature of 120 C before its use in the reactor.

The substrate was arc treated under the normal optimal conditions required for nanotube growth (inter-electrode gap of 5 mm and a tape speed of 3 mm/s). The arc gap was also varied and the samples were analysed in the SEM to explore the effect of the catalyst on nanotube presence and growth.

3.2 Field emission from nanotubes:

Field emission from nanotubes has been widely studied since the first report of emission from nanotubes at low applied fields[192, 193]. Carbon nanotubes have demonstrated superior properties and stable emission at low field compared to Spindt type emitters due to their unique geometrical shape[3, 203]. Various prototypes of flat panel displays[122] and alternatives to luminescent tubes[18] have also been successfully demonstrated using carbon nanotube emitters acting as cathodes[236]. Gas ionisation sensors have also been realized using carbon nanotube emitters and offer much promise against the commercially available large and bulky gas sensors[127, 238]. Carbon nanotubes grown on carbon cloth from CVD have exhibited the lowest turn-on field and superior emission properties suggesting that the substrate itself assist electron emission[11]. Since our process directly deposits nanotubes onto a conducting substrate and employs an arc discharge, our nanotubes are expected to exhibit superior emission properties. A luminescent tube and a gas sensor are hence designed to test the field emission properties of the in-house substrate grown nanotubes.

3.2.1 *Luminescent tube:*

This section describes the design of luminescent tube which allows us to characterise the field emission properties of our substrate grown nanotubes. The idea of designing a luminescent tube in a non-planar geometry was conceived due to its apparent

advantages over a planar geometry[18]. The luminescent tube design is the result of an investigation of the nanotube prototype field emission display devices and the commercial cathode ray tube design. Some of the initial design can be found in the report of Marthosa[19]. The design requires careful thought on five main parts namely the cathode, anode, phosphor selection, getter selection and system assembly as well as a suitable vacuum system for its efficient operation. The basic lamp design of Marthosa[19] was improved and various parts were modelled in SolidWorks, the schematics and assembly model are show in Fig. 3.13.

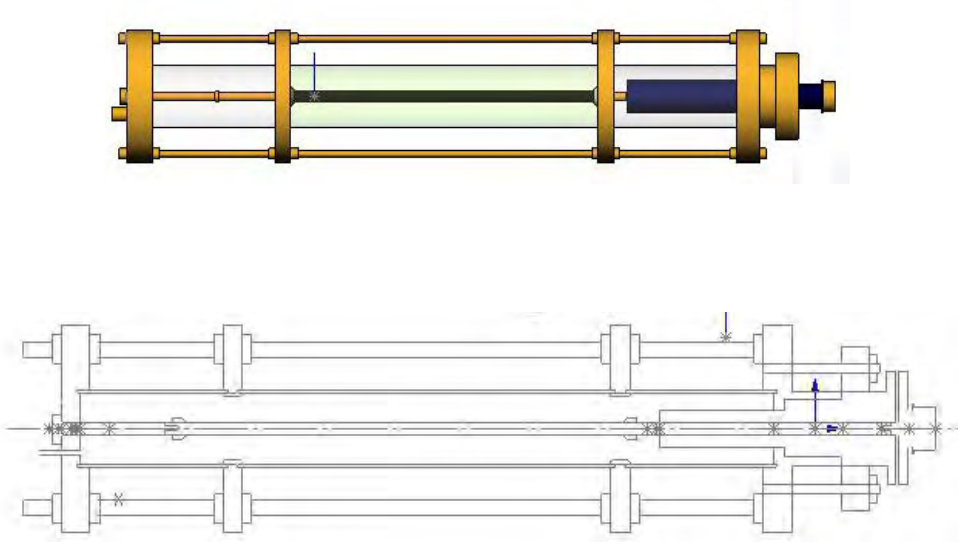

Fig.3. 13 Assembly model and schematics of the first design of a luminescent tube from *SolidWorks.*

The cathode in the first design is a live brass rod (6 mm diameter) located in the middle of the vacuum chamber about which a sample of substrate grown nanotubes is wrapped. The ends of the substrate are tied to the rod using a plastic tie at each end. The diameter of the cathode can be increased to allow the gap between the electrodes to be varied, if desired. The cathode is designed to be removable from one end of the assembly to facilitate sample change.

The anode is a glass tube (40 mm outside diameter) of thickness 2 mm coated with a layer of Indium Tin Oxide (ITO) and phosphor on the inside of the glass tube. Boron Nitride (BN) rod grade and High Density Poly-ethylene (HDPE) are used as insulating materials. BN (7 mm diameter) is used in the immediate vicinity of the cathode due to its high resistivity (10^{14} Ω/cm). HDPE (15 mm diameter) with a resistivity of ~10^{8} Ω/cm is used as the other major insulator next to BN due to the

brittle nature of BN. The whole cathode assembly was housed in a vacuum tight chamber by clamping the phosphor coated glass tube and an uncoated glass tube using four threaded bolts and nuts. All the glass tubes were then sealed using rubber 'O' rings. The uncoated glass tube was electrically isolated from both the anode and cathode.

One of the important parts in the tube design was the assembly of all components since glass comprises a major component of the design. The sealing process should not degrade the anode or the device structure. Vacuum glue capable of sealing glass-glass and glass-metal is commonly used in various demonstrated prototypes. High vacuum grease was used to prevent any vacuum leakages at the glass metal interface.

Although many of the parts were fabricated early, the lamp could not be assembled due to the difficulty in procuring a conducting phosphor coated glass tube. After an extensive search and effort, the phosphor coated glass was procured from Solaronix, from Switzerland. The phosphor coated glass tube was susceptible to breakage due to stress imparted by tightening the bolts to reduce vacuum leakages from the glass-metal interface, thereby often needing replacement. Due to the cost of obtaining spare phosphor coated glass tubes, another test cell (an ionisation sensor) was designed separately to test the field emission properties of nanotubes.

A newer version of luminescent tube was designed by assembling standard fittings (size QF40, ISO ref NW40). This comprised of a standard single pin 12 kV, 30 A electrical feed-through (part number EFT 1213098B from Kurt J. Lesker company) and a sealed off HV series dome shaped glass adapter (part number 463022 from MDC vacuum) to fit the feed through. A copper tube (OD 18 mm) was designed to sit on the feed-through and the arc-treated sample was wrapped around the copper tubing. The phosphor coated glass was housed inside the dome shaped adapter arranged in an annular configuration with the nanotube laden copper, as shown in Fig. 3.14.

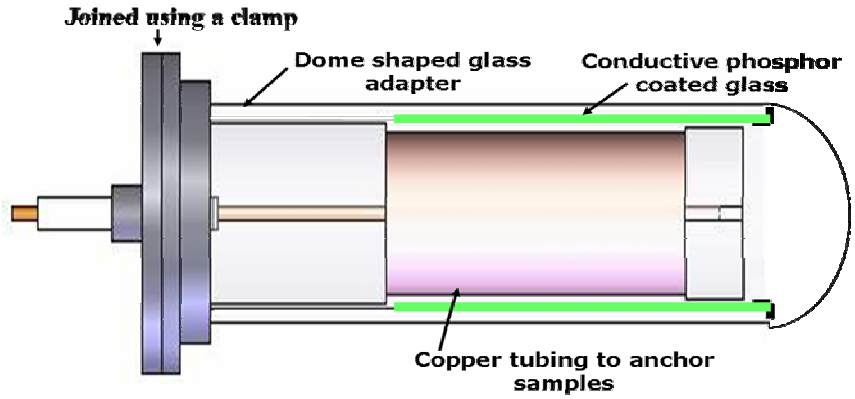

Fig.3. 14 Schematic of the luminescent tube and picture of the luminescent tube set up.

3.2.2 *Ionisation sensor:*

The design of the ionisation sensor is adapted from the basic design of the luminescent tube and was designed by Batty[20]. The designs were modelled using SolidWorks, which aided the sensors construction and considerably reduced design errors and construction time. The assembly model and schematics are shown in Fig. 3.15.

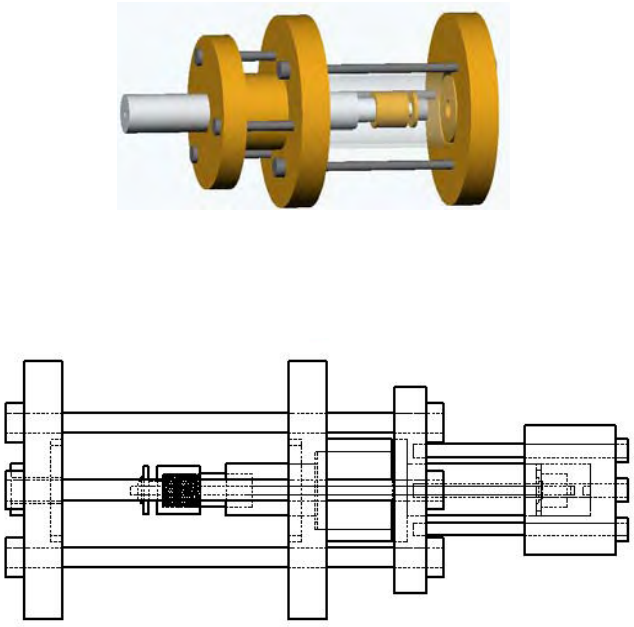

Fig.3. 15 Assembly model of the sensor and its schematics from *Solidworks*.

The sensor consists of two brass discs mounted axially facing each other acting as electrodes. The cathode is a circular brass plate (22 mm diameter) housed on a live brass rod of diameter 2 mm. The total disc area available for emission is 275 mm^2. The anode is also a circular brass plate (20 mm diameter) threaded onto an insulating support (7 mm diameter) designed to have a linear travel of 1.5 mm per revolution. The thread is designed to allow the gap between the electrodes to be varied in the range of 1 to 5 mm. The cathode is designed to be removable from the outer part of electrode assembly to be able to easily change and anchor different nanotube samples, as shown in Fig. 3.16.

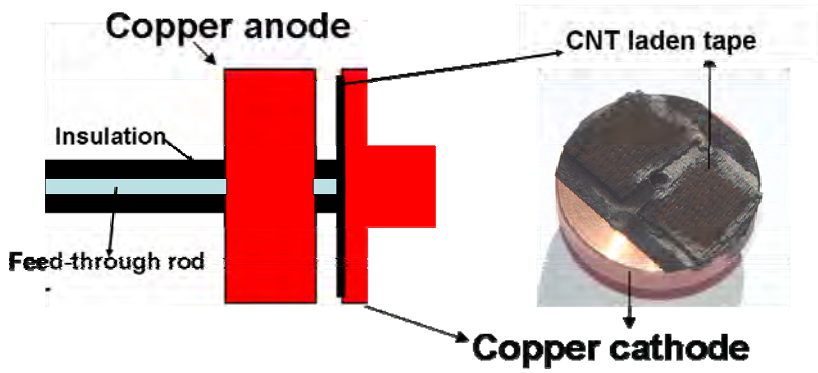

Fig.3. 16 Picture of removable copper cathode with nanotube laden carbon substrate and view of the cathode with nanotubes struck to the inner surface.

Boron Nitride (BN) rod grade and High Density Polyethylene (HDPE) were used as insulating materials in the sensor construction. BN was threaded to accommodate the anode and was also used to separate the two electrodes due to its high resistivity (10^{14} Ω/cm). HDPE was used as the other major insulator away from the electrodes due to the cost and brittle nature of BN.

The electrode assembly was housed in a vacuum tight chamber by clamping a glass tube with the electrode assembly using a threaded rod and nuts (8 mm diameter). The glass tube allowed visual access of the sensor during its operation. The ends of the glass tube were ground down to a smooth finish and sealed at either ends using rubber 'O' rings. The use of glue such as Araldite was considered during construction to fix the glass, but was ruled out due to the possibility of de-gassing under exposure to vacuum. Further detailed diagrams and assembly models can be found in the report of Batty[20].

The designed sensor failed to maintain the necessary vacuum required for performing field emission tests. Clamping the glass tube with "O" rings contributed to a major source of leak and a system vacuum better than 10^{-4} mbar could not be achieved. Hence, a new sensor was designed by procuring and assembling a custom made QF40 flange size HV series double ended glass adapter (part number 462022 from MDC vacuum and a 12 kV, 30 A electrical feed-through (part number EFT 1213098B from Kurt J. Lesker company), both of which had standard vacuum fittings (flange size QF40). The schematic of such an assembled sensor is shown in Fig. 3.17. An ultimate vacuum of 1.8 x 10^{-5} mbar could be achieved using the above combination and was sufficient to perform field emission measurements.

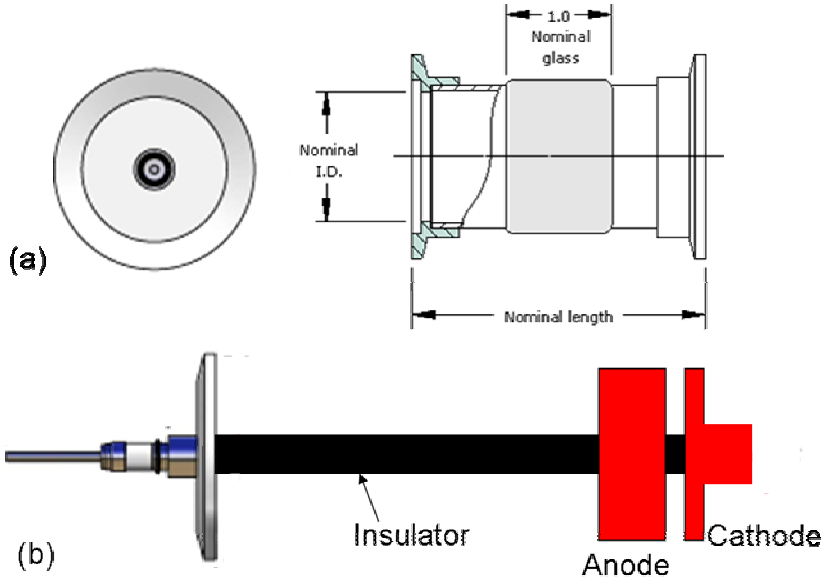

Fig.3. 17 (a) A double sided glass adapter and **(b)** electrical feed through with the electrode assembly.

3.2.2.1 Vacuum system:

The vacuum system was the key component of the sensor design. Various research groups have stated that a vacuum of 1.33 x 10^{-6} mbar is necessary to achieve stable field emission from nanotubes[7, 193, 260]. However conventional Cathode Ray Tube (CRT) systems widely operate at a base pressure of 10^{-4} mbar and nanotubes have also shown stable emission and increased current densities at 10^{-4} mbar[229].

The high vacuum in our system was achieved by using a combination of two pumps obtained from an old mass spectroscope system. They were a two-stage rotary vane

pump and a turbo-molecular pump. The two-stage rotary vane pump (Edwards E2M2) was used as a backing pump for the turbo-molecular pump (TMP50). The two-stage pump had an absolute vacuum of 2.5 x 10^{-4} mbar without a gas ballast. The vacuum pressure was measured using a Pirani model 1005 gauge. However the pump could only achieve an ultimate pressure of 6.5 x 10^{-4} mbar inspite of measures to minimise the leaks.

The turbo-molecular pump was the source pump used to achieve the desired vacuum for the sensor operation. This pump was connected to the sensor cell through the backing pump to reduce the cell pressure from atmospheric to low vacuum. An ultimate vacuum of 1.8 x 10^{-5} mbar could be achieved only using the above combination, though the turbo-molecular pump has an absolute vacuum of 10^{-7} mbar. This discrepancy was attributed to leaks in the system and in vacuum lines. A number of measures were taken to reduce the leaks in the system such as removing redundant joints and fittings, reducing excess length in vacuum lines and applying a thin layer of vacuum grease to all the rubber seals. Even with the above measures, the system vacuum reduced to a value of only 1.3 x 10^{-5} mbar.

Pressure gauges: The whole system comprised of three pressure gauges. The high vacuum gauge was a Penning gauge (Edwards CP25-K) connected to the turbo-molecular pump and was used to observe the pressure close to the vacuum sufficient for sensor operation. The low vacuum gauge was a Pirani gauge (Edwards PRM10) and was used to measure the pressure in the gas transfer line until the vacuum was sufficient to switch on the turbo molecular pump. The other gauge was a back up gauge (Penning) connected to the cell to observe any variations in system cell vacuum. The Pirani and Penning gauges were monitored on a Pirani Penning 1005 digital controller/indicator.

A third vacuum pump was thought to be essential to achieve a better vacuum in the system. A brief research on the type of pumps capable of delivering vacuum in the 10^{-6}-10^{-9} mbar range was conducted. Based on the research on various types of leaks, it was thought that a better vacuum was difficult to obtain for our system. The different sources that contribute to low vacuum in our system can be summarised as follows:

1. **Leaks**. These may be real leaks due to passageways through the vacuum wall from outside the chamber or virtual leaks due to gas being trapped in localities from which it can emerge only slowly into the vacuum surroundings.

2. **Vaporisation**. Often unintentionally, but sometimes of necessity, materials which exert a significant vapour pressure are present in a chamber, contributing a gas load. Water vapour from imperfectly dried components is, in general, troublesome because it slows down the initial evacuation process.
3. **Outgassing**. This term describes the release of gas from the internal surface of the vacuum wall and the surfaces of components inside the chamber. It forms the principal source of gas in many systems and limits the degree of vacuum, which can be achieved.
4. **Process generated gas and/or injection**. Many processes carried out in vacuum cause the release of gas, often from materials that are heated. For example in vacuum degassing applications, metals are heated to high temperature to rid of the dissolved gas inside the metals. In some applications a gas (mixture) must be injected into the vacuum chamber. Obviously this will give a gas load as well.
5. **Others**. Depending on the type(s) of pump(s) used in a given application, there may be a tendency for the vapour of lubricants to "back-stream" into the vacuum chamber.

After careful considerations of our design limitation, it was decided that an ultimate vacuum of 1.3×10^{-5} mbar was the best achievable vacuum for our system.

3.2.2.3 Electrical equipment:

Fig. 3.18(a-b) illustrates the key pieces of the electrical equipment used in sensor operation. Initially a positive HV supply (Philips PW 4221) having a range of 600-6000 V was used as the supply feed unit. However this power supply got damaged while in operation and was replaced by a negative supply (Glassman MK series) having a power range of 0-10 kV and a current output of 0-7.5 mA. The HV output was reduced using a voltage dropper consisting of a series of zena diodes which produced a constant drop of 400 V to accommodate any sudden variations. The power supply had an automatic current regulation and provided protection against overload, short circuit and arcing.

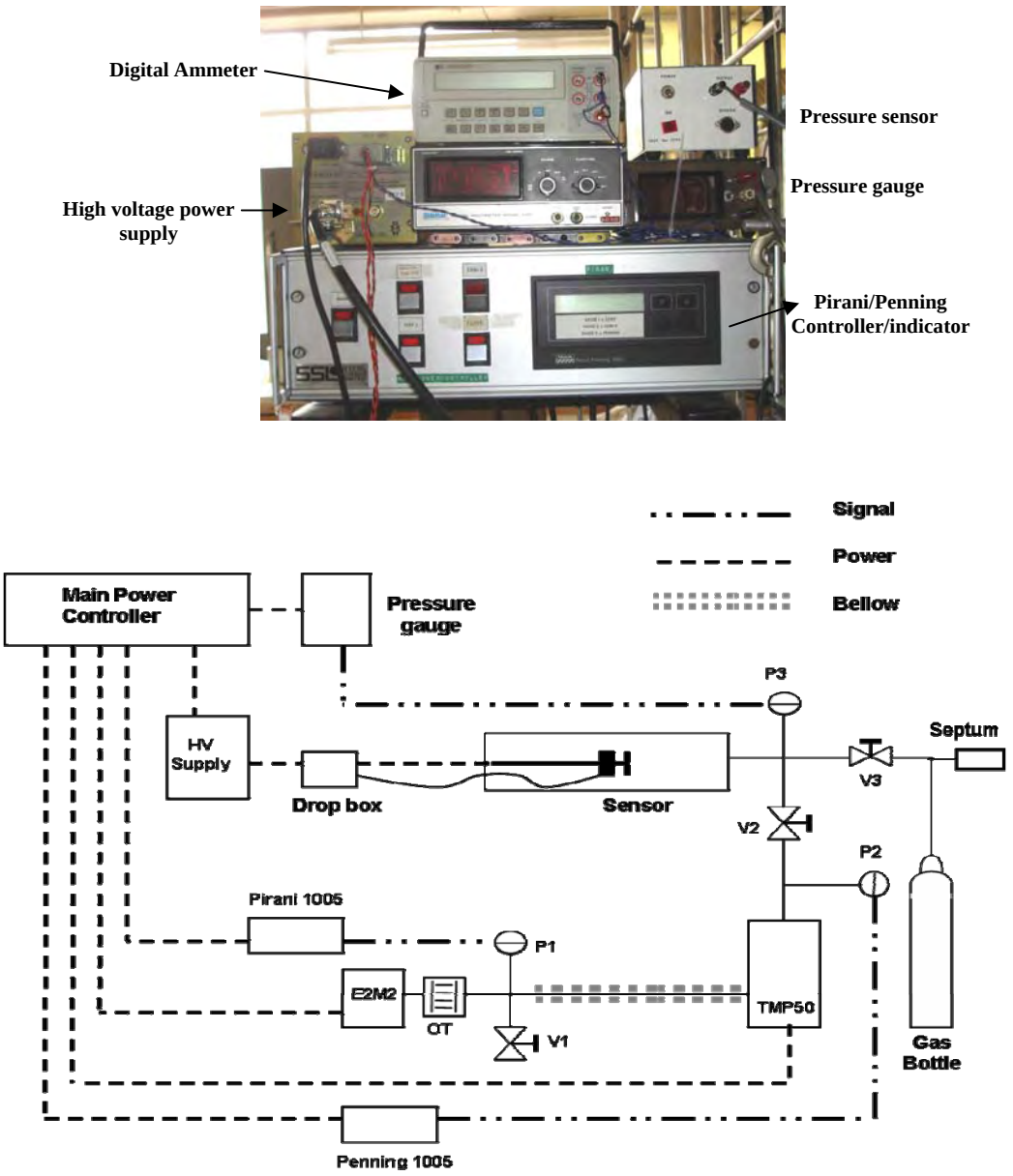

Fig.3. 18 (a) Picture of the electrical supply used for ionisation sensor and **(b)** flow diagram showing key components of the ionisation sensor.

The voltage was measured using an analogue AVO meter. The resistance across the electrodes was measured using a multimeter (HP3468A) prior to applying any voltage. The resistance measurement was performed to assess any bridging/shorting of the electrodes. The multimeter read "O.VLD MOHM" for no bridging and a value of ~ 7 kΩ when bridging occurred. This also aided in verification that the observed current was due to electron emission and not due to conduction.

The supplier specifies that the power supply monitors current by measuring voltage with an accuracy of 0.01%. The multimeter was also used to detect the current due to electron emission (A multimeter reading of 1V corresponds to a current of 1 mA).

3.2.2.4 Sample preparation:

The treated path on the carbon fibres was carefully cut using a scalpel. The cut sections were attached to the cathode using a double-sided conductive carbon tape. Fraying often occurred at the sample ends resulting in a short circuit within the system. The frayed ends of the fibres were also prevented from sticking out by overlaying the conductive tape at its cut ends. Although this helped reduce bridging of the electrodes, it was not possible to eliminate individual fibres from fraying and the sensor had to be operated at large electrode gaps (1 to 4 mm). The use of conductive carbon tape was abandoned after a few runs in favour of conductive carbon glue/ paint (Manufacturer: ProSciTech, Australia, Make: I003)

The new method of sample preparation involved the use of conductive carbon glue which is widely used in sample preparation for SEM. The glue was pasted on to the cut ends of the samples and is allowed to settle for a few minutes. The sample was then heated in an oven operating at 110 C for about 5 min to vaporise all the solvent (isopropyl alcohol) used in the carbon glue/paint. The use of glue eliminated fraying and bridging of the electrodes, facilitating smooth operation of the sensor. The sample-laden cathode was fixed to its position and a visual check was performed to observe any bridging.

3.2.2.5 Gas supply:

The following gases were to be tested using the sensor. The gas flow was monitored using a regulator from the gas bottle. A gauge pressure sensor was initially used to ensure the sensor chamber was not over pressurised. The sensor displayed a reading between 0-10 V for pressure corresponding to 0-20 kPa. The flow diagram of the sensor with all the key components is, as shown in Fig. 3.18(b).

3.2.2.6 Sensor operating procedure:

The following steps constitute a typical operating procedure. The nanotube samples were loaded into the sensor and the gap was set to a desired value. All the valves were ensured to be closed and the gas supply (if any) should be off.

- The power was turned on at the main power controller (switch labelled 'Mains').
- The Edwards backing pump was turned on by switching on the switch labelled 'E2M2' in the main controller and then by pushing the 'start' green button.
- The Valve (V2) between the sensor and the high speed turbomolecular pump was opened to pump down the base pressure in the sensor chamber to low vacuum.
- The high speed turbomolecular pump (switch labelled 'TMP50') was switched on when the Penning gauge in the controller reached a constant value.
- The high voltage supply was turned on when the sensor chamber was evacuated to a pressure of 2×10^{-5} mbar obtained by reading the Penning gauge in the controller.
- The ammeter (HP3468A) was switched on and was programmed to read current in the microampere range.
- The sensor chamber was injected with a known volume of desired gas (at one atm pressure) using a syringe through the septum by opening valve V3 and closing V2. The pressure inside the sensor was given by the reading of the Penning on the controller.
- The voltage was increased in steps of 50 V and read using the analogue AVO meter until breakdown was achieved or till profuse arcing occurs for no gas flow.
- The corresponding parameters were recorded. The breakdown voltage and current were ensured to be accurate by repeating the previous step and finally increasing the voltage in finer steps of 1-2 V, where if possible.

3.3 Single nanotube measurements:

This section describes the experimental method of anchoring single nanotube samples to study field emission from individual nanotubes. Various attempts were made to put nanotubes onto tungsten filaments commonly used as cathodes in SEM. The nanotube attached tungsten filaments were to be used as an emission source inside the SEM by applying different voltages.

Initial trials of mounting individual nanotubes on tungsten filaments consisted of scraping the arc treated substrate surface with the help of a scalpel. The separated fibres and nanotubes were then collected in a Petri dish filled with 5 ml of acetone. The filament from the SEM was then dipped into the solution to attach nanotubes to it and dried in an oven operating at 100 C for 10 minutes. The samples were then analysed in a SEM to trace individual nanotubes sticking to the filament. Unfortunately, no nanotubes were found in any of the trails but carbon fibres were instead found sticking to the tungsten filament.

The other method involved the use of a conductive carbon paint to attach individual nanotubes on the filament. In this method, a blob of conductive carbon paint was put on the tip of the tungsten filament which was then rubbed over the arc treated surface. The samples were then dried in an oven operating at 100 C for 5 minutes. This method was successful, as individual nanotubes were seen protruding from the tungsten filament as shown in Fig. 3.19(a-b)

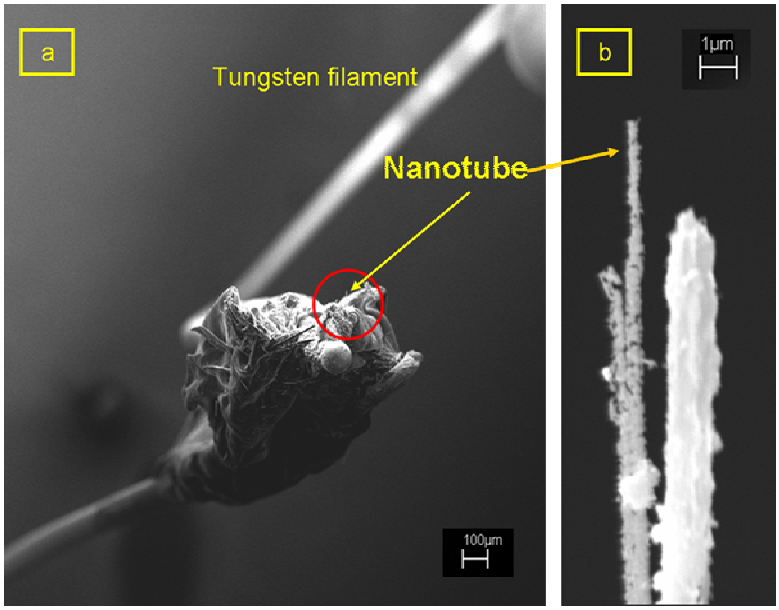

Fig.3. 19 SEM images of (a) distribution of a single nanotube on tungsten filament circled in red and **(b)** nanotube at high magnification coated with conductive carbon paint.

4.0 Field emission from individual nanotubes

The first few sections of this chapter provide a detailed literature review of the current studies on field emission from a single carbon nanotube (both MWNT and SWNT). The effect of temperature on the physical properties of nanotubes (thermal conductivity and electrical resistivity) are summarised from various studies. A suitable thermal conductivity and electrical resistivity value was identified from the above studies and were used for simulation.

The modelling studies and the effect of different parameters on field emission from a single nanotube were carried out by the author of this thesis. The simulation results provide information on the onset of Joule heating from a single nanotube.

4.1 Introduction:

Carbon nanotubes exhibit exceptional field emission behaviour due to their high aspect ratio, conductivity and inertness. Carbon nanotubes have been shown to be perfect candidates for vacuum microelectronics and considered a good replacement for Spindt type emitters. Various applications like field emission displays (FED), cathode ray tube type lighting elements, magnetic field sensors, plasma starters, microwave tubes, X-ray tubes and semi-conductor devices have been demonstrated using carbon nanotube as emitters. These applications characterise emission from a multitude of nanotubes as films, patterned arrays or from nanotubes dispersed in a conductive matrix to increase the total emission current or to achieve large emission areas. Most of the studies on nanotubes focus on the statistical properties of a large number of collective nanotubes. The experimentally measured results are an average from nanotubes that are structurally diverse in diameters, length and helical angles. Therefore it is difficult from these to understand the effect of various factors affecting the mechanism of field emission measurements. The intrinsic physics of field emission from individual nanotubes are then obscured since emission is influenced by many intrinsic factors. Hence it is beneficial to study field emission from individual nanotubes through experiments and/or simulations.

Experiments on individual nanotubes provide further details of the mechanism occurring during field emission and the reasons for emitter failure. It also provides an accurate characterisation of a nanotubes work function, turn-on voltage, current density and field enhancement factor. It is also possible to determine optical parameters like reduced brightness, angular current densities, virtual source size and tip temperatures which is beneficial to using them as single electron beam sources.
The experimental technique of studying emission from individual nanotubes involves the measurement of current-voltage (IV) curves, measurement of the electron energy distribution, field emission microscopy and in-situ studies within a transmission electron microscope and scanning tunnelling microscope.

4.2 Field emission from a single nanotube:

Field emission from individual nanotubes has been deeply investigated by several groups. The small dimensions of nanotubes make their characterisation and manipulation difficult, prohibiting the use of commonly well established techniques. Among the various techniques used, in situ TEM and SEM studies have provided important insights into the behaviour and destruction of nanotubes during field emission. Other techniques like field emission microscopy, STM and AFM have also been a major tool in investigating the properties of individual nanotubes. Field emission from individual nanotubes is influenced by various parameters. Factors like the type of nanotubes, tip structure, temperature and adsorbates affect field emission to a large extent.

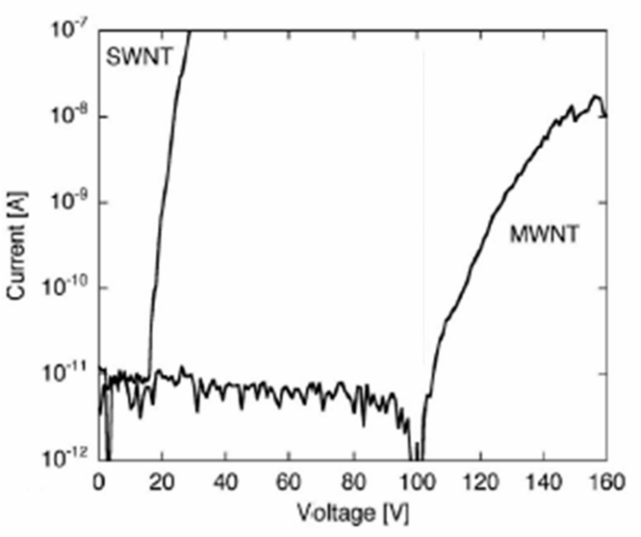

Fig.4. 1 I-V curves acquired from a SWNT rope and on a MWNT showing the onset voltage for each emitter[261].

Fig. 4.1 shows the I-V curves of a MWNT and SWNT rope of similar length measured at a constant inter-electrode distance. The turn-on voltage for the SWNT rope is considerably lower than that of a MWNT. This decrease in turn-on voltage for the SWNT rope is attributed to high field enhancement at their tips due to their smaller diameters. It has also been shown by some theoretical calculations and STM measurements that the electronic properties of the tip and the cylindrical part of the tube are different for SWNTs and MWNTs. SWNTs display a characteristic 1D character whereas MWNTs exhibit essentially graphitic character indicating high localised states for SWNT. Similarly the turn-on voltage for opened MWNTs is considerably higher than that of closed MWNTs as shown in Fig. 4.2. This factor is attributed to the energy and intensity of the localised states at its tips. Simulations have shown that the local density of states at closed tips reaches values at least 30 times higher than that in the cylindrical part of nanotube[262]. This leads to an increased electron supply and thus lower turn-on voltages for closed cap nanotubes. However, very recent results[206, 207] have shown low threshold voltages and high field enhancement for field emission from the side walls of MWNTs (when compared to their tips).

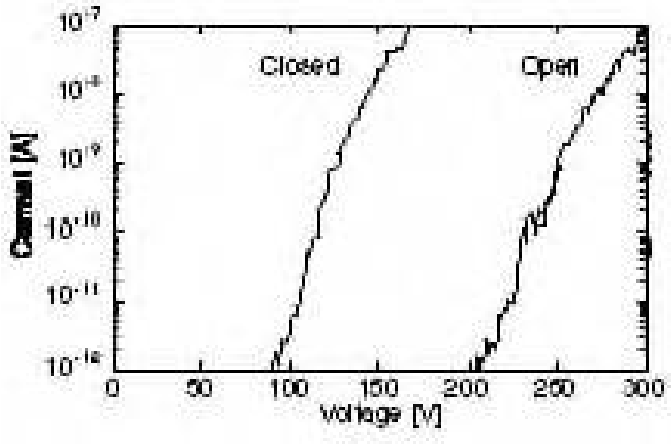

Fig.4. 2 Current-voltage characteristics of an individual open and closed MWNT[263].

Various studies have shown a current saturation effect in the field emission behaviour of carbon nanotube films[222, 223, 264]. Several mechanisms have been proposed to explain this saturation phenomenon which is believed to be a direct result of adsorbates affecting the field emission mechanism. A current saturation mechanism for individual nanotube has only been studied for SWNT[222]. It was found that adsorbates play an important role in current saturation and that adsorbate states enhance the field emission current of an individual nanotube by two to three orders of magnitude at lower voltages as shown in Fig. 4.3. Desorption of adsorbates at higher voltages causes current saturation, until it's desorption at high fields. The field emission pattern after desorption match the properties of a clean individual nanotube[222]. Therefore current saturation is not an intrinsic property of a nanotube. An individual MWNT is expected to exhibit a similar mechanism[265], but there has been no report to this date investigating current saturation mechanisms for individual MWNT.

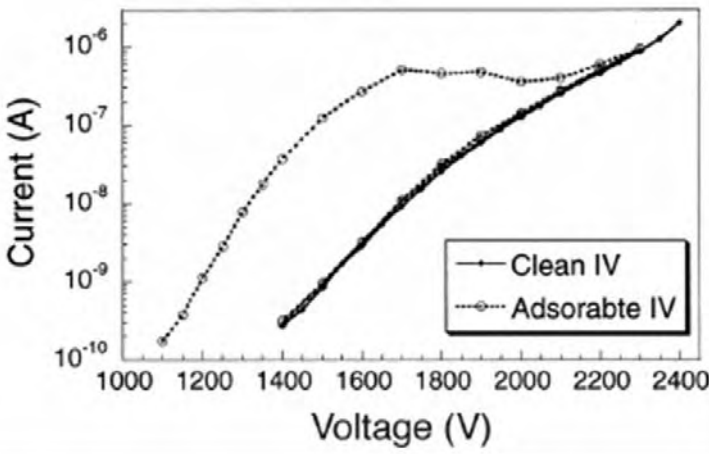

Fig.4. 3 Current-voltage characteristics of a single SWNT with and without adsorbates[222].

The field emission behaviour of an individual clean nanotube is stable and reproducible over a large current range[226]. The Fowler-Nordheim plot is linear over this current range but deviates from linearity at extremely high currents. The experimental results from an individual nanotube and nanotube films reveal a non-linear Fowler-Nordheim behaviour during high current emission. This behaviour at high field is attributed to strong Ohmic heating resulting in increased tip temperatures. This is also evident in the observation of a “knee” like decrease in the slope of the Fowler-Nordheim plot at high applied fields as shown in the inset of Fig. 4.4. Various reports have shown resistive heating of individual nanotubes corresponding to temperature rises of 2000 K for emission currents in the microampere range during field emission[210, 216]. This Joule heating is of importance since it can be one of the origins of current saturation and also destruction in nanotubes.

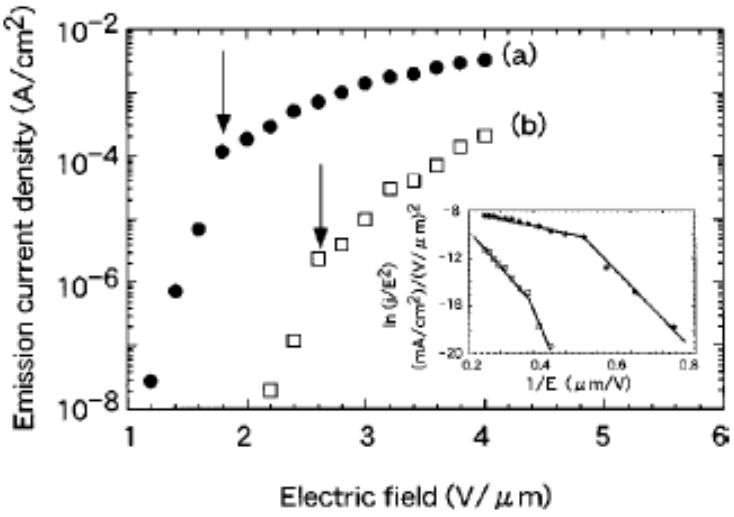

Fig.4. 4 Current density vs electric field for a carbon nanotube. Inset: corresponding F-N plot. (Arrows indicate the onset of saturation)[266]

The onset of Joule heating results in a sudden increase in current emission from nanotubes due to thermally enhanced electron emission, as shown in Fig. 4.5. Carbon nanotube tips suffer a rapid change in structure at high currents and often undergo sudden destruction. This change in their apex structure does not occur gradually, but rather abruptly accompanied by a sudden drop in emission current. Various mechanisms have been proposed to explain the structural change assumed due to resistive heating of a nanotube tip at high currents[267]. It is not yet clear whether this

damage is due to segment-by-segment peeling process of the graphitic layers or due to a layer by layer stripping process. Rinzler[192] proposed an unravelling process of carbon chains followed by field-induced fragmentation to explain this sudden damage while Dean[211] proposed field evaporation of carbon atoms at the end of the nanotube causing length reduction, resulting in an emission current decrease. Whatever, there appears to be a current limit for an individual nanotube dictated by thermally assisted evaporation.

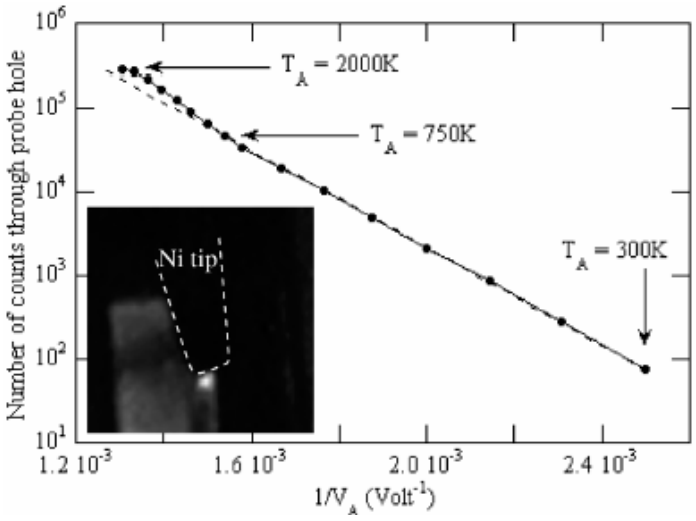

Fig.4. 5 F-N plot of current induced heating of nanotubes for a MWNT. Field emission current increases significantly above F-N line at T=750K[268].

Some simulation reports have also shown evidence of a self-repair mechanism (Fig. 4.6) of nanotube tips in which open ended tubular nanotube caps rearrange and close at high currents[267, 269]. This process is expected to depend on the type of nanotube (radius, length, defects, amorphous content) and its contact with the support/base. This Joule heating is also known to permit nanotube cleaning (removal of adsorbates) without the aid of an external temperature. This can be initiated by significantly increasing the emission current, leading to either damage/repair of the nanotube tip. This also indicates the maximum current one can extract from a nanotube.

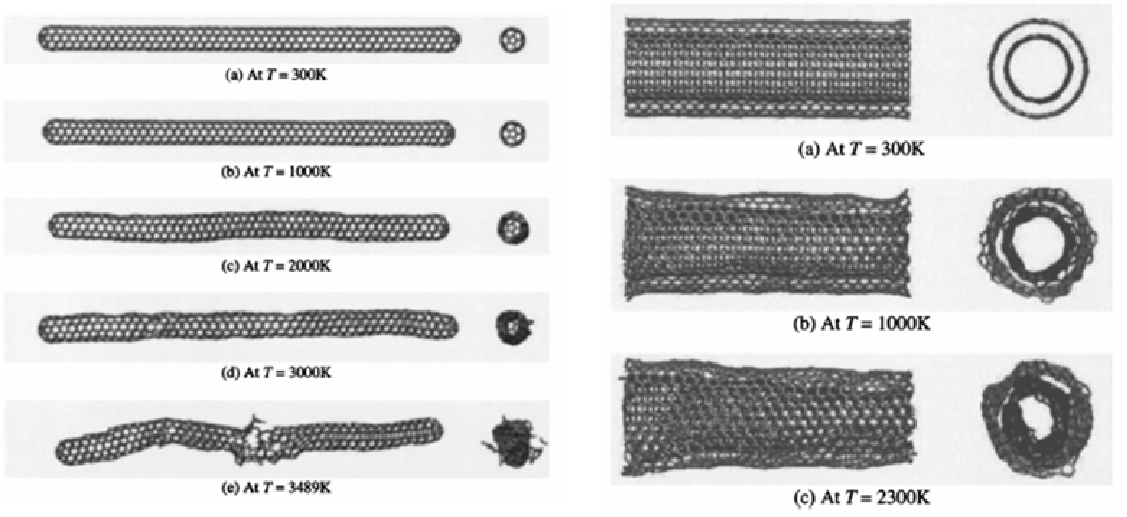

Fig.4. 6 Simulation of SWNT destruction at various temperatures and evidence of tip closure (self repair mechanism) for a MWNT at various temperatures[269].

Hence, it is essential to understand the behaviour of nanotubes at high current densities and the extent of Joule heating through modelling and simulations. Despite the importance of Joule heating on field emission, there have been very few studies on modelling the current-induced heating of nanotubes[210, 270, 271]. The computational issues still remains unsolved since the complexity of nanotubes makes these analytical approaches difficult. Finite element analysis (FEA) has been quite successful in modelling macroscale phenomenon and there have been several interesting studies of microscale structures.

However, theoretical and experimental studies on the variation of electronic and thermal properties within individual nanotubes with temperature are absolutely vital to understand and/or simulate field emission from individual nanotubes.

4.3 Modelling field emission from a single nanotube:

In this study, we use finite element commercial software Comsol Multiphysics 3.2 to compute and simulate the electric field near the tip of a multiwall nanotube and model its thermal behaviour due to current flow. This approach is likely to apply better to MWNT than SWNT since it assumes properties taken from bulk measurements. We first formulate the potential distribution and the local electric field distribution near the nanotube tip to calculate the local current density. Then, we studied the heat

conduction and temperature variation at the tip at various total currents by coupling the Laplace equation with Fourier's law of conduction. The physical properties of various types of nanotubes are assumed the same, since there has been no previous distinction for different types of nanotubes and/or nanotubes produced from different methods. The variation of their physical properties with temperature is also not characterised completely. A detailed overview of this is given in the following section. The assumed values of electrical resistivity, thermal conductivity, work function values are 1.2 x 10^{-6} Ω-m[272], 990 W/m-K (From Comsol Multiphysics) and 5 eV[273] respectively at a temperature of 20 C.

4.3.1 *Thermal conductivity (k):*

The relevant physical properties of nanotubes are very important to this modelling. It is interesting to examine thermal conductivity values for nanotubes in light of high conductivity values exhibited by other carbon forms like graphite and diamond. An unusually high thermal conductance is expected for nanotubes due to their sp^2 bonding and large phonon mean path in their bond network. The bulk thermal conductivity of nanotubes is estimated to be in the range of 150-6600 W/m-K[274-278]. Thermal conductivity of SWNTs is theoretically predicted to be comparable to the highest thermal conductivity ever measured and exceeding the k(T) value of isotopically pure diamond by a factor of 2 at room temperature[274]. However, the thermal conductivity varies greatly and is highly anisotropic, with their axis having higher values than in other directions. There is also a significant gap between experimentally measured results and theoretical predictions. This is probably due to the uncertainty of thermal resistance in tube-tube junctions and the effect of the volume filling factor while conducting bulk conductivity measurements with nanotube composites[275]. Therefore it is desirable and necessary to investigate individual nanotubes to achieve reliable and accurate information. This will help us to understand and predict heat transport along nanotubes for their various applications.

So far only a few experimental results of thermal conductivity for an individual SWNT[269, 279, 280] and MWNT[269, 275, 276, 281] have been reported. A SWNT is expected to exhibit much higher thermal conductivity than a MWNT, but the

reported k(T) values for both types of nanotubes are very similar and are hard to distinguish. This is because experiments tend to measure 'k' values for a bundle of several SWNTs, due to the difficulty in the manipulation technique for an individual SWNT. It can only be deduced from all the experimental and theoretical calculations that thermal conductivity (SWNT and MWNT) increases with increasing temperatures showing an asymptote near 300 K, and decreasing above this temperature, as shown in Fig. 4.7.

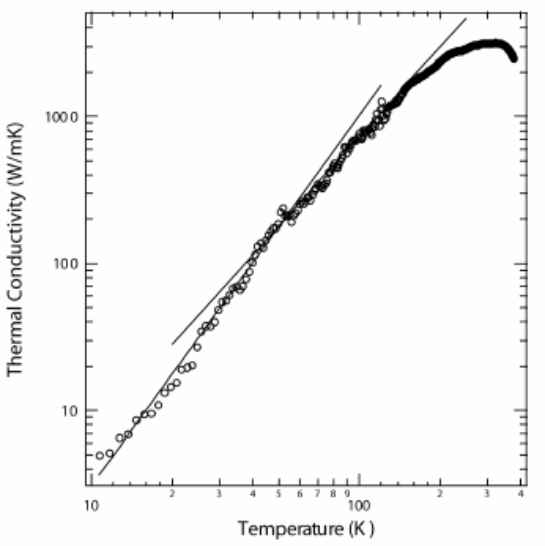

Fig.4. 7 Relationship between thermal conductivity and temperature for an individual MWNT with a diameter of 14 nm[282].

It is clearly seen from Fig. 4.7 that nanotubes exhibit a temperature power law relationship with thermal conductivity at low temperatures suggesting quantum effects. The thermal conductivity of a MWNT follows a 2-D system dependency due to their larger diameters and narrow temperature scale for quantum effects[274]. The thermal conductivity of 2-D sheet systems generally follow a T^2 temperature dependence as observed experimentally for an individual MWNT[283, 284].

Fig. 4.8 shows the relationship of thermal conductivity with nanotube diameter for a SWNT and a MWNT (where d_0 and d_i are outer and inner diameters of nanotubes respectively). It is seen that the thermal conductivity of a SWNT at room temperature increases as its diameter decreases. Similarly, the thermal conductivity increases as the number of multi-walled layers decreases for a MWNT[280]. The diameter-dependent thermal conductivity indicates that the interaction of phonons and electrons

affect the thermal conductivity values. Zhang[277] studied the effects of chirality, isotope purity and nanotube length on thermal conductivity in SWNTs. They showed that thermal conductivity is insensitive to chirality of nanotubes. However, the presence of isotope impurities changed the temperature dependence of nanotubes and suppressed their thermal conductivity up to 60%. The effect of nanotube length on thermal conductivity is still unknown. Maruyama[285] and Che[286] proposed that the thermal conductivity of nanotubes converges to a constant value for nanotubes longer than the phonon mean free path while others have observed that thermal conductivity is independent of nanotube length[276, 287].

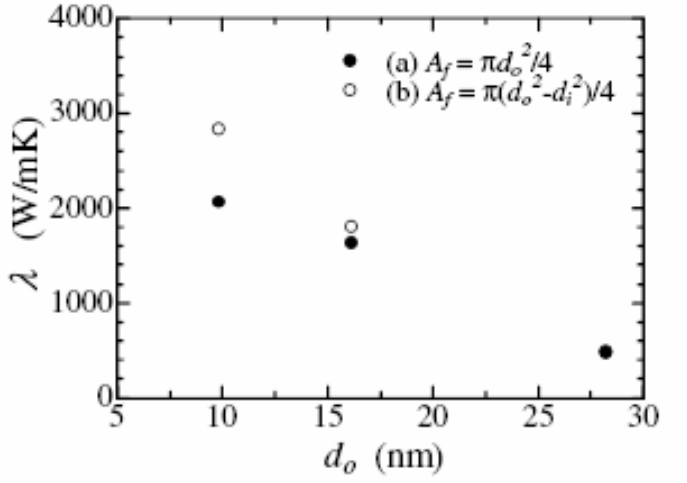

Fig.4. 8 Thermal conductivity of a SWNT (o) and MWNT (⌾) at different diameters at room temperature[280].

Thermal conductivity values for different nanotube types from both experiments and simulations are summarized in Table 4.1. It is seen that the thermal conductivity values along the tube axis for different types of nanotubes varies from 25-6600 W/m-K for bulk CNT samples, CNT films, and individual MWNTs and SWNTs. In fact, the thermal conductivity of nanotubes is highly anisotropic, with values perpendicular to the tube axis usually two orders lower than that along the axis. Choi[275] predicted a thermal conductivity value of 5.6 W/m-K in a direction perpendicular to the tube compared to 950 W/m-K along the tube axis. The highly anisotropic properties in thermal conductivity and the large difference between single-tube and bulk measurements suggest that more extensive studies are needed.

Author	Method of fabrication	Nanotube type	Thermal conductivity at room temperature, W/m-K
Berber et. al	Simulations	Isolated SWNT	6600
Hone et. al	Arc discharge	SWNT films and ropes	200
Small et. al	n/a	SWNT mat	35
Yi et. al	CVD	MWNT	25
Kim. et. al	Arc discharge	Individual MWNT	3000
Jiang. et. al	Microwave Plasma CVD	MWNT film	200
Fujii. et. al	Arc discharge	Individual SWNT	2000
Choi. et. al	n/a	Individual MWNT	650-830

Table 4. 1 Summary of thermal conductivity values for different types of nanotubes.

4.3.2 *Electrical resistivity:*

Electron transport in nanotubes is one of the more intensively studied topics in nano-electronics. This interest is due to its potential for various applications, from single electron transistors, semiconductor nanowires, field effect transistors, metallic nano-constrictions to other molecular nanostuctures.

Most of the research in this field has been performed on SWNTs which exhibit ballistic transport over mesoscopic distances[288]. Single walled nanotubes can also be metallic or semi-conducting based on their atomic arrangement. They are also shown to act as genuine quantum wires with conduction occurring through well separated, discrete electronic states that are quantum-mechanically coherent over different lengths[289]. They also exhibit an anomalous behaviour of conductivity as a function of temperature.

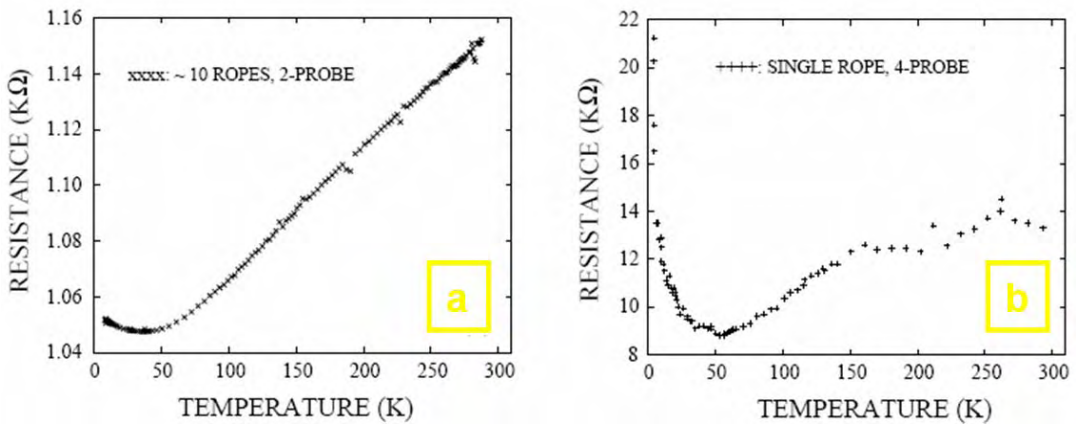

Fig.4. 9 Temperature dependent resistivity of different forms of SWNT **(a)** 10 ropes using 2 pt. probe and **(b)** 1 rope using 4 pt. probe[290].

Fig. 4.9 displays the temperature dependence of resistance for different forms of SWNT. It is seen that the resistivity decreases at low temperatures till a certain crossover point, and then increases linearly with temperature. However, to date, single-tube transport has only been measured at low temperatures and this linear increase in resistivity behaviour has been confirmed to extend only till 580 K[290]. Various mechanisms have been proposed by authors to explain this anomalous behaviour and this is beyond the scope of our study here. The resistance of SWNT at room temperature reported by various research groups are mostly in the range of 1-10 kΩ/μm[272], though Fischer[291] obtained data for a SWNT above 50 K to fit an equation of the form $A+CT-DT^2$. If conduction is assumed to be through the entire cylindrical cross sectional area of the tube, the resistivity of a SWNT at room temperature can be taken as 2×10^{-6} Ω-m[272].

Electron transport through MWNT is more complex since each shell can have different chiralities. The weak interactions between the walls in MWNT are similar to interlayer interactions in graphite. The intra-layer conductance in MWNT can be several orders of magnitude larger than the interlayer conductance[292]. Conductance measurements for MWNTs are complex since its values depend on how the contact is made with individual layers. In practice, most of the current flows through the outermost shell[293]. The transport mechanism occurring in a MWNT is very uncertain since some studies have concluded that MWNTs are ballistic at room temperature[294], while others have concluded that the transport is ohmic[295].

Several groups have reported electrical resistivity results for MWNTs and none of the initial results reveal metal like characteristics[291]. In general, the resistivities of arc grown MWNTs compare well with arc-grown graphite fibres[296] and ropes of SWNTs whose resistivities are ~10^{6} Ω-m[297].

The electrical resistivity of individual nanotubes is also sensitive to structural variations[298]. The electrical conductivity shows reversibility corresponding to the deformation process within the elastic limit when stretched. However nanotubes undergo structural defects when the applied stress exceeds its elastic limit. Its electrical conductivity is also not restored to its original state when the stress is released[298].

4.3.3 *Simulation method*

The Comsol Multiphysics simulation package is used in this study to investigate the field emission and thermal properties of a single nanotube. The following assumptions were made to the model;

- The fields and the geometry of the model are axially symmetric.
- Variables (electric field and temperature) varies only along the length of nanotube (y-direction)
- Constant electrical and thermal conductivity values.
- Nottingham effect (tip cooling due to electron emission) and radiation are not considered.
- No thermal contribution to the total emission current from nanotube.

The initial geometry used to model the nanotube is shown in Fig. 4.10. Simulations have been performed assuming the nanotube is a cylinder with a hemi-ellipsoidal cap of 20 nm major radius and 15 nm minor radius. Most simulations were done with a configuration as in Fig. 4.10 *i.e* diameter of 30 nm and 4 μm in length with the nanotube anchored on a tungsten ellipsoidal base (3 μm width and 1.25 μm height) acting as the cathode. The anode is located at a distance of 12 μm from the nanotube tip arranged in a diode configuration. Simulations were performed accounting for changes in field emission characteristics by varying nanotube diameters, lengths and the inter-electrode gap. The nanotube was assumed to have a constant electrical

resistivity, thermal conductivity, work function, with values of 1.2 x 10^{-6} Ω-m[272], 990 W/m K and 5 eV[273] respectively. The software computes the local electric field at the nanotube tip by dividing the emitter tip into fine grids with graded grid size as shown in Fig. 4.10, and by solving the Laplace equation.

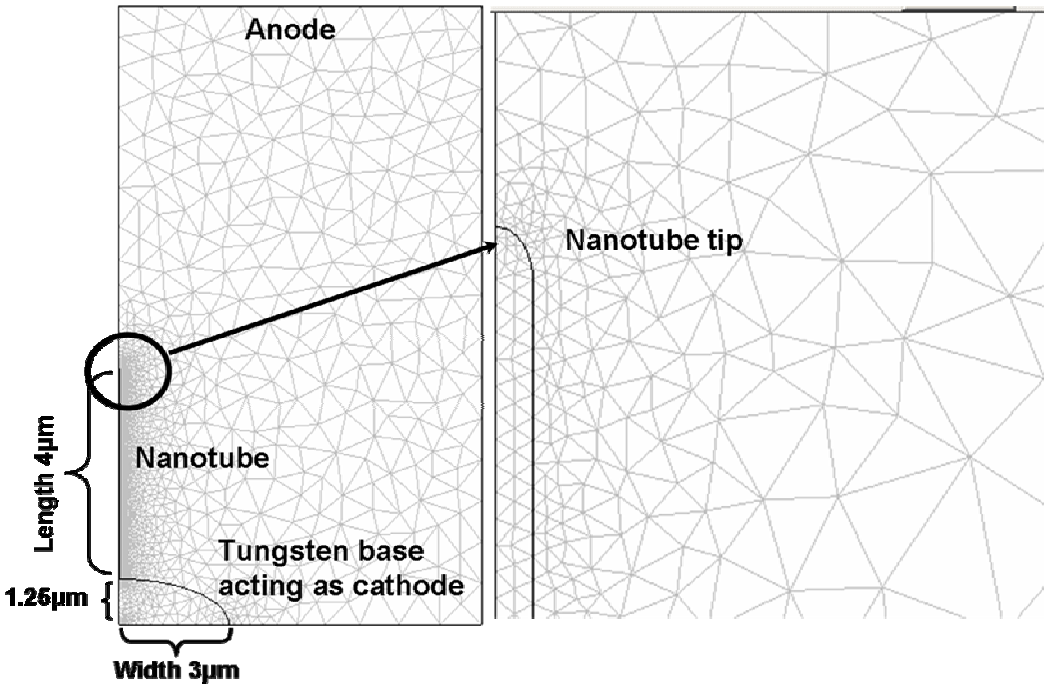

Fig.4. 10 Model definition with mesh consisting of triangular elements.

The local current density at the nanotube tip is obtained from the Fowler-Nordheim (FN) equation.

$$J = A.\ E^2/Ø.\ \exp\ (-BØ^{3/2}/E) \text{----------} (4.1)$$

Where E is the local electric field obtained from the solver. The total current from the nanotube tip was obtained from numerical integration of current density from the FN equation over the tip surface.

As discussed in the previous sections, a nanotube tip heats up when an electric current flows through it due to its electrical resistance. This resistive or Joule heating is noticeable when the current from a nanotube reaches several mA or few hundreds of µA[299]. The resistive heating is proportional to the magnitude of current density from the nanotube tip and its intrinsic resistance. Resistive heating is directly included as a variable in FEMLAB and is used as the source term for heat transfer when it is coupled with the Laplace equation, to evaluate temperature within the nanotube for various currents. This multiphysics coupling facilitates the calculation of nanotube tip

temperature values at different voltages. The simulations were done with increasing current, until a current is reached at which the tip temperature value attains ~ 3800 K.

4.3.4 *Simulation results:*

Fig. 4.11 shows a streamline plot of the electric field at the nanotube (60 nm diameter, 6 μm long) tip for an applied voltage of 600 V. The electric field concentrates at the nanotube tip causing local field enhancement. The enhancement factor is defined as the ratio between the resultant local field at the protrusions, to the applied field. Therefore

$$ß = E_{loc}/ E_{app} \text{----------(4.2)}$$

The applied electric field across the electrodes in a diode configuration is given by E_{app} = V/d, where V is the applied voltage across (z-plane) the electrodes and 'd' is the spacing between the tungsten cathode and the anode. With an applied bias of 600 V the applied electric field is calculated as;

$$E_{app} = V_{app}/d = 600/1.275 \times 10^{-5} = 4.70 \times 10^{7} \text{ V/m----------(4.3)}$$

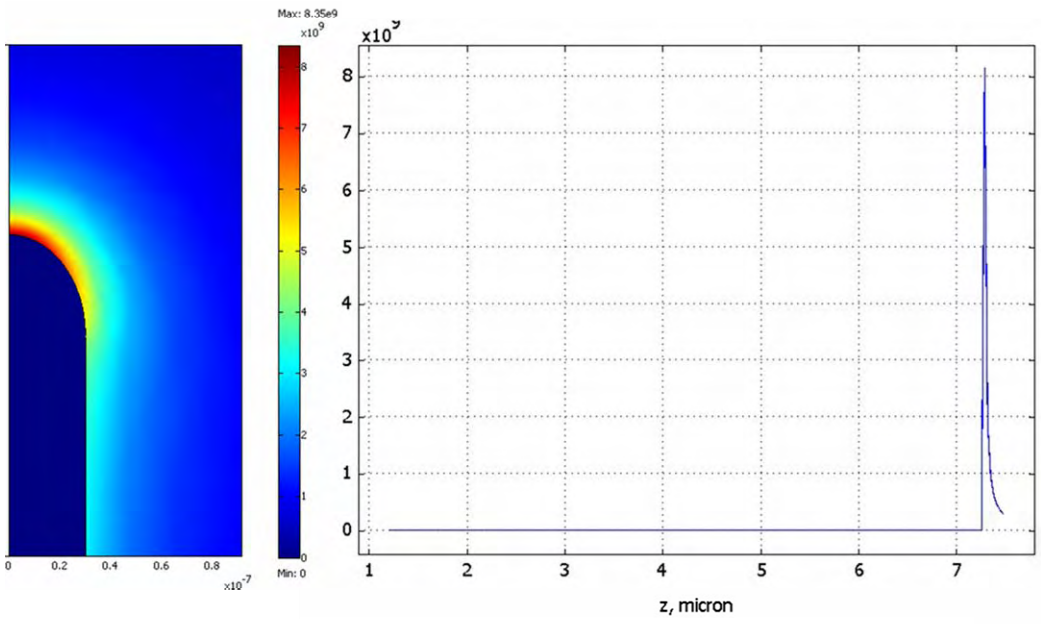

Fig.4. 11 Electric field distribution showing the electric field by a color and extrusion plot of E_{loc} along the nanotube length showing a maximum occurring right at the tip at 600 V.

It is hard to precisely know the topology of the emitting surface during simulations since the tip irregularities greatly contribute to local field enhancement and current emission. The nanotube tip was divided into various sized mesh. The resultant maximum local field at the nanotube tip as seen from Fig. 4.11 is $E_{loc} = 8.35 \times 10^9$ V/m. Thus we obtain an enhancement factor of

$$\beta = E_{loc}/ E_{app} = 8.35 \times 10^9/4.7 \times 10^7 = 168.6\text{----------}(4.4)$$

Many field emission experiments with nanotubes use small inter-electrode separations since high electric fields are attained at small separation gaps. The field enhancement is dependent on $E_{loc,}$ which along with turn-on voltage is very sensitive to the separation distance for a given applied voltage 'V'[300]. Fig. 4.12 shows the dependence of E_{loc} on the gap between the nanotube (60 nm diameter, length 4 μm) obtained from simulations, when the anode is arranged in a diode configuration. However, $E_{loc/} E_{app}$ is always constant for a given inter-electrode gap.

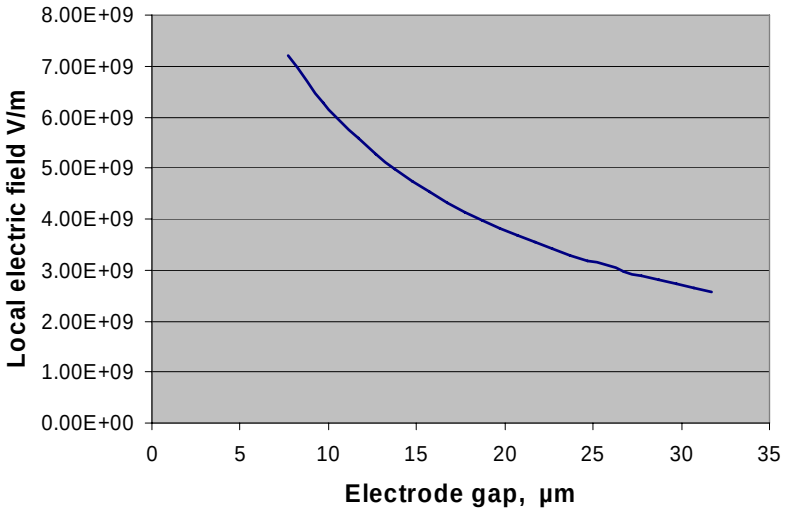

Fig.4. 12 Dependence of local electric field on emitter-anode gap for an applied voltage of 600 V.

It shows that the gap between the emitter and anode has a significant effect on the local electric field, thereby on the total emission current. However, very few experimental reports on individual nanotubes relating the effect of emitter-anode gap are available making comparisons difficult. The effect of length and diameter of nanotubes on the total current, current density, joule heating and field enhancement is

studied systematically by varying the length and radius between 6-11 μm and 10-60 nm respectively. The simulated values of the enhancement factor as a function of length (a constant diameter of 48 nm) and radius of the nanotube (a constant length of 5.83 μm) is shown in Fig. 4.13.

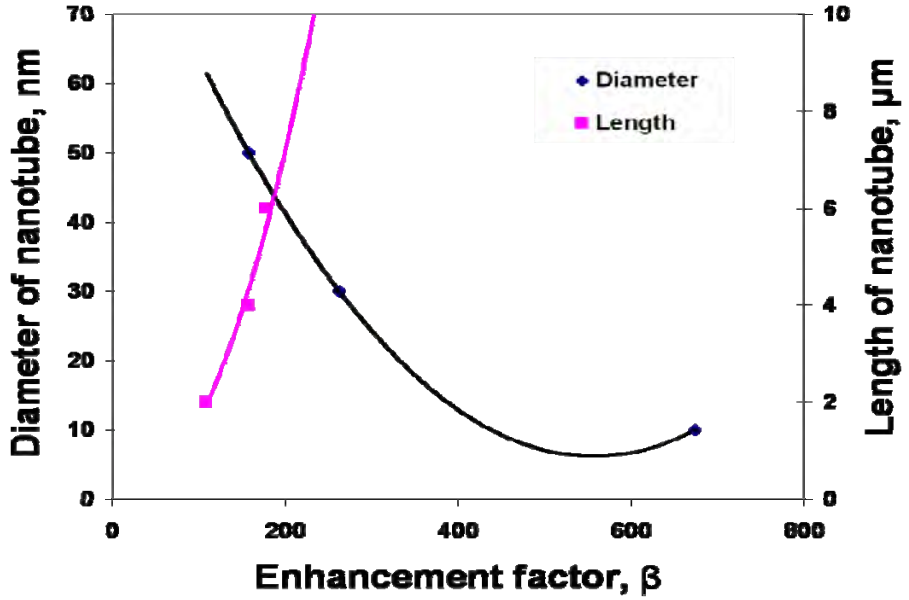

Fig.4. 13 Variation of field enhancement factor at different lengths and diameters of nanotubes from simulation of this work.

One such simulation was to test the experimental results of field emission properties by Minh[301]. Minh obtained enhancement factors in the range 208-249 for a 24 nm diameter, 5.83 μm length nanotube, arranged in a diode configuration, with an inter-electrode gap of 13 μm. They also measured the resistance of individual nanotubes using two contact methods to find the conductivities of their nanotube to be 10^{-6} Ω m. Simulations were performed under the above conditions with similar values of nanotube diameter, length, conductivity and inter electrode gap and were compared with the experimental results of Minh[301]. The simulations predicted an enhancement factor of 242 which were in good agreement with the experimental results. The experimental results revealed breakdown (sudden drop in emission current) on the nanotube emitter at currents between 0.2 and 2 mA (current densities of 10^{11}-10^{12} A/m^2 averaged over the whole tip area). However, our simulations predicted a significantly higher breakdown (tip temperatures ≥ 3600 K) current of 8 mA but at the same tip current densities (averaged values over the whole tip) observed in experiments. This discrepancy is thought to be due to the thermal conductivity

values of nanotubes. There was no mention of thermal conductivity values in the results reported by Minh[301], but we assumed the highest reported value of 3000 W/m-K for our simulations.

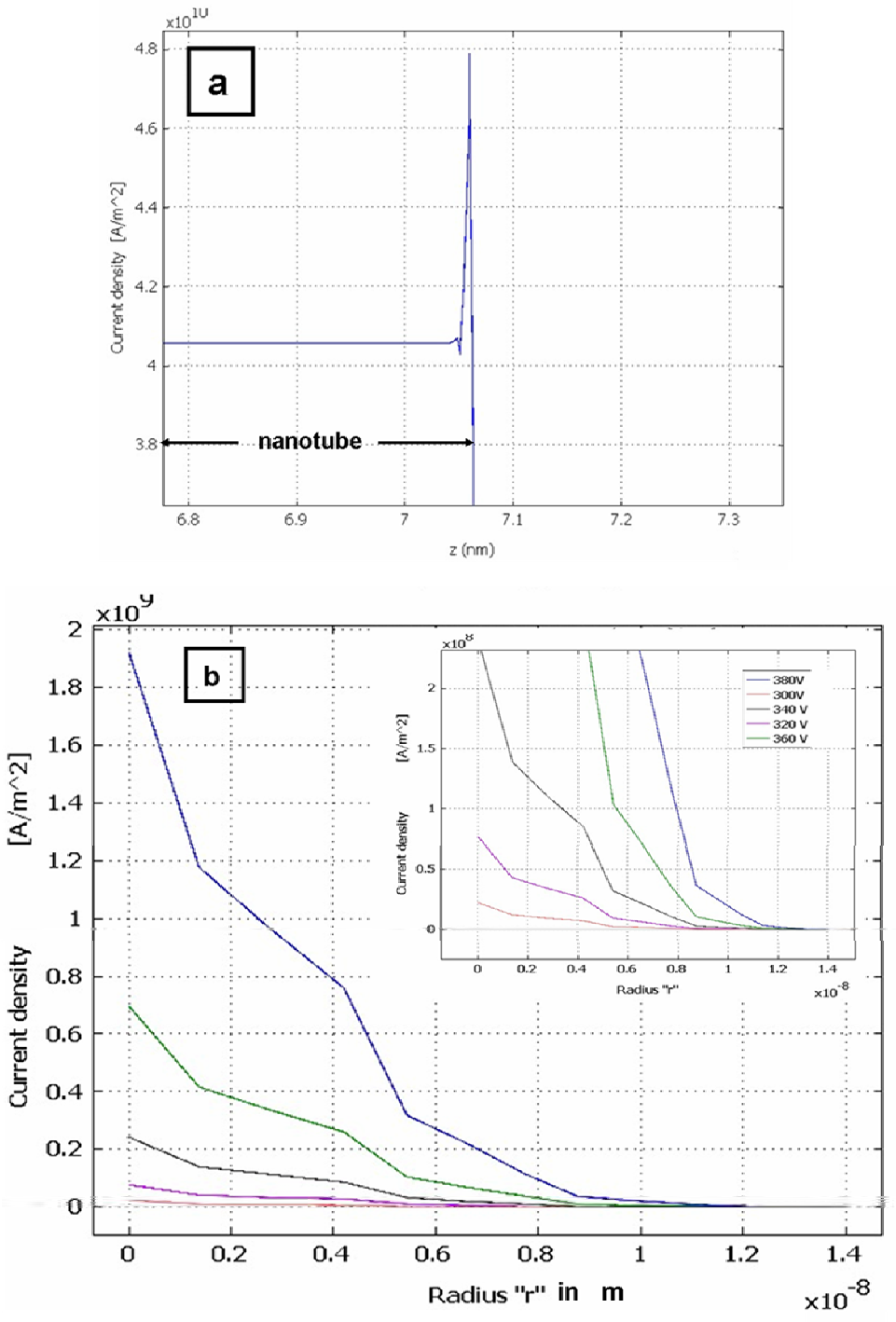

Fig.4. 14 Simulation results showing variation of current density (a) inside a nanotube along a part of its length (z) and (b) showing increasing emission(current density) from the nanotube tip with applied voltage along its radius. The inset shows increased current density from its tips at different applied voltages.

Fig. 4.14 shows the simulated internal current density map along the length of the nanotube. There was no variation in current density within the nanotube and all the emission occurs from the top of the nanotube tip. It was also observed that the emission area of the nanotube tip increases with increasing current density. This observation points out that the common way of plotting current (by averaging current over the tip area) versus voltage 'V' in experiments might not reveal the actual behaviour of a nanotube during field emission. It was also observed that the onset of heating occurs only once emission is from the entire area of nanotube tip.

Larger field enhancement is observed for nanotubes with greater lengths and smaller diameters. Fig. 4.15(a-b) shows the simulated J_{avg}-V ($J = I/\pi r^2$) curves for nanotubes with different diameters (for a length of 5.83 μm) and length (at a diameter of 24 nm) respectively. It predicts that the turn-on voltage is significantly reduced for nanotubes with smaller diameters and longer lengths. This is in agreement with experimental results of Hu[302] and Hansen[303] where they obtained low turn-on voltages for nanotubes with smaller diameters and longer lengths. The simulations also agree well with experimental results that short nanotubes are capable of carrying larger current densities than longer nanotubes[304]. [The tip temperature of a 60 nm diameter, 6 μm long nanotube reaches ~3600 K (T_{max}) at a current density of $1.65 \times 10^{11} A/m^2$ (current of 18 mA) when compared to $3.34 \times 10^{11} A/m^2$ (current of 8 mA) for a 2 μm long nanotube for the same temperature]. Experimental values for current density in the range of 10^{11}-10^{12} A/m^2 has been obtained for individual nanotubes[272] by electrically stressing the nanotube until their breakdown. Thus maximum current densities obtained before emitter burn out during our simulations agrees well with the experimental results of maximum current densities for individual nanotubes[272].

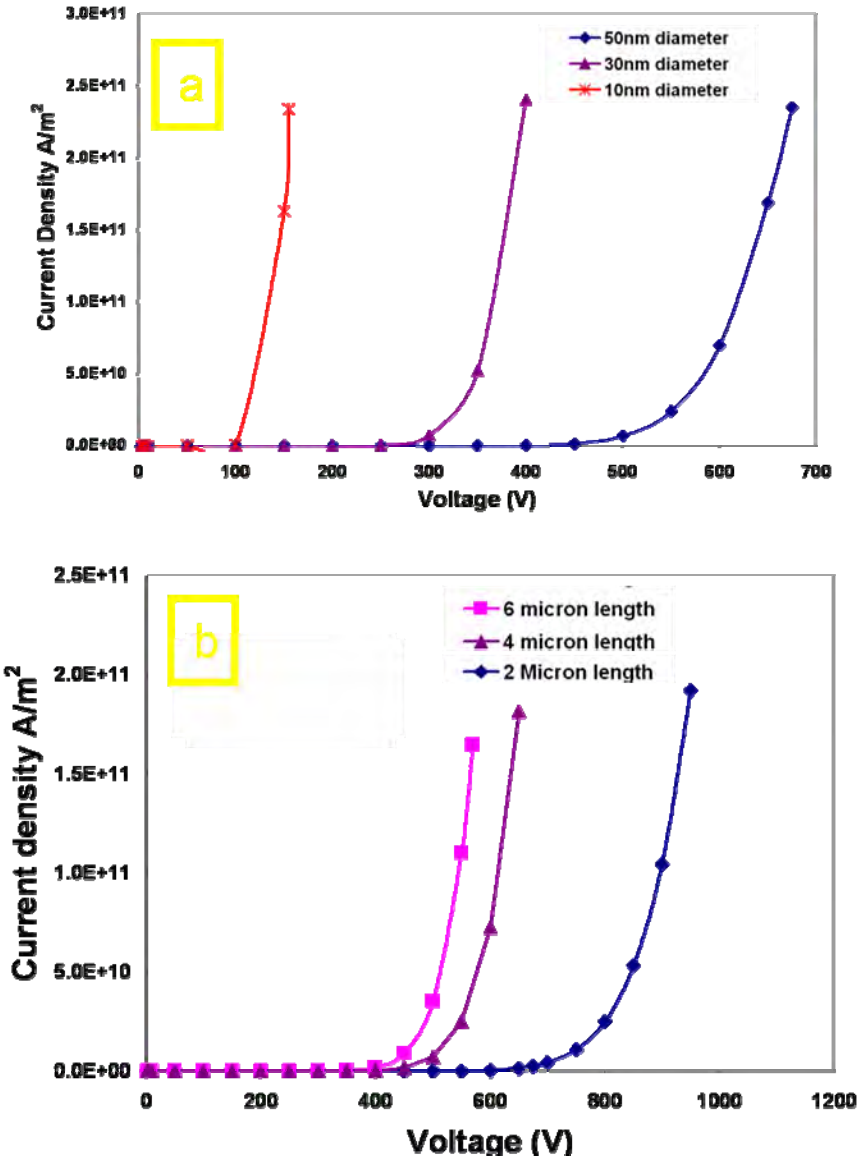

Fig.4. 15 Simulated values of current density at **(a)** different diameters and **(b)** different lengths.

Experiments have shown that the temperature rises during field emission of individual nanotubes of up to 2000 K measured using field emission (FE) electron spectroscopy for current in the μA range[212]. The simulation results [Fig 4.16(a-b)] show that smaller diameter nanotubes attain higher tip temperatures at lower voltages. Fig. 4.16(b) also validates that longer nanotubes emit at relatively low voltages[304] and burn out much faster when compared to shorter nanotubes[305]. This low turn-on voltage and higher currents from longer nanotubes is due to the combined effect of temperature and field emission (Thermo-field emission). The exponential rise in tip temperature is also consistent with experimental results where a sudden burn out of

emitter occurs for a small change in voltage above certain current density values[270, 304].

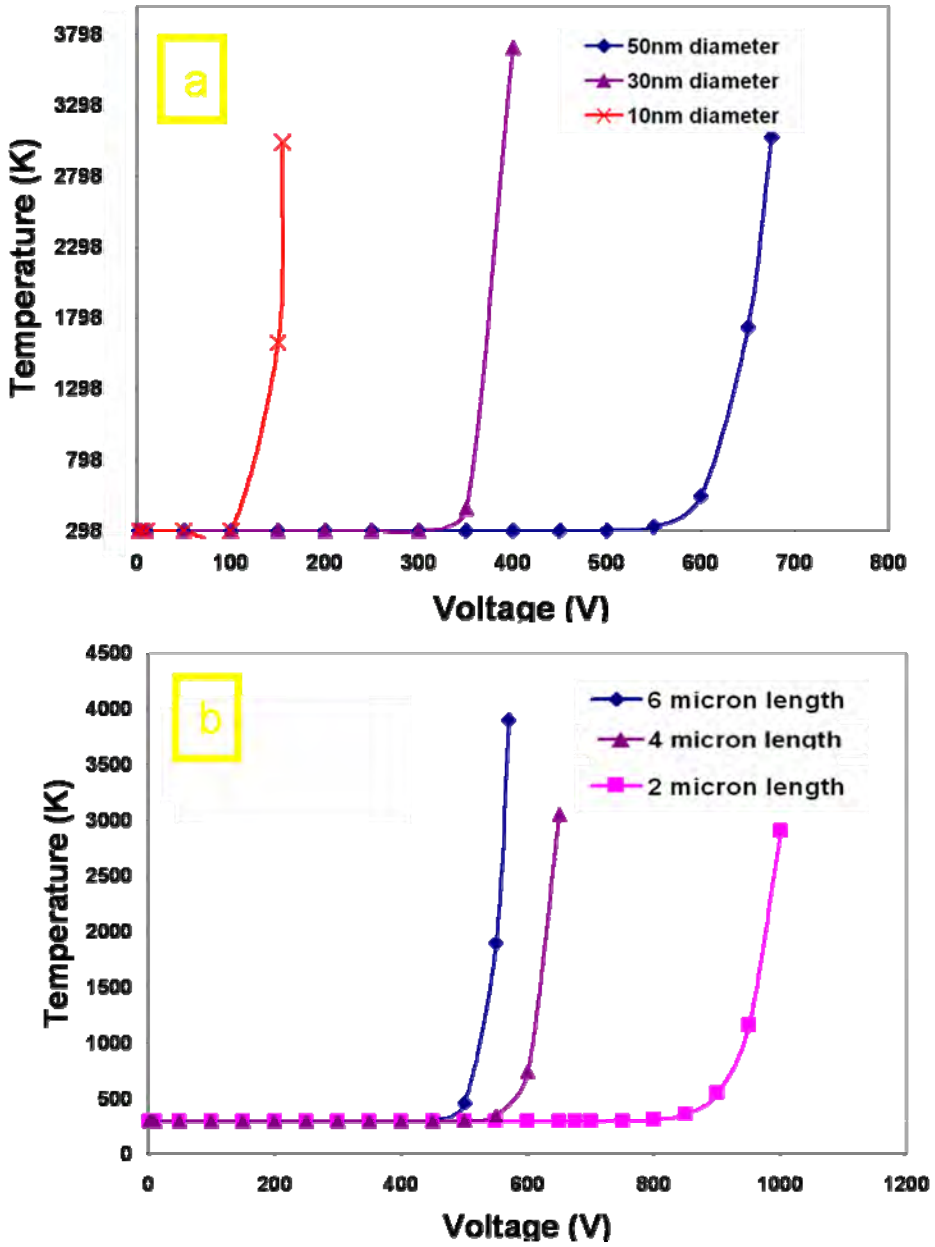

Fig.4. 16 Joule heating of nanotubes at (a) different diameters and (b) different length.

There has been no reliable experimental report of temperature measurements of individual nanotubes during field emission studies. However, depending on the geometrical properties (length and radius) and intrinsic properties (resistivity and thermal conductivity) of nanotubes, heating effects are known to arise at currents in the 0.1 μA to 100 μA range for different nanotubes[210, 306]. The thermal

conductivity of nanotubes is estimated to be in the range of 150-6000 W/m-K[271]. However, there is a significant gap between experiment measurements and theoretical predictions of temperature rises. Our simulation predicts heating effect to arise in the 100 µA to mA range. This anomaly can be due to the assumed constant intrinsic values of electrical resistivity and thermal conductivity. The tip temperature obtained for a 60 nm diameter, 6 µm long nanotube is ~3600 K at 990 W/m-K compared to ~6300 K (ignoring sublimation) at 600 W/m-K because no phase change is included in our model. The simulation also predicts temperature increases without limit as a function of increasing current.

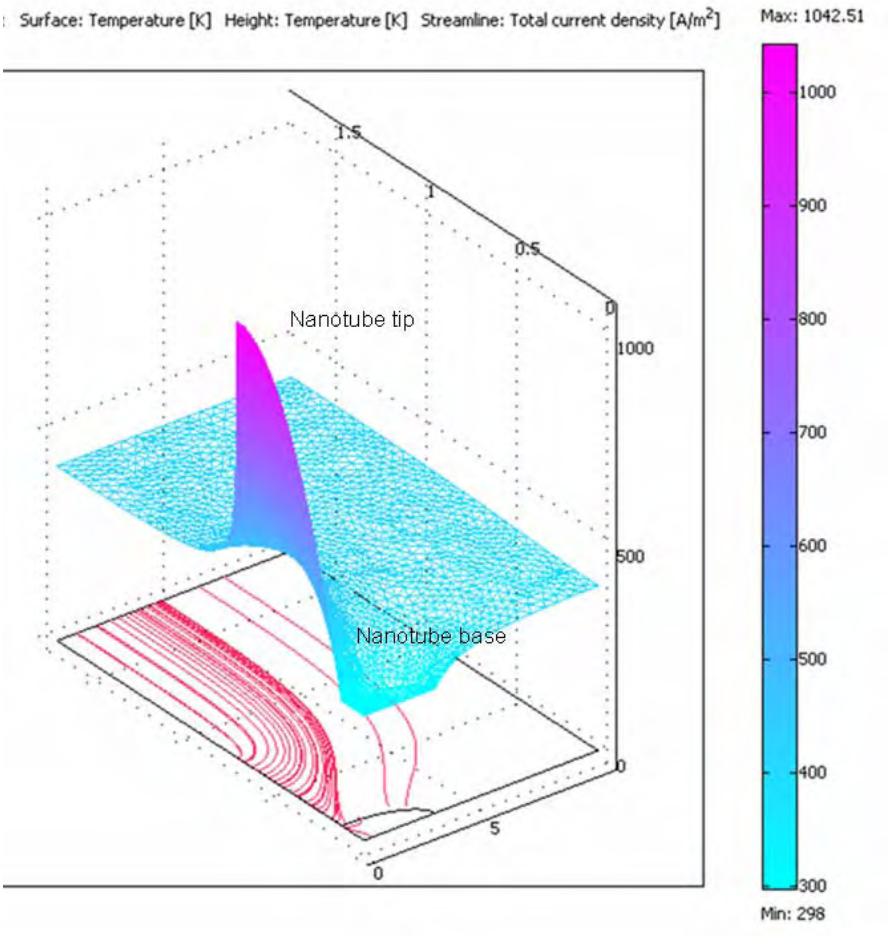

Fig.4. 17 Simulated temperature profile for Milne[272] model nanotube at an applied voltage of 380 V. The figure clearly depicts joule heating originating from the nanotube tip and a decrease in temperature along its length towards the base. **Simulation conditions:** Length – 5.83 µm, diameter – 24 nm with an inter-electrode distance of 13 µm.

The simulations also predicted that the Joule heating originates at the from nanotube tip for high current densities. Fig. 4.17 shows the simulated temperature profile along the length of nanotube. It can be clearly observed that heating originates from the nanotube tip. The temperature starts to decrease along its length towards the base of the nanotube.

This is important since nanotubes are known to undergo structural changes in their tip structure at high fields. These changes can be due to splitting of their apex, shortening or closing of their end caps.

4.4 Conclusion:

The highly anisotropic properties of thermal and electrical conductivity values and the large difference between single-tube and bulk measurements suggest that more extensive studies are needed to provide appropriate property values. The observed anomaly for higher currents obtained from simulation (8 mA in comparison to 2 mA from experiments) is attributed to the assumed constant physical properties of the nanotube. This model also predicts that heating controls the maximum current sustained by the nanotube. There is a need for better experimental results on individual nanotubes characterising the effects of length, radius, temperature and electrode spacing on field emission. The deviations between experimental results and simulations (based on theory) will then shed light on fundamental processes like temperature dependence of physical properties of nanotubes and finally to temperature induced modification.

However, both experiments and this simulation indicate that heat dissipation and thermal breakdown in nanotubes can be minimised by using short nanotubes with smaller diameters. Shorter nanotubes are capable of carrying larger current densities before thermal breakdown occurs. Carbon nanotubes grown using the arc discharge technique are also preferred due to its high temperature during production and lower defects in their structure.

5.0 Results

5.1 Analysis:

The continuous process developed in this thesis is designed for carbon nanotube growth on a substrate acting as an anode. The arc treated substrate surface was analysed using Scanning Electron Microscopy (SEM). The sample substrates were coated with a conductive film of gold since good sample conductivity is essential for this method of analysis. After nanotube deposition, a 2 nm gold film was placed over each sample by treating it in a thin film deposition unit (4 minutes at 20 mA). For SEM analysis, the samples were glued to the object slide using a double-sided sticky carbon tape for analysis.

5.2 Standard:

The samples were analysed in both in a low resolution SEM and FESEM to determine the any occurrence of carbon nanotubes and a conclusion was drawn relating it to various operating conditions/parameters inside the reactor. The highest resolution achieved in both the SEMs was 5 nm and a mention of diameters in this section constitutes an error of ± 5 nm. The structures observed were identified to be nanotubes when their diameters were less than 100 nm. A quantitative analysis of nanotube yield was very difficult, so an impression of the quantity of nanotubes in comparison with each other is stated. The length and diameter distribution of nanotubes was hard to quantify from the micrographs. The statistical software (Sigma Scan Pro 5.5) was used for micrographs with high magnification to analyse nanotube diameters and lengths. The nanotubes were said to be ‘abundant’ if their distribution was spread uniformly over the arc treated area. The nanotubes were said to be ‘plentiful’ if their coverage on the sample surface was dense (more than 50 - 70%). ‘Very few nanotubes’ was a condition where the distribution of nanotubes was sparse (coverage less than 30%). This condition was usually associated with patches/ segments of nanotubes occurring on the substrate sample. ‘No nanotubes’ were said to

be observed if their coverage was arbitrary (less than 5% of the observed sample surface). Besides the above conditions, the following types of carbon forms were commonly observed, as shown in Fig. 5.1.

- Nanorods: Tubular structures with diameters in the range of 200 nm-1 µm.
- Cauliflower like forms: Round carbon deposits resembling a cauliflower with their diameters in the micron range.
- Sintered carbon deposits.
- Flake-like carbon forms.

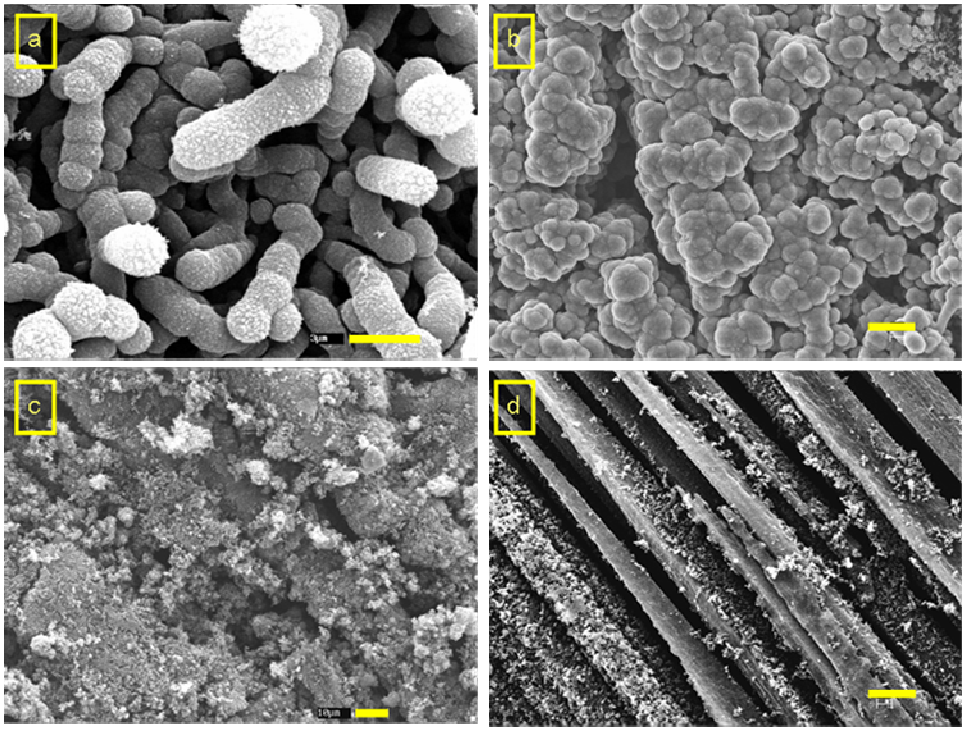

Fig.5. 1 Different types of commonly observed carbon forms. (a) Carbon nanorods (b) Cauliflower like carbon forms (c) Sintered deposits and (d) Flake like carbon forms.

5.3 Influence of the type of substrate:

The aim of the first series of runs was to determine the most suitable substrate for depositing carbon nanotubes. Three different types of substrate were thus chosen and

experimented with. All the tapes showed a distinctive arc treated path with a width between 7-14 mm after arc treatment.

The Carbonics Gmbh substrate (section 3.1.3.5) which could endure prolonged exposure to the arc was used for most of the runs. The path of the arc on this substrate appeared as grey or black colour and could clearly be observed by eye. The width of the arc attachment was found to vary with the inter electrode gap, ranging from 7 mm at smaller gaps of 3 mm to about 14 mm at the largest gap of 7 mm. The arc treated path appeared to be black at smaller gaps and grey in colour at the largest gap. Variation of various arc parameters like arc gap, tape speed could easily be achieved with Carbonics due to its high specific weight and thickness. The rupture strength of the tape decreased significantly when operated at the smallest arc gap and low tape speeds, but appeared to sustain its original strength at larger arc gaps and higher speed. Carbon nanotubes were generally found on these tapes at certain optimum parameters. Fig. 5.2(a-b) shows a typical arc treatment path and nanotube occurrence on a Carbonics substrate.

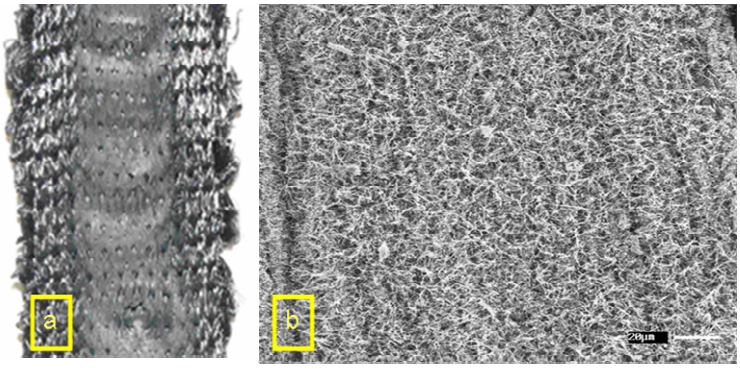

Fig.5. 2 (a) Typical arc treated path on a Carbonics substrate (actual size) and **(b)** enlarged view of carbon nanotube distribution in the arc treated area. *(Scale bar – 20 µm)*

It was hard to assess the occurrence of carbon nanotubes on the inner filaments of the substrate beneath the outer fibres from SEM images. However, the growth/deposition of nanotubes appeared to be confined to only a few layers of fibres at the arc treated side (tape facing the cathode). No nanotubes could be observed on the opposite side (touching the anode) of the arc-treated path, as shown in Fig. 5.3(a-b), though a black coloured line could be seen on the anode side outlining the periphery of the arc treatment. (approximately equal to the diameter of the anode)

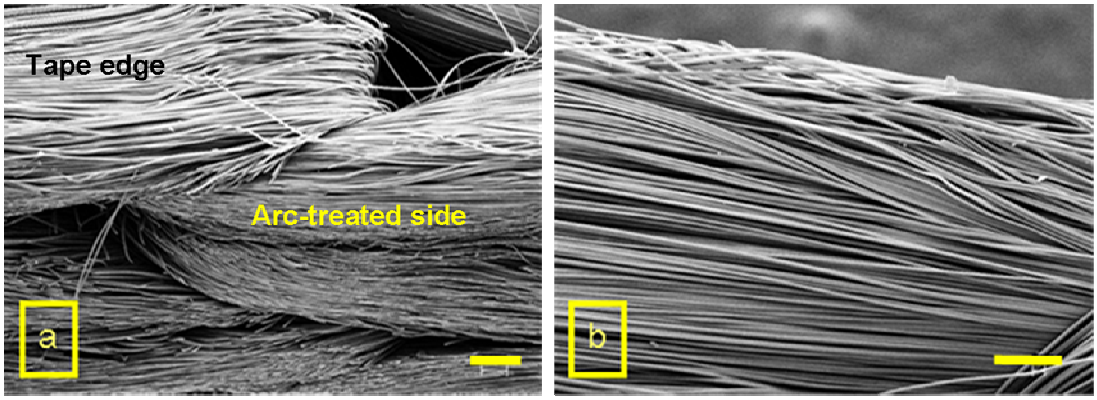

Fig.5. 3 (a) Edge view of the tape showingcarbon nanotube distribution on Carbonics substrate *(Scale bar-200 µm)* and **(b)** SEM image of the opposite end of substrate showing no signs of nanotube.*(Scale bar – 100 µm)*

Sigmatex tapes were hard to work with due to their smaller thickness (0.8 mm) and texture. The path of the arc treatment for these tapes always appeared black in colour and could clearly be seen by eye. The upper filament layers of arc treatment were often vaporised through at smaller inter-electrode gaps and slow speeds. The arc often burnt holes through the tape for prolonged exposure to the arc. These tapes were seldom chosen while experimenting with arc parameters and were used only once optimum parameters were known. Abundant nanotubes could be observed on this substrate type for a range of arc parameters close to the general optimum. The nanotubes obtained on this substrate appeared to have smaller diameters and were associated with fewer impurities when compared with nanotube occurrence on the Carbonics substrate operating at the same parameters. No nanotubes could be seen on the opposite end side to the arc treated path but a black colouration could be seen over the whole arc treated area. Carbon foam-like forms was also found on some samples. Fig. 5.4 shows an overview of the arc-treated path and nanotube occurrence on a Sigmatex substrate.

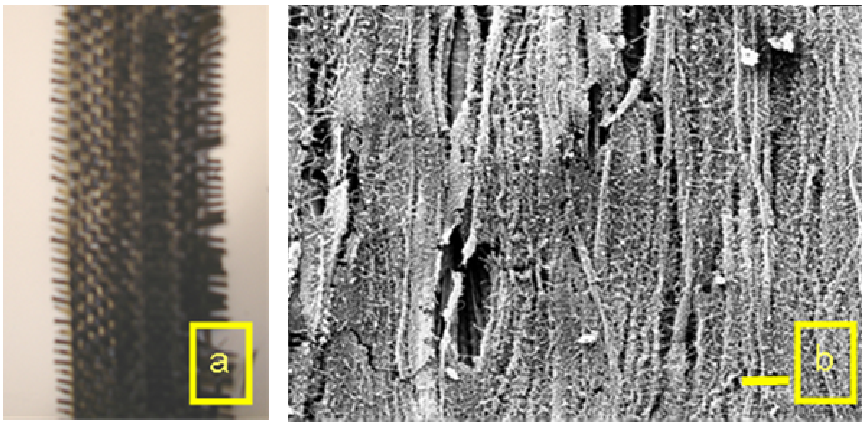

Fig.5. 4 (a) Typical arc treated path on a Sigmatex substrate (actual size) and **(b)** Enlarged view showing carbon nanotube distribution in the arc treated area. *(Scale bar – 20 µm)*

The third type of tape tested was the uni-directional carbon substrate and this was the hardest to work with. The glass binder which held individual fibres of the tape together always vaporised before reaching the spot of arc discharge. This often led to extreme fraying of the fibres and resulted in bridging across to the cathode. The speed of the tape or the arc gap had to be increased eventually to avoid any short and to obtain some form of arc treatment on the tape. This always resulted in non-optimum parameters for nanotube production.

The arc treatment for the uni-directional tape was always somewhat uncontrolled and sometimes a bunch of fibres adhered to the anode during the tape movement. This often led to intermittent arc treatment on the tape for short distances (< ~200 mm). No nanotubes were observed on any of the uni-directional tapes and their analysis often revealed only small spherical carbon forms.

5.4 Influence of inter-electrode gap:

The arc gap is one of the major parameters which influence the formation of carbon nanotubes. The aim of these experiments was to find the favourable arc gap for carbon nanotube growth and to identify the substrate temperatures at this gap. This would also help in predicting a plausible carbon nanotube growth mechanism in arcs. The runs to find the optimal arc gap for carbon nanotube occurrence were performed using the Carbonics substrate. A constant tape speed of 3 mm/s was maintained during these

runs. The arc current was 16 A and a 3 mm diameter cathode (impurity < 6 ppm) was used. The inter-electrode gap was varied in the range of 2-8 mm. The arc became highly unstable and wandered for arc gaps larger than 8 mm resulting in sheen-like treatment on the substrate. An arc gap of less than 2 mm often resulted in burning a hole through the tape. The short arc gap range (2-4 mm) led to graded arc treatment on the substrate which is grey and black in colour and was accompanied by hissing. The arc operated in a quiet mode for the 4-6 mm gap range. The appearance of the arc path at these arc gaps was always grey in colour with a black tinge at the periphery of the arc treated path.

The substrate surface temperature was deduced using the image intensity method as described in Chapter 3 (section 3.1.4.2) and in the report of Yusoff[307]. A temperature profile across the arc attachment on the substrate was obtained at each arc gap. Fig. 5.5 shows the temperature profile of the substrate surface at various arc gaps. The highest substrate temperature of ~3850 K was obtained for an arc gap of 2.7 mm. The temperature dropped to ~3650 K as the arc gap was increased to 5.0 mm. The substrate temperature increased again to ~3800 K when the arc gap was enlarged to 7.8 mm.

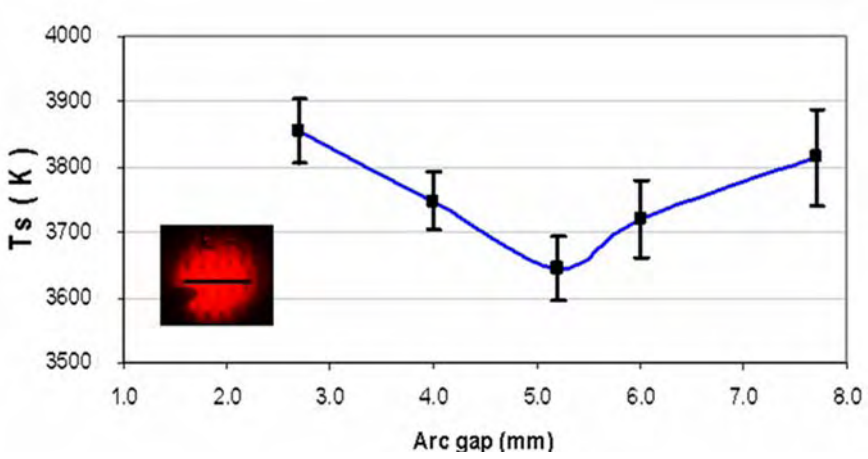

Fig.5. 5 Substrate temperature for different arc gaps for a current of 16 A, with a substrate velocity of 3 mm/s. *(The inset in the graph shows the substrate surface during arc treatment)*

The width of arc treatment on the substrate also varied with the change in inter electrode gap, as shown in Fig. 5.6(a-c). The width of the arc treated path was around 6 mm at an arc gap of 3 mm with grey and black coloured patch like deposits. The width of the arc treatment increased (8-10 mm) with a uniform grey coloured treatment at an arc gap of 5 mm. The arc was more widespread at an arc gap of 8 mm

and with a sheen-like treatment on the substrate. The anodic current densities estimated from the momentary area of arc attachment on the substrate are given in Table. 5.1.

Arc gap (mm)	Current density (A/mm^2)
2.7	0.566
4.0	0.610
5.2	1.261
6.0	0.885
7.7	0.720

Table 5. 1 Anode current densities at various gaps.

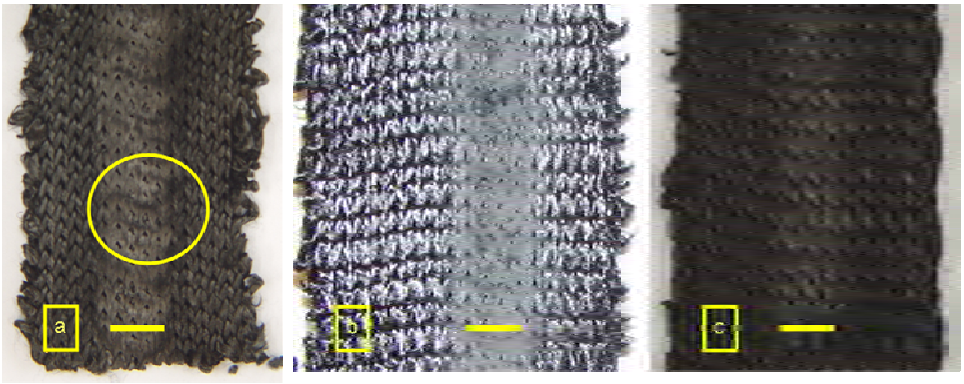

Fig.5. 6 Substrate surface depicting width and type of arc attachment at different inter electrode gap **(a)** arc gap of 3 mm showing patch like deposits (circled in yellow) **(b)** arc gap of 5 mm showing a increase in width and uniform treatment and **(c)** arc gap of 8 mm showing sheen like treatment.[Scale bar = 6 mm]

Fig. 5.7(a-e) shows the micrographs of nanotubes obtained at various gaps in the range of 2-8 mm. Abundant nanotubes with lengths of around 8 µm and with minimal presence of other elemental carbon forms were obtained at an arc gap of 5.2 mm as shown in Fig. 5.7(c). Few nanotubes, with smaller lengths (~4 µm) were obtained for short arc gaps (range 2-4 mm) and these were associated with nanoparticles. These substrate deposits resembled pine trees with large nanorods at the bottom as shown in Fig. 5.7(a)-(b). The micrograph obtained at long arc (range 6-8 mm) showed few or no signs of nanotubes as shown in Fig. 5.7(d), but the micrographs at the longest arc gap range usually depicted crumbled mass of carbon forms, as shown in Fig. 5.7(e).

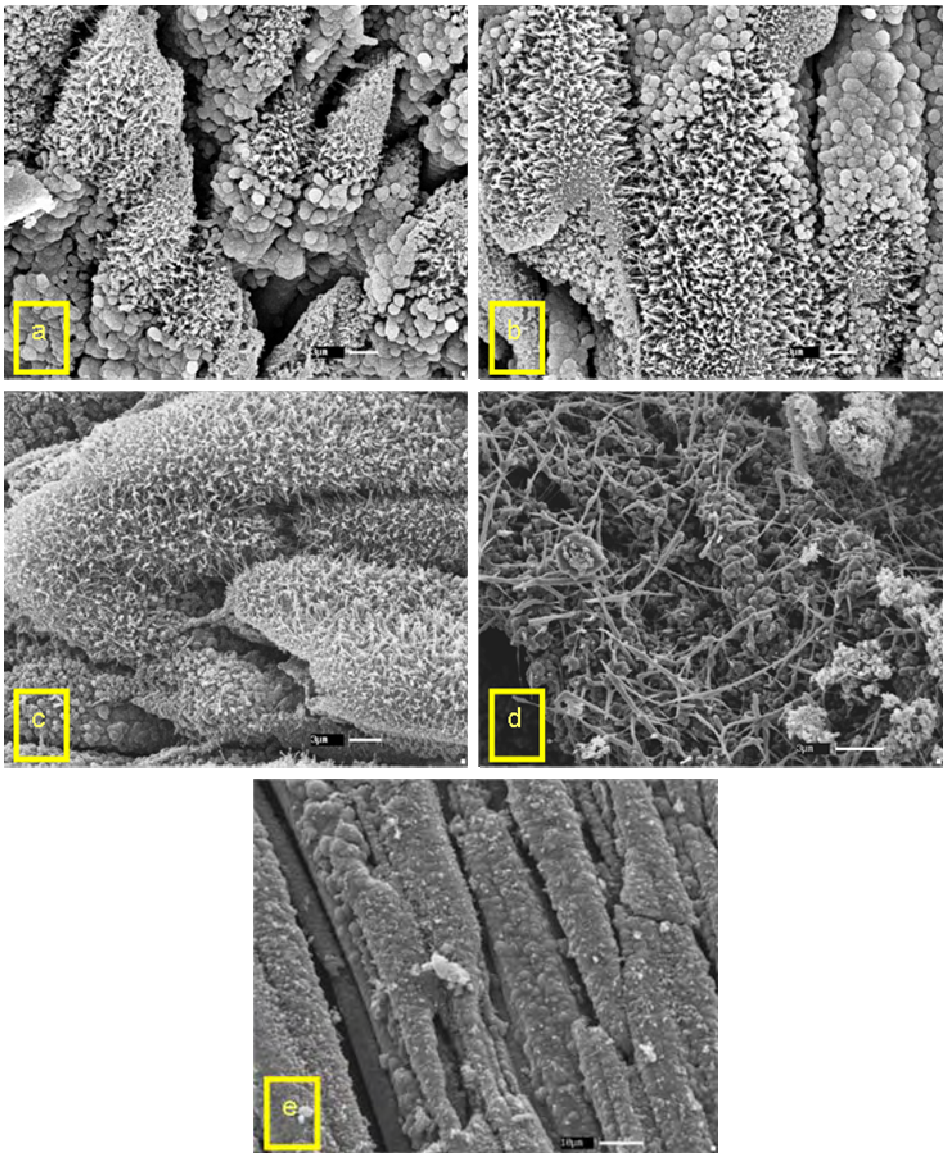

Fig.5. 7 SEM of the substrate at different arc gap [X]. **(a)** X=2.7 mm, depicting nanorods at the bottom. **(b)** Short arc-X=3.5 mm, showing an increase in density of nanotubes over nanorods. **(c)** X=5.2 mm, optimal gap with evenly distributed nanotubes. **(d)** X=6.0 mm, nanotubes apparently start to sinter with appearance of other carbon forms. **(e)** Long arc-X=7.7 mm, deposits apparently sintered into useless mass. (*Micrographs (a)-(d) have a scale bar of 3 µm, and (e) has a scale bar of 10 µm)*

Experiments were performed with a 8 mm diameter cathode and a 3 mm diameter cathode at high currents to observe the validity of the optimal arc gap range for different values of cathodic current density.

5.4.1 3 mm diameter cathode runs:

The first set of experiments comprised of 20 A current on a 3 mm diameter cathode with the tape speed set at 3 mm/s. The tape was excessively damaged when operated with an inter-electrode gap of less than 5 mm. The operative range of arc gaps with the above parameters was 5-12 mm, above which the arc became highly unstable. The substrate temperatures revealed substantially higher temperatures over the explored gap range as shown in Fig. 5.8.

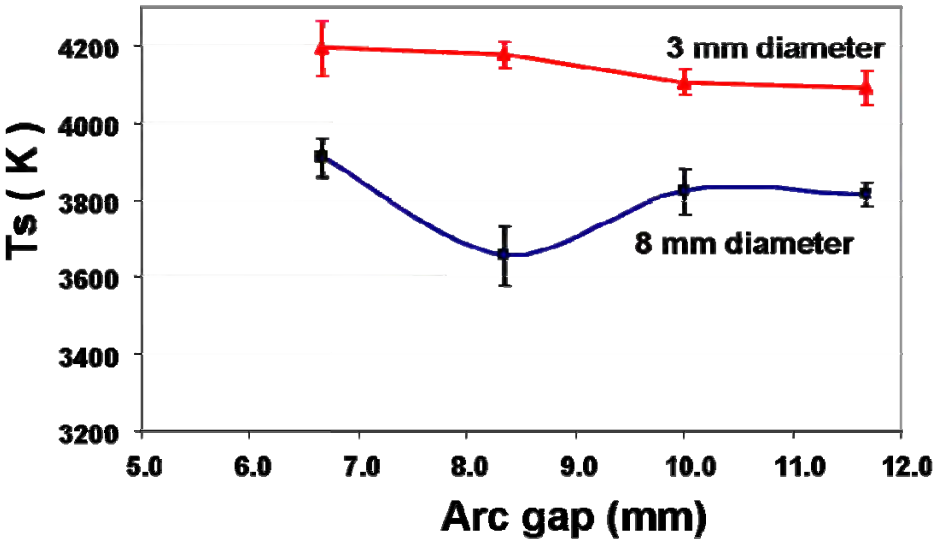

Fig.5. 8 Substrate surface temperatures at different arc gaps for a current of 20 A and a substrate velocity of 3mm/s.

The tape speed was also varied between 3 mm/s to 5 mm/s to obtain a stable arc attachment on the tape at short arc (2-5 mm) and to reduce the tape damage. However, average substrate temperatures close to 4100 ± 100 K were observed at all gaps under the various explored parameters. No nanotubes were observed under the explored gap range of 5-12 mm. The micrographs reveal the occurrence of cauliflower-like carbon forms distributed uniformly at all arc gaps associated with little or no nanoparticles as shown in Fig. 5.9(a-d). Large nanorods with no signs of nanotubes were observed in the long arc (10-12 mm) range, as shown in Fig. 5.9(d).

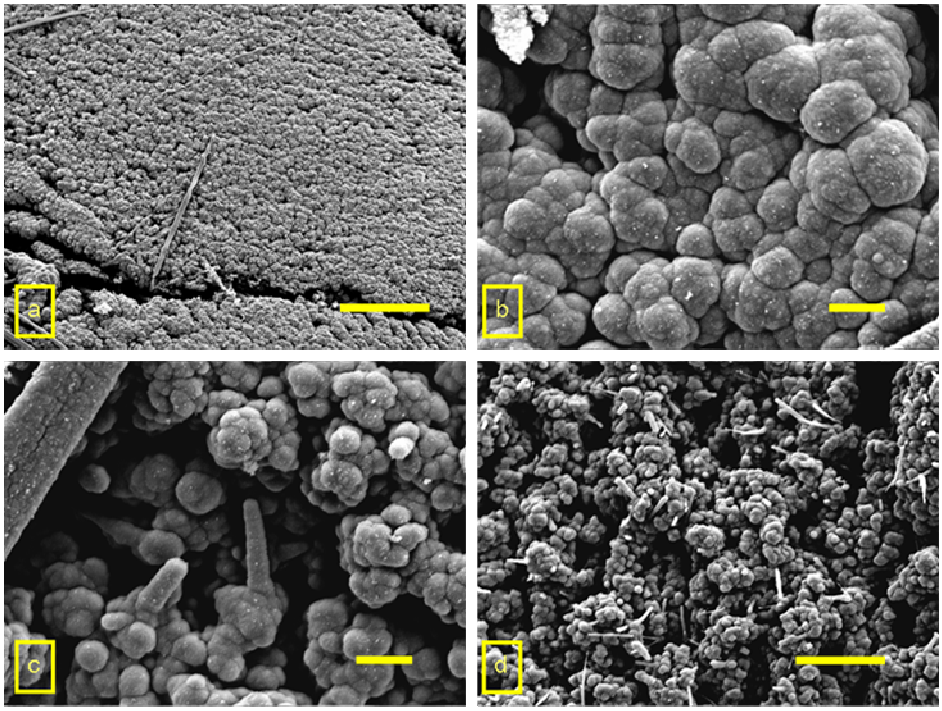

Fig.5. 9 SEM of the substrate at different arc gap [X] for 3 mm diameter cathode at a tape velocity of 3 mm/s and current of 20 A. **(a)-(c)** shows cauliflower like carbon forms for an arc gap of 6.4, 8.4 and 10 mm respectively and **(d)** showing increased number of carbon nanorods at an arc gap of 12 mm. [*Micrographs (a) and (d) have a scale bar of 20 µm, with (b) and (c) having a scale bar of 5 µm]*

5.4.2 *8 mm diameter cathode runs:*

The other set of experiments were performed with 20-22 A on 8 mm diameter cathode operating at a tape velocity of 3 mm/s to explore the optimal arc gap for nanotube formation. The average substrate temperatures obtained with an 8 mm diameter cathode was substantially lower than the temperatures observed when operated with a 3 mm diameter cathode as shown in Fig. 5.8. A considerably higher substrate temperature of ~3850 K was obtained for an arc gap of 6.5 mm. The temperature dropped to ~3650 K as the arc gap was increased to 8 mm. The substrate temperature increased again to ~3800 K for long arcs (10-12 mm).

Fig. 5.10(a-e) depicts the morphology of nanotubes obtained over the gap range of 4-12 mm. Plentiful nanotubes [Fig 5.10(c)] were observed at an arc gap of 8 mm corresponding to an average substrate temperature of ~ 3650 ± 50 K. Cauliflower like forms were obtained for short arc gaps (5 mm) and large nanorods were seen as the gap increased to 6.4 mm. The micrographs obtained at long arc (range 10-12 mm)

showed few signs of nanotubes [Fig.5.10(d-e)]. Etched fibres with sharp and pointed tips were obtained at the largest arc gap of 12 mm [Fig 5.10(e)] associated with flake like carbon deposits on individual fibres. Abundant nanotubes [Fig 5.10(e)] associated with many impurities were obtained at an arc gap of ~8.2 mm. However, the length of nanotubes obtained at the optimal arc gap of 8.2 mm (around 3 µm) was shorter than the length of nanotubes observed at an arc gap of 10 mm (~6 µm).

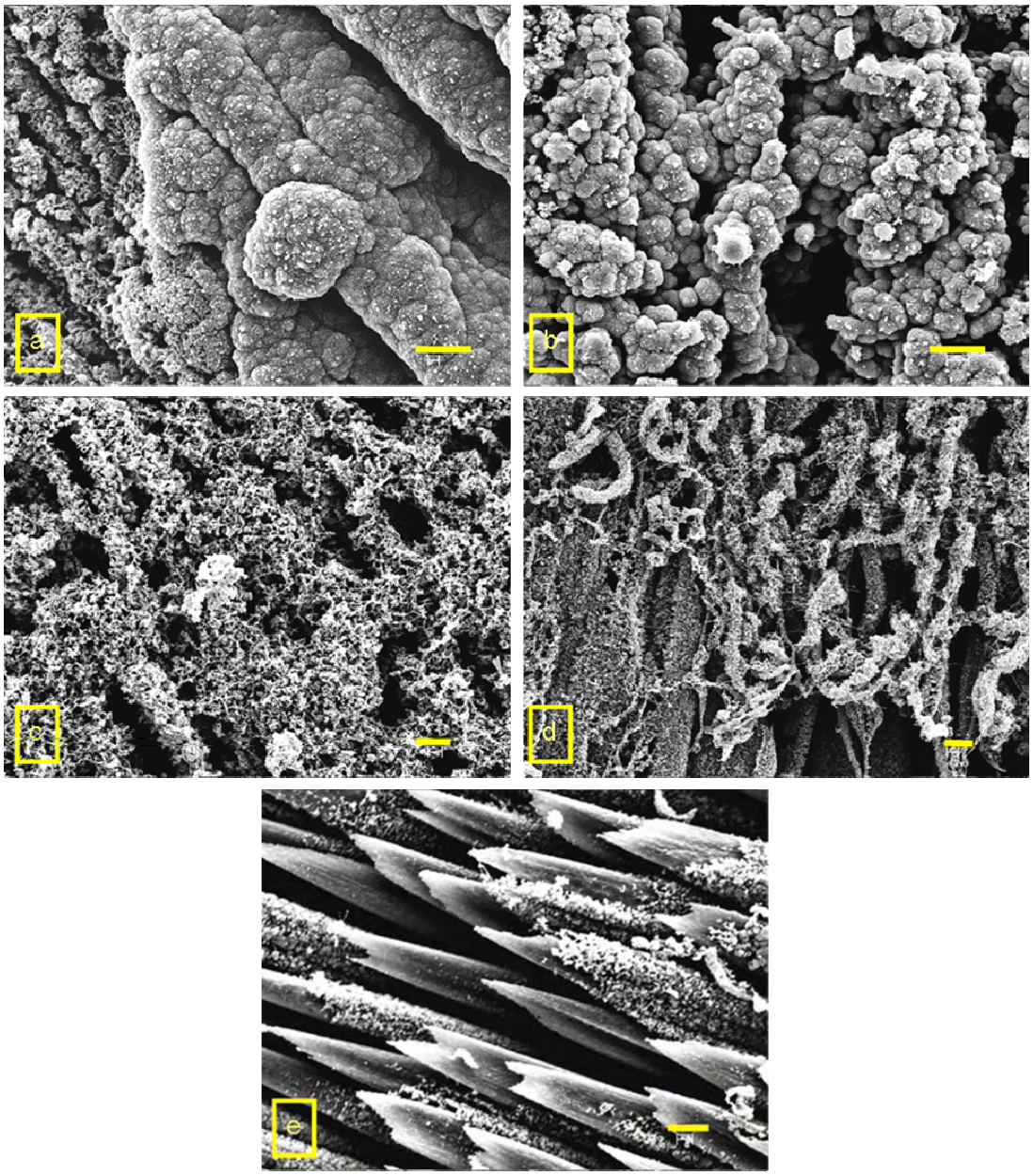

Fig.5. 10 SEM of the substrate at different arc gap [X] for 8 mm diameter cathode at a tape velocity of 3 mm/s and 20 A. **(a)** X=5.0 mm, depicting cauliflower like forms and other impurities **(b)** X=6.4 mm, showing an increase in density of nanorods. **(c)** X=8.2 mm, optimal gap with evenly distributed nanotubes. **(d**) X=10.0 mm showing less dense carbon nanotubes with longer lengths and **(e)** X=12.0 mm showing etched carbon fibres associated with flake like deposits. [All *Micrographs have a scale bar of 5 µm]*

5.5 Influence of substrate velocity:

The aim of these experiments was to find the optimum substrate velocity and to observe its influence on the substrate temperature to be able to relate it to carbon nanotube formation. The details of these experiments are explained in Chapter 3 (section 3.1.5.2). An optimum arc gap of ~5 mm for a current of 16 A and cathode diameter of 3 mm as found from our earlier experiments was maintained for all the runs.

Fig. 5.11 shows the temperature profile of the substrate surface at various velocities. A temperature of ~3750 K was observed at a tape velocity of 0.8 mm/s which decreased to 3650 K at a tape velocity of 2.5 mm/s. The average substrate surface temperature increased again to 3750 K at a tape velocity of 4.2 mm/s before decreasing back to 3600 K at a velocity of 5.6 mm/s.

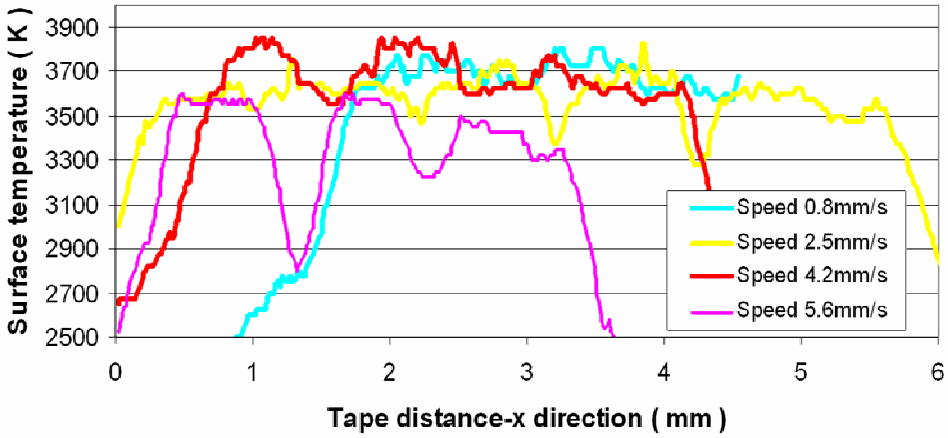

Fig.5. 11 Temperature of the substrate at various velocities for an arc gap of 5 mm for a 3 mm diameter cathode at a current of 16 A. *(Error in temperature measurements ±50 K)*

The tape velocity also influenced the nanotube yield as shown in Fig. 5.12(a-e). Spherical carbon forms were observed at a velocity of 0.8 mm/s with a greater presence of nanotubes at a speed of 2.5 mm/s. Abundant nanotubes were seen at a tape velocity of 3 mm/s whereas honeycomb-like structures were observed at a velocity of 4.2 mm/s. Graphitic flakes were observed on individual carbon fibres for a tape velocity of 5.6 mm/s.

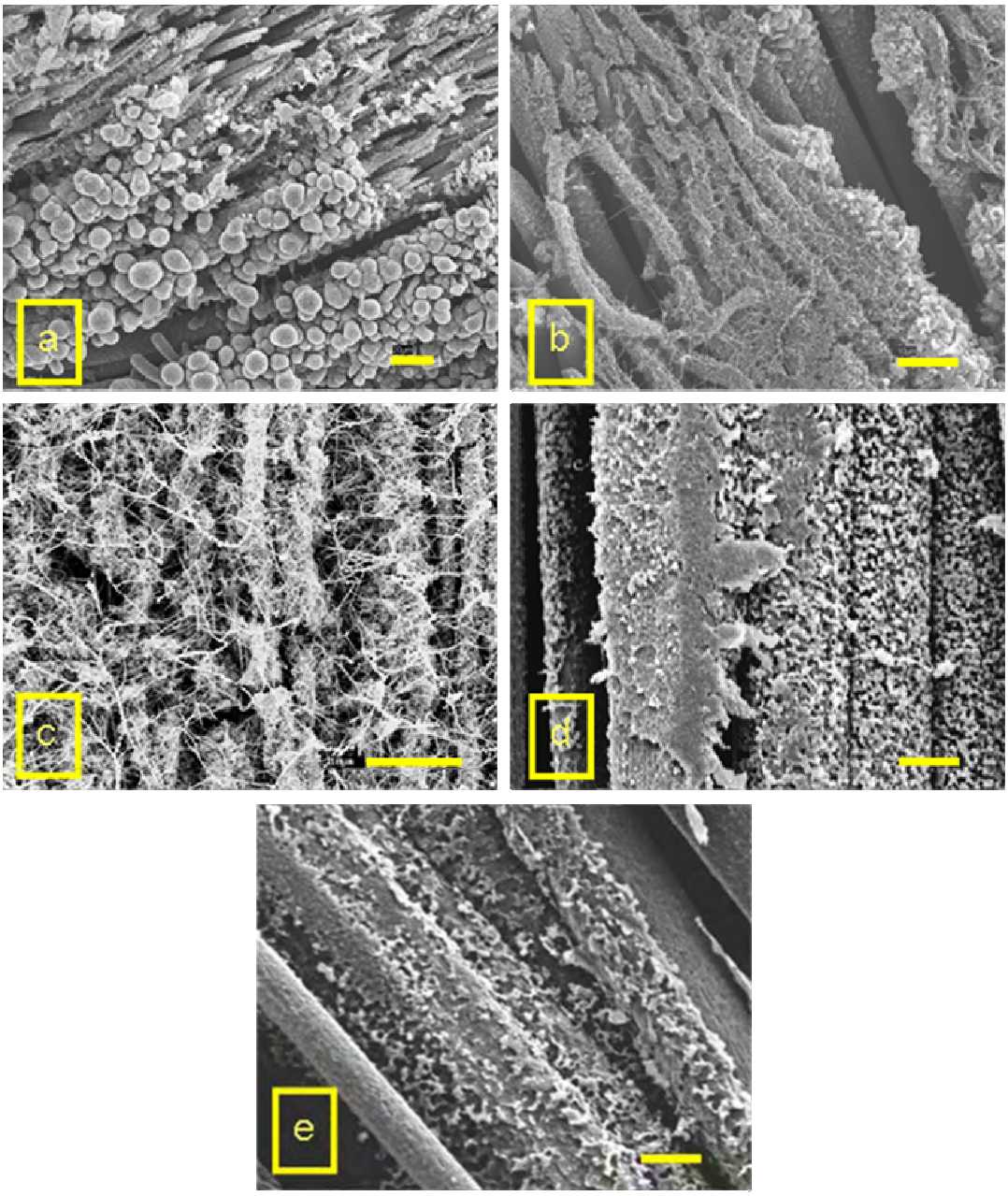

Fig.5. 12 SEM of substrate surface at different velocities [V]for 3 mm diameter cathode at a current of 16 A.**(a)** V=0.8 mm/s, depicting cauliflower like deposits due to large size and density of carbon **(b)** V=2.5 mm/s, showing nanotubes with other carbon forms **(c)** V=3 mm/s, showing nanotubes deposited on original carbon fibre frame work. **(d)** V=4.2 mm/s, honey comb like structures on fibre with sintering. **(e)** V=5.6 mm/s, showing fused graphitic flakes on individual fibre. *[All micrographs have a scale bar of 10 µm]*

5.6 Effect of flushing:

The aim of these experiments was to observe any change in nanotube purity by providing a gas/gas mixture flow through the porous anode during arc discharge. The room temperature velocity profiles and the effect of anodic flushing on various substrate types were earlier investigated by Querrioux[17] and can be found in his report. However, the existence of an optimum gap range and substrate speed was not identified during his experiments. The calibration chart relating rotameter flow rates with actual flow rate of nitrogen gas through the anode can be found in Appendix F. In this work, Carbonics and Sigmatex tapes demonstrated common effects on the arc. The arc attachment was stable for flow in the range of 0-0.6 L/min for Carbonics tape above which the attachment became highly unstable. The Sigmatex tapes could endure only low flushing velocities through the anode. The arc attachment for Sigmatex tapes was stable for flow rates up to 0.3 L/min above which the arc wandered and became highly unstable. However, providing this anodic flushing had no significant effect on average substrate temperatures for both types of substrate. The average substrate temperature remained essentially constant at 3700 ± 50 K, as shown for the Carbonics tape in Fig. 5.13(a).

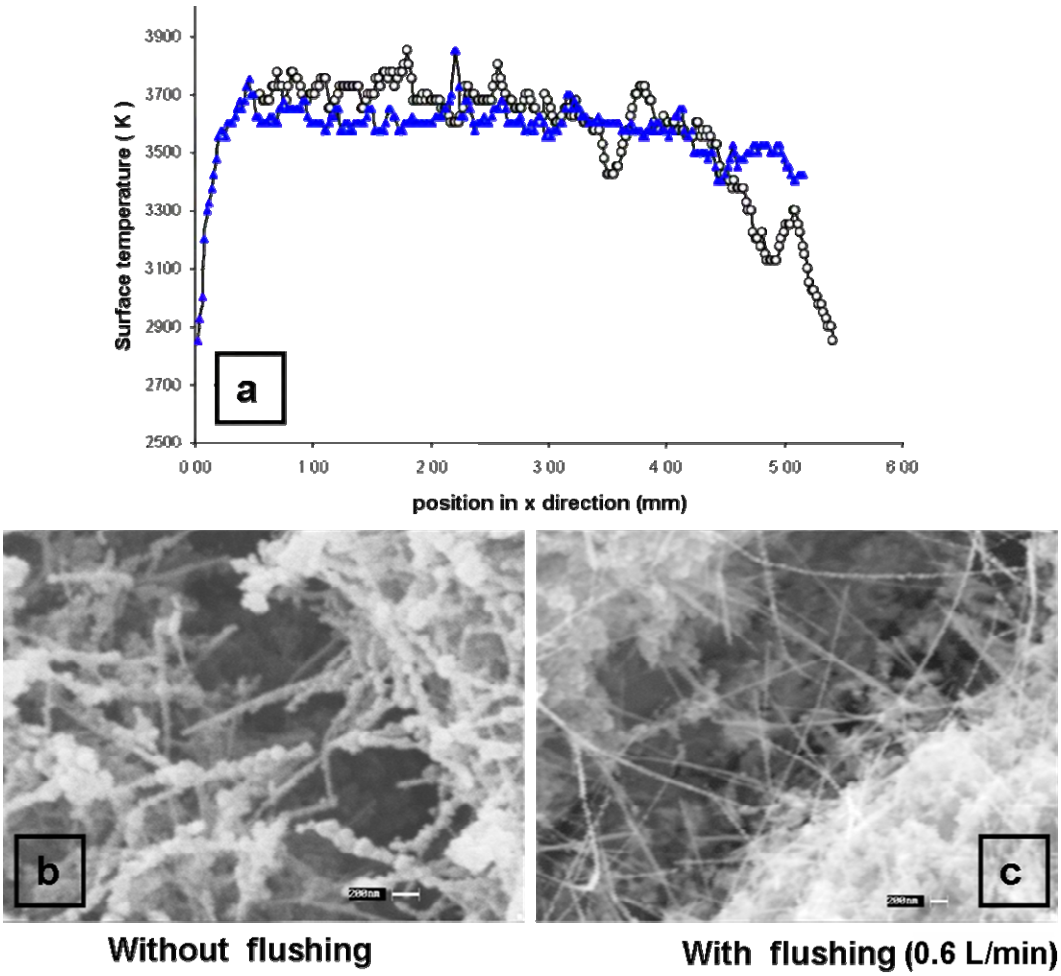

Fig.5. 13 (a) Substrate surface temperature across the Carbonics substrate at 5.2 mm gap at 16 A current for , —O— no flow and —▲— 0.6 L/min nitrogen flow showing little variation and **(b, c)** SEM showing the effect of flushing using a Ar-N_2 gas mixture. *(Scale bar-200 nm)*

Fig 5.13(b) shows micrographs of the substrate surface and some difference in nanotube quantity and quality obtained by flushing compared to no anodic flow. Some nanotubes devoid of other carbon forms are observed when the substrate is flushed by Ar – N_2 gas mixture in spite of little variation in the substrate surface temperature.

These increases in the gas velocity through the anode appear to cause a small shift in nanotube diameter distribution to lower values, as shown in Fig. 5.14. The micrographs were analysed using the Sigma Scan software. However, the number density of nanotubes remained relatively constant as the flow velocity increases. The average diameter of nanotubes was ~ 45 ± 5 nm at a flushing velocity of 0.19 m/s when compared to an average diameter of ~60 ± 5 nm at 0.15 m/s. It is also seen from Fig. 5.14(d) that some nanotubes with diameters in the 10 nm range were observed at the maximum flushing velocity of 0.19 m/s.

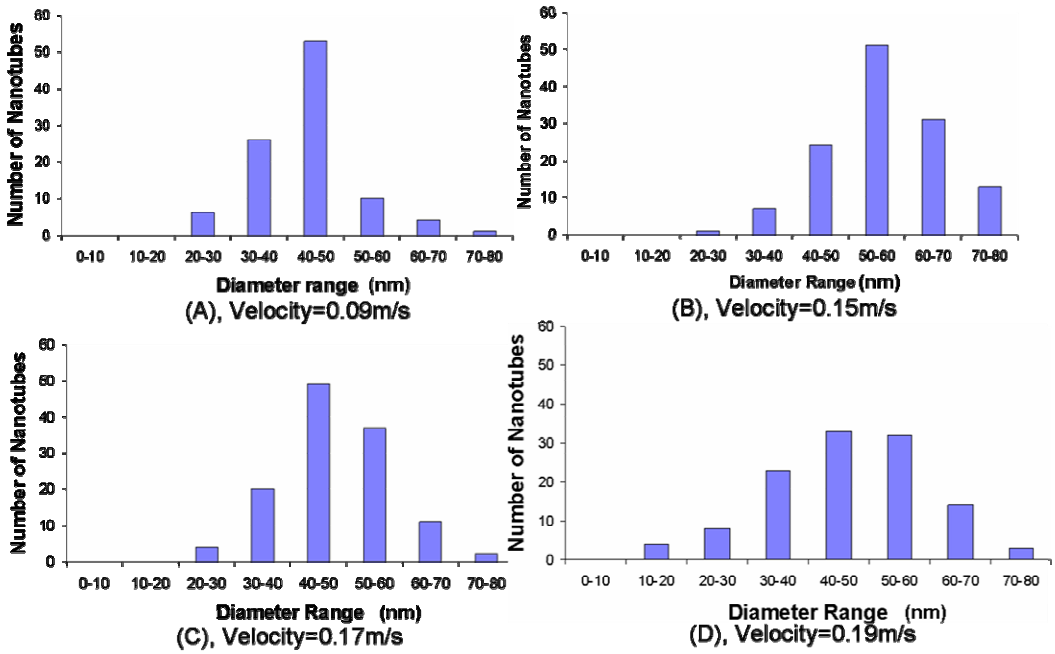

Fig.5. 14 Histogram of carbon nanotube diameters at various flushing velocities. The diameters of nanotubes were analyses using Sigma Scan Pro 5.5 software. *[Note: nanotubes with smaller diameters start to appear at higher flushing velocities]*

5.7 Influence of inert gas concentration:

The objective of these runs was to explore the effect of different inert gases and their concentration on the substrate surface temperature and subsequently on carbon nanotube occurrence. This set of experiments were performed with helium and argon as buffer gases in the reaction chamber, not only added to nitrogen but also pure at 1 atm. The concentration of argon and helium when mixed with nitrogen was varied in the range of 0-50,000 and 0-20,000 ppm respectively. The initial set of experiments was performed in a pure inert gas at 1 atm to find the optimal gap range. The effect of inert gas concentration on nanotube occurrence was analysed by mixing the gases with nitrogen at the optimal arc gap in the range mentioned above.

5.7.1 *Argon:*

Fig. 5.15 shows the temperature profile of the substrate surface for gaps in the range of 3-8 mm. A substrate temperature of ~4000 K was obtained for an arc gap of 3.4 mm. The temperature dropped to ~3850 K as the arc gap was increased to 5 mm. The substrate temperature dropped further to ~3750 K when the arc gap was enlarged to 6.6 mm, increasing to ~3800 K as the gap was further increased to 8 mm.

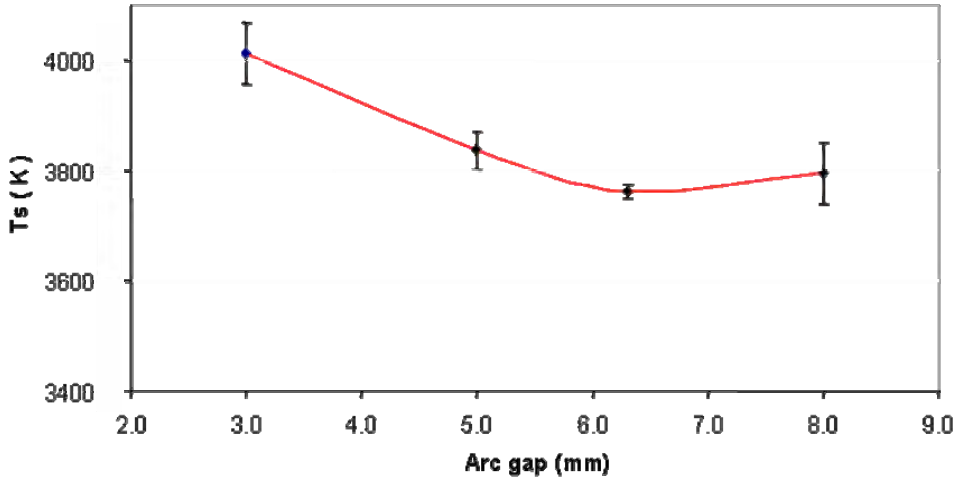

Fig.5. 15 Temperature of the substrate at various arc gaps for a current of 16 A and tape speed of 3 mm/s in a complete argon atmosphere. *(Error in temperature measurements ±50 K)*

Fig. 5.16(a-c) shows the corresponding micrographs obtained over the explored gap range. The number density of nanotubes produced with argon was substantially lower than that produced when nitrogen was used as a buffer gas. Abundant nanotubes were observed at the smallest arc gap of 3.4 mm [Fig. 5.16(a)] but they were short and had larger diameters. Cauliflower like carbon forms were observed at an arc gap of 5 mm and were associated with very few patches of nanotubes, as shown in Fig. 5.16(b). Nanotubes with very small diameters and longer lengths (of the order of 10 μm) were observed at a gap of 6.6 mm. These nanotubes were distributed like spider web on individual carbon fibres of the substrate [Fig 5.16(d)]. The micrographs at the longest gap range showed no signs of nanotubes as shown in Fig. 5.16(c).

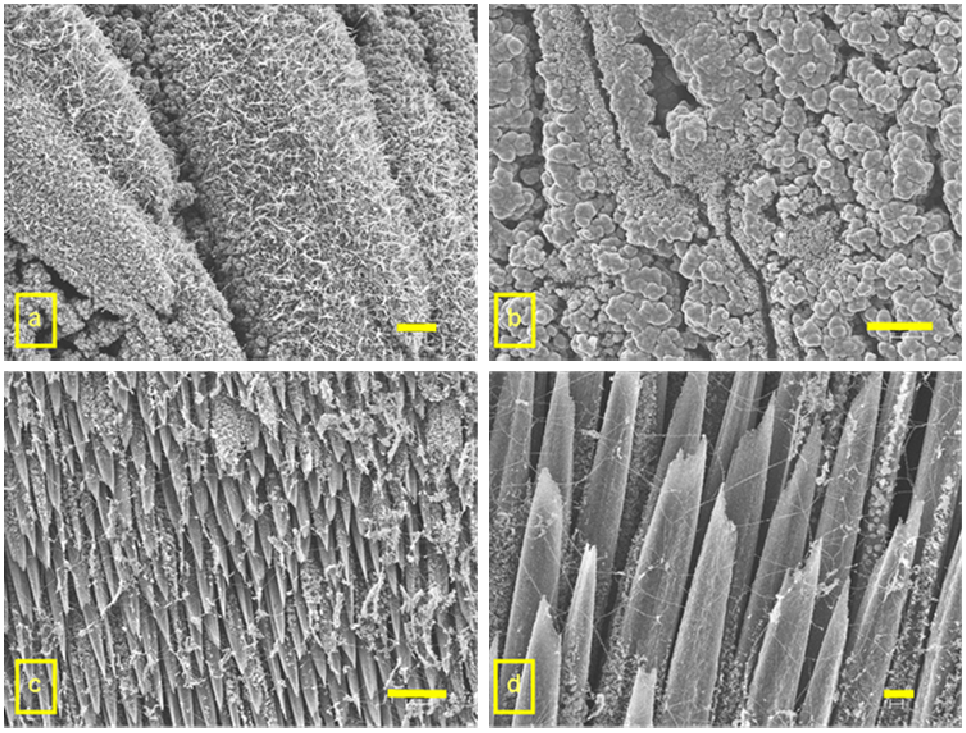

Fig.5. 16 SEM of the substrate at various arc gaps in a pure Argon atmosphere **(a)** Arc gap=3.4 mm illustrates uniform distribution of nanotubes **(b)** Arc gap= 5 mm shows cauliflower like carbon forms **(c)** Arc gap=6.6 mm showing etched carbon fibres but associated with very fine and long carbon nanotubes and **(d)** High resolution SEM depicting the spider web like distribution of nanotubes on individual fibre tips.*[Micrographs (a)-(c) have a scale bar of 20 µm and (d) has a scale bar of 5 µm]*

The concentration of argon was varied in the range of 0-38,000 ppm by mixing it with nitrogen after the optimal gap range for nanotube occurrence on the substrate was identified in a pure argon atmosphere. The details of the experiments were outlined in Chapter 3 (section 3.1.5.3) and the corresponding calibration charts relating capillary (ID – 1/16 inch) pressure drop and resulting concentration can be found in Appendix E. The inter-electrode gap and tape velocity was set to an optimum value of 3.4 mm and 3 mm/s respectively. The arc current used was 16 A and Carbonics tapes were used. The change in argon concentration did not influence carbon nanotube yield as shown in Fig. 5.17. Abundant nanotubes/nanorods with larger diameters in the range of 400-450 nm were observed at all concentrations. This was substantially higher when compared to the nanotube diameter range of 100-140 nm obtained with no argon flow into the reactor (only nitrogen).

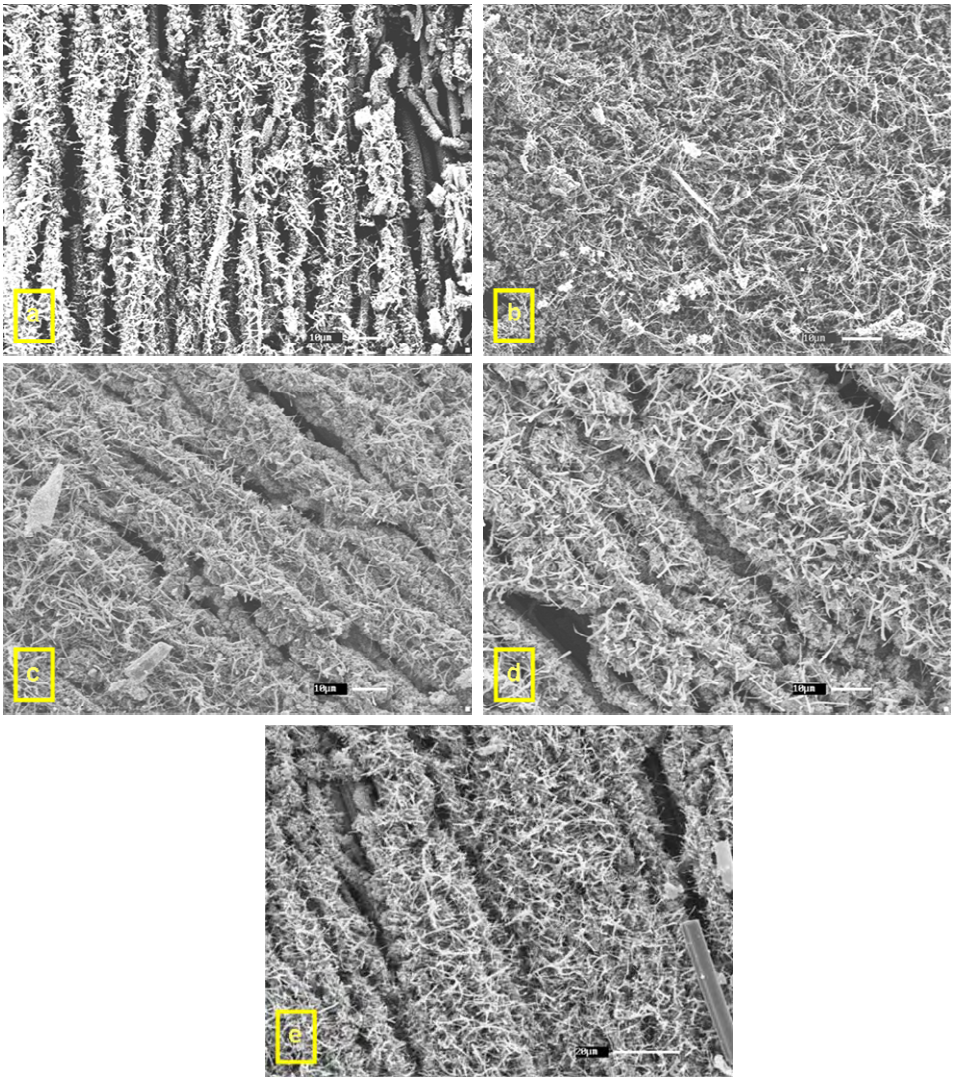

Fig.5. 17 SEM images of carbon nanotube distribution at various argon concentration. **(a)-(e)** shows uniformly distributed carbon nanotubes on the substrate with little or no variation for argon concentration of 4000-38000 ppm respectively. *[All micrographs have a scale bar of 10 µm)*

However, a significant decrease in nanotube diameters was observed at all concentrations when the gas mixtures were flushed through the anode at velocities of 1-1.3 L/min. The average diameters of carbon nanotubes reduced to a range of 60-80 nm as shown in Fig. 5.18, but there was no major change in nanotube yield/distribution at different concentrations.

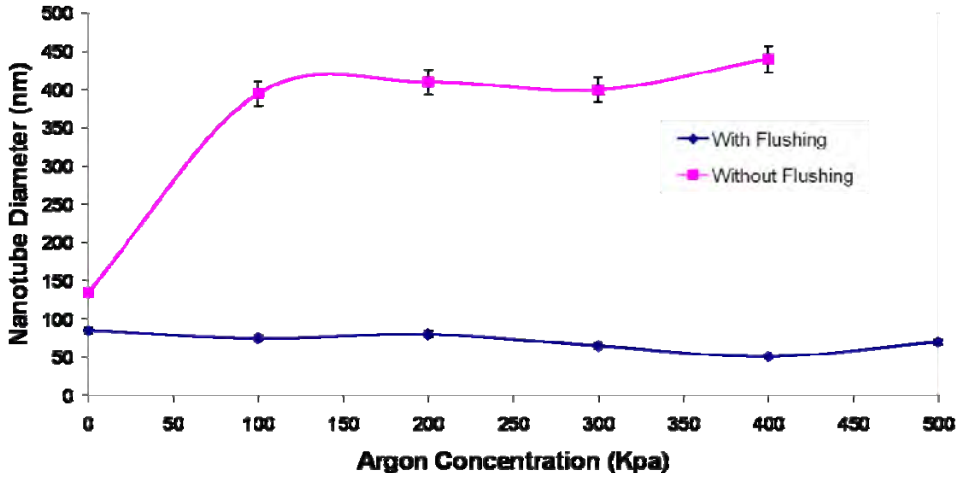

Fig.5. 18 Change in carbon nanotube diameter when Ar-N gas mixture was flushed through the anode at a flow rate between 1-1.3 L/min.

5.7.2 *Helium:*

The effect of helium gas on nanotube yield and occurrence was also investigated for our continuous reactor. The first set of experiments constituted an effort to find the optimal gap range and the second set of experiments were then performed at the optimal gap to explore the effect of helium concentration by mixing it with nitrogen.

Fig. 5.19 shows the average temperature of the substrate surface at various arc gaps. It was seen that the substrate surface temperature under a helium atmosphere was lower (< 3800 K) than the sublimation temperature of graphite for any inter-electrode gap. It was observed that the substrate temperatures were noticeably lower than the temperatures obtained under an argon atmosphere. The anode surface temperatures seem to be independent of the arc gap. Substrate temperatures close to around ~3700 K were obtained for arc gaps of 3.3, 5.0 and 8 mm. A lowest temperature of ~ 3600± 50 K was obtained for an arc gap of 6.3 mm.

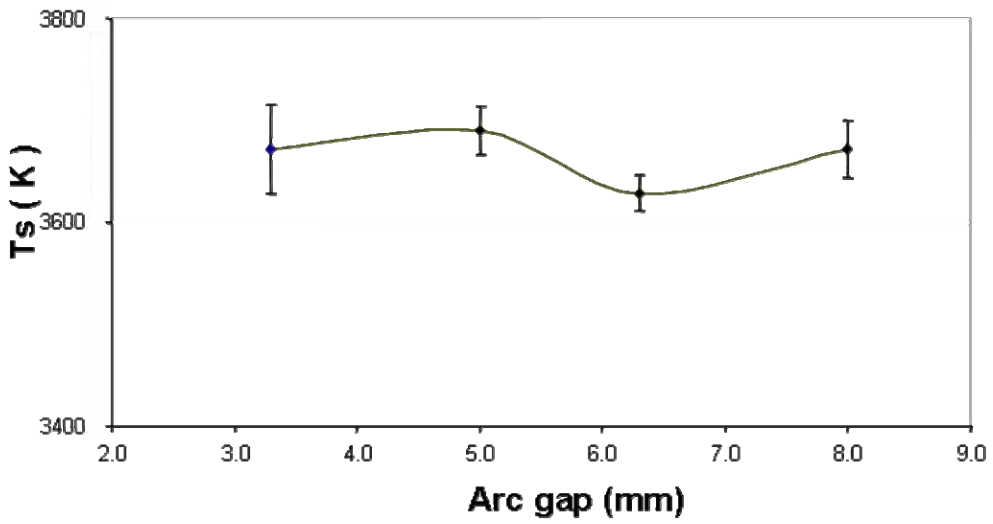

Fig.5. 19 Temperature of the substrate at various arc gaps for a current of 16A and tape speed of 3 mm/s in a complete Helium atmosphere. *(Error in temperature measurements ±50 K)*

It was found that no nanotubes were found under the explored gap range of 3-8 mm when operated under a helium atmosphere. Fig. 5.20(a-d) depicts the SEM images and morphology of carbon deposits on the substrate at various gaps. Spherical carbon forms and carbon nanorods were seen at an arc gap of 3.4 mm. Some nanotubes were observed as the arc gap was increased to 5 mm but they were confined to very few spots on the substrate, as shown in Fig. 5.20(b). Sharp and pointed etched carbon fibres were observed at the gap was further increased to 6.3 mm [Fig. 5.20(c)]. No nanotubes were found at the largest arc gap of 8 mm but this condition was associated with different carbon forms and impurities, as shown in Fig. 5.20(d).

No further experiments were performed to analyse the effect of helium concentration on nanotube occurrence as it was found that no or very little nanotubes were produced in the runs above.

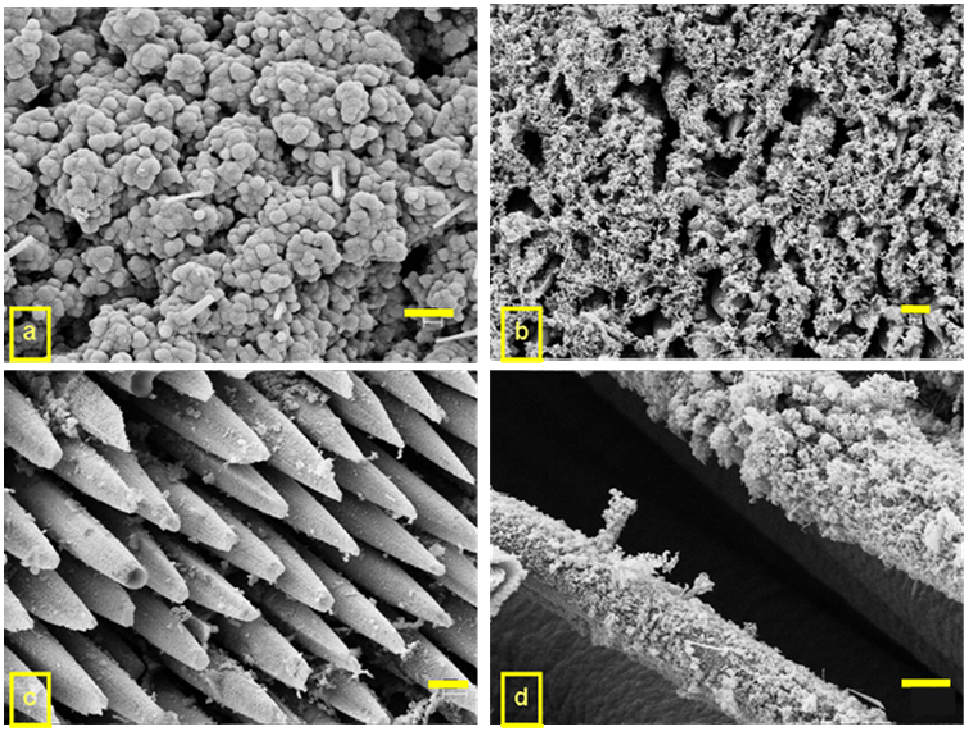

Fig.5. 20 SEM images depicting distribution of carbon nanotubes at various arc gaps in a complete Helium environment. **(a)** Arc gap= 3.4 mm showing cauliflower like carbon forms associated with nanorods **(b)** Arc gap= 5 mm showing carbon nanotubes but confined to very few spots on the substrate surface **(c)** Arc gap=6.3 mm showing sharp pointed etched carbon fibres and **(d)** Arc gap=8 mm showing individual carbon fibres covered with different carbon forms and impurities. *[All micrographs have a scale bar of 5 µm]*

5.8 Influence of oxygen in nitrogen:

The objective of these experiments was to find the effect of oxygen concentration on nanotube occurrence and purity in the reactor. Previous experiments performed by Ulubay[15] suggested that the purity of nanotubes increased for increasing oxygen concentration from 0-9000 ppm. However, subsequent experiments by Archer[16] revealed no nanotubes in the presence of oxygen but found dense mats of nanotubes in the presence of nitrogen and argon atmospheres. The existence of an optimum gap for nanotube formation was not characterised by either Ulubay[15] or Archer[16] and hence it was essential here to determine the exact effect of oxygen concentration on nanotube occurrence inside the reactor keeping the gap at the optimum value. The correlation curve relating capillary pressure drop and resulting concentration for

oxygen when mixed with a nitrogen flow rate of 10 L/min has been adapted from Ulubay and can be found in Appendix E.

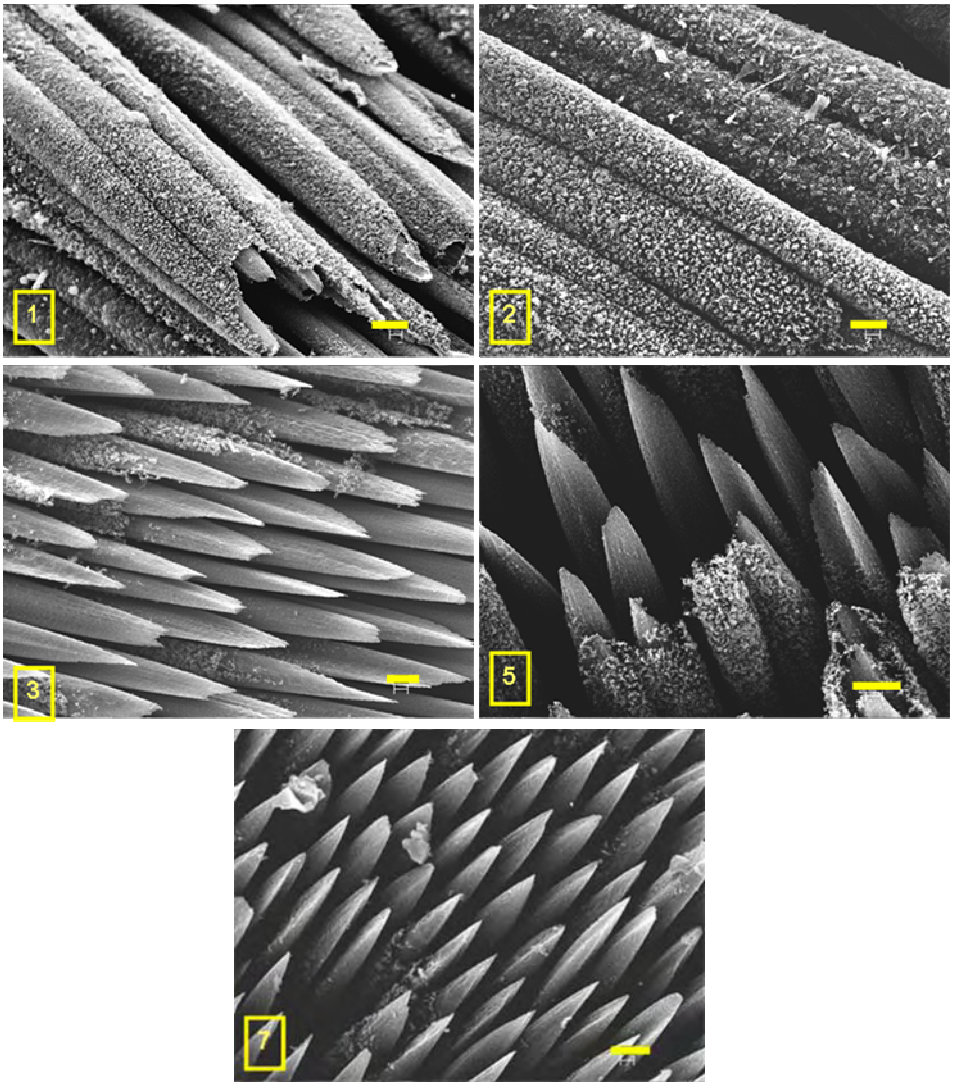

Fig.5. 21 SEM images of the substrate surface at different oxygen concentrations in nitrogen at an optimal arc gap of 5 mm for a 3 mm diameter cathode at 16 A, performed with no anodic flush **(a)** 990 ppm depicts honeycomb-like structures on individual fibres **(b)** 2200 ppm shows very few carbon forms and many impurities on individual fibres **(c)** 3560 ppm illustrates clean individual carbon fibres with sharp tips with no other carbon forms and **(d)-(e)** reveal uniformly etched individual carbon fibres with very sharp tips and no other carbon forms for subsequent increase in concentration to 6250 ppm and 8800 ppm respectively. *[All micrographs have a scale bar of 5 µm and (1) =(a)=(100 kPa)=990 ppm, (5)=(d)=(500 kPa)= 6250 ppm and (7)=(e)=(700 kPa)=8800 ppm]*

Fig. 5.21(a-e) depicts the morphology of nanotubes obtained under the explored oxygen concentration of 0-9000 ppm. The occurrence of carbon forms and nanotubes decreased rapidly as the oxygen concentration was increased. Honeycomb-like

structures are observed at concentrations of 990 ppm [Fig. 5.21(a)]. Flake like carbon forms and fewer honeycomb structures were seen as the concentration increased to 2200 ppm, as shown in Fig. 5.21(b). Etched individual fibres start to appear as the concentration was further increased to 3560 ppm. Uniformly distributed individual fibres with sharp tips (~150 nm diameter) and with no evidence of any fine carbon forms were seen at the highest concentration of 8880 ppm, as shown in Fig. 5.21(e).

5.9 Influence of other parameters:

5.9.1 *Graphite foils anchoring and gaseous hydrocarbon:*

The aim of these experiments was (a) use an alternative/additional carbon source and (b) to find out whether heating a carbon solid to anode temperature was sufficient to produce nanotubes. Graphite foils were anchored onto the tape by either sewing them using a cotton fibre/ carbon fibre or by stapling them using a pin. These experiments were unsuccessful since the cotton fibre could not endure temperatures reached during arcing and the foil often fell down. Some traces of black spots were observed on graphite foils when the tape speed was increased. No carbon nanotubes could be found on either the burnt graphite foils (either side) or the substrate when analysed in a SEM.

Another set of experiments was performed using benzene as an additional carbon source to boost nanotube yield. The experimental procedure for reactor runs performed using benzene is detailed in Chapter 3, section 3.1.5.3. These runs were performed with the traditional arc discharge technique without the presence of a substrate. The reactor could not be operated for more than 2 min as thick soot deposition was observed on the observational ports. One of the runs also caused a fire inside the reactor possibly due to a high concentration of benzene (or less flushing duration). Thick soot deposition was observed at even the lowest concentration of benzene which made operating the reactor difficult.

5.9.2 *Pre-treatment:*

Previous to some runs, the Carbonics and Sigmatex tapes were subjected to pre-treatment by Joule heating to investigate any changes in nanotube quality. This was performed after observing fumes from the reactor when Sigmatex tapes were used. The tapes were cut for specific lengths and a current of ~5 A is passed for a known time until the tape got red hot and the glow spread evenly along the tape. The tape was then weighed to account for any weight loss. No weight loss was observed for the Carbonics tape but a weight loss of 1.6 wt% was found for Sigmatex tapes. This value was very close to the value stated by the manufacture as the resin content, which could have been vaporised due to Joule heating.

No fumes were observed during experiments with a pre-treated tape. The pre-treatment also seemed to have no effect on nanotube distribution or quality for both kinds of substrates.

5.9.3 *Substrate direction:*

The direction of the tape motion (up or down) inside the reactor influenced the area of arc treatment on the substrate. All the runs in this work were performed with the tape moving up. It was observed that the arc attachment was more widespread when the tape moved up when compared to that with downward motion of the tape. This might be due to the effects of plasma buoyancy and surface adhesion on the substrate (Fig. 5.22). Querrioux[17] found broken patches of nanotube deposit and some untreated fibres when the substrate moved up. However, parameters like arc gap and tape speed were not characterised during his runs, so there were large fluctuations in his findings. There was also no detectable change in nanotube morphology or occurrence with the change in substrate direction[17]. Operating the reactor with an upward motion of the tape resulted (in the resent study) in an overall increase in the number of carbon nanotubes, only due to an increase in the area of arc treatment.

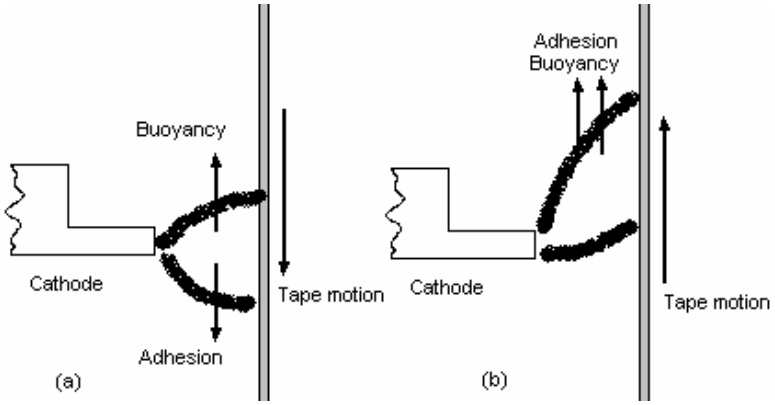

Fig.5. 22 Arc attachment relating to the direction of substrate (a) Downward motion showing smaller arc attachment and (b) upward motion showing diffuse arc attachment used for the runs in this work.

5.10 Tape screening:

The width of arc treatment varied when one or many of the parameters were changed. A screening of the arc treated area was performed to observe changes in nanotube occurrence and morphology across its cross section. Fig. 5.23 shows a representative sample of an arc treated path on the substrate. An arbitrary centre line along the arc treated path was marked corresponding to certain co-ordinates in the SEM stage. Pictures were taken when the nanotube morphology changed noticeably starting from the centre along the arrow (Fig. 5.23) until the periphery of arc treatment.

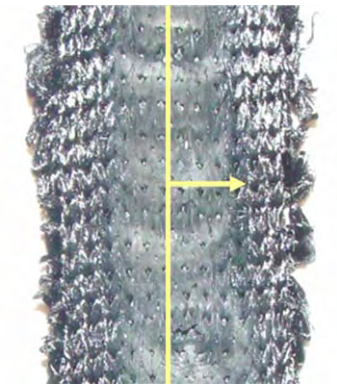

Fig.5. 23 Screening path along an arc treated Carbonics substrate with the arrow showing the direction of SEM analysis.

The distribution of carbon nanotubes along the arc-treated area when the substrate was in contact with the anode is as shown in Fig. 5.24(a-e). Carbon nanotubes with

few impurities and smaller diameters were generally observed at the centre of arc treatment as shown in Fig. 5.24(a). The average diameter of nanotubes increased from 250 nm to 350 nm as we move away from the centre of the arc treatment, towards the periphery as shown in Fig. 5.24(c-d). Nanotubes also appeared to fuse themselves into thicker nanorods near the periphery of the arc-treated path on the substrate as shown in Fig. 5.24(e). However, average diameters of carbon nanotubes in the range of 60-80 nm were obtained when gas mixtures were flushed through the anode at different velocities in the range of 0.05-0.2 m/s (0.09 – 0.6 L/min anode flow).

However, a major variation to this general trend was observed when the tape was not in contact with the anode. The change in nanotube morphology across the cross section of the tape when it was moving at a distance of 1 mm from the anode is as shown in Fig. 5.25. Although, carbon nanotubes with smaller diameters were observed at the centre of the arc attachment [see Fig. 5.25(a)], their diameters increased significantly as we moved away from the centre as shown in Fig. 5.25(c). Carbon nanorods start to appear just next to the centre of the tape associated with nanorods (diameters as large as 1 μm) with large cauliflower like forms [see Fig. 5.25(e)] observed at the periphery of arc treatment.

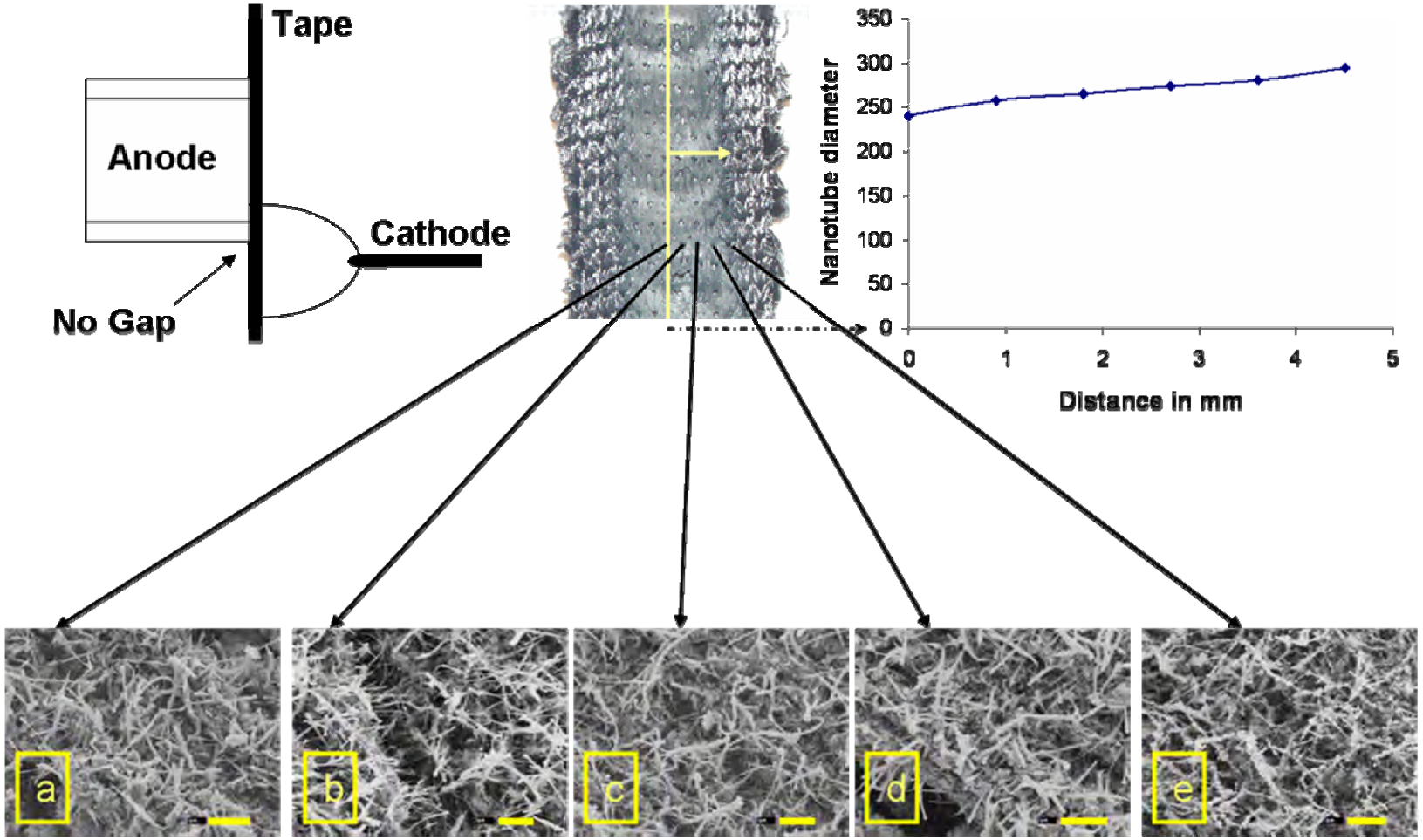

Fig.5. 24 Diameter distribution and micrographs of carbon nanotubes along the arc-treated path on the substrate when the substrate was in contact with anode. Note: Individual carbon nanotubes appear to fuse themselves into thicker nanorods [(d), (e)] as we move towards the periphery of the arc treatment. *[All micrographs have a scale bar of 5 µm] Conditions: 3 mm dia cathode, 16 A, 3mm/s tape velocity with no flushing*

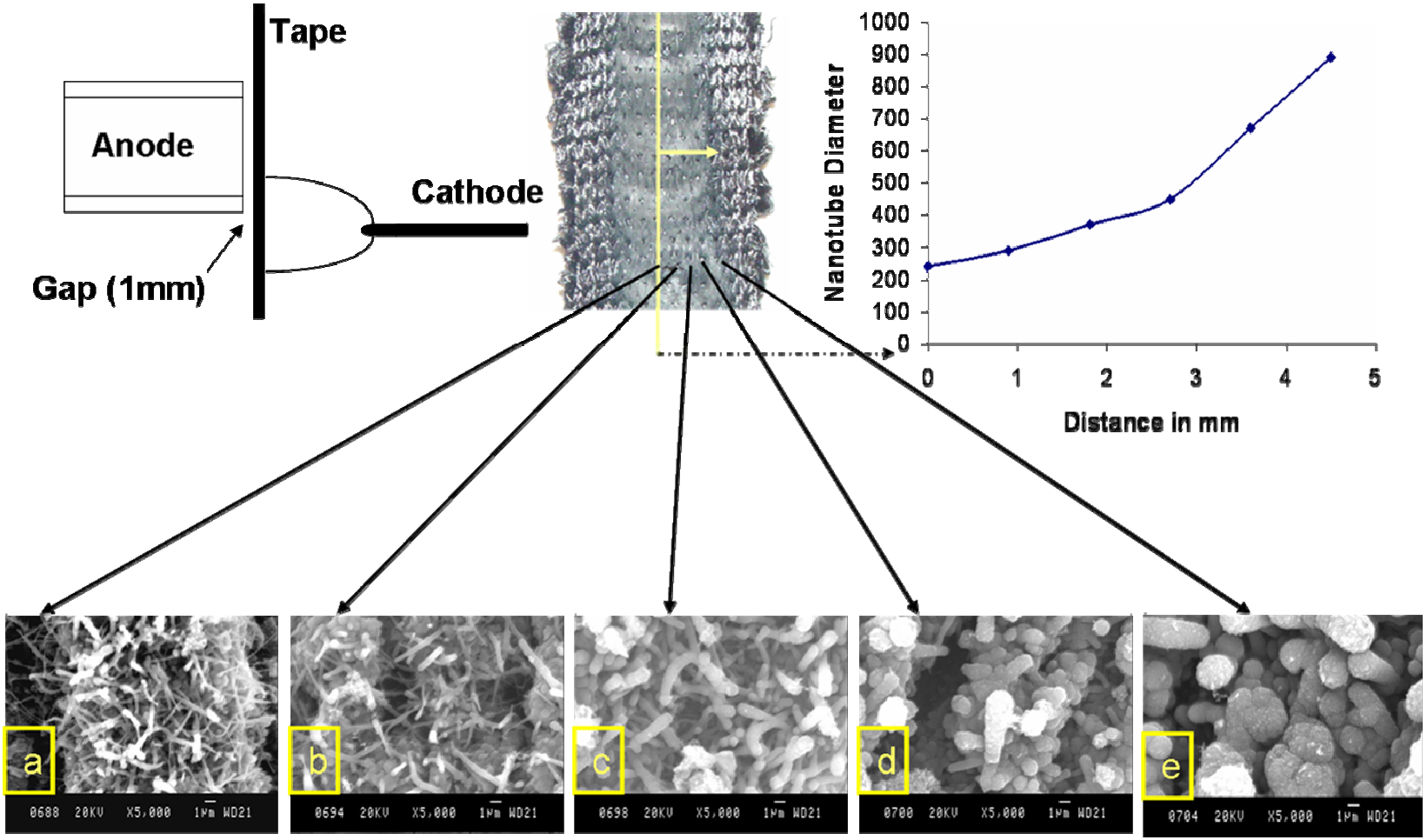

Fig.5. 25 Diameter distribution and micrographs of carbon nanotubes along the arc-treated path on the substrate when the substrate was not in contact with anode. (b)-(c) Individual carbon nanotubes appear to fuse themselves into thicker nanorods with (e) showing cauliflower like occurrence as we move toward the periphery. *[All micrographs have a scale bar of 1 μm] Conditions: 3 mm dia cathode, 16 A, 3mm/s tape velocity with no flushing.*

5.11 Influence of Catalyst:

5.11.1 *Nickel:*

The highest relative yield and most uniform carbon nanotube distribution on the substrate were obtained when nickel was used as a catalyst nanoparticle. The distribution, morphology and number density of carbon nanotubes produced with a nickel concentration of 0.03 at% were similar to nanotubes produced without any catalyst. The sample preparation method is detailed in the report of Ostilliger[259] and the concentration of catalyst was measured using EDS. The nanotubes appear rigid and have longer lengths associated with impurities as shown in Fig. 5.26. This appearance is similar to the morphology of nanotubes produced without any catalyst presence on the substrate.

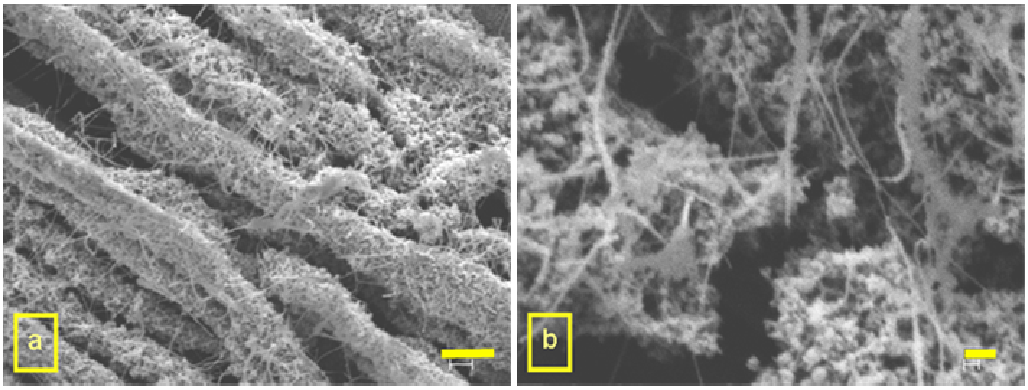

Fig.5. 26 (a) Morphology of the substrate at 0.03 at% Ni catalyst *[Scale bar-5 µm]* and **(b)** higher magnification depicting longer rigid nanotubes *[Scale ba -600 nm]*

However, higher concentrations of nickel on the substrate seem to have a major influence on the number of nanotubes produced on the substrate. The surface morphologies of the substrate produced at nickel concentrations of 0.9 at% for gaps in the range of 3-7 mm are shown in Fig. 5.27(a-e). Carbon nanotube growth appears to be favoured over a range of arc gaps and no optimal gap could be identified. However, dense growth of finer nanotubes was observed at a gap range of 5-6 mm, as shown in Fig. 5.27(c-d). The micrographs at the largest arc gap of 6.8 mm [Fig. 5.27(e)] were mostly associated with carbon honeycomb like structures but also revealed the presence of finer nanotubes. Surprisingly, no nanotubes were seen at an

arc gap of 4.5 mm, but instead the micrographs depicted different carbon morphologies and impurities.

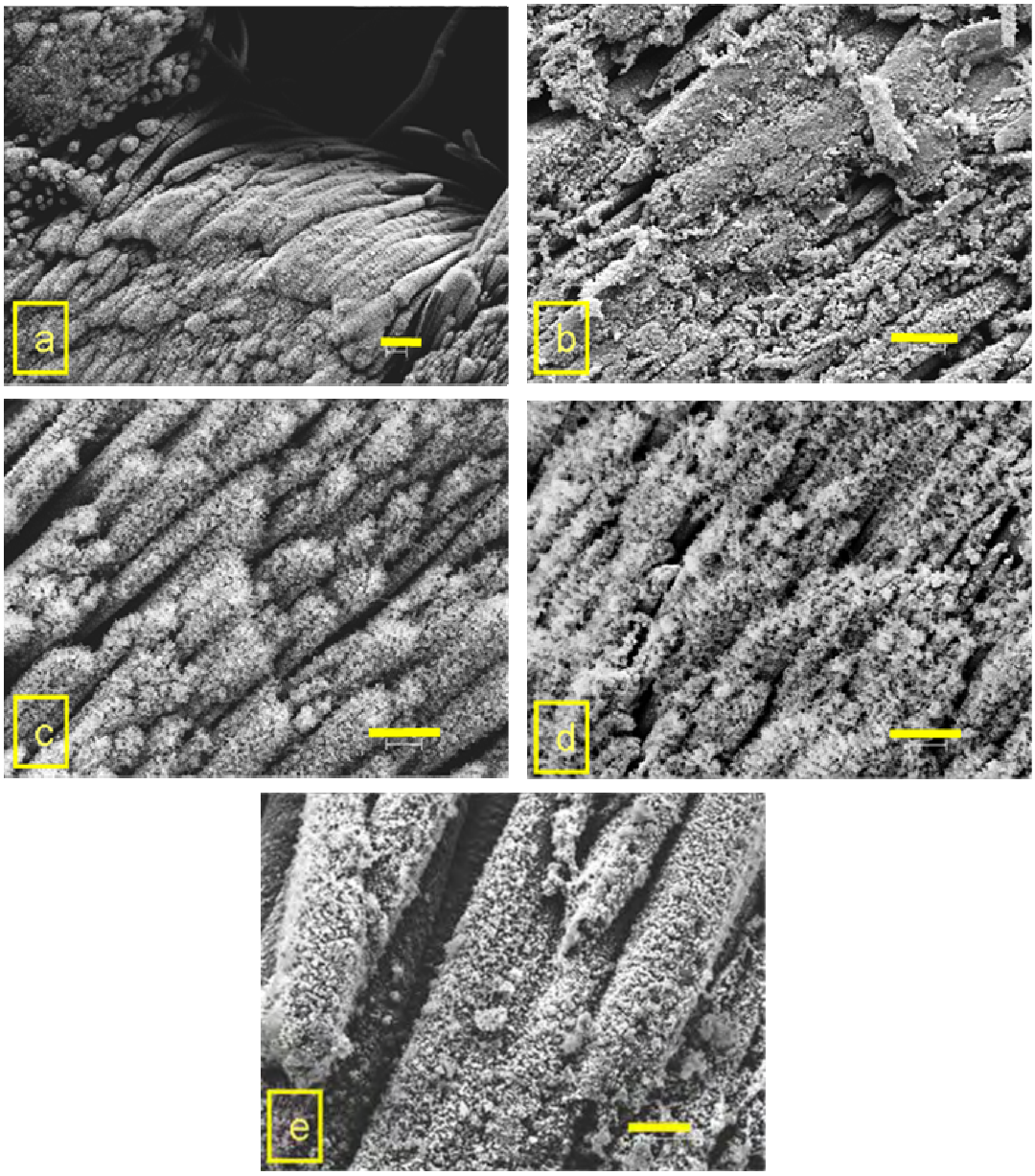

Fig.5. 27 SEM of the substrate surface at various gaps in the presence of 0.9 at% Ni catalyst for a 3 mm diameter cathode at 16A and a substrate speed of 3mm/s. **(a)** arc gap of 3.4 mm showing uniform distribution of nanotubes **(b)** arc gap of 4.5 mm showing presence of various carbon morphologies **(c)** arc gap of 5.3 mm showing dense distribution of finer nanotubes on individual fibres **(d)** arc gap of 6mm showing consistent nanotube distribution and **(e)** arc gap of 6.8 mm depicting carbon honeycomb like structures associated with nanotubes. *[All micrographs have a scale bar of 20 µm with (a) having a scale bar of 40 µm and (e) with a scale bar of 10 µm]*

Besides the above carbon forms, carbon nanotubes growing from large spherical catalyst clusters were also commonly seen on the substrate surface as shown in Fig. 5.28 (a-b). There was no change in the gap dependence (compared with 0.9 at% nickel) and nanotube occurrence when the concentration of nickel was reduced to 0.4 at%. Dense contorted finer structures were obtained at the arc gap range of 5-6 mm as shown in Fig. 5.28 (b).

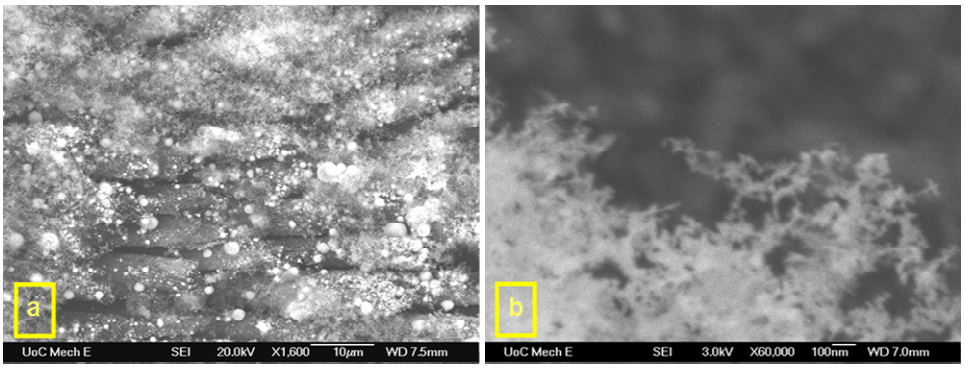

Fig.5. 28 (a) SEM of the substrate surface depicting carbon nanotube growth from spherical catalyst particles *[Scale bar -10 μm]* and **(b)** high magnification of nanotubes obtained at an arc gap range of 5-6 mm in presence of Ni catalyst. *[Scale bar- 100 nm]*

5.11.2 *Iron:*

The experiments performed with iron distributed using commercially available Ferrofluid (10 nm) produced very little or no carbon nanotubes. The morphology of the substrate at an arc gap of 1.8 mm revealed overnucleation or overgrowth of carbon forms resembling rod like deposits, as shown in Fig. 5.29(a). Carbon nanotubes were confined to very few spots on the carbon substrate even at the optimal gap range of 5 mm as shown in Fig. 5.29(b). Various carbon morphologies like sintered carbon, carbon honeycomb-like structures and patches of nanotubes were also seen at various gaps. Large size iron particles were frequently observed on the fibre surface. The micrographs at the largest gap of 6.5 mm were almost identical to untreated carbon substrate except for a few catalyst particles, as shown in Fig. 5.29(c).

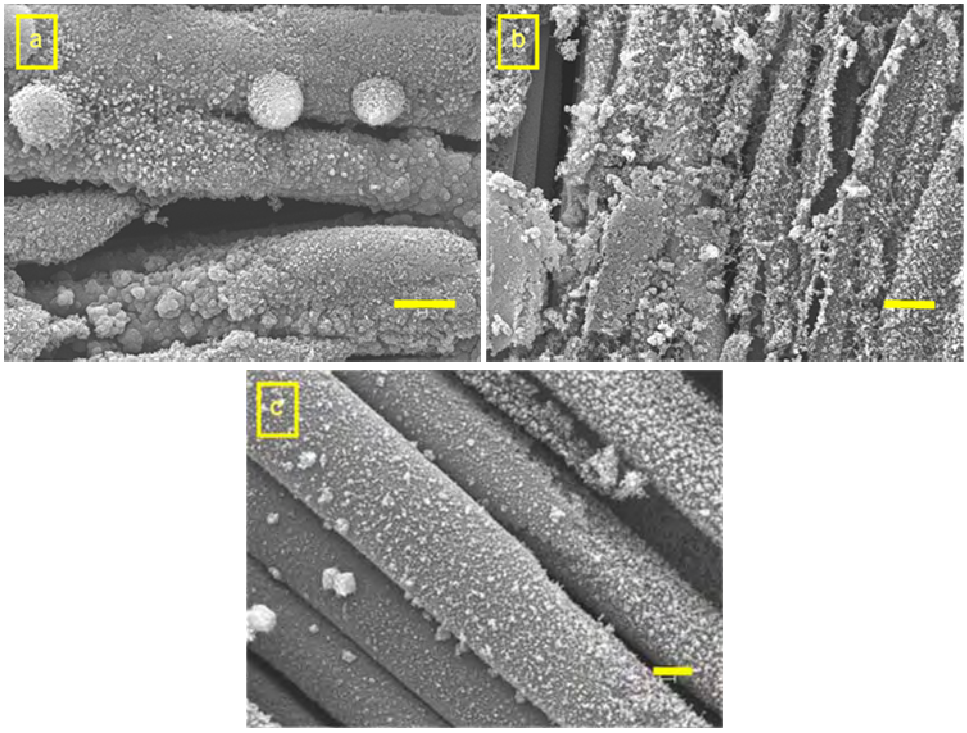

Fig.5. 29 SEM images of the substrate surface at various gaps in the presence of an Fe catalyst distributed using diluted Ferrofluid solution **(a)** arc gap of 1.8 mm showing rod like carbon deposits **(b)** arc gap of 5 mm showing patches of nanotubes and crumbled carbon forms and **(c)** arc gap of 6.5 mm depicting catalyst particles and untreated individual fibres. *[All micrographs have a scale bar of 5 µm with (a) having a scale bar of 10 µm]*

An improved method of distributing iron nanoparticles on the substrate was carried out by distributing iron oxide particles using a wet-impregnation method. The morphology of nanotubes appeared to be similar to the ones produced using a nickel catalyst, but their distribution was less uniform. Patches of fine nanotubes resembling raft on fibres were observed at smaller arc gaps. However, their growth appeared to be largely confined to the surface of large catalyst particles, as shown in Fig. 5.30(b). Carbon nanotubes growing from large spherical catalyst clusters were commonly seen on the substrate surface, as shown in Fig. 5.30(c).

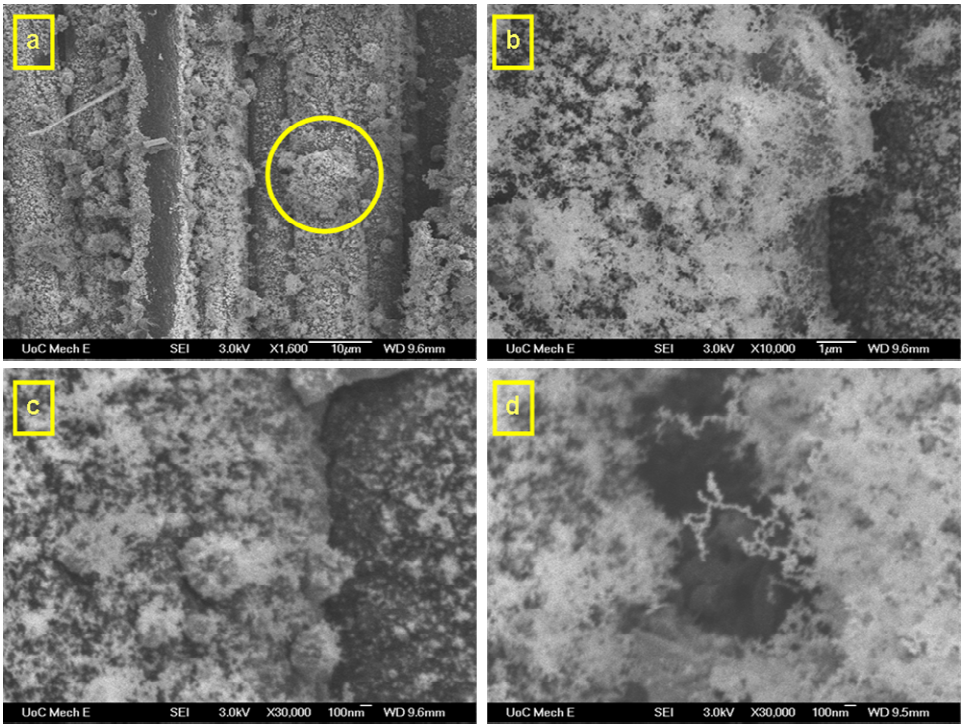

Fig.5. 30 Micrographs of the substrate surface in presence of 0.9 at% Fe catalyst **(a)** arc gap of 4 mm showing patches (circled) of nanotubes **(b)** higher magnification of the circled patch **(c)** micrograph illustrating carbon nanotube growth on catalyst and **(d)** magnified image of nanotubes produced.

5.11.3 *Bimetallic catalyst:*

The presence of a bimetallic catalyst mixture consisting of 0.5 at% nickel and 0.5 at% iron had a major influence on the carbon nanotube distribution. Uniform web-like carbon nanotubes were consistently distributed over the entire arc treated surface for gaps in the range of 4-6 mm, as shown in Fig. 5.31(a). However, high magnification micrographs revealed similar nanotube morphologies (fine and contorted) to that produced using individual catalysts. The major distinguishing feature with nanotubes produced using a bimetallic catalyst was their uniform occurrence over a wider arc gap range (3.4 mm-6 mm).

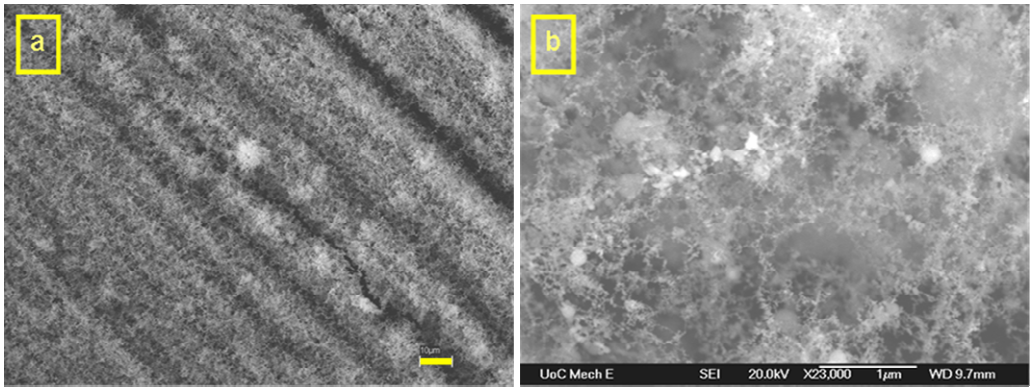

Fig.5. 31 Micrographs of the substrate surface in the presence of 0.5 at% Fe/Ni catalyst each **(a)** consistent distribution of nanotubes on the substrate *[Scale bar-10 μm]* and **(b)** web like fine carbon nanotubes. *[Scale bar-1 μm]*

Overall, carbon nanotube formation was strongly influenced by the type and concentration of catalyst. Abundant carbon nanotube formation occurred when Ni and a bimetallic catalyst of 0.5 at% Ni and Fe was used. Carbon nanotubes were more uniformly distributed and were found in a wider gap range when its formation was influenced by a bimetallic catalyst. The growth of nanotubes appeared to be confined only to the surface of the catalyst when iron was used as a catalyst. No carbon nanotube formation occurred when 10 nm size iron nanoparticles (Ferrofluid) were used as a catalyst. Carbon nanotubes appeared to have similar morphologies (contorted and fine) at high magnification irrespective of the catalyst type. However, a major distinction that was evidently visible was the difference in nanotubes produced with no catalyst on the substrate. Carbon nanotubes produced without any presence of catalyst were multiwalled, rigid and were associated with impurities and nanoparticles, as shown in Fig. 5.32(a). Carbon nanotubes produced in the presence of catalyst also appeared to be multiwalled, but were contorted and associated with few impurities (traces of catalyst particles), as shown in Fig. 5.32(b).

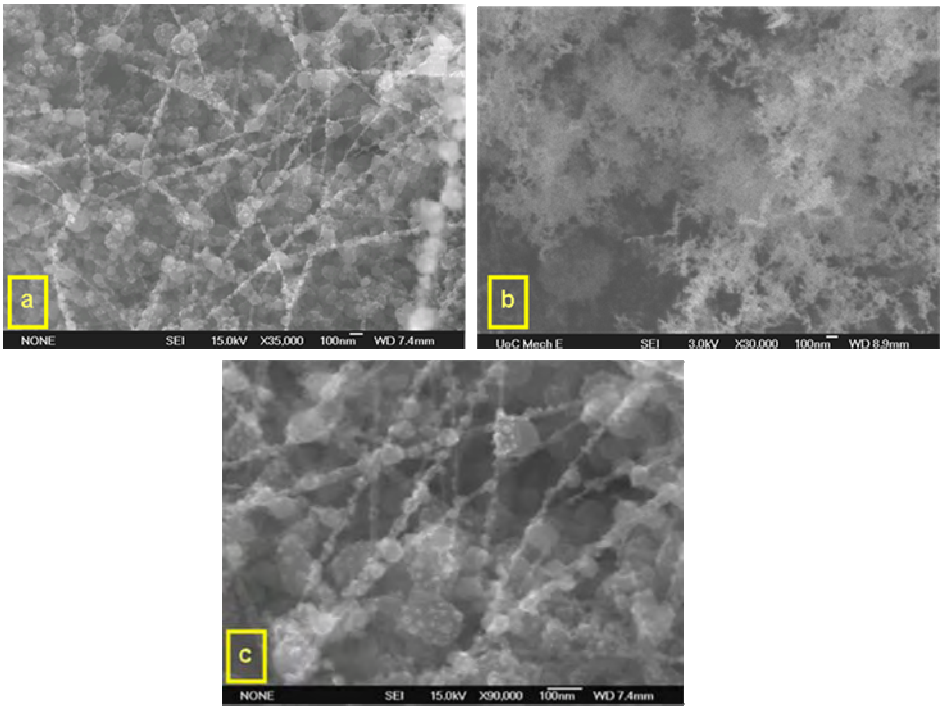

Fig.5. 32 (a) High magnification SEM of the substrate surface showing **(a)** long rigid carbon nanotubes associated with nanoparticles **(b)** fine contorted and short carbon nanotubes **(c)** multi-walled nanotubes with 4 walls. *[Scale bar-100 nm]*

All the samples coated with catalysts were characterised using X-ray analysis (EDS) to analyse catalyst distribution and concentration. Fig. 5.33 shows the EDS spectrum of the catalyst loaded substrate samples in presence of nickel, iron and a bimetallic mixture of iron-nickel respectively. It was seen that the nickel catalyst was evenly distributed when compared to iron catalyst nanoparticles which formed aggregates. Fig. 5.33(c) also shows the EDS of a bimetallic substrate sample confirming an equal concentration of nickel and iron.

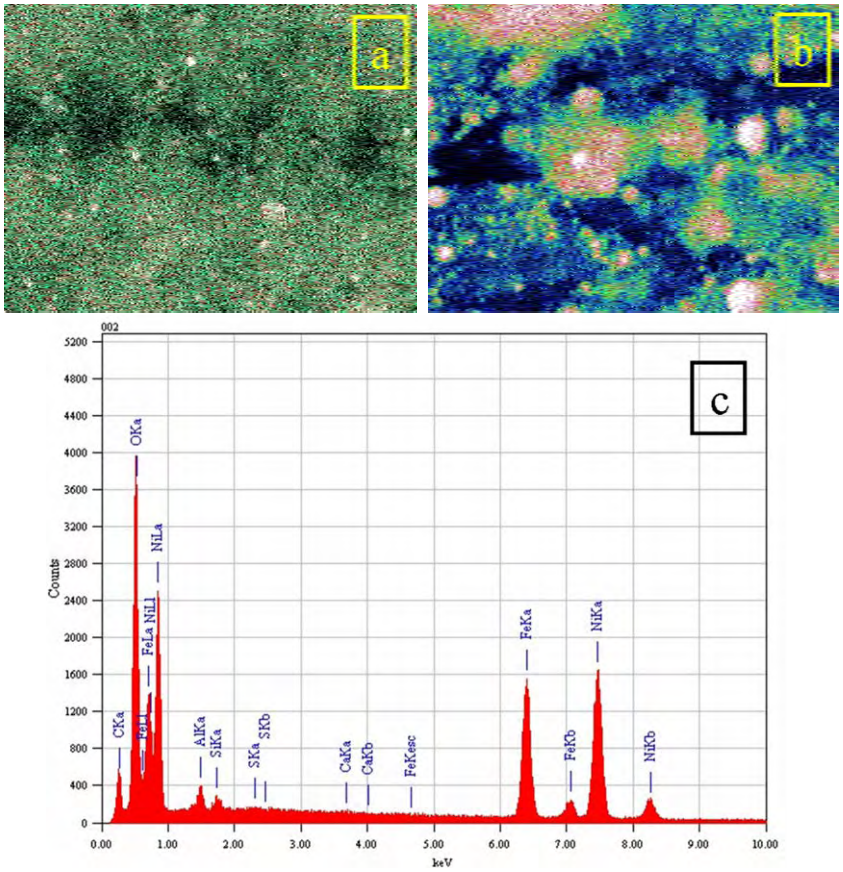

Fig.5. 33 X-ray analysis (EDS) of a catalyst coated substrate sample for (a) nickel-showing evenly distributed catalyst particles, (b) iron-showing catalyst aggregates and (c) 0.5 at% bimetallic mixture of Ni-Fe plotted for intensity of the peak, showing an equal concentration of nickel and iron.

5.12 High speed video:

The most common feature seen during arc discharge was emission of small bright particles from the cathode, as shown marked with an arrow in Fig. 5.34(a). High speed video analysis was performed to observe the type, size and velocities of particulates emitted during the arc discharge, providing an opportunity to understand the arc discharge process better. The visible particulate emission ceased when spectroscopic grade graphite rods were used as the cathode instead of electrodes which had impurities of < 6 ppm. However, there was no change in nanotube occurrence irrespective of the electrode type, when analysed by SEM. The high speed video images also revealed particulate emission from the substrate acting as an anode and the flow profiles near arc attachment, as shown in Fig. 5.34(b).

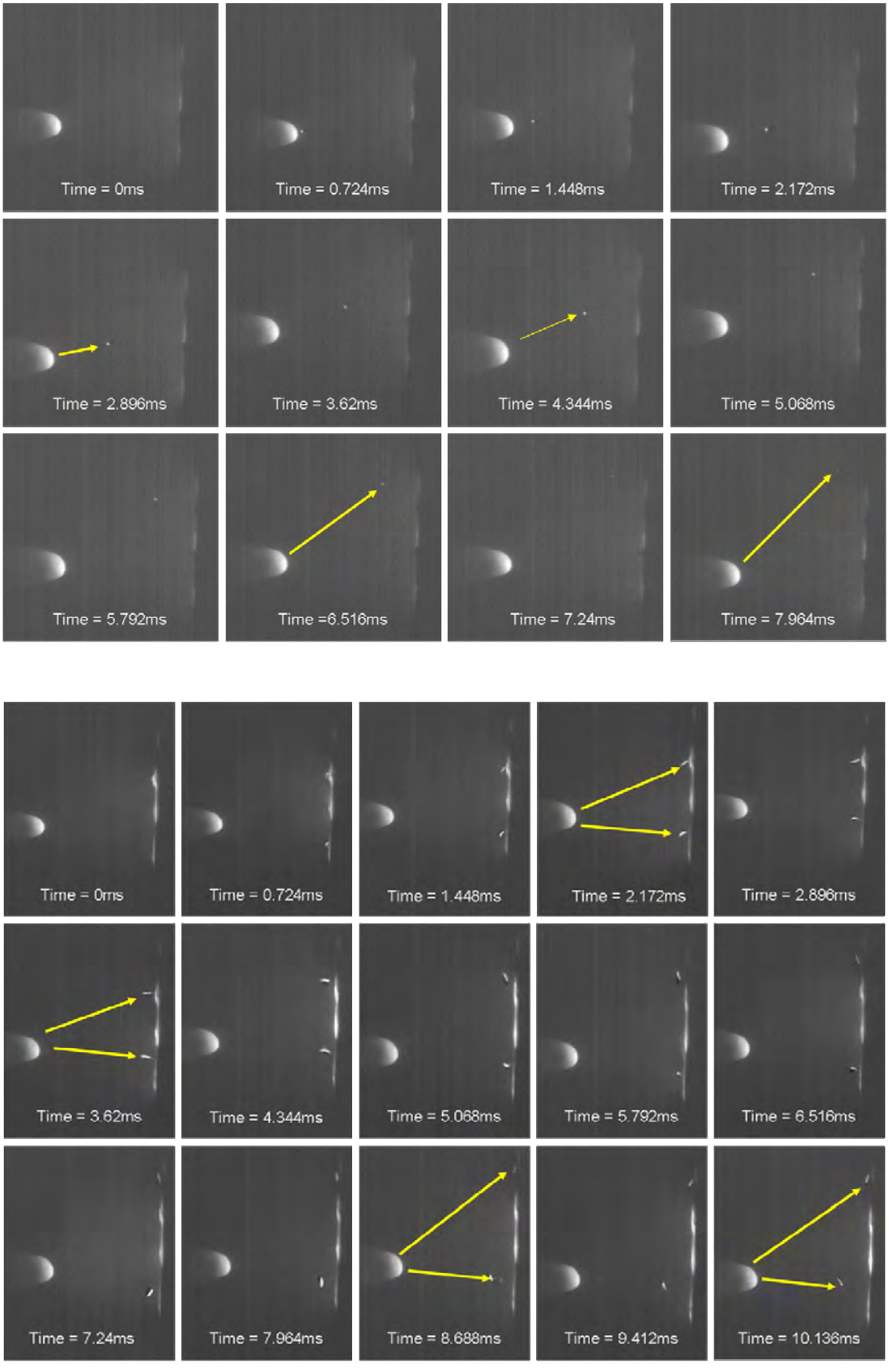

Fig.5. 34 High speed video images showing particulate emission at an interval of 0.724 ms from **(a)** cathode and **(b)** carbon substrate [Note: These runs were performed at an optimal arc gap of 5 mm using a 3 mm diameter cathode at an arc current of 16A].

5.13 Field emission properties:

The field emission properties of nanotubes were tested in a field emission chamber using the simple diode configuration. The arc-treated substrate was carefully cut and glued onto a copper plate using a double sided sticky tape. The loose ends of the cut tape were coated with a conductive carbon paint to avoid fraying and bridging the electrodes during field emission tests. The base pressure of the field emission chamber was around 3 x 10^{-5} mbar. The result of the first voltage sweep usually showed unstable current or current fluctuations. The measurements were carried out in alternate sweeps of up and down until the results were identical to the previous sweeps as shown in Fig. 5.35. The field emission current was quite reproducible and stable after this conditioning process and this was performed on all samples before extracting field emission characteristics.

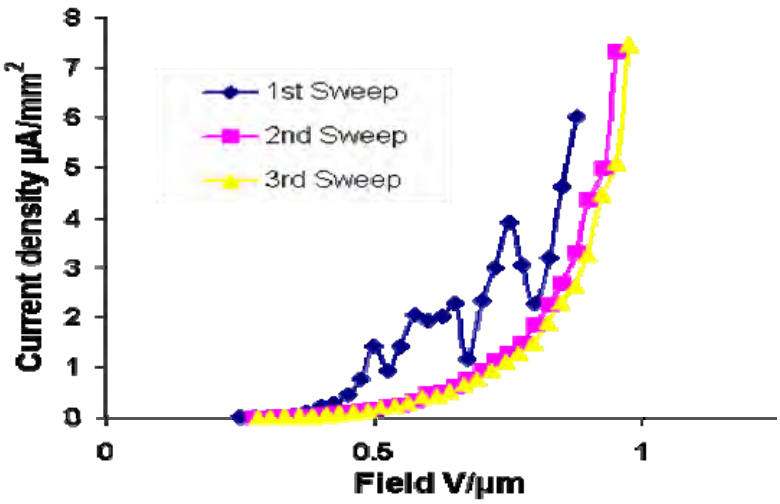

Fig.5. 35 Change in field emission characteristics of carbon nanotubes grown on carbon cloth using a mixture of Fe/Ni catalyst during consecutive voltage sweeps.

5.13.1 *Carbon nanotubes produced with the aid of a catalyst/catalyst mixture:*

The field emission characteristics of carbon nanotubes produced using different catalysts and catalyst mixtures at different vacuum gaps are shown in Fig. 5.36(a-c). The field emission characteristics are represented by a plot of current density versus

the macroscopic electric field. It was observed that nanotube samples produced using nickel, iron and a mixture of Ni/Fe produced similar emission characteristics. This confirms that field emission from nanotube films are governed only by the areal density of nanotubes and not influenced by different conductivities imparted by specific catalysts. Fig. 5.37 shows the Fowler-Nordheim plots with different vacuum gaps for various carbon nanotube samples. The plots form a reasonably straight line, indicating that the FN theory approximately fits the field-emission behaviour of all our samples. Furthermore, field emission behaviour of carbon nanotubes with different gaps was also investigated. The turn-on field[1] decreases monotonously from 0.35 V/μm to 0.23 V/μm when the vacuum gap was increased from 1.5 mm to 4 mm, while the voltage applied increased to 900 V from 550 V to obtain the same emission current density of 1 $\mu A/mm^2$

[1] Turn-on field is defined as the field required to obtain an emission current density of 1 $\mu A/cm^2$

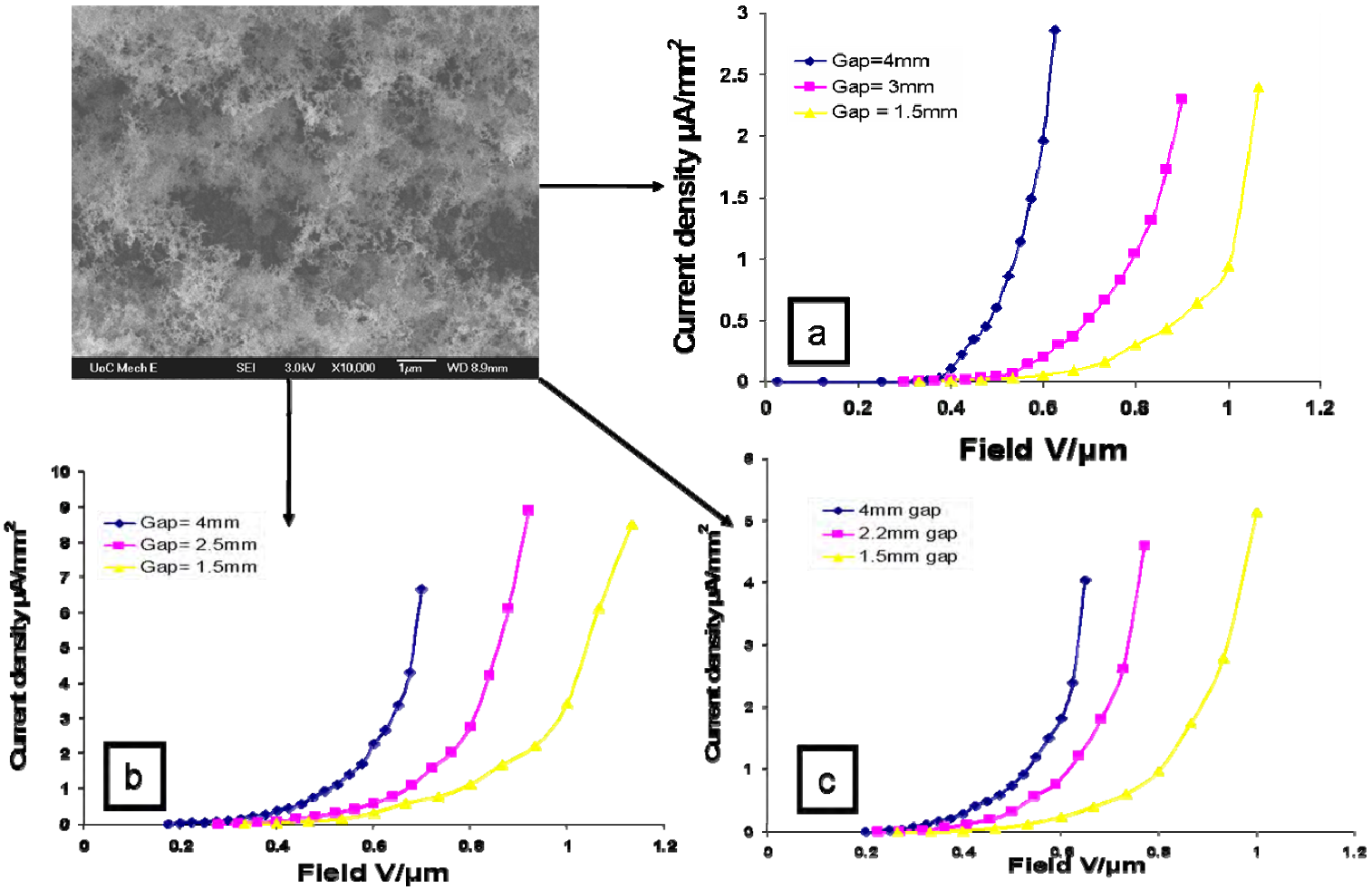

Fig.5. 36 Field emission characteristics of nanotubes on carbon cloth produced at different vacuum gap using (a) nickel (b) iron and (c) a mixture of Fe/Ni catalyst.

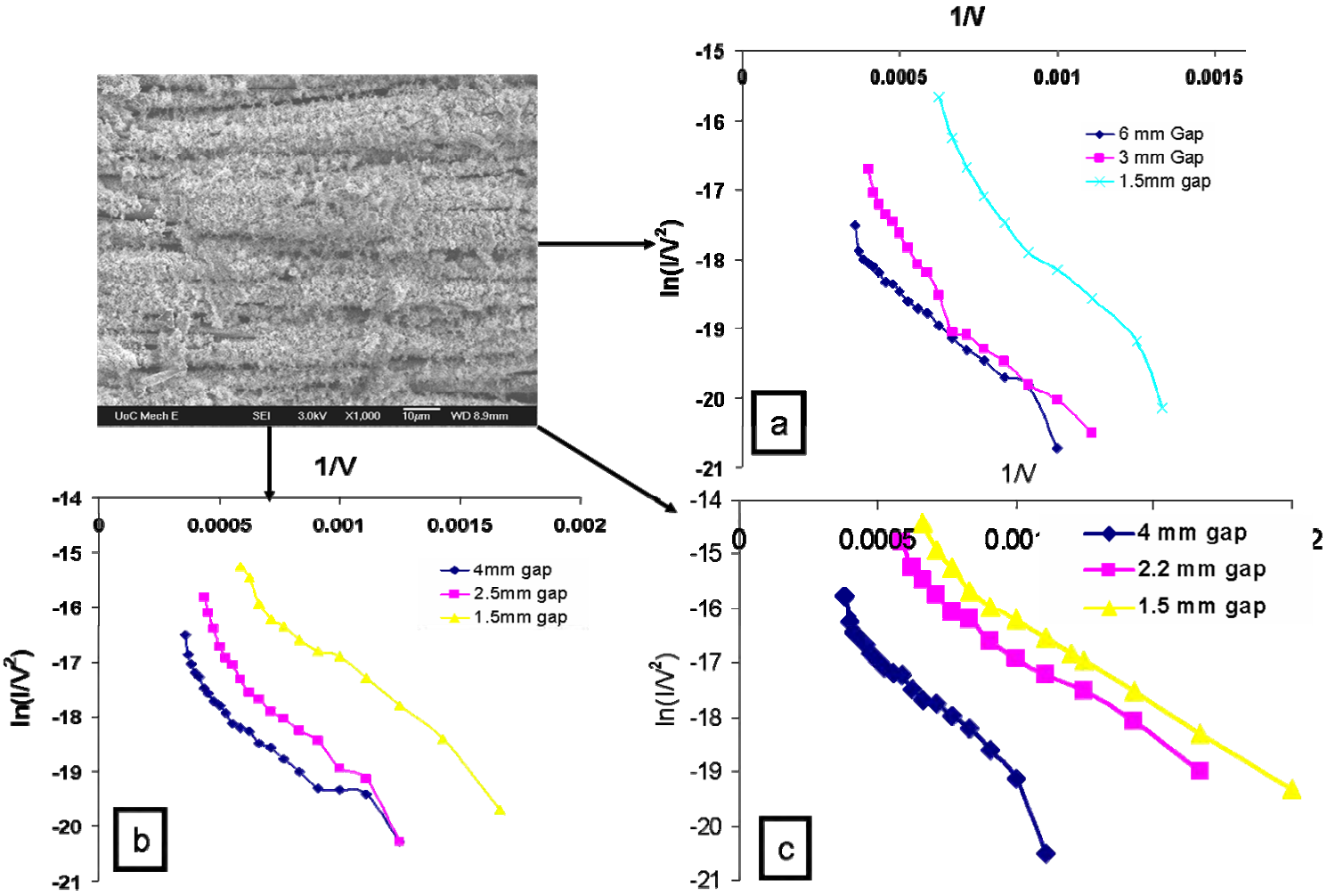

Fig.5. 37 Fowler-Nordheim plot at different vacuum gaps for different nanotube samples produced using (a) nickel (b) iron and (c) mixture of nickel and iron catalyst.

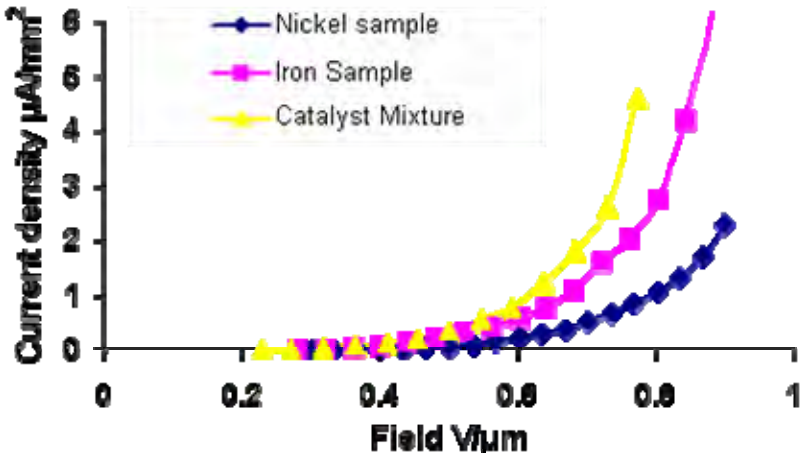

Fig.5. 38 Field emission properties of nanotubes produced using different catalysts at a vacuum gap of 2.5 mm.

Fig. 5.38 shows the field emission characteristics of nanotube samples produced using different catalysts when the gap between carbon cloth and anode was 2.5 mm. It is quite evident that nanotubes produced using a catalyst mixture exhibits low turn on field. However, when the vacuum gap was reduced to 1.5 mm, samples produced using iron catalyst and a catalyst mixture exhibited similar emission characteristics as shown in Fig. 5.39. This similarity can be attributed to identical morphology/similar distribution of carbon nanotubes produced using different catalyst and catalyst mixture, as shown in previous section.

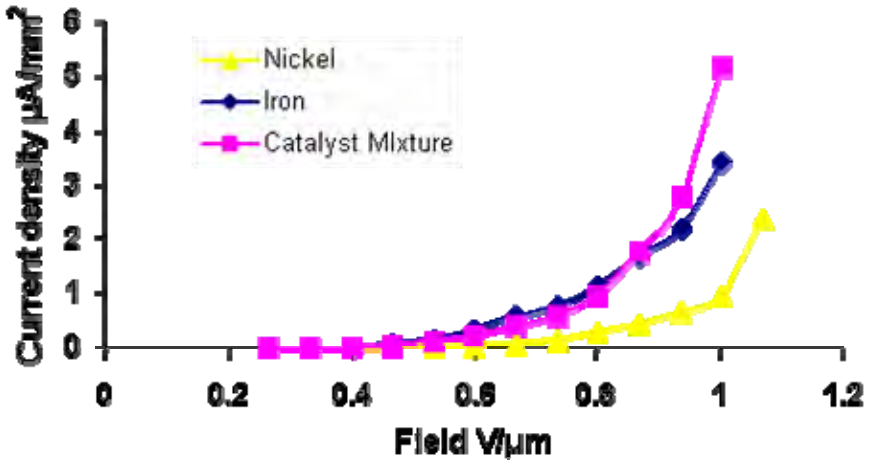

Fig.5. 39 Field emission properties of nanotubes produced using different catalysts at a vacuum gap of 1.5 mm.

The samples were analysed in the SEM after field emission studies. Fig. 5.40 shows very little change in morphology of nanotube obtained before and after field emission studies. The number of nanotubes appeared to have somewhat decreased after field emission experiments but their number density was still large. Finer structures could still be seen widely distributed over the entire sample area as shown in Fig. 5.40(d).

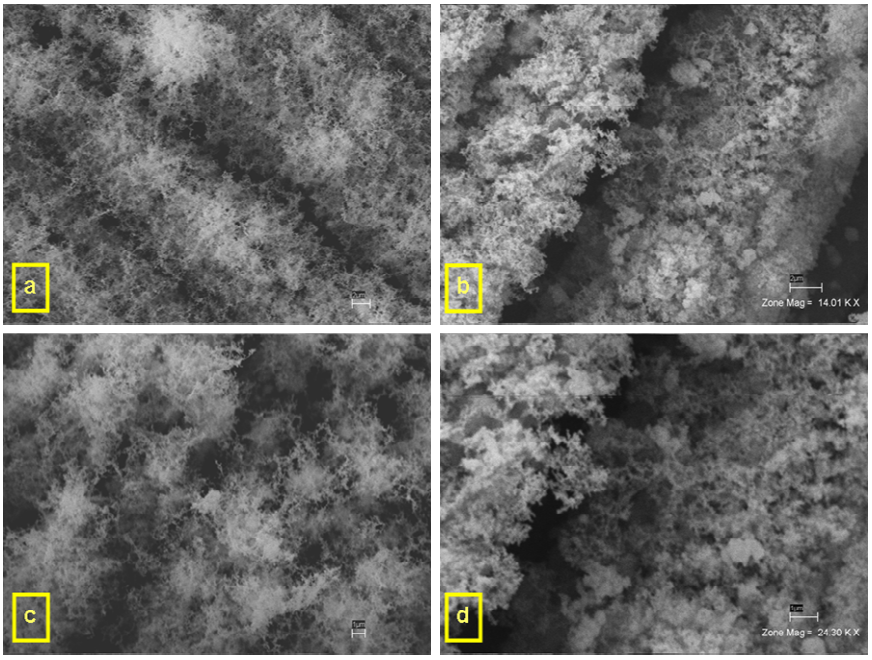

Fig.5. 40 Micrographs of substrate surface **(a)** before and **(b)** after field emission tests. High magnification images **(c)** and **(d)** revealing presence of fine structures before and after field emission tests respectively. *[Micrographs (a) and (b) have a scale bar of 2 µm with (c) and (d) having a scale bar of 1 µm]*

5.13.2 *Carbon nanotubes produced without the aid of a catalyst/catalyst mixture:*

The field emission characteristics of different morphologies of nanotubes were also explored. Fig. 5.41 shows the measured emission current density as a function of applied electric field for untreated, etched (obtained by treating with oxygen) and nanotube laden substrates produced without any catalyst. The inset in the Fig. 5.41 shows the

corresponding FN curves for the explored samples. It was seen that the emission characteristics of nanotubes produced with and without any catalyst presence were similar. No appreciable current emission was obtained from the untreated carbon substrate (virgin tape) and its corresponding FN equation was not a straight line. A significantly higher field was required by sharp pointed etched carbon fibre samples for field emission. It was also observed that the emission current for etched samples were highly unstable and the applied field had to be increased with time to maintain a certain current density.

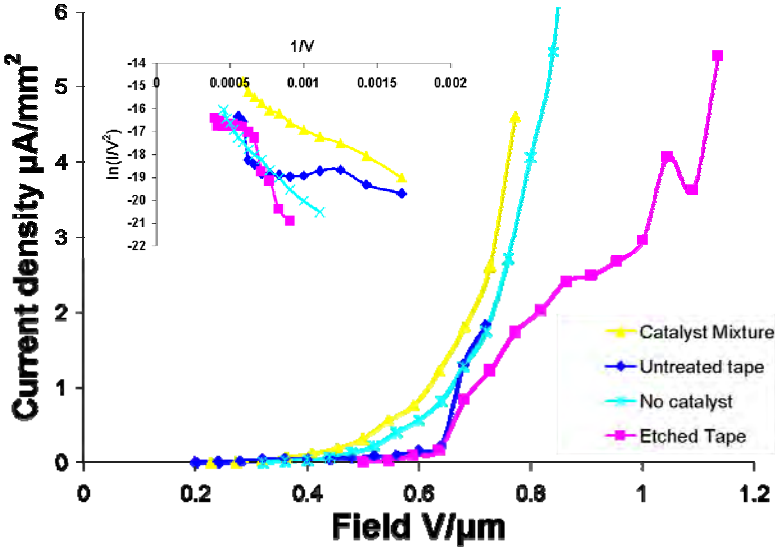

Fig.5. 41 Current density versus field curves for different forms of carbon on various substrates. The inset in the figure is the corresponding FN curve.

Surprisingly, the electron field emission characteristics of nanotubes produced on the thicker type of Carbonics tape (2 mm) produced significantly better emission characteristics. Sharp etched pointed fibre like morphology on Carbonics substrates exhibited the lowest turn-on voltage of 0.24 V/m (possibly due to presence of nanotube on their tips) of all the tested samples as shown in Fig. 5.42. The inset of Fig. 5.42 shows the corresponding F-N plot.

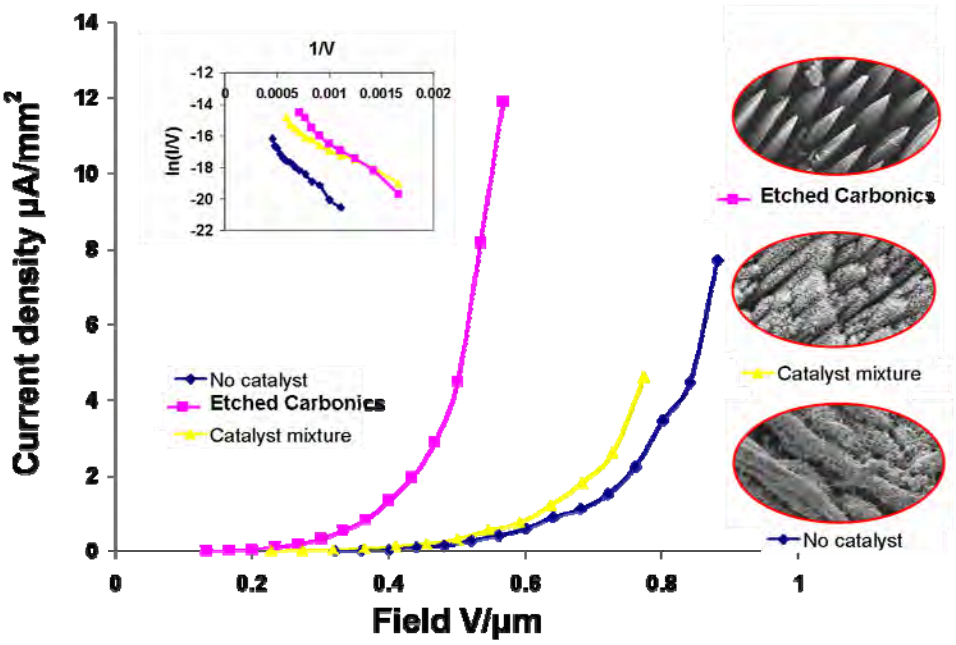

Fig.5. 42 Current density-electric field (J-F) curves of electron field emission from carbon nanotubes and etched carbon on different types of Carbonics substrate.

Table 5.2 shows the average field amplification factor (ß) of all the samples calculated from the slope of FN curve assuming a work function of nanotubes to be 4.8 eV. The average turn on voltage was reached at an applied field of 0.38, 0.30 and 0.28 V/µm for samples produced using nickel, iron and Fe/Ni mixture respectively at a vacuum gap of 2.5 mm.

Sample	Catalyst content	Enhancement factor (β)	Turn-on Voltage V/µm
Etched Carbonics	n/a	3.50E+04	0.24
Catalyst Mixture	0.5 at% Fe/Ni	4.42E+04	0.28
Iron	0.9 at%	3.82E+04	0.3
Etched thinner Carbonics	n/a	1.67E+04	0.33
Nickel	0.9 at%	4.11E+04	0.38
No Catalyst	No Catalyst	2.69E+04	0.55

Table 5. 2 Field enhancement factor and turn-on field at a vacuum gap of 2.5 mm for different samples.

Furthermore, the relationship of the field enhancement factor with vacuum gap for different types of nanotube samples was also investigated. Fig. 5.43 shows the relationship of field enhancement factor variation with the vacuum gap*'d'*. It shows that β depends on d with a relationship of β α d. It should be noted that such a relationship between β and d is universal for carbon nanotube field emitters. Ex: β increased from 19300 to 70400 when the vacuum gap was increased from 1.5 mm to 4 mm for nanotubes produced using a catalyst mixture.

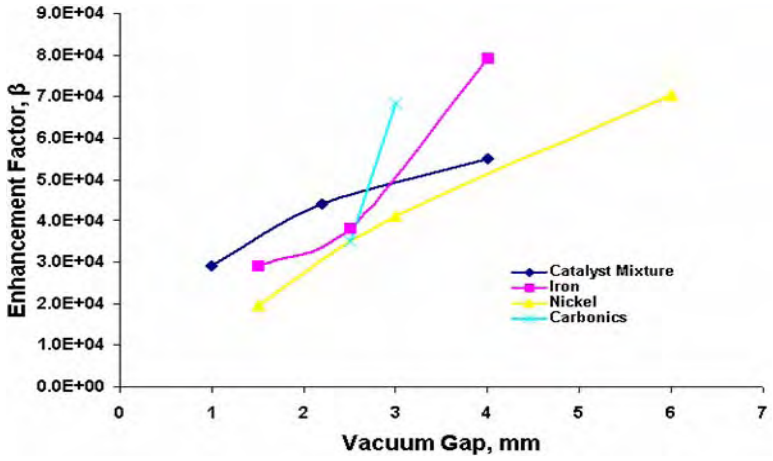

Fig.5. 43 Relationship of field enhancement factor *β* and vacuum gap *d* for various samples of carbonics tape.

5.14 Field ionisation sensor:

The field emission properties of nanotubes were used to sense different gases in a gas sensing device. The sensor works on the basis of fingerprinting the ionisation characteristics of distinct gases[127, 238]. The operating procedure and design of the gas sensor has been detailed in Chapter 3, section 3.2.2. The nanotube sensor was used to detect the identity of various gas species, such as helium, argon, carbon dioxide, oxygen, nitrogen, hydrogen and dry air. Tests performed with bare copper electrodes and a copper cathode with sticky carbon tape (with no nanotubes) demonstrated significant higher breakdown voltages for different gases. Fig. 5.44 shows the breakdown voltages of various tested gases at room temperature and at a gas concentration of 1.84 x 10^{-4} mol/L.

The anode cathode separation for all the tests was maintained at 2.5 mm. It was seen that each individual gas exhibited distinct breakdown behaviour with hydrogen displaying the lowest (305 V) and oxygen showing the highest breakdown voltage (570 V). Note that gases like oxygen and hydrogen are easier to distinguish due to their large separation in breakdown voltage when compared to gases like nitrogen and oxygen.

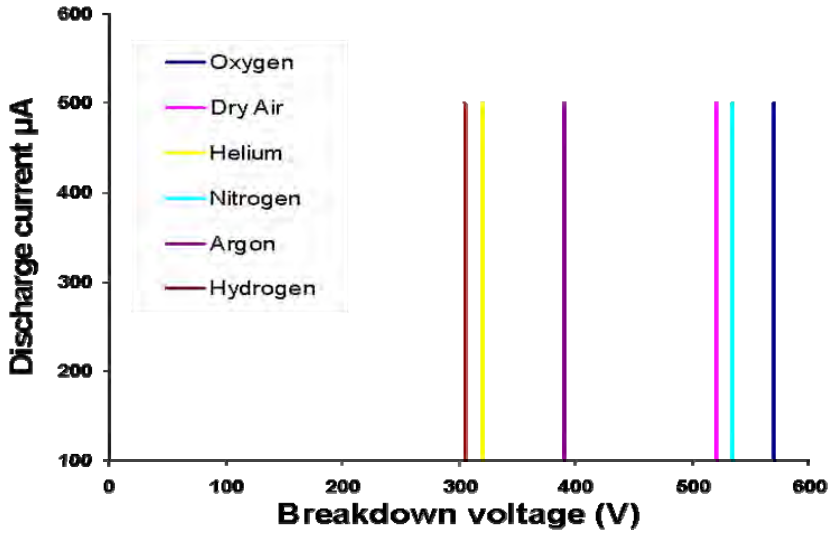

Fig.5. 44 Current-Voltage (I-V) curves of different gases showing distinct breakdown voltages at 2.5 mm gap for a nanotube cathode produced using 0.9 at% Ni ; oxygen displays the highest and hydrogen the lowest.

The effect of gas concentration on breakdown voltage was also recorded over a gas concentration range of 10^{-5} to 10^{-3} mol/L. The gas concentration was controlled by administering a controlled volume of gas to the sensor cell through a septum from a syringe. The breakdown voltage was defined as the voltage necessary for self sustaining current discharge. Fig. 5.45 shows the effect of concentration on the breakdown voltages of argon, carbon dioxide, oxygen and nitrogen. The break down voltage does not vary significantly for each of argon, helium and nitrogen for the range of explored gas concentrations (Note: these tests were done at different total gas pressures due to a constant volume of the test chamber). However, the breakdown voltage of oxygen and carbon dioxide increased significantly with increasing concentration. This increase in breakdown voltage was observed only for high electronegative gases (gases that easily

attach electrons) like carbon dioxide and oxygen. This is because oxygen atoms are known to preferentially adsorb on nanotube tips affecting their field emission characteristics. However, the breakdown voltage of Ar, He and N_2 to some extent was unique and depended mainly on the electric field, being only weakly affected by concentration. Hence, the identity of each gas can be established by monitoring the breakdown voltage of the gas.

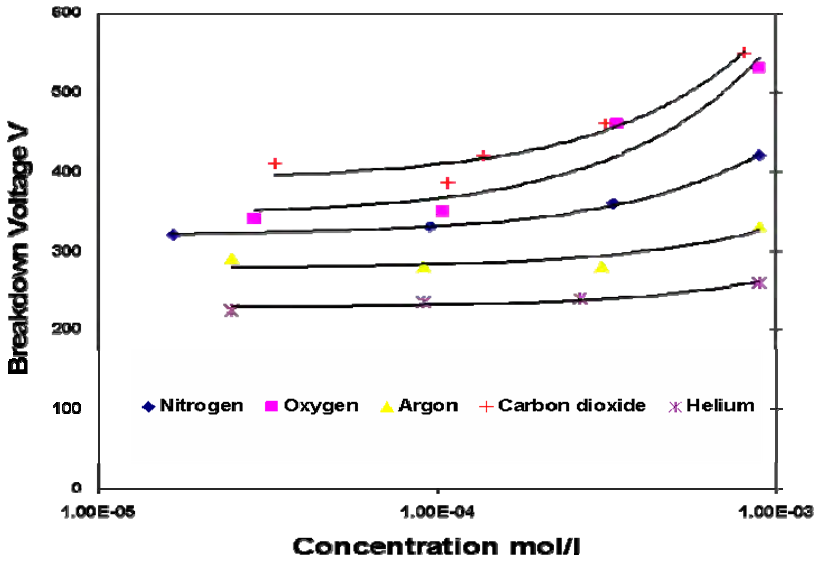

Fig.5. 45 Effect of gas concentration on breakdown voltage for various gases for a nanotube cathode.

We also obtained significantly lower breakdown voltages of individual gases as the inter-electrode spacing was reduced to a 1.2 mm gap, as shown in Fig. 5.46(a). The breakdown voltage for helium reduced from 320 V at a vacuum gap of 2.5 mm to 225 V at a gap of 1.2 mm. Fig 5.46 (b) shows the breakdown voltage for argon (1.84×10^{-4} mol/L) as a function of vacuum gap inside the sensor for two types of electrodes. The breakdown voltages for copper electrodes with no nanotubes reduced from 680 V at a gap of 4 mm to 365 V at a gap of 1.5 mm, whereas the copper-nanotube film electrode (1 mm thick Carbonics tape with 0.5 at% each of Fe/Ni) exhibited a breakdown voltage of 380 V at 4 mm to 290 V at 1.2 mm gap. The observed low breakdown voltages of different gases for distances as large as 1.2 mm are exceptional. These results are helpful to develop portable sensors from carbon nanotube cathodes which can be achieved by operating at much lower gaps.

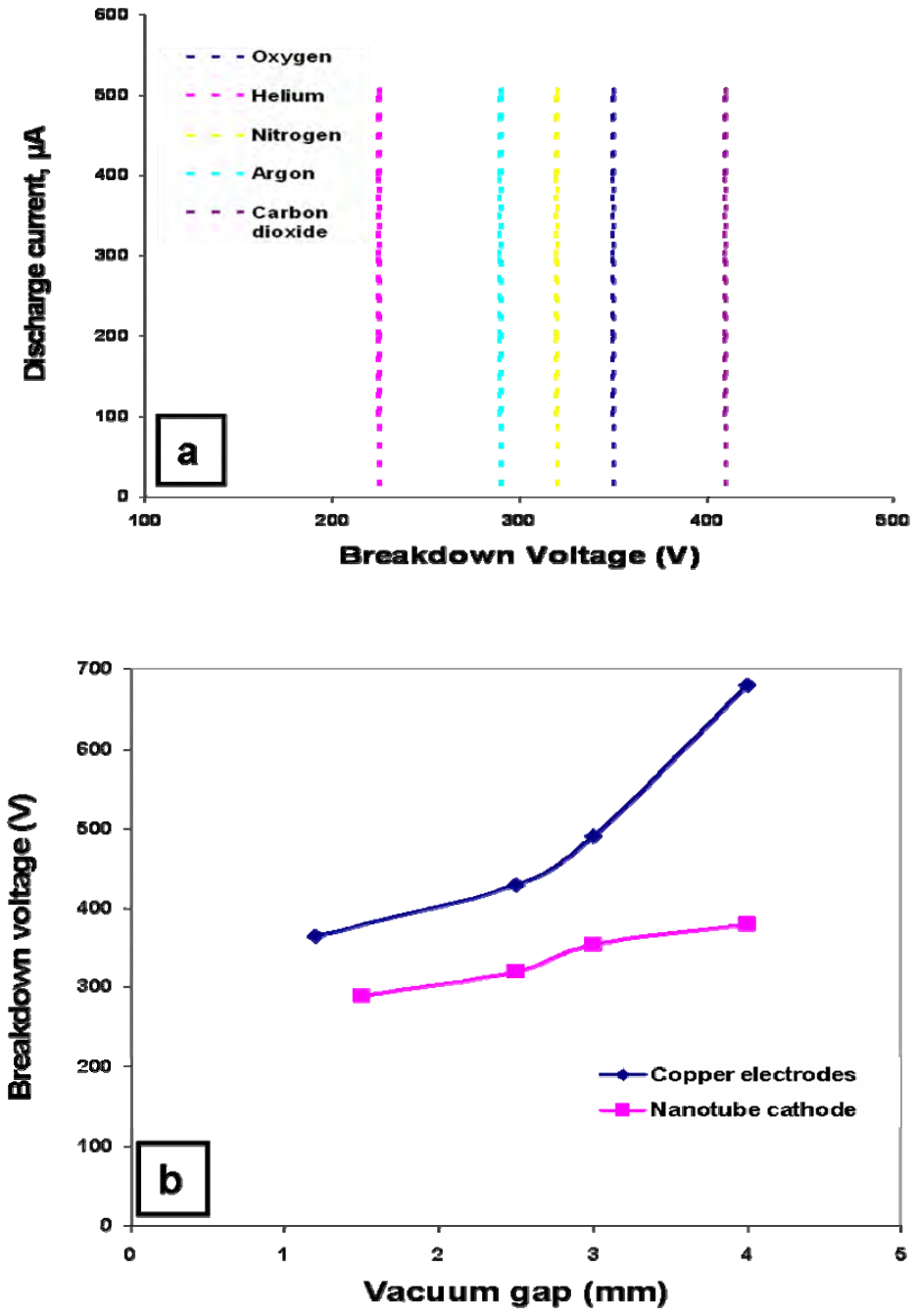

Fig.5. 46 (a) Current-Voltage (I-V) curves of different gases showing distinct breakdown voltages for a nanotube cathode at 1.2 mm gap and **(b)** effect of electrode separation on breakdown voltage of argon for bare copper electrodes and cathode with a nanotube film.

5.15 Luminescent tube:

The field emission properties of nanotubes were extended to non-planar geometries by demonstrating the operation of a cylindrical luminescent tube in a diode configuration. The luminescent tube works on the basis of "conversion" of electrons into photons by striking a conductive transparent glass electrode coated with phosphor. The operating procedure and the design of the luminescent tube were detailed in Chapter 3, section 3.2.1. An ultimate vacuum of 2 x 10^{-5} mbar was achieved inside the luminescent tube prior to its operation and the gap between the conductive phosphor coated glass and nanotube samples was maintained at 2.5 mm. The nanotube samples demonstrated low turn-on fields (0.27 V/μm) and stable current emission at low voltages.

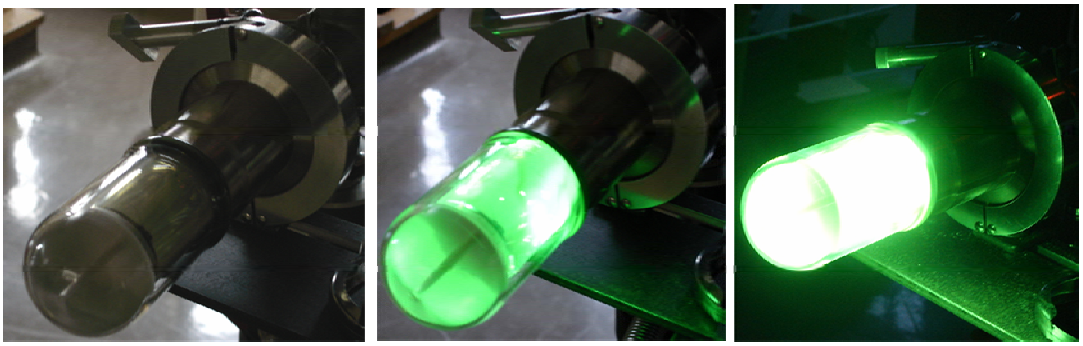

Fig.5. 47 Luminescent tube at different voltages produced using nanotubes produced using mixture of 0.5 at% Fe/Ni catalyst, the emitted current density at 2.6 kV corresponds to 1.1 mA/mm^2.

Fig. 5.47 is a picture of the lamp setup at different applied voltages. The longer nanotubes were burnt off by applying a voltage of 4 kV before making any current measurements. Emission occurs from some sparse spots on the sample at low voltages (1 kV, 50 μA) which increases and becomes more uniform as the voltage is further increased (2.8 kV, 3.38 mA). The brightness also increases with applied voltage. The J-V characteristic of the sample was recorded after several upsweep and down sweep runs until the emission was stable and reproducible, as shown in Fig. 5.48(a). The emission current was stable and the fluctuation was about 5% at a current density of 43 μA/mm^2, as shown in Fig. 5.48(b).

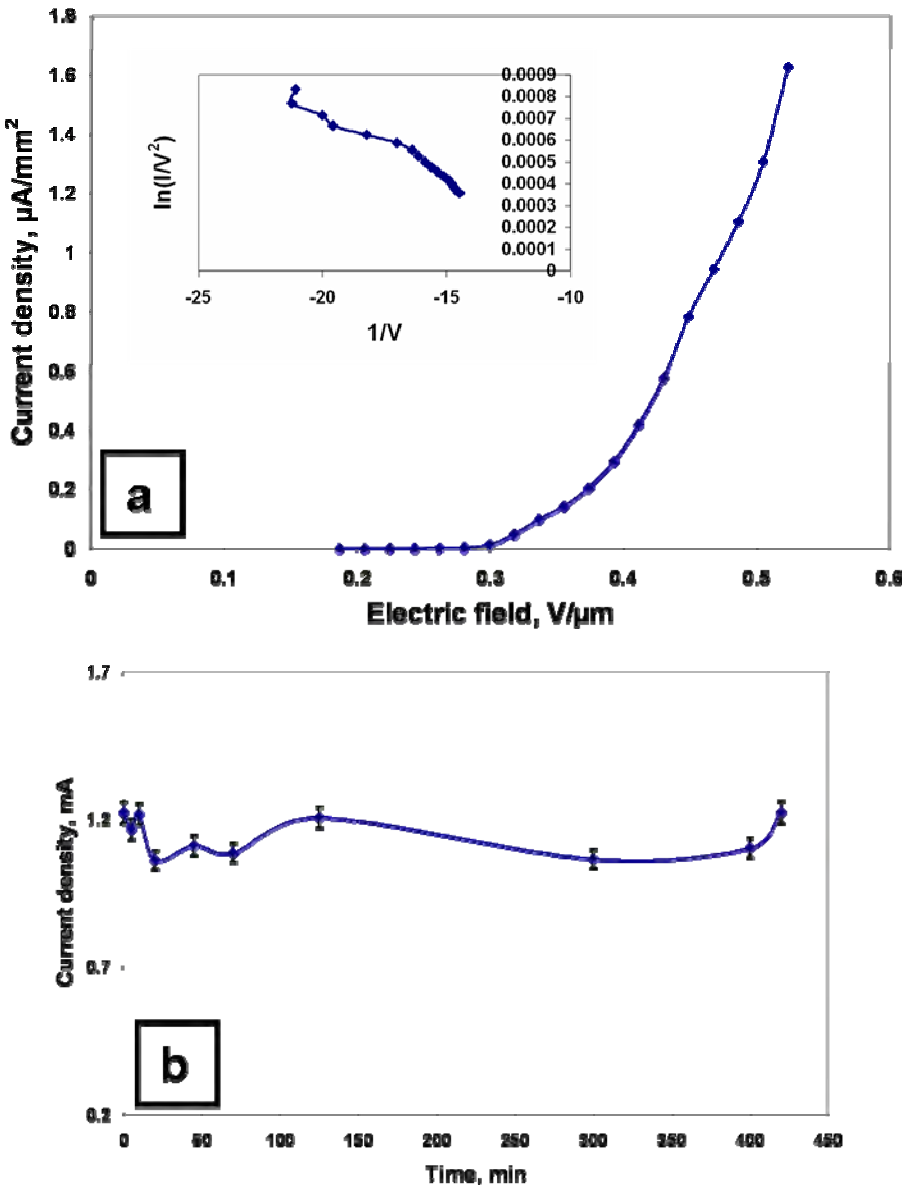

Fig.5. 48 (a) Current-voltage characteristics of the luminescent lamp produced using a sample of nanotube laden Carbonics tape (1mm thick) produced using 0.9 at% Ni catalyst, with the corresponding FN curve, **(b)** current stability of the lamp during operation.

This cylindrical geometry exhibits lower operating voltages as demonstrated by other groups[18, 308]. Our lamp has not been optimised (e.g. for phosphor efficiency) but this first example shows similar or better efficiency than a standard tungsten filament bulb (see Fig. 5.49) and are expected to be well suited for field emission applications. Other

potential applications include a portable X-ray device, secondary electrodes for space thrusters, and cheap and efficient flat panel devices.

Fig.5. 49 Comparison of the NT lamp operating at 14 W (3.3 kV, 4.2 mA) with an incandescent tungsten 15 W lamp.

6.0 Discussion:

6.1 Carbon nanotube formation:

The major emphasis in research activity of carbon nanotubes in recent years has been in production and characterisation. The formation mechanism of carbon nanotubes in CVD systems is well understood and documented[309, 310]. A detailed understanding of carbon nanotubes formation in high energy systems such as arc discharge and laser ablation is still lacking. So far, it has been impossible to determine their growth mechanism in arcs from direct experimentation. However, several qualitative models have been proposed by various researchers, but there is no agreement yet on a full and self-consistent theory of nanotube formation in arc/laser plasma.

The most recognised and commonly accepted theory of nanotube formation in arcs is based on the model put forth by Gamaly[311]. They considered various physical parameters of the plasma near the cathode surface like the space and time distribution of density, velocity and temperature of carbon vapours, electric charge, potential, electric field and deduced a model for nanotube formation. Based on the above parameters they found a thin layer of carbon vapour next to the electrode surface and speculated that to be the most appropriate area for nanotube formation. They explained their model based on the interaction of two major groups of carbon vapour with different velocity distributions in the arc discharge plasma. The first group has an undirected flux and Maxwelllian velocity distribution corresponding to the temperature of the arc. The second group has a directed flux comprising of ions, which have been accelerated in the electric field between the electrodes with higher velocities. Based on the interaction between the above specie groups near the cathode, they explained nanotube formation to occur in three major steps---- *seed formation, tube growth and growth termination.*

The model explained seed formation for tube growth to occur from nanoparticles, which are formed by a process of carbon cluster growth starting from C_2. This reacting region is dominated by carbon vapour with Maxwellian distribution and without any axis of

symmetry. The tube formation and growth was explained from the interaction of directed carbon comprising of ions, colliding and attaching to the cathode surface. The model explained termination of tube growth to occur from termination of directed ion current caused by current instabilities, and the tube end capping by rearrangement of carbons having Maxwellian (isotropic) velocity distribution in the absence of current. The model described the formation of multi-walled nanotubes to occur from attachment and annealing of carbons on the growing tube from isotropically distributed carbons (Maxwellian).

Another model suggested by Smalley[312] assumed that nanotubes can only grow in plasma by an open ended “pentagon road” mechanism. He suggested nanotube growth to occur from the addition of small clusters of carbon from the gas phase through an open ended mechanism. The energy to prevent the nanotube from closing and to stabilise the open configuration during growth is proposed to be due to a high electric field. Although their model was supported by molecular dynamic calculations, the growth of nanotubes by methods like heat treatment could not be explained.

The above two well accepted models favours the open ended growth mechanism for nanotubes. However, Endo[313] suggested a growth mechanism which favoured a closed-end mechanism. They suggested that nanotubes grow by insertion of carbon atoms into closed fullerenes in the vicinity of pentagonal rings on their surface. The strain caused by insertion of small carbon fragments is equilibrated by rearrangement resulting in extension of initial fullerene cages. They found support for their idea in experiments carried out by Ulmer[314], where larger fullerenes were grown from C60 and C70 by addition of small carbon fragments. This model is not accepted, as it has problems describing multi-walled nanotubes growth.

6.2 New growth mechanism:

All the current models explain nanotube growth by addition of carbon clusters resulting from collision of smaller carbon precursors. The location for these collisions and growth is disputable since some speculate nanotube growth to occur in plasma and others on the surface of electrode/substrate. We speculate that nanotube formation is related to the concentration and composition of vapour phase close to the anode/substrate surface. Except for a small fraction of gaseous ions affected by local electric field, this vapour is expected to be close to equilibrium (both in temperature and vapour pressure) with the carbon surface at least within several mean-free-paths of it, where the nanotubes grow. Thus direct condensation of carbon from this vapour on the surface will closely follow evaporation in rate, and any part of this condensation which forms nanotubes will increase with the general exchange rate. This implies that faster nanotube growth should be favoured at higher temperatures near the sublimation temperature of the substrate surface. A temperature drop of 100 K from the sublimation temperature corresponds approximately to a 50% reduction of carbon vapour in equilibrium with the anode surface [315] and we found nanotubes at lower substrate surface temperatures. This expected behaviour contradicts our observations, casting doubt on the proposal that small gaseous species are precursors to nanotubes.

Abrahamson[257] proposed the presence of small crystallites (size < 3 nm resulting from aggregation of graphitic fragments) near the anodic surface resulting from the breakup of electrode surface during arc operation. He suggested that the observed temperature of the surface was in fact the temperature of these suspended particles, which are at their equilibrium temperature at the arc total pressure (here 1 atmosphere), considerably lower than the expected sublimation temperature of bulk graphite (3950 K) because of the surface free energy. This is observed in arc discharge in the form of a milky coloured plasma in front of the electrode surface. Therefore, the smaller the particles the lower was the observed temperature. Using this model we expect the lowest temperature to correspond to the finest particles, i.e. those in the last stage of breakup – graphene fragments. Hence, we observed the formation of nanotubes at a maximum concentration

of graphene fragments, *i.e.* lower temperatures. These fragments naturally lend themselves to addition and building of nanotube, and so there is no conflict under this scenario with the observed temperature dependence of nanotube growth.

Our experimental results provide evidence that nanotube growth occurs on the substrate at a certain optimum temperature range[307]. This is supported by the fact that nanotubes were found to occur over a narrow temperature range under the various explored parameters. The presence/growth of nanotubes at temperatures lower than the reasonable sublimation temperatures of graphite suggests that carbon vapour is unlikely to be responsible for nanotube growth.

The contribution of electric field in nanotube growth has largely remained neglected so far. A strong electric field is expected to be present close to the electrode surface due to the large potential drop in a space of about 12 μm above the electrode surface. This large potential drop is due to high resistance caused by the interaction of hot gas with a relatively cold electrode leading to less ionisation. Fig. 6.1 gives an idea of the potential drop in the space between the electrodes:

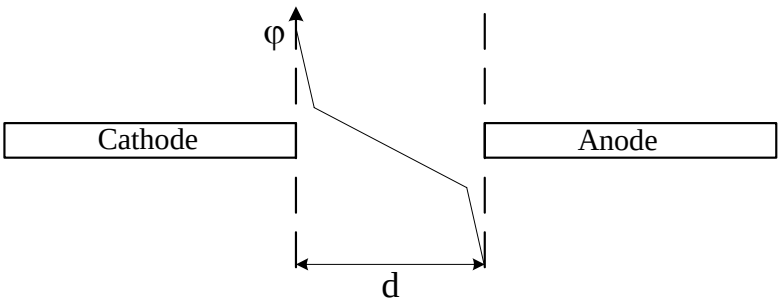

Fig.6. 1 Potential drop in the space between the electrodes.

We have seen that the surface morphology of substrate/carbon fibres are not smooth and consist of numerous protrusions. These protrusions are expected to disturb equi-potential planes and cause distortions in the electric field as shown in Fig. 6.2. A new theory of nanotube growth is presented based on this distortion of electric field.

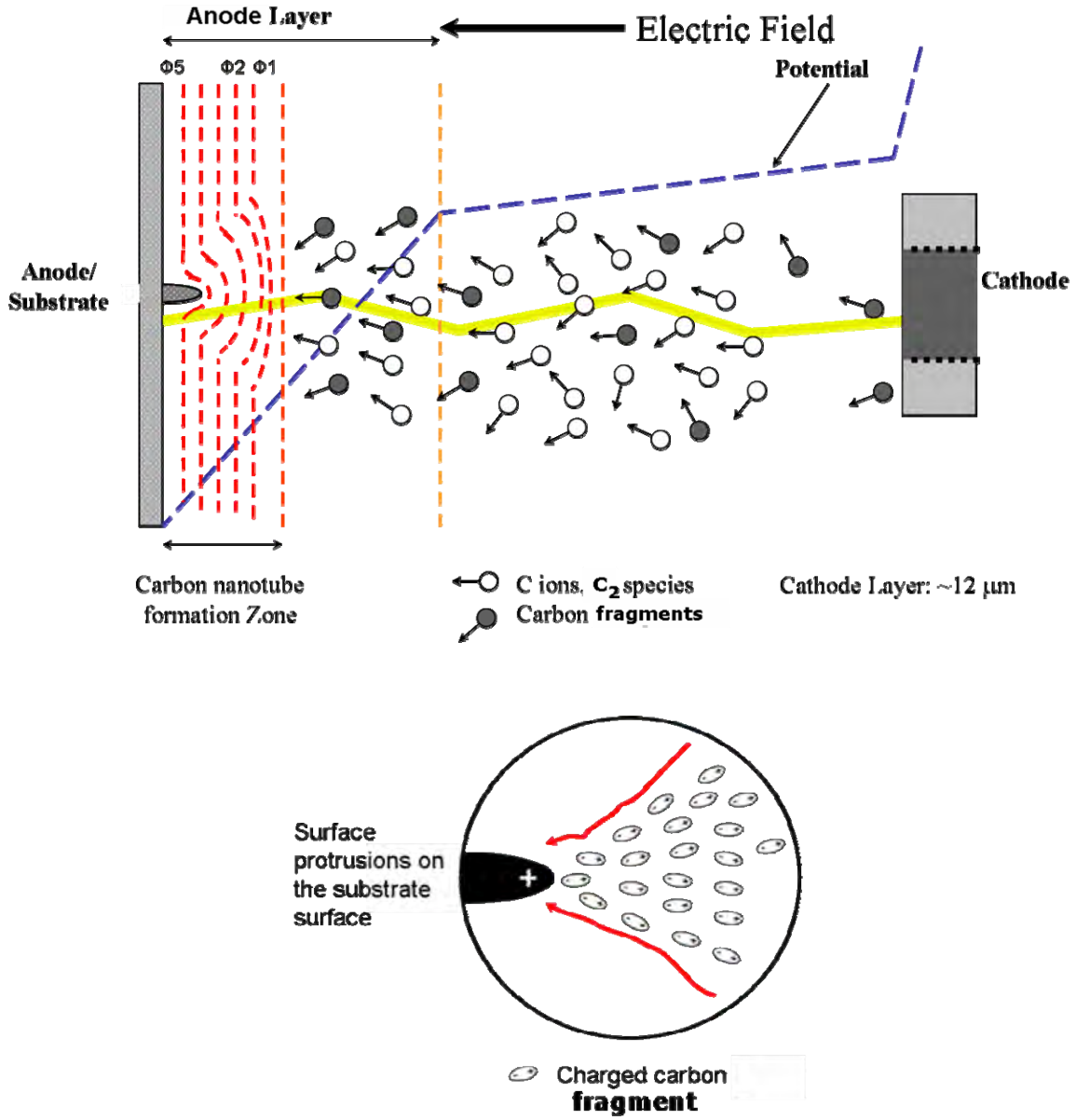

Fig.6. 2 Carbon nanotube formation mechanism, the red curves indicate constant potentials and **(b)** showing acceleration of charged carbon fragments towards anode surface due to polarisation.

This electric field will activate the motion of negatively charged particles toward the anode and positively ones towards the cathode. Thus, a global field polarisation occurs in plasma due to a self induced magnetic field from which small clusters/graphitic fragments of carbon particles (polarised) near the electrode surface are accelerated towards its surface. Any collision of these fragments is expected to result in their agglomeration to larger particles away from the plasma sheath. However, these fragments

get directed toward the distorted electric field near the electrode surface due to protrusions within the plasma sheath. This distorted electric field then collects charged carriers (graphitic fragments) like a funnel which naturally lend themselves to addition and building of nanotube. The growth is expected to speed up with increasing length of nanotube, due to higher distortion of electric field. Thus the growing nanotube tips become preferred sites for further addition of polarised carbon fragments and more material is deposited than on the surrounding anode surface. As the flux of the charged carbons keeps following the electric field lines, an elongated structure (nanotube) keeps growing. This elongated structure is speculated to be the base of a multiwalled carbon nanotube. The nanotube growth is terminated when the arc becomes unstable due to fluctuations in voltage, current or convection of plasma gas.

The occurrence of nanotubes only at the centre of arc treated path when the substrate is not touching the anode (non-contact mode) emphasizes the effect of electric field for nanotube growth in arcs. We speculate nanotube formation over the entire arc treated area (when the substrate acts as anode) to the effect of electric field. The electric field keeps the nanotubes from getting closed and aids in addition of graphitic fragments (resulting from collision of charged clusters) due to polarisation when the substrate is in contact with the anode. This also explains the formation of dense nanotubes on the thinner Sigmatex tapes (0.2 mm thick) when compared to Carbonics substrate (2 mm thick). When the substrate is not in contact with the anode, nanotube growth is dictated only by the state of carbon particles near the substrate surface due to a reduced influence of electric field. The increased thickness of nanotubes and occurrence of different carbon impurities from the centre to the periphery of arc treated patch confirms the importance of electric field. The above model thus can also explain the influence of electric field for nanotube growth in arcs.

6.3 Effect of inter-electrode gap:

Altering the arc gap over the range 1.4 mm to 7 mm at a tape speed of 3 mm/s showed large changes in surface temperature between 3850 K and 3650 K and also revealed radically different forms of carbon deposits. A gradual drop in anode surface temperature was observed, with a minimum of 3650 K at around a 5 mm arc gap, rising again as the gap was further increased. The SEM observations revealed nanotubes only at the minimum temperature of 3650 K. This is a significant find for distinguishing broad candidates for precursors to nanotubes and supports our new growth mechanism. The smaller the particles (graphene fragments), the lower is the observed temperature. This was obtained only at a specific arc gap of 5 mm and is responsible for favourable nanotube formation. Using this model we expect the lowest temperature to correspond to the finest particles at this arc gap, i.e. those in the last stage of breakup – graphene fragments. Where we observe the formation of nanotubes then corresponds to a maximum concentration of graphene fragments. These fragments naturally lend themselves to addition and building of nanotubes, and so there is no conflict under this scenario with the observed temperature dependence of nanotube growth. This explains the observation of nanotube formation/growth only at specific arc gap ranges, in comparison with no nanotubes at other arc gap values.

6.4 Effect of flushing:

The observations made on flushing nitrogen through the substrate into the arc were that 1) fewer nanocrystallites were found attached to the nanotubes at higher flushing flow, 2) the observed surface temperature did not alter appreciably (~3650 ± 50 K), and 3) the number concentration of nanotubes is little changed but the diameter is smaller.

If we take the gaseous precursor model, the temperature of the gas close to the nanotubes does not change, but the carbon vapour is expected to dilute with increasing nitrogen flow. Thus if the nanocrystallites were deposited from this diluted vapour, fewer of them would be expected, in accord with our experiments. Also thinner nanotubes may be

expected in agreement with observations. However, we cannot account for any mechanism for a constant number of nanotubes, nor for a constant temperature irrespective of gas flow.

The suspended particle model results in expected deposition of nanocrystallites on the growing nanotubes similar to a filter deposition. Additional nitrogen gas flow away from the surface increases the outward velocity, so the advected particles spend less time in the vicinity, and so have less chance to diffuse to nanotubes and stick there. Observation of the heated surface from the other side of the arc still includes seeing all the suspended crystallites even though they are further out from the surface. Thus the observed temperature is not expected to change, as observed, but purer nanotubes are seen.

6.5 Effect of substrate speed:

Altering the substrate speed over the range 0.8 to 5.6 mm/s at a gap of 5 mm showed small changes in surface temperature between 3750 and 3650 K but showed radically different forms of carbon deposit. At the lowest speed, cauliflower forms resulted, then nanotubes at 3 mm/s, and above this honeycomb-like structures dominated. Significantly, the appearance of the arc attachment changed for speeds above 3 mm/s, from being coherent and steady below this value, to a more unsteady wandering attachment.

The fall-off in temperature at the highest speed of 5.6 mm/s may be explained by a heating rate/thermal capacitance effect but the almost steady temperature at lower speed cannot be similarly explained. If we accept that nanocrystallites are present, they are likely to influence the temperature in this manner. They may also influence the conductivity of the anode arc attachment, encouraging a uniform coherent attachment where they (nanotubes) are plentiful, and causing the transition to an unstable attachment where they are sparse. Deposition to the various forms is also likely to be related to this availability of nanocrystallites.

However, there appears to be a time effect on the arc instability, which is not covered by the simple presence of suspended nanocrystallites. While all other parameters are held

constant (arc gap, current, gas flows), when the duration of the arc attachment on the anode becomes longer than a critical value, instability occurs. This exposure time corresponds to the time of travel of any point on the substrate as it passes across the attachment. The critical time is that for a speed of 3 mm/s where a mat of nanotubes are observed on cool down. For a span of 8 mm of the arc-treated high temperature region, the critical duration is 8/3 = 2.7 s. In previous work[17] we have observed a layer of nanotubes beneath the spherical nodules or "cauliflowers" which are found at slower speeds (longer time). Thus it appears that nanotubes are deposited within ~2.7 s and any longer exposure to the arc attachment covers them with other types of deposits. Then either nanotubes or cauliflowers on the surface encourage a stable diffuse arc attachment, but a shorter time than that necessary for nanotube deposition promotes unstable operation. We must reach the conclusion that nanotube or cauliflower surface detail is necessary for the diffuse arc attachment.

6.6 Effect of Inert gas:

The importance of inert gas and its pressure on nanotube formation has been studied by various research groups. Helium gas at a pressure of 500 Torr[42, 316] is known to be the most suitable gas for nanotube production compared to argon[43, 50] and nitrogen[317]. However, helium did not appreciably influence nanotube formation in our reactor at any arc gap, but use of argon resulted in a shift in the optimum arc-gap for nanotube deposition. (an optimal gap of 5.2 mm in presence of N_2 compared to 3.4 mm in presence of argon). This is surprising since nanotube formation is known to be favoured in helium atmospheres due to a more softer cooling, and fullerene formation is favoured under argon atmospheres due to high temperatures. Dense nanotubes were commonly found only in the presence of nitrogen. Abrahamson[257] reported that the state of vapour near the anode surface in the vicinity of growing carbon nanotubes will be largely carbon molecules and fragments, rather than the surrounding gas. Thus the type of inert gas or the surrounding gas near the nanotube formation zone is not expected to influence nanotube production. The lower substrate temperature values (3650 K) observed when

the reactor was operated under helium atmospheres are may be due to the high ionisation potential of helium (the thermal conductivity of argon is about eight times smaller than helium and is expected to change the kinetics of nanotube formation). However, we cannot explain a mechanism for no/little nanotube growth (very inhomogeneous) in helium in spite of favourable growth temperatures. Similarly, we cannot account for nanotube growth that was observed at substantially higher substrate temperatures (3850 K) in argon atmospheres. But our observation is consistent with the reports of Farhat[316] where they observed a very inhomogeneous nanotube distribution in helium when compared to argon. However, we speculate that the effect of the inert gas is not expected to be appreciable since our reactor always operates at atmospheric pressure. This is in agreement with the reports of Farhat[316] in which they found no influence of pressure on nanotube structure when operating with a single inert gas (argon or helium) but only observed change in nanotube density.

6.7 Effect of catalyst:

The discovery of single walled nanotubes using a catalyst, and its superior properties over multi-walled nanotubes for certain applications has initiated extensive research on the influence of different catalysts on nanotube growth. Catalyst like Fe, Ni, Co and other transition metals are commonly used for nanotube growth in arc and CVD systems[318-321]. In general, it is noticed that the catalytic activity is much better when a mixture of catalysts are supported on an active support, than their presence individually or unsupported[322, 323]. The use of a heterogeneous catalyst leads to improved yield of nanotubes in arc systems and provides an ability to control their diameters for CVD systems[319, 320]. In this work, iron, nickel and a mixture of Ni/Fe catalyst were used as catalysts to investigate their effect on nanotube growth in our system.

The use of iron as a catalyst did not have a major influence on nanotube growth. The occurrence of no nanotubes when Ferrofluid (particle size of 10 nm) was used, can be attributed to a lack of catalyst presence or due to a non-uniform distribution of catalyst

particles on the porous carbon substrate. This is supported by SEM micrographs where we hardly observed any catalyst particles on individual substrate fibres. However, nanotubes were observed only at the optimal arc gap when iron nanoparticles were distributed using wet impregnation on the substrate surface. The growth of nanotubes is expected by the interaction of molten catalytic particles and carbon species near the substrate surface. It is speculated that at high temperatures, the diffusion rate of iron particles into carbon fibres is increased and the possibility of nanotube growth is reduced. The presence of nanotubes at the optimal arc gap indicates that nanotube growth is favoured only at lower temperatures in arcs even in the presence of iron as a catalyst. Zhu[323] found nanotubes in a limited temperature range of 650-800C using Iron as catalyst on a substrate in a thermal CVD system. A similar effect may be thought to occur in arc systems at a certain optimum temperature (maximum carbon fragments) where the catalyst particle is saturated with carbon fragments leading to carbon nanotube growth.

We observed nanotube growth over a broad arc gap range when nickel was used as a catalyst. This can be attributed to high activity of nickel compared to iron[324]. It has been observed quite commonly in CVD systems that the growth rate of nanotubes using a nickel catalyst is higher than that on iron.

The use of a bimetallic mixture of Fe/Ni (0.5 at %) resulted in nanotube occurrence over a wider arc gap range than that obtained by using a nickel catalyst. This indicates that the complex nature of the iron-nickel alloy catalyst exerts a significant influence on growth of nanotubes, as compared with pure iron or a pure nickel catalyst. This result is consistent with other studies of increased nanotube yield in arc discharge using bimetallic catalysts[319, 325].

However, the catalytic influence of bimetallic catalysts on nanotube growth in arc discharge has remained an open question. Available results suggest that the catalytic particles rapidly assemble to form an alloy in a region of high carbon density leading to nucleation and growth of nanotubes. This is found to happen only when the catalyst particles reach a certain critical size. The decrease in temperature leads to decreased

solubility of carbon into the catalyst/alloy and results in its segregation onto the catalyst surface. This forms the seed for nanotube growth from where it grows by further addition of graphitic fragments by a mechanism described earlier.

7.0 Conclusion

A feasible method of depositing carbon nanotubes continuously at atmospheric pressure on a substrate in real time has proved the validity of the reactor. The advantage of this method is its ability to deposit nanotubes directly on a carbon substrate eliminating the need for further treatment. Parameters like inter-electrode gap, substrate speed were found to be vital in obtaining high yields of nanotubes on the substrate. An inter-electrode gap of ~ 5.2 mm and a substrate velocity of ~3 mm/s were found to be ideal for copious carbon nanotube occurrence on the substrate. Nanotubes were also grown in nitrogen, argon and helium atmospheres, which indicated that nanotube formation occurs within a thin boundary layer of carbon vapour containing nanocrystallites, graphene fragments near the electrode surface and is therefore independent of the surrounding atmosphere. The influence of oxygen during cool down was found to be crucial for the purity of nanotubes, but no optimum could be achieved in the explored concentration range. Overall, carbon nanotube formation was strongly influenced by the type and concentration of catalyst. Carbon nanotubes produced with a Ni and Ni/Fe catalyst were finer, contorted and were associated with fewer impurities than nanotubes produced without a catalyst.

Carbonics and Sigmatex tapes proved to be suitable for the process and copious amounts of nanotubes were found on the thinner Sigmatex tape, once optimum parameters were identified. The growth/deposition of nanotubes appeared to be confined to only a few layers of fibers at the arc treated end, but the inner fibers were not covered with nanotubes. No nanotubes were found on unidirectional substrates as the tapes could not endure arc treatment for a longer time due to melting of glass binder which holds all the fibers together.

A new growth model is introduced to explain the formation of nanotubes. In this model nanotube formation is explained to occur from polarisation of carbon species near the

electrode surface and by addition of graphene fragments and nanocrystallites. This suggests that carbon vapour is unlikely to be responsible for nanotube growth.

For most applications, it is essential for nanotubes to be firmly attached to a substrate to benefit from their exceptional mechanical and electrical properties. The nanotube-laden substrate samples were tested for their field emission properties. The samples exhibit low turn-on voltage and excellent current stability in their operation as a luminescent tube and in a gas ionisation sensor.

Theoretical modelling of the behaviour of a single nanotube during field emission was performed using finite element analysis software (COMSOL 3.2) to understand the effect of various physical parameters on field emission. The results reveal that resistive heating (temperature) limits the maximum current carried by an individual nanotube.

References:

1. D. Riehl L. Vivien, F. Hache and E. Anglaret *Optical limiting properties of carbon nanotubes.* Physica B, 2002. **323**(1-4): p. 233-234.
2. J. P. Lu, *Novel magnetic properties of Carbon Nanotubes.* Physical Rreview Letters, 1995. **74**(7-13): p. 1123-1126.
3. M. Croci J-M Bonard, C. Klinke, R. Kurt, O. Noury, N. Weiss., *Carbon nanotube films as electron field emitters.* Carbon, 2002. **40**: p. 1715-1728.
4. N De Jonge and J-M Bonard., *Carbon nanotube electron sources and applications.* Proceedings of the Royal Society of London. Series A, 2004. **362**: p. 2239-2266.
5. J. Robertson, *Realistic applications of CNT's*, in *Materials Today*. October 2004. p. 46-52.
6. Z. Dong Yang, B. Huang, Y. Liu, L. Yan, F-Y. Li, Hu-Lin, *Enhanced wear resistance and micro-hardness of polystyrene nanocomposites by carbon nanotubes.* Materials Chemistry and Physics, 2005. **94**(1): p. 109-113.
7. A.N. Obraztsov, *Vacuum electronic applications of nano-carbon materials*, in *NATO-Advance Study Institute (ASI) Nanoengineered Nanofibrous Materials*. 2003, Drextel University: Antalya, Turkey. p. 327-338.
8. J. Cumings M. Ishigami, Zettl A, Chen S., *A simple method for the continuous production of carbon nanotubes.* Chemical Physics Letters, 2000. **319**(5-6): p. 457-459.
9. R. Jacques Andrews, D. Rao, A. M. Derbyshire, F. Qian, D. Fan, X. Dickey, E. C. Chen, J., *Continuous production of aligned carbon nanotubes: a step closer to commercial realization.* Chemical Physics Letters, 1999. **303**(5-6): p. 467-474.
10. J. No Kim, K. Lee, C. Jin, *Growth and field emission of carbon nanotubes on electroplated Ni catalyst coated on glass substrates.* Journal of Applied Physics, 2001. **90**(5): p. 2591-2594.
11. D. Z. Wang S. H. Jo, J. Y. Huang, W. Z. Li, K. Kempa and Z. F. Ren, *Field emission of carbon nanotubes grown on carbon cloth.* Applied Physics letters, 2004. **85**(5): p. 810-813.
12. O Smiljanic, Dellero T, Serventi A, Lebrun G, Stansfield B. L, Dodelet J. P, Trudeau M, Desilets S., *Growth of carbon nanotubes on Ohmically heated carbon paper*. Chemical Physics Letters, 2001. **342**(5-6): p. 503-509.
13. J.C Siew and Keen, *Production of Carbon nanotubes by electric arc method* 2000, Deparment of Chemical and Process Engineering, University Of Canterbury.: Christchurch.
14. Hill A. M and P. Mani, *Carbon nanotube production by the electric arc method*. 2001, Department of Chemical and Process Engineering, University Of Canterbury: Christchurch.
15. C. Ulubay, *Development and testing of a continuous reactor for deposition of carbon nanotubes on a substrate*, in *Chemical Engineering*. 2002, University of Canterbury: Christchurch. p. 1-100.

16. R. H. Archer, *Carbon nanotube production via an electric arc*, in *Chemical Engineering*. 2002, University Of Canterbury: Christchurch.
17. T. Querrioux, *Carbon nanotube continuous production.*, in *Chemical and Process Engineering Department, Masters Thesis*. 2004, University of Canterbury: Christchurch. p. 1-116.
18. Stockli T. Bonard J-M, Noury O., Chatelain A., *Field emission from cylindrical carbon nanotube cathodes: Possibilities for luminescent tubes.* Applied Physics Letters, 2001. **78**(18): p. 2775-2777.
19. S. Marthosa, *Carbon nanotubes in a field emission lamp.* 2003, University of Canterbury: Christchurch. p. 1-23.
20. R. B. Betty, *Gas Ionisation sensor utilising carbon nanotubes* 2004, University of Canterbury.: Christchurch. p. 1-36.
21. W. Lamb Kratschmer, Lowell D. Fostiropoulos, K. Huffman, Donald R., *Solid C60: a new form of carbon.* Nature, 1990. **347**(6291): p. 354-358.
22. Chia-Chun S. P.Chen, Kelty, Lieber, Charles M., *Superconductivity at 30 K in caesium-doped C60.* Nature, 1991. **352**(6332): p. 223-225.
23. S. Iijima, *Helical microtubules of graphitic carbon.* Nature, 1991. **354**(6348): p. 56-58.
24. Roger Bacon, *Growth, Structure, and Properties of Graphite Whiskers.* Journal of Applied Physics, 1960. **31**(2): p. 283-290.
25. P. G. Wiles and J. Abrahamson, *Carbon fibre layers on arc electrodes--I : Their properties and cool-down behaviour*. Carbon, 1978. **16**(5): p. 341-349.
26. D. S. Bethune, Klang, C. H.,de Vries, M. S.Gorman, G.Savoy, R.Vazquez, J.Beyers, *Cobalt-catalysed growth of carbon nanotubes with single-atomic-layer walls.* Nature, 1993. **363**(6430): p. 605-607.
27. S. Iijima, T. Ichihashi, *Single-shell carbon nanotubes of 1-nm diameter*. Nature, 1993. **363**(6430): p. 603-605.
28. Dresselhaus G Saito R, Dresselhaus M. S., *Physical properties of carbon nanotubes*. 1999, London: Imperial College Press. 1-259.
29. N Wang Z K Tang, X X Zhang, J N Wang, C T Chan and Ping Sheng, *Novel properties of 0.4 nm single-walled carbon nanotubes templated in the channels of AlPO4-5 single crystals.* New Journal of Physics, 2003. **5**: p. 146.
30. P. J. F. Harris, *Carbon nanotubes and related structures: new materials for the twenty-first century*. 1999: Cambridge University Press.
31. David Tomanek, *Science and Application of Carbon Nanotubes*. 2002.
32. A. J Zambano, Talapatra, S, Lafdi, K, Aziz, M. T, McMillin, W, Shaughnessy, G, Migone, A. D, Yudasaka, M, Iijima, S, Kokai, F, Takahashi, K., *Adsorbate binding energy and adsorption capacity of xenon on carbon nanohorns.* Nanotechnology, 2002(2): p. 201-204.
33. NEC Laboratories, *Carbon Nanotube*, in *http://www.labs.nec.co.jp/Eng/innovative/E1/02.html*. 2002.
34. Shik Chi Tsang Peter J. F. Harris, John B. Claridge and Malcom L. H. Green, *HIgh-resolution Electron Microscopy Studies of a Microporous Carbon produced by Arc-evaporation.* J. Chem. Soc. Faraday. Trans., 1994. **90**(8): p. 2799-2802.
35. *Carbon nanofibers*, in *http://www.ep2.physik.uni-wuerzburg.de/ag_fricke/graphic/fibers/carbon_nf.html*.

36. *What is Carbon nanofoam?*, in http://www.wisegeek.com/what-is-carbon-nanofoam.htm.
37. A. Salleh, *Crazy carbon nanofoam loves magnets*, in *News in Science*. 2004, ABC Science online.
38. M. Zacek, *Aerogely a kosmicky prach*, in *Aldebaran Bulletin*. 2004.
39. Janke Dittmer Paul Alivisatos, Wendy Huynh, Robert Sanders, *Solar Cells Flexible Enough To Be Painted On Surfaces*, in *Daily University Science News*. 2002.
40. L. Kalaugher, *Nano test tubes get a reaction*, in www.nanotechweb.org. November 2004.
41. Anvar A. Zakhidov and Walt A. de Heer Ray H. Baughman, *Carbon nanotubes-the route towards applications.* Science, 2002. **297**(787-792).
42. H. Zhang, Wang, D. Xue, X. Chen, B. Peng, Shaoqi, *The effect of helium gas pressure on the formation and yield of nanotubes in arc discharge.* Journal of Physics D: Applied Physics, 1997(3): p. L1-L4.
43. N. N. Kolesnikov D. N. Borisenko, M. P. Kulakov,V. V. Kveder, *Growth of Carbon Nanotubes(CNTs) in electric arc discharge in Argon.* International Journal of Nanoscience, 2002. **1**(3-4): p. 235-246.
44. K Shimotani, Anazawa, K, Watanabe, H, Shimizu, M., *New synthesis of multi-walled carbon nanotubes using an arc discharge technique under organic molecular atmospheres.* Applied Physics A: Materials Science & Processing, 2001. **73**(4): p. 451-454.
45. N. Sano, Charinpanitkul, T. Kanki, T. Tanthapanichakoon, Wiwut, *Controlled synthesis of carbon nanoparticles by arc in water method with forced convective jet.* Journal of Applied Physics, 2004. **96**(1): p. 645-649.
46. Miki Yatsuki Hirofumi Takikawa, Tateki Sakakibara and Shigeo Itoh *Carbon nanotubes in cathodic vacuum arc discharge.* J. Phys. D: Appl. Phys., 2000. **33**: p. 826-830.
47. S. H Jung, Kim, M. R, Jeong, S. H, Kim, S. U, Lee, O. J, Lee, K. H, Suh, J. H, Park, C. K,, *High-yield synthesis of multi-walled carbon nanotubes by arc discharge in liquid nitrogen.* Applied Physics A: Materials Science & Processing, 2003. **76**(2): p. 285-286.
48. M. Ikeda H. Takikawa, K. Hirahara, Y. Hibi, Y. Tao, P. A. Ruiz, Jr. , T. Sakakibara, S. Itoh and S. Iijima, *Fabrication of single-walled carbon nanotubes and nanohorns by means of a torch arc in open air* Physica B, 2002. **323**(1-4): p. 277-279.
49. X. K Wang, Lin, X. W, Dravid, V. P, Ketterson, J. B, Chang, R. P. H., *Carbon nanotubes synthesized in a hydrogen arc discharge.* Applied Physics Letters, 1995. **66**(18): p. 2430-2432.
50. A. Scott S. Farhat, C. D, Lefrant, M. L. Loiseau, S. Journet, de La Chapelle, C. Bernier, Patrick, *Diameter control of single-walled carbon nanotubes using argon--helium mixture gases.* The Journal of Chemical Physics, 2001. **115**(14): p. 6752-6759.
51. A Huczko, Lange, H, Byszewski, P, Poplawska, M, Starski, A, *Fullerene Formation in Carbon Arc: Electrode Gap Dependence and Plasma Spectroscopy.* Journal of Physical Chemistry A, 1997. **101**(7): p. 1267-1269.

52. H Lange, Baranowski, P, Huczko, A, Byszewski, P, *An optoelectronic control of arc gap during formation of fullerenes and carbon nanotubes.* Review of Scientific Instruments, 1997. **68**(10): p. 3723-3727.
53. X. K Wang, Lin, X. W, Dravid, V. P, Ketterson, J. B, Chang, *Stable glow discharge for synthesis of carbon nanotubes.* Applied Physics Letters, 1995. **66**(4): p. 427-429.
54. Omote Hideki Sugai Toshiki, Bandow Shunji, Tanaka Nobuo, Shinohara Hisanori, *Production of fullerenes and single-wall carbon nanotubes by high-temperature pulsed arc discharge.* The Journal of Chemical Physics, 2000. **112**(13): p. 6000-6005.
55. Rahul Shastry and John Abrahamson, *Carbon Nanotube Electrodes as Supercapacitors*. 2007, Canterprise Limited: Christchurch. p. 1-7.
56. Satsuki Kamo Seiji Akita, Yoshikazu Nakayama, *Diameter Control of Arc Produced Multiwall Carbon Nanotubes by Ambient Gas Cooling.* Jpn. J. Appl. Phys., 2002. **41**(4B): p. L487-L489.
57. José Gino Venegas Romero John G Huber, James David Spivey e Carlos Alberto Luengo *A bench arc-furnace facility for fullerene and single-wal nanotube synthesis.* Quím. Nova 2001. **24**(6): p. 898-900.
58. D. S. Tang, Xie,S. S.Chang,B. H.Sun,L. F.Liu,Z. Q.Zou,X. P.Li,Y. B.Ci,L. J.Liu,W.Zhou,W. Y. and G. Wang, *Effect of acetylene in buffer gas on the microstructures of carbon nanotubes in arc discharge.* Nanotechnology, 2002. **4**: p. L1-L4.
59. R. Dubrovsky, V. Bezmelnitsyn, and Yu. Sokolov, *Reduction of cathode carbon deposit by buffer gas outflow.* Carbon, 2005. **43**(4): p. 796-802.
60. S-D Wang, Chang M-H, Cheng J-J, Chang H-K, L. Kenneth, Ming-Der, *Unusual morphologies of carbon nanoparticles obtained by arc discharge in deionized water.* Carbon, 2005. **43**(6): p. 1322-1325.
61. Julien Marie Houjin Huang, Hisashi Kajiura, and Masafumi Ata *Improved Oxidation Resistance of Single-Walled Carbon Nanotubes Produced by Arc Discharge in a Bowl-like Cathode* Nano Letters, 2002. **2**(10): p. 1117-1119.
62. M. Kato H. Takikawa, Y. Hibi, T. Sakakibara, T. Tahara, S. Itoh, *Transformation of graphite into multi-walled carbon nanotubes by AC torch-arc.* Physica B, 2002. **323**: p. 287-289.
63. S. Hiroyuki Yokomichi H., Ichihara M., S. Fumiko, Itoh K., Kishimoto N., *Effects of high magnetic field on the morphology of carbon nanotubes and selective synthesis of fullerenes.* Applied Physics Letters, 1999. **74**(13): p. 1827-1829.
64. J. C. Bae, Yoon Y. J., Baik, H. Koo, Lee, S-J, Song, K. Moon, *Effect of a rotating electrode on the formation of single-walled carbon nanotubes.* Applied Physics Letters, 2003. **82**(13): p. 2154-2156.
65. T. Mieno, *Characteristics of the gravity-free gas-arc discharge and its application to fullerene production.* Plasma Physics and Controlled Fusion, 2004(1): p. 211-219.
66. M Kanai, Koshio, A, Shinohara, H, Mieno, T, Kasuya, A, Ando, Y, Zhao, X., *High-yield synthesis of single-walled carbon nanotubes by gravity-free arc discharge.* Applied Physics Letters, 2001. **79**(18): p. 2967-2969.

67. T. Guo, Nikolaev, P., Thess, A., Colbert, D. T., and Smalley, R. E., *Catalytic growth of single-walled nanotubes by laser vaporization.* Chemical Physics Letters, 1995. **243**(1-2): p. 49-54.
68. C. D. Scott, Arepalli, S., Nikolaev, P., and Smalley, R. E., *Growth mechanisms for single-wall carbon nanotubes in a laser-ablation process.* Applied Physics A: Materials Science & Processing, 2001. **72**(5): p. 573-580.
69. R.D. de Fouw M. Daenen, B. Hamers, P.G.A. Janssen, K. Schouteden, M.A.J. Veld, *The Wondrous World of Carbon Nanotubes*. 2003, Eindhoven University of Technology. p. 1-96.
70. Pavel Nikolaev Ting Guo, Andrew G. Rinzler, David Tománek, Daniel T. Colbert, and Richard E. Smalley, *Self-Assembly of Tubular Fullerenes.* J. of. Phys. Chem., 1995. **99**: p. 10694-10697.
71. CVD, in *http://www.fy.chalmers.se/atom/research/nanotubes/experimental.xml*: Goteborg.
72. M. S Kabir, Morjan, R. E, Nerushev, O. A, Lundgren, P, Bengtsson, S, Enokson, P, Campbell, E. E. B., *Plasma-enhanced chemical vapour deposition growth of carbon nanotubes on different metal underlayers.* Nanotechnology, 2005(4): p. 458-466.
73. S Hofmann, Ducati, C, Robertson, J, Kleinsorge, B., *Low-temperature growth of carbon nanotubes by plasma-enhanced chemical vapor deposition.* Applied Physics Letters, 2003. **83**(1): p. 135-137.
74. C. J. Lee, Kim, D. W. Lee, T. J. Choi, Young C. P., Young S. K., Won S. Lee, Young H. Choi, Won B. Lee, N. S. Kim, J. M. Choi, Yong G. Yu, S. Chang, *Synthesis of uniformly distributed carbon nanotubes on a large area of Si substrates by thermal chemical vapor deposition.* Applied Physics Letters, 1999. **75**(12): p. 1721-1723.
75. Sun Z Guo PS, Chen YW, Zheng ZH *A novel approach to mass synthesis of raw CNTs for printed field emission cathodes by chemical vapour deposition* Materials Letters, 2006. **60**(7): p. 966-969.
76. F Rohmund, Morjan, R. E, Ledoux, G, Huisken, F, Alexandrescu, R., *Carbon nanotube films grown by laser-assisted chemical vapor deposition.* Journal of Vacuum Science & Technology B: Microelectronics and Nanometer Structures, 2002. **20**(3): p. 802-811.
77. G. S Choi, Cho, Y. S, Hong, S. Y, Park, J. B, Son, K. H, Kim, D. J., *Carbon nanotubes synthesized by Ni-assisted atmospheric pressure thermal chemical vapor deposition.* Journal of Applied Physics, 2002. **91**(6): p. 3847-3854.
78. *Chemical Vapour Deposition*, in *http://en.wikipedia.org/wiki/Chemical_vapour_deposition*.
79. C. Bower, Zhou, O Zhu, W. Werder, D. J. Jin, Sungho, *Nucleation and growth of carbon nanotubes by microwave plasma chemical vapor deposition.* Applied Physics Letters, 2000. **77**(17): p. 2767-2769.
80. David Mann Guangyu Zhang, Li Zhang, Ali Javey, Yiming Li, Erhan Yenilmez, Qian Wang, James P. McVittie, Yoshio Nishi, James Gibbons, and Hongjie Dai *Ultra-high-yield growth of vertical single-walled carbon nanotubes: Hidden roles of hydrogen and oxygen* Proceeding of the National Academy of Sciences of the United States of America, 2005. **102**(45): p. 16141-16145.

81. J.P. Hare N. Grobert, W.K. Hsu, H.W. Kroto, M. Terrones, D.R. M. Watson and Y. Q. Zhu, *New advances in the creation of nanostuctured materials.* Pure and Applied Chemistry., 1999. **71**(11): p. 2125-2130.
82. W. K. Hsu, Terrones, M., Hare, J. P., Terrones, H., Kroto, H. W., Walton, D. R. M., *Electrolytic Formation of Carbon Nanostructures.* Chemical Physics Letters, 1996. **261**: p. 161-166.
83. Randall L. Vander Wal, Hall, Lee J., Berger, Gordon M, *Optimization of Flame Synthesis for Carbon Nanotubes Using Supported Catalyst.* Journal of Physical Chemistry B, 2002. **106**(51): p. 13122-13132.
84. T. Pichler E. Borowiak-Palen, X. Liu, M. Knupfer, A. Graff, O. Jost, W. Pompe, R. J. Kalenczuk and J. Fink, *Reduced diameter distribution of single-wall carbon nanotubes by selective oxidation* Chemical Physics Letters, 2002. **363**(5-6): p. 567-572.
85. Shigemitsu Tsutsui Hisashi Kajiura, Houjin Huang and Yousuke Murakami, *High-quality single-walled carbon nanotubes from arc-produced soot* Chemical Physics Letters, 2002. **364**(5-6): p. 586-592.
86. M. E. Anderson E. Farkas, Z. H. Chen, A. G. Rinzler, *Length sorting cut single wall carbon nanotubes by high performance liquid chromatography* Chemical Physics Letters, 2002. **363**(1-2): p. 111-116.
87. I. Mart, Callejas M. A, Benito, A. M. Cochet, M. Seeger, T. Ans, oacute, N, A. Schreiber, J. Gordon, C. Marhic, C. Chauvet, O. Maser, W. K., *Modifications of single-wall carbon nanotubes upon oxidative purification treatments.* Nanotechnology, 2003(7): p. 691-695.
88. D.D.L. Chung, ed. Carbon fiber Composites. 1994, Butterworth-Heinemann: Boston.
89. N. Murdie, *Introduction to carbon technologies,* ed. E.A.H.a.F.R.-R. H. Marsh. 1997, Alicante: Universidad. 597-634.
90. D. Jacques R. Andrews, D. Qian and E. C. Dickey, *Purification and structural annealing of multiwalled carbon nanotubes at graphitization temperatures* Carbon, 2001. **39**(11): p. 1681-1687.
91. Chung-Yang Lee Fu-Hsiang Ko, Chu-Jung Ko and Tieh-Chi Chu, *Purification of multi-walled carbon nanotubes through microwave heating of nitric acid in a closed vessel* Carbon, 2005. **43**(4): p. 727-733.
92. Chung-Yang Lee Chu-Jung Ko, Fu-Hsiang Ko, Hsuen-Li Chen and Tieh-Chi Chu, *Highly efficient microwave-assisted purification of multiwalled carbon nanotubes* Microelectronic Engineering, 2004. **73-74**: p. 570-577.
93. N. Xie Zhang, J. Guers, M. Varadan, Vijay K., *Chemical bonding of multiwalled carbon nanotubes to SU-8 via ultrasonic irradiation.* Smart Materials and Structures, 2003(2): p. 260-263.
94. G. Marom H. D Wagner L. Vaisman, *Dispersions of Surface-Modified Carbon Nanotubes in Water-Soluble and Water-Insoluble Polymers.* Advanced Functional Materials, 2006. **16**(3): p. 357-363.
95. M. E. Anderson Elaine Farkas, Z. Chen, A. G. Rinzler, *Length sorting cut single wall carbon nanotubes by high performance liquid chromatography* Carbon, 2002. **363**(1-2): p. 111-116.

96. Y. K. Chen K. L. LuR. M. Lago, M. L. H. GreenP. J. F. HarrisS. C. Tsang, *Mechanical damage of carbon nanotubes by ultrasound.* Carbon, 1996. **34**(6): p. 814-816.
97. Rinat O. Esenaliev Konstantin B. Shelimov, Andrew G. Rinzler, Chad B. Huffman and Richard E. Smalley, *Purification of single-wall carbon nanotubes by ultrasonically assisted filtration* Chemical Physics Letters, 1998. **282**(5-6): p. 429-434.
98. Thomas W. Ebbesen Ajit Krishnan Michael M. J. Treacy Erik Dujardin, *Purification of Single-Shell Nanotubes.* Advanced Materials, 1998. **10**(8): p. 611-613.
99. F. Assi, *Recent developments in technologies for filtration*. 2005, Baverstam Assosiates Inc.
100. Jonathan Stickel Thomas Abatemarco, Jonathan Belfort,Brian P. Frank,P. M. Ajayan and Georges Belfort, *Fractionation of Multiwalled Carbon Nanotubes by Cascade Membrane Microfiltration.* Journal of Physical Chemistry B, 1999. **103**: p. 3534-3538.
101. S. Banerjee Tae-Jin Park, T. Hemraj, Benny, S. S. Wong, *Purification strategies and purity visualization techniques for single-walled carbon nanotubes.* Journal of Materials Chemistry, 2006. **16**: p. 141-154.
102. A. M. Rao S. Bandow, K. A. Williams, A. Thess, R. E. Smalley, and P. C. Eklund, *Purification of Single Wall Carbon Nanotubes by Microfiltration.* Journal of Physical Chemistry B, 1997. **101**: p. 8839-8842.
103. *Scanning Electron Microscope*, in http://en.wikipedia.org/wiki/Scanning_electron_microscope.
104. J.T. Sparrow J.W.S. Hearle, P.M. Cross, *The Use of the Scanning Electron Microscope*. 1972, Oxford: Pergamon Press.
105. T. Belin, Epron F. , *Characterization methods of carbon nanotubes: a review.* Materials Science and Engineering B, 2005. **119**(2): p. 105-118.
106. H. J. Guntherodt and Wiesendanger R., *Scanning Tunneling Microscopy II*. 1995, Springer Verilag: Berlin.
107. H. J Guntherodt. R. Wiesendanger, *Scanning Tunneling Microscopy II: Further Applications and Related Scanning Techniques* Springer Series in Surface Sciences. 1992, Berlin: Springer-Verlag
108. H. J. Guntherodt R. Wiesendanger *Scanning Tunneling Microscopy III: Theory of Stm and Related Scanning Probe Methods* Springer Series in Surface Sciences. 1997, Berlin: Springer Verlag
109. R. Wiesendanger H.J. Guntherodt, *Scanning Tunneling Microscopy I: General Principles and Applications to Clean and Adsorbate-Covered Surfaces* Springer Series in Surface Sciences. 1992, Berlin: Springer Verlag
110. Omicron Nanotechnology, in http://www.omicron.de/index2.html?/results/two_dimensional_imaging_of_electronic_wavefunctions_in_carbon_nanotubes/~Omicron. 2002.
111. A. Govindaraj S. R. C. Vivekchand *A new method of preparing single-walled nanotubes.* Proceedings of the Indian Academy of Sciences (Chemical Sciences), 2003. **115**(5-6): p. 509-518.

112. M. Zuo Gao, J. M. Twesten, R. D. Petrov, I. Nagahara, L. A. Zhang, R., *Structure determination of individual single-wall carbon nanotubes by nanoarea electron diffraction.* Applied Physics Letters, 2003. **82**(16): p. 2703-2705.
113. J. F. Henrard Colomer, L. Launois, P. Van Tendeloo, G. Lucas, A. A. Lambin, Ph, *Interpretation of electron diffraction from carbon nanotube bundles presenting precise helicity.* Physical Review B (Condensed Matter and Materials Physics), 2004. **70**(7): p. 075408-5.
114. Gress S.B. McKee Christian P. Deck, and Kenneth S. Vecchio, *Synthesis Optimization and Characterization of MultiwalledCarbon Nanotubes.* Journal of Electronic Materials, 2006. **35**(2): p. 211.
115. A. Loiseau L. Henrard, C. Journet, P. Bernier, *Study of the symmetry of single-wall nanotubes by electron diffraction.* The European Physical Journal B, 1999. **13**: p. 661-669.
116. *SIMAGIS® Nanotubes*, in *http://smartimtech.com/nanotubes.htm*.
117. Gene Dresselhaus Mildred Dresselhaus, T Ebbesen and Riichiro Saito *Carbon Nanotubes*, in *Physics World*. Jan.1998.
118. S. G. Janssen Lemay, J. W. van den Hout, M. Mooij, M. Bronikowski, M. J. Willis, Peter A., Smalley R. E., Kouwenhoven L., P. Dekker, Cees, *Two-dimensional imaging of electronic wavefunctions in carbon nanotubes.* Nature, 2001. **412**(6847): p. 617-620.
119. J. U. Lee, P. P. Gipp, and C. M. Heller, *Carbon nanotube p-n junction diodes.* Applied Physics Letters, 2004. **85**(1): p. 145-147.
120. M. Gehring Pourfath, A. Ungersboeck, E. Kosina, H. Selberherr, S. Cheong, B. H. Park, W. J., *Separated carrier injection control in carbon nanotube field-effect transistors.* Journal of Applied Physics, 2005. **97**(10): p. 106103-3.
121. S. J. Radosavljevic Wind, M. Appenzeller, J. Avouris, Ph, *Transistor structures for the study of scaling in carbon nanotubes.* Journal of Vacuum Science & Technology B: Microelectronics and Nanometer Structures, 2003. **21**(6): p. 2856-2859.
122. Young Hee Lee et.al. Won Bong Choi, *Carbon nanotubes for full colour field emission displays.* Jpn. J. appl. Phys, 2000. **39**: p. 2560-2564.
123. D. S. Chung N. S. Lee, I. T. Han, J. H. Kang, Y. S. Choi, H. Y. Kim, S. H. Park, Y. W. Jin, W. K. Yi, M. J. Yun *Application of carbon nanotubes to field emission displays* Diamond and Related Materials, 2001. **10**(2): p. 265-270.
124. H. Tanemura Sugie, M. Filip, V. Iwata, K. Takahashi, K. Okuyama, F., *Carbon nanotubes as electron source in an x-ray tube.* Applied Physics Letters, 2001. **78**(17): p. 2578-2580.
125. S. Sakai Senda, Y. Mizuta, Y. Kita, S. Okuyama, F., *Super-miniature x-ray tube.* Applied Physics Letters, 2004. **85**(23): p. 5679-5681.
126. G. R. Myneni C. Dong, *Carbon nanotube electron source based ionisation guage.* Applied Physics letters, 2004. **84**(26): p. 5443-5445.
127. Woo S-Y Choi I-M, *Application of carbon nanotube field emission effect to an ionization gauge.* Applied Physics Letters, 2005. **87**(17): p. 173104-3.
128. Xu X. Xiao T, Liao K., *Characterization of nonlinear elasticity and elastic instability in single-walled carbon nanotubes.* Journal of Applied Physics, 2004. **95**(12): p. 8145-8148.

129. S. Falvo Paulson, M. R. Snider, N. Helser, A. Hudson, T. Seeger, A. Taylor, R. M. Superfine, R. Washburn, S., *In situ resistance measurements of strained carbon nanotubes.* Applied Physics Letters, 1999. **75**(19): p. 2936-2938.
130. V. Ravikumar P. M. Ajayan, J.-C. Charlier, *Surface Reconstructions and Dimensional Changes in Single-Walled Carbon Nanotubes.* Physical Review Letters, 1998. **81**(7): p. 1437-1440.
131. *Properties and Applications of Carbon Nanotubes*, in *http://www.cheaptubesinc.com/applications.htm*.
132. Tzu-Chieh Wei Ulas C. Coskun, Smitha Vishveshwara, Paul M. Goldbart, Alexey Bezryadin, *h/e Magnetic Flux Modulation of the Energy Gap in Nanotube Quantum Dots* Science, 2004. **304**(5674): p. 1132-1134.
133. B. Dumé, *Carbon nanotubes go magnetic*, in *Physics Web*. March. 2004.
134. Minett A.I. Moulton S.E., Wallace G.G., *Carbon Nanotube Based Electronic and Electrochemical Sensors* Sensor Letters, 2005. **3**(3): p. 183-193.
135. K. B. Hulteen Jirage, J. C. Martin, Charles R., *Nanotubule-Based Molecular-Filtration Membranes.* Science, 1997. **278**(5338): p. 655-658.
136. D. A Lu, A. Shih, Amy Y., Cruz-Chu, E. Freddolino, P. L. Arkhipov, A. Schulten, Klaus, *The role of molecular modeling in bionanotechnology.* Physical Biology, 2006(1): p. S40-S53.
137. Peter J. Sadler Shik Chi Tsang Zijian Guo, *Immobilization and Visualization of DNA and Proteins on Carbon Nanotubes.* Advanced Materials, 1998. **10**(9): p. 701-703.
138. C. Waje Wang, M. Wang, X. Tang, J. M. Haddon, R. C. Yan, Y. S., *Proton Exchange Membrane Fuel Cells with Carbon Nanotube Based Electrodes.* Nano Letters., 2004. **4**(2): p. 345-348.
139. W. Wang Li, X. Chen, Z. Waje, M. Yan, Y. S., *Carbon Nanotube Film by Filtration as Cathode Catalyst Support for Proton-Exchange Membrane Fuel Cell.* Langmuir, 2005. **21**(21): p. 9386-9389.
140. Gregory P. Meisner Gary G. Tibbetts, Charles H. Olk, *Hydrogen storage capacity of carbon nanotubes, filaments, and vapor-grown fibers* Carbon, 2001. **39**(13): p. 2291-2301.
141. Hongwei Zhu Xuesong Li, Lijie Ci, Cailu Xu, Zongqiang Mao, Bingqing Wei, Ji Liang and Dehai Wu, *Hydrogen uptake by graphitized multi-walled carbon nanotubes under moderate pressure and at room temperature* Carbon, 2001. **39**(13): p. 2077-2079.
142. A. Park Chambers, C. Baker, R. T. K. Rodriguez, N. M., *Hydrogen Storage in Graphite Nanofibers.* Journal of Physical Chemistry: B, 1998. **102**(22): p. 4253-4256.
143. S. M. An Lee, K. H. Lee, Y. H. Seifert, G. Frauenheim, T., *A Hydrogen Storage Mechanism in Single-Walled Carbon Nanotubes.* Journal of American Chemical Society., 2001. **123**(21): p. 5059-5063.
144. K.E.H. Gilbert A.C. Dillon, P.A. Parilla, C. Horbacewicz, J.L. Alleman, K.M. Jones, and M.J. Heben., *Hydrogen Storage in Carbon Single-wall Nanotubes*. 2002, National Renewable Energy Laboratory.

145. S. Hossain R. O. Loutfy, and M. Y. Saleh *Carbon Nanotubes as Anodes in Rechargeable Lithium-Ion Cells*. 2002, John H. Glenn Research Center: Cleveland, Ohio.
146. Bousquet C. Maurin G., Henn F., Bernier P., Almairac R., Simon B., *Electrochemical intercalation of lithium into multiwall carbon nanotubes* Chemical Physics Letters, 1999. **312**(1): p. 14-18.
147. H. Gao Shimoda, B. Tang, X. P. Kleinhammes, A. Fleming, L. Wu, Zhou O., *Lithium Intercalation into Opened Single-Wall Carbon Nanotubes: Storage Capacity and Electronic Properties.* Physical Review Letters, 2001. **88**(1): p. 015502.
148. B. Bower Gao, C. Lorentzen, J. D. Fleming, L. Kleinhammes, A. Tang, X. P. McNeil, L. E. Wu, Y. Zhou, O., *Enhanced saturation lithium composition in ball-milled single-walled carbon nanotubes.* Chemical Physics Letters, 2000. **327**(1-2): p. 69-75.
149. *Future of flight: High times*, in *The Economist*. Dec.11 2003.
150. M. Coleman Cadek, J. N. Ryan, K. P. Nicolosi, V. Bister, G. Fonseca, A. Nagy, J. B. Szostak, K. Beguin, F. Blau, W. J., *Reinforcement of Polymers with Carbon Nanotubes: The Role of Nanotube Surface Area.* Nano Letters., 2004. **4**(2): p. 353-356.
151. S. Sinturel Bhattacharyya, C. Salvetat, J. P. Saboungi, M. L., *Protein-functionalized carbon nanotube-polymer composites.* Applied Physics Letters, 2005. **86**(11): p. 113104-3.
152. Kinloch I. A. Li Y-L , Windle A. H., *Direct Spinning of Carbon Nanotube Fibers from Chemical Vapor Deposition Synthesis.* Science, 2004. **304**(5668): p. 276-278.
153. L P Roschier, J. Martin, M. Hakonen, P. Paalanen, M.Tapper, U., Kauppinen E. I., Journet C., Bernier P., *Single-electron transistor made of multiwalled carbon nanotube using scanning probe manipulation.* Applied Physics Letters, 1999. **75**(5): p. 728-730.
154. R. J. Hofmann Luyken, F., *Concepts for hybrid CMOS-molecular non-volatile memories.* Nanotechnology, 2003(2): p. 273-276.
155. D. Srivastava, M. Menon, and P. M. Ajayan, *Branched Carbon Nanotube Junctions Predicted by Computational Nanotechnology and Fabricated through Nanowelding.* Journal of Nanoparticle Research, 2003. **5**(3): p. 395-400.
156. A. Henny Bachtold, M. Terrier, C. Strunk, C. Schonenberger, C. Salvetat, J. P. Bonard, J. M. Forro, L., *Contacting carbon nanotubes selectively with low-ohmic contacts for four-probe electric measurements.* Applied Physics Letters, 1998. **73**(2): p. 274-276.
157. V. Martel Derycke, R. Appenzeller, J. Avouris, P. H, *Carbon Nanotube Inter- and Intramolecular Logic Gates.* Nano Letters., 2001. **1**(9): p. 453-456.
158. Y. C. Raravikar Chen, N. R. Schadler, L. S. Ajayan, P. M. Zhao, Y. P. Lu, T. M. Wang, G. C. Zhang, X. C., *Ultrafast optical switching properties of single-wall carbon nanotube polymer composites at 1.55 mu m.* Applied Physics Letters, 2002. **81**(6): p. 975-977.
159. G. Levy Nagy, M. Scarmozzino, R. Osgood, Jr R. M. Dai, H. Smalley, R. E. Michaels, C. A. Flynn, G. W. McLane, G. F., *Carbon nanotube tipped atomic*

force microscopy for measurement of [less-than] 100 nm etch morphology on semiconductors. Applied Physics Letters, 1998. **73**(4): p. 529-531.
160. H. Akita Y. Nishijima, S. Hohmura, Ken I. Yoshimura, Nakayama, S. H. Takeyasu, Kunio, *Microprocess for fabricating carbon-nanotube probes of a scanning probe microscope.* Journal of Vacuum Science & Technology B: Microelectronics and Nanometer Structures, 2000. **18**(2): p. 661-664.
161. Y. C. Wang Chang, D. C. Chang, C. S. Tsong, Tien T., *Easy method to adjust the angle of the carbon nanotube probe of an atomic force microscope.* Applied Physics Letters, 2003. **82**(20): p. 3541-3543.
162. Franklin N. Dai H., Han J., *Exploiting the properties of carbon nanotubes for nanolithography.* Applied Physics Letters, 1998. **73**(11): p. 1508-1510.
163. I. Kong Heller, J. Heering, H. A. Williams, K. A. Lemay, S. G. Dekker, C., *Individual Single-Walled Carbon Nanotubes as Nanoelectrodes for Electrochemistry.* Nano Letters., 2005. **5**(1): p. 137-142.
164. J. S. Bunch, T. N. Rhodin, and P. L. McEuen, *Noncontact-AFM imaging of molecular surfaces using single-wall carbon nanotube technology.* Nanotechnology, 2004(2): p. S76-S78.
165. Stanislaus S. Wong, Woolley A. T., Odom T., Wang H., J-L Kim, P. Vezenov, Dimitri V. Lieber, Charles M., *Single-walled carbon nanotube probes for high-resolution nanostructure imaging.* Applied Physics Letters, 1998. **73**(23): p. 3465-3467.
166. J.T.-W. Yeow N. Sinha, *Carbon nanotubes for biomedical applications.* IEEE Transactions on Nanobioscience, 2005. **4**(2): p. 180-195.
167. L. Kalaugher, *Nanotechnology bulks up artificial muscles*, in *http://nanotechweb.org/articles/news/5/3/18/*. 28 Mar.2006.
168. J. Kjelstrup-Hansen S. Dohn, D. N. Madsen, K. Mølhave, P. Bøggild, *Multi-walled carbon nanotubes integrated in microcantilevers for application of tensile strain.* Ultramicroscopy, 2005. **105**: p. 209-214.
169. Andrei N. Khlobystov David A. Britz, Kyriakos Porfyrakis, Arzhang Ardavan and G. Andrew D. Briggs, *Chemical reactions inside single-walled carbon nano test-tubes.* Chemical Communications, 2005. **1**: p. 37-39.
170. Lin Y. Liu G, *Carbon Nanotube-Templated Assembly of Protein* Journal of Nanoscience and Nanotechnlogy, 2006. **6**(4): p. 948-953.
171. Wang X Li W, Chen Z, Waje M, Yan Y., *Carbon nanotube film by filtration as cathode catalyst support for proton-exchange membrane fuel cell.* Langmuir, 2005. **21**: p. 9386-9389.
172. C. Zhu, *Lecture Notes, Surfaces and Interfaces*. 2002, Department of ECE, National University of Singapore.
173. K. L Jensen, *Theory of Field Emission*. Vacuum Microelectronics, ed. W. Zhu. 2001: John Wiley & Sons, Inc. 33-104.
174. O. W. Richardson, *Electron Emission from Metals as a Function of Temperature.* Physical Review, 1924. **23**(2): p. 153.
175. J. A. Venables. *Lecture Notes*. July 1996 [cited; Available from: venables.asu.edu/sphy/sectA2.doc
176. J. C. Miller, *The role of adsorbates on field emission*, in *Physics*. 2002, College of William and Mary: Virginia.

177. R. H. Fowler, Nordheim, L., *Electron Emission in Intense Electric Fields.* Proceedings of the Royal Society of London. Series A, 1928. **119**(781): p. 173-181.
178. Shimoi A. Yuasa K., Ohba I., Oshima C., *Modified Fowler-Nordheim Field-Emission Formulae from a Nonplanar-Emitter Model.* ArXiv Condensed Matter e-prints, 25 Nov 2003. **1**.
179. D. A. Bergeron Kirkpatrick, G. L. Czarnaski, M. A. Hickman, J. J. Chow, G. M. Price, R. Ratna, B. L. Schoen, P. E. Stockton, W. B. Baral, S. Ting, A. C. Schnur, J. M., *Demonstration of vacuum field emission from a self-assembling biomolecular microstructure composite.* Applied Physics Letters, 1992. **60**(13): p. 1556-1558.
180. D. A. Kirkpatrick, Mankofsky, A., Tsang, K. T., *Analysis of field emission from three-dimensional structures.* Applied Physics Letters, 1992. **60**(17): p. 2065-2067.
181. Renner C. H. Niedermann P. H., Kent A. D., Fischer O., *Study of field-emitting microstructures using a scanning tunneling microscope.* Journal of Vacuum Science & Technology A: Vacuum, Surfaces, and Films, 1990. **8**(1): p. 594-597.
182. P. H. He Cutler, Jun Miskovsky, N. M. Sullivan, T. E. Weiss, B. *Theory of electron emission in high fields from atomically sharp emitters: Validity of the Fowler--Nordheim equation*. in *Fifth international vacuum microelectronic conference*. 1993. Vienna (Austria): AVS.
183. G. Ehrlich, *An atomic view of adsorption.* Brit. J. Appl. Phys., 1964. **15**: p. 349.
184. S. G. Walton J. C. Tucek, R. L. Champion, *Ion-induced secondary electron and negative ion emission from Mo/O.* Surface Science, 1998. **410**(2-3): p. 258-269.
185. J. L. Uscinski, *Adsorbates effects on Field Emission.*, in *Physics Department*. 2003, College of William and Mary: Williamsburg,Virginia. p. 1-31.
186. G. A. Dyuzhev G. Baksht, A. M. Martsinovskiy,B. Ya. Moyzhes, G. Ye. Pikus, E. B. Sonin and V. G. Yur'yev., *Emission and adsorption processes (TIC Electrodes)*, in *Thermionic Converters and Low-Temperature Plasma*
1978, Technical Information Center - U.S. Department of Energy.
187. T. J. Lewis, *Some Factors Influencing Field Emission and the Fowler-Nordheim Law.* Proceedings of the Physical Society. Section B, 1955. **68**(11): p. 938-943.
188. W. Zhu, C. Bower, G. P. Kochanski, S. Jin *Field emission properties of diamond and carbon nanotubes* Diamond and Related Materials 2001. **10**(9-10): p. 1709-1713.
189. J. Robertson J J. B. Cui, Miln W. I., *Field emission site densities of nanostructures carbon films deposited by a cathodic arc.* Journal of applied physics, 2001. **89**(10): p. 5707-5711.
190. Wilson D. A R. V. Latham, *The development of a high-definition cathode-ray tube using a carbon-fibre field-emission electron source.* Journal of Physics E: Scientific Instruments, 1982. **15**(10): p. 1083-1092.
191. Y Tzeng and R V Latham N S Xu, *Similarities in the 'cold' electron emission characteristics of diamond coated molybdenum electrodes and polished bulk graphite surfaces.* Journal of Physics D: Applied Physics., 1993. **26**(10): p. 1776-1780.

192. J. H. Hafner A.G. Rinzler, P. Nikolaev,L. Lou, S.G. Kim, D. Tomanek, D. Colbert, R E Smalley, *Unravelling nanotubes: field emission from an atomic wire.* Science, 15 Sep 1995. **269**: p. 1550-1553.
193. A. Châtelain Walt A. de Heer , D. Ugarte, *A Carbon Nanotube Field-Emission Electron Source.* Science, 1995. **270**(5239): p. 1179-1180.
194. A. Iriguchi Sawada, M. Zhao, W. J. Ochiai, C. Takai, M. *Emission site control in carbon nanotube field emitters by focused ion and laser irradiation*. in *Papers from the 14th International Vacuum Microelectronics Conference*. 2003. Davis, California (USA): AVS.
195. Yong C. Sohn Kim, K. H. Cho, Y. M. Yoo, Eun H., *Vertical alignment of printed carbon nanotubes by multiple field emission cycles.* Applied Physics Letters, 2004. **84**(26): p. 5350-5352.
196. J-H Moon Park, J-S Han, J-H Berdinsky, A. S. Yoo, J-B Park, C-Y Nam, J-W Park, J. Lee, C. G. Choe, D. Hyeon, *Stable and high emission current from carbon nanotube paste with spin on glass.* Journal of Vacuum Science & Technology B: Microelectronics and Nanometer Structures, 2005. **23**(2): p. 702-706.
197. J. I. Lee Sohn, S. Song, Y-H Choi, S-Y Cho, K-k Nam, Kee-Soo, *Patterned selective growth of carbon nanotubes and large field emission from vertically well-aligned carbon nanotube field emitter arrays.* Applied Physics Letters, 2001. **78**(7): p. 901-903.
198. Z. P. Huang Z. F. Pen, J. W. Xu, J. H. Wang, P. Bush, M. P. Siegel and P. N. Provencio., *Synthesis of large arrays of well-aligned carbon nanotubes on glass.* Science, 1998. **282**: p. 1105-1107.
199. Y. Tu S. H. Jo, Z. P. Huang and D. L. Carnahan,D. Z. Wang and Z. F. Ren, *Effect of length and spacing of vertically aligned CNT on field emission properties.* Applied Physics letters, 2003. **82**(20): p. 3520-3522.
200. N. S. Xu S. Z. Deng, J. B. Liu, Jun Chen, Y. L. Ke, J. C. She, *Field electron emission properties from aligned carbon nanotube bundles of different density.* Surface and Interface Analysis., 2004. **36**(5-6): p. 501-505.
201. Valdrè U. Edgcombe C. J., *Microscopy and computational modelling to elucidate the enhancement factor for field electron emitters.* Journal of Microscopy 2001. **203**(2): p. 188-194.
202. N. Weiss J.-M. Bonard, T. Stöckli, L. Forró , K. Kern, A. Châtelain, *Tuning the Field Emission Properties of Patterned Carbon Nanotube Films.* Advanced Materials, 2001. **13**(3): p. 184-188.
203. K.B.K. Teo W.I. Milne, G. A. J. Amaratunga, P. Legagneux, L. Gangloff, V. Semet, V. Thien Binh and O. Groening. , *Carbon nanotubes as field emission sources.* Journal of Materials Chemistry, 2004. **14**: p. 933-943.
204. D. V. Novikov G. N. Fursey, G. A. Dyuzhev, A. V. Kotcheryzhenkov, P. O. Vassiliev, *The field emission from carbon nanotubes.* Applied surface science, 2003. **215**: p. 135-140.
205. O. Zhou Y. Cheng, *Electron field emission from carbon nanotubes.* Comptes Rendus Physique, 2003. **4**: p. 1021-1033.
206. Chai G. and C. Lee, *Electron emission from the side wall of an individual multiwall carbon nanotube.* Carbon, 2007. **45**(2): p. 281-284.

207. Shaw D. T. Chen Y., Guo L., *Field emission of different oriented carbon nanotubes.* Applied Physics Letters, 2000. **76**(17): p. 2469-2471.
208. M. Reed D Carnahan, Z. Ren, K. Kempa, *Field emission from arrays of Carbon Nanotubes.*, in *Nanolab Inc.* 1998, Physical Sciences Inc., Boston College.
209. L. Groening Nilsson, O. Emmenegger, C. Kuettel, O. Schaller, E. Schlapbach, L. Kind, H. Bonard, J. M. Kern, K., *Scanning field emission from patterned carbon nanotube films.* Applied Physics Letters, 2000. **76**(15): p. 2071-2073.
210. S. T. Purcell P. Vincent, C. Journet, Vu T. Binh, *Modelization of resistive heating of carbon nanotubes during field emission.* Physical Review B 2002. **66**(7-15): p. 075406.
211. K A. Dean, T P. Burgin, and B R. Chalamala, *Evaporation of carbon nanotubes during electron field emission.* Applied Physics Letters, 2001. **79**(12): p. 1873-1875.
212. P. Vincent S. T. Purcell*, C. Journet, and Vu Thien Binh, *Hot Nanotubes: Stable Heating of Individual Multiwall Carbon Nanotubes to 2000 K Induced by the Field-Emission Current.* physical Review Letters, 2002. **88**(10): p. 105502.
213. P. V. Pikhitsa Altman I. S, Choi M., *Two-process model of electron field emission from nanocarbons: Temperature effect.* Journal of Applied Physics, 2004. **96**(6): p. 3491-3493.
214. J. Jia C. M. Tan, W. Yu, *Temperature dependence of the field emission of multiwalled carbon nanotubes.* Applied Physics Letters, 2005. **86**(26): p. 263104-3.
215. A. G. Umnov and V. Z. Mordkovich, *Field-induced evaporation of carbon nanotubes.* Applied Physics A: Materials Science & Processing, 2001. **73**(3): p. 301-304.
216. M. Jonsson Sveningsson, M. Nerushev, O. A. Rohmund, F. Campbell, E. E. B., *Blackbody radiation from resistively heated multiwalled carbon nanotubes during field emission.* Applied Physics Letters, 2002. **81**(6): p. 1095-1097.
217. Salvetat J. P. Bonard J. M., Stockli T., ForrÃ L., ChÃ¢telain A., *Field emission from carbon nanotubes: perspectives for applications and clues to the emission mechanism.* Applied Physics A: Materials Science & Processing, 1999. **69**(3): p. 245-254.
218. Jan Andzelm Amitesh Maiti, N Tanipipat and P Von Allmen, *Effect of adsorbates on field emission from carbon nanotubes.* Physical Review Letters, 8 October,2001. **87**(15): p. 155502.
219. Kenneth A. Dean, Paul von Allmen, and Babu R. Chalamala, *Three behavioral states observed in field emission from single-walled carbon nanotubes.* Journal of Vacuum Science & Technology B: Microelectronics and Nanometer Structures, 1999. **17**(5): p. 1959-1969.
220. K. A. Dean, P. vonAllmen, and B. R. Chalamala. *Thermal field emission behavior of single walled carbon nanotubes*. 1998.
221. S. C. Jeong Lim, H. J. Park, Y. S. Bae, D. S. Choi, Y. C. Shin, Y. M. Kim, W. S. An, K. H. Lee, Y. H., *Field-emission properties of vertically aligned carbon-nanotube array dependent on gas exposures and growth conditions.* Journal of Vacuum Science and Technology A., 2001. **19**(4): p. 1786-1789.

222. K A. Dean and B R. Chalamala, *Current saturation mechanisms in carbon nanotube field emitters.* Applied Physics Letters, 2000. **76**(3): p. 375-377.
223. Hersam M. Collins P. G., Arnold M., Martel R., Avouris Ph., *Current Saturation and Electrical Breakdown in Multiwalled Carbon Nanotubes.* Physical Review Letters, 2001. **86**(14): p. 3128-3131.
224. C. Dong, Gupta M. C., *Influences of the surface reactions on the field emission from multiwall carbon nanotubes.* Applied Physics Letters, 2003. **83**(1): p. 159-161.
225. Akihiro Takakura and Yahachi Saito Koichi Hata, *Field emission from multiwall carbon nanotubes in controlled ambient gases, H2, CO, N2 and O2.* Ultramicroscopy, 2003. **95**: p. 107-112.
226. Babu Chalamala Kenneth A. Dean, *Current saturation mechanisms in carbon nanotube field emitters.* Appl Physics letters, 2000. **76**(3): p. 375-377.
227. G. Cao M. Grujicic, *Enhancement of field emission in carbon nanotubes through adsorption of polar molecules.* Applied Surface Science, 2003. **206**: p. 167-177.
228. S. Jeon Lee, D. Young, *Effect of degassed elements on the degradation behavior of carbon nanotube cathodes in sealed field emission-backlight units.* Applied Physics Letters, 2006. **88**(6): p. 063502-3.
229. T.S. Kim D.H. Kim, B.K. Ahn, H.Y. Shin, Dong-Gu Lee, H.K. Cho, Y. R. Cho *A Study of the Degradation Mechanism for Carbon Nanotubes in Field Emitter Applications* Materials Science Forum, 2005. **475-479**: p. 1771-1776.
230. Frédéric Maier Jean-Marc Bonard, Thomas Stöckli, André Châtelain, Walt A. de Heer, Jean-Paul Salvetat and László Forró, *Field emission properties of multiwalled carbon nanotubes.* Ultramicroscopy, 1998. **73**(1-4): p. 7-15.
231. Takeshi Nishiyama Yahachi Saito, Taka-aki Kto, Shin-ichiro Kondo and Toshihiko Tanaka, *Field emission properties of Carbon nanotubes and their application to display devices.* Mol. Cryst. Liq. Cryst. Vol, 2002. **387**(84): p. 303.
232. D. Y. Zhang Zhong, G. Y. Liu, S. Sakurai, T. Wang, E. G., *Universal field-emission model for carbon nanotubes on a metal tip.* Applied Physics Letters, 2002. **80**(3): p. 506-508.
233. C. J. Edgcombe Richard G. Forbes, and U. Valdrè *Some comments on models for field enhancement.* . Ultramicroscopy, 2003. **95**(57): p. 57-65.
234. Jean-Paul Salvetat Jean-Marc Bonard, Thomas Stöckli, Walt A. de Heer, László Forró, and André Châtelain, *Field emission from single wall carbon nanotube films.* Appl Physics letters, 1998. **73**(7): p. 918-920.
235. Joseok Chae Seon Mi Yoon, Jung Sang Suh., *Comparison of the field emissions between highly ordered carbon nanotubes with closed and open tips.* Applied Physics letters, 2004. **84**(5): p. 825-827.
236. S. Uemura Y. Saito, *Field emission from carbon nanotubes and its application to electron sources.* Carbon, 2000. **38**(2): p. 169-182.
237. G. Z. Qiu Yue, Q. Gao, Bo Cheng, Y. Zhang, J. Shimoda, H. Chang, S. Lu, J. P. Zhou, O., *Generation of continuous and pulsed diagnostic imaging x-ray radiation using a carbon-nanotube-based field-emission cathode.* Applied Physics Letters, 2002. **81**(2): p. 355-357.

238. Nikhil Koratkar Ashish Modi, Eric Lass, Bingqing Wei, Pulickel M. Ajayan, *Miniaturized gas ionization sensors using carbon nanotubes* Nature, 2003. **424**: p. 171-174.
239. M E Read. *CNT based cathode for microwave tubes*. in *Particle accelerator conference*. 2001. Chicago.
240. R. Simendinger Rosen, W. Debbault, C. Shimoda, H. Fleming, L. B. Stoner, Zhou O., *Application of carbon nanotubes as electrodes in gas discharge tubes.* Applied Physics Letters, 2000. **76**(13): p. 1668-1670.
241. D. S. Chung, Choi W. B. Kang, J. H. Kim, H. Y. Han, I. T. Park, Y. S. Lee, Y. H. Lee, N. S. Jung, J. E. Kim, J. M. *Field emission from 4.5 in. single-walled and multiwalled carbon nanotube films*. in *Papers from the 12th international vacuum microelectronics conference*. 2000. Darmstadt (Germany) and Wroclaw (Poland): AVS.
242. Q. H. Wang, M. Yan, and R. P. H. Chang, *Flat panel display prototype using gated carbon nanotube field emitters.* Applied Physics Letters, 2001. **78**(9): p. 1294-1296.
243. W. B. Jin Choi, Y. W. Kim, H. Y. Lee, S. J. Yun, M. J. Kang, J. H. Choi, Y. S. Park, N. S. Lee, N. S. Kim, J. M., *Electrophoresis deposition of carbon nanotubes for triode-type field emission display.* Applied Physics Letters, 2001. **78**(11): p. 1547-1549.
244. Y. W.; Jung Jin, J. E.; Park, Y. J.; Choi, J. H.; Jung, D. S.; Lee, H. W.; Park, S. H.; Lee, N. S.; Kim, J. M.; Ko, T. Y.; Yoo, Ji-Beom; Park, Chong-Yun *Triode-type field emission array using carbon nanotubes and a conducting polymer composite prepared by electrochemical polymerization.* Journal of Applied Physics, 2002. **92**(2): p. 1065-1068.
245. Takeshi Nishiyama Yahachi Saito, Taka-aki Kto, Shin-ichiro Kondo and Toshihiko Tanaka, *Field emission from carbon nanotubes and its application to cathode ray tube lighting elements.* Appl Surface Science, 1999. **146**: p. 305-311.
246. J. Yang Zhang, G. Cheng, Y. Gao, B. Qiu, Q. Lee, Y. Z. Lu, J. P. Zhou, O., *Stationary scanning x-ray source based on carbon nanotube field emitters.* Applied Physics Letters, 2005. **86**(18): p. 184104-3.
247. F. M. Charbonnier, J. P. Barbour, and W. P. Dyke, *Resolution of field-emission x-ray sources.* Radiology, 1975. **117**(1): p. 165-172.
248. G. S. Hallenbeck, *Clinical evaluation of the 350-kV chest radiography system.* Radiology, 1975. **117**(1): p. 1-4.
249. Yann Lamy Niels de Jonge, *High brightness electron beam from a multi walled carbon nanotube.* Nature, 2002. **420**: p. 393-395.
250. K. B. K. Teo W. I. Milne, G. A. J. Amaratunga, R. Lacerda, P. Legagneux, G. Piriob, V. Semet and V. Thien Binh *Aligned carbon nanotubes/fibers for applications in vacuum microwave devices.* Current Applied Physics, 2004. **4**(5): p. 513-517.
251. W. Bower Zhu, C. Zhou, O. Kochanski, G. Jin, S., *Large current density from carbon nanotube field emitters.* Applied Physics Letters, 1999. **75**(6): p. 873-875.
252. F.Paschen, Wied. Ann., 1889. **37**(69).

253. X D Bai Zhi Xu, E G Wang and Zhong L Wang, *Dynamic in situ field emission of a nanotube at electromechanical resonance.* Journal of Physics: Condensed Matter, 2005. **17**(46): p. L507-L512.
254. P. Vincent S. T. Purcell, C. Journet, Vu T. Binh, *Tuning of Nanotube Mechanical Resonances by Electric Field Pulling.* Physical Review Letters, 2002. **89**: p. 276103-276107.
255. Hamister. V.C. Chaney. N. K., *The properties of carbon at the arc temperature.* Transactions of the Electrochemical Society, 1934. **67**: p. 301.
256. R. Murphy M. Cadek, B. McCarthy, A. Drury, B. Lahr, R. C. Barklie, M. in het Panhuis, J. N. Coleman and W. J. Blau *Optimisation of the arc-discharge production of multi-walled carbon nanotubes* Carbon, 2002. **40**(6): p. 923-928.
257. J. Abrahamson, *Graphite sublimation temperatures, carbon arcs and crystallite erosion.* Carbon, 1974. **12**(2): p. 111-118.
258. S. H. Wang Jo, D. Z. Huang, J. Y. Li, W. Z. Kempa, K. Ren, Z. F., *Field emission of carbon nanotubes grown on carbon cloth.* Applied Physics Letters, 2004. **85**(5): p. 810-812.
259. Kerstin Otillinger, *Deposition of carbon nanotubes on a continuously fed substrate by arc-discharge using Fe and Ni catalysts*, in *Chemical and Process Engineering*. 2006, University of Canterbury: Christchurch. p. 1-42.
260. T. Utsumi, *Vacuum microelectronics: Whats new and exciting.* IEEE Transaction of Electron devices., 1991. **38**(10): p. 2276-2283.
261. Dean K A. Bonard J-M, Coll, B F. Klinke, Christian, *Field Emission of Individual Carbon Nanotubes in the Scanning Electron Microscope.* Physical Review Letters, 2002. **89**(19): p. 197602.
262. Jean-Paul Salvetat Jean-Marc Bonard, Thomas Stöckli, and André Châtelain László Forró. *Why are Carbon nanotubes such excellent field emitters??* in *6th Foresight Conference on Nanotechnology*. 2003. Santa Clara, CA.
263. Jean-Paul Salvetat Jean-Marc Bonard, Thomas Stöckli, László Forró, André Châtelain. *Why are carbon nanotubes such excellent field emitters??* in *The Sixth Foresight Conference on Molecular Nanotechnology*. 1998. California.
264. Y. X. Liang, Q. H. Li, and T. H. Wang, *Current saturation in multiwalled carbon nanotubes by large bias.* Applied Physics Letters, 2004. **84**(17): p. 3379-3381.
265. S. Wang Gupta, Y. Y. Garguilo, J. M. Nemanich, R. J., *Imaging temperature-dependent field emission from carbon nanotube films: Single versus multiwalled.* Applied Physics Letters, 2005. **86**(6): p. 063109-3.
266. M. Hirakawa H. Murakami, C. Tanaka, H. Yamakawa, *Field emission from well aligned patterned CNT emitters.* Applied Physics letters, 2000. **76**(13): p. 1776-1778.
267. M Doytcheva, M Kaiser, and N de Jonge, *In situ transmission electron microscopy investigation of the structural changes in carbon nanotubes during electron emission at high currents.* Nanotechnology, 2006. **17**(13): p. 3226-3233.
268. S. T. Vincent Purcell, P. Journet, C. Binh, Vu Thien, *Hot Nanotubes: Stable Heating of Individual Multiwall Carbon Nanotubes to 2000 K Induced by the Field-Emission Current.* Physical Review Letters, 2002. **88**(10): p. 105502.

269. K. M. Wong Liew, C. H. He, X. Q. Tan, M. J., *Thermal stability of single and multi-walled carbon nanotubes.* Physical Review B (Condensed Matter and Materials Physics), 2005. **71**(7): p. 075424-6.
270. M A Kuroda, Leburton J-P, *Joule heating induced negative differential resistance in freestanding metallic carbon nanotubes.* Applied Physics Letters, 2006. **89**(10): p. 103102-3.
271. Xin-She Yang, *Modelling heat transfer of carbon nanotubes.* Modelling and Simulation in Materials Science and Engineering, 2005. **13**(6): p. 893-902.
272. W. I. Teo Milne, K. B. K. Chhowalla, M. Amaratunga, G. A. J. Lee, S. B. Hasko, D. G. Ahmed, H. Groening, O. Legagneux, P. Gangloff, L., *Electrical and field emission investigation of individual carbon nanotubes from plasma enhanced chemical vapour deposition.* Diamond and Related Materials, 2003. **12**(3-7): p. 422-428.
273. Han J Zhao J, Lu J P, *Work functions of pristine and alkali-metal intercalated carbon nanotubes and bundles.* Physical Review B, 2002. **65**(19): p. 193401.
274. J. Hone, *Carbon Nanotubes: Thermal Properties*, in *Encyclopedia of Nanoscience and Nanotechnology*, M. Dekker, Editor. 2004.
275. Y. Poulikakos Choi T, D. Tharian, J. Sennhauser, Urs, *Measurement of thermal conductivity of individual multiwalled carbon nanotubes by the 3-omega method.* Applied Physics Letters, 2005. **87**(1): p. 013108-3.
276. D. Jiang Z Yang, Q. Chen, G. Yoon, S. F. Ahn, J. Wang, S. G. Zhou, Q. Wang, Q. Li, J. Q., *Thermal conductivity of multiwalled carbon nanotubes.* Physical Review B, 2002. **66**(16): p. 165440.
277. G Zhang and B Li, *Thermal conductivity of nanotubes revisited: Effects of chirality, isotope impurity, tube length, and temperature.* The Journal of Chemical Physics, 2005. **123**(11): p. 114714-4.
278. S K Berber, Young-Kyun, TomÃ¡nek D., *Unusually High Thermal Conductivity of Carbon Nanotubes.* Physical Review Letters, 2000. **84**(20): p. 4613.
279. J. Whitney Hone, M. Piskoti, C. Zettl, A., *Thermal conductivity of single-walled carbon nanotubes.* Physical Review B, 1999. **59**(4): p. R2514.
280. Zhang X Fujii M, Xie H, Ago H, Takahashi K, Ikuta T, Abe H, Shimizu T,, *Measuring the Thermal Conductivity of a Single Carbon Nanotube.* Physical Review Letters, 2005. **95**(6): p. 065502-4.
281. Da Jiang Yang, et al., *Thermal conductivity of multiwalled carbon nanotubes.* Physical Review B, 2002. **66**(16): p. 165440.
282. J. P. Small, L. Shi, and P. Kim, *Mesoscopic thermal and thermoelectric measurements of individual carbon nanotubes.* Solid State Communications, 2003. **127**(2): p. 181-186.
283. P. Shi Kim, L. Majumdar, A. McEuen, P. L., *Thermal Transport Measurements of Individual Multiwalled Nanotubes.* Physical Review Letters, 2001. **87**(21): p. 215502-4.
284. W. Lu Yi, L. Dian-lin, Zhang Pan, Z. W. Xie, S. S., *Linear specific heat of carbon nanotubes.* Physical Review B, 1999. **59**(14): p. R9015.
285. Y. Igarashi S. Maruyama, Y. Taniguchi and J. Shiomi, *A molecular dynamics simulation of heat conduction in a carbon nanotube.* Microscale Thermophysical Engineering, 2005. **to be submitted**.

286. J A Che, T. Iii, W. A. Goddard, *Thermal conductivity of carbon nanotubes.* Nanotechnology, 2000. **11**(2): p. 65-69.
287. J. Wang and J-S Wang, *Carbon nanotube thermal transport: Ballistic to diffusive.* Applied Physics Letters, 2006. **88**(11): p. 111909-3.
288. A. Hansson and S. Stafstrom, *Intershell conductance in multiwall carbon nanotubes.* Physical Review B (Condensed Matter and Materials Physics), 2003. **67**(7): p. 075406-6.
289. J. Devoret Tans S, Michel H., Dai H., Thess A., Smalley R. E. ,Geerligs L. J., Dekker C., *Individual single-wall carbon nanotubes as quantum wires.* Nature, 1997. **386**(6624): p. 474-477.
290. E. J. Mele C. L. Kane, R. S. Lee, J. E. Fischer, P. Petit, H. Dai, A. Thess, R. E. Smalley, A. R. M. Verschueren, S. J. Tans and C. Dekker *Temperature-dependent resistivity of single-wall carbon nanotubes.* Europhysics Letters, 1998. **41**(6): p. 683-688.
291. J. E. Dai Fischer, H. Thess, A. Lee, R. Hanjani, N. M. Dehaas, D. L. Smalley, R. E., *Metallic resistivity in crystalline ropes of single-wall carbon nanotubes.* Physical Review B, 1997. **55**(8): p. R4921.
292. K. Liu, et al., *Electrical transport in doped multiwalled carbon nanotubes.* Physical Review B, 2001. **63**(16): p. 161404.
293. M C Bockrath, David H, Lu J, Rinzler A. G, Smalley R. E, Balents L, McEuen P. L. , *Luttinger-liquid behaviour in carbon nanotubes.* Nature, 1999. **397**(6720): p. 598-601.
294. Poncharal P Frank S, Wang Z. L, Heer W. A. , *Carbon Nanotube Quantum Resistors.* Science, 1998. **280**(5370): p. 1744-1746.
295. A. Fuhrer Bachtold, M. S. Plyasunov, S. Forero, M. Anderson, Erik H. Zettl, A. McEuen, Paul L., *Scanned Probe Microscopy of Electronic Transport in Carbon Nanotubes.* Physical Review Letters, 2000. **84**(26): p. 6082.
296. A. Bachtold C. Schönenberger, C. Strunk, J.-P. Salvetat, L. Forró *Interference and Interaction in multi-wall carbon nanotubes.* Applied Physics A: Materials Science & Processing 1999. **69**(3): p. 283-295.
297. Lee R Thess A., N. Pavel, Dai, H Petit, P. Robert, J. Xu, C. Lee, Y H Kim, S G, Rinzler A G. ,Colbert D ,T. Scuseria G E., Tomanek D, Fischer J E., Smalley R E., *Crystalline Ropes of Metallic Carbon Nanotubes.* Science, 1996. **273**(5274): p. 483-487.
298. T. Kuzumaki and Y. Mitsuda, *Dynamic measurement of electrical conductivity of carbon nanotubes during mechanical deformation by nanoprobe manipulation in transmission electron microscopy.* Applied Physics Letters, 2004. **85**(7): p. 1250-1252.
299. P. J. Graugnard de Pablo, E. Walsh, B. Andres, R. P. Datta, S. Reifenberger, R., *A simple, reliable technique for making electrical contact to multiwalled carbon nanotubes.* Applied Physics Letters, 1999. **74**(2): p. 323-325.
300. Vallance R. R Hii K-F, Chikkamaranahalli S, B. Menguc, M. Pinar, Rao A. M., *Characterizing field emission from individual carbon nanotubes at small distances.* Journal of Vacuum Science & Technology B: Microelectronics and Nanometer Structures, 2006. **24**(3): p. 1081-1087.

301. Phan Ngoc Tuyen Minh, Le T. T. Ono, T. Miyashita, H. Suzuki, Y. Mimura, H. Esashi, Masayoshi. *Selective growth of carbon nanotubes on Si microfabricated tips and application for electron field emitters*. in *Papers from the 14th International Vacuum Microelectronics Conference (IVMC2002) and the 48th International Field Emission Symposium (IFES)*. 2003. Lyon, France: AVS.
302. Yuan Hu and C. H. Huang. *Computer simulation of the field emission properties of multiwalled carbon nanotubes for flat panel displays*. in *Papers from the 14th International Vacuum Microelectronics Conference (IVMC2002) and the 48th International Field Emission Symposium (IFES)*. 2003. Lyon, France: AVS.
303. M. Hansen Sveningsson, K. Svensson, K. Olsson, E. Campbell, E. E. B., *Quantifying temperature-enhanced electron field emission from individual carbon nanotubes.* Physical Review B (Condensed Matter and Materials Physics), 2005. **72**(8): p. 085429-5.
304. M. Ducati Chhowalla, C. Rupesinghe, N. L. Teo, K. B. K. Amaratunga, G. A. J., *Field emission from short and stubby vertically aligned carbon nanotubes.* Applied Physics Letters, 2001. **79**(13): p. 2079-2081.
305. M A. Kuroda, Cangellaris A., Leburton J-P, *Nonlinear Transport and Heat Dissipation in Metallic Carbon Nanotubes.* Physical Review Letters, 2005. **95**(26): p. 266803-4.
306. T. Hidaka Fujieda, K. Hayashibara, M. Kamino, T. Matsumoto, H. Ose, Y. Abe, H. Shimizu, T. Tokumoto, H., *In situ observation of field emissions from an individual carbon nanotube by Lorenz microscopy.* Applied Physics Letters, 2004. **85**(23): p. 5739-5741.
307. Hamdan M. T. Querrioux Yusoff, R. Shastry, J. Abrahamson, , *Nanotube deposition in a continuous arc reactor for varying arc gap and substrate temperature.* Current Applied Physics, 2006. **6**(3): p. 422-426.
308. T Nishiyama Y. Saito, T-A Kto, S-I Kondo, T. Tanaka, *Field emission properties of Carbon nanotubes and their application to display devices.* Molecular Crystals and Liquid Crystals, 2002. **387**(84): p. 303.
309. B. Little Reginald, *Mechanistic Aspects of Carbon Nanotube Nucleation and Growth.* Journal of Cluster Science, 2003. **V14**(2): p. 135-185.
310. J. F. Lai Z. Y. Juang, C. H. Weng, J. H. Lee, H. J. Lai, T. S. Lai and C. H. Tsai, *On the kinetics of carbon nanotube growth by thermal CVD method* Diamond and Related Materials, 2004. **13**(11-12): p. 2140-2146.
311. E. G. Gamaly and Ebbesen T. W., *Mechanism of carbon nanotube formation in the arc discharge.* Physical Review B, 1995. **52**(3): p. 2083.
312. D. T.; Zhang Colbert, J.; McClure, S. M.; Nikolaev, P.; Chen, Z.; Hafner, J. H.; Owens, D. W.; Kotula, P. G.; Carter, C. B.; Weaver, J. H.; Rinzler, A. G.; Smalley, R. E. , *Growth and Sintering of Fullerene Nanotubes.* Science, 1994. **266**(5188): p. 1218-1222.
313. M. Endo and H. W. Kroto, *Formation of carbon nanofibers.* J. Phys. Chem., 1992. **96**: p. 6941-6944.
314. Campbell E. E B Ulmer G, Kuhnle R., Busmann H. G, Hertel I. V., *Laser mass spectroscopic investigations of purified, laboratory-produced C60/C70.* Chemical Physics Letters, 1991. **182**(2): p. 114-119.

315. W. W. Lozier and M. R. Null, *The low current carbon arc and the properties of graphite near the sublimation temperature.* Carbon, 1978. **16**(5): p. 313-339.
316. de La Chapelle Farhat Samir, Marc Lamy Loiseau, Annick Scott, Carl D, Lefrant, Serge Journet, Catherine Bernier, Patrick, *Diameter control of single-walled carbon nanotubes using argon--helium mixture gases.* The Journal of Chemical Physics, 2001. **115**(14): p. 6752-6759.
317. György Radnóczi Bernadett Veisz, *Growth model for arc-deposited fullerene-like nanoparticles.* Microscopy Research and Technique, 2005. **67**(2): p. 100-105.
318. Anne-Claire Dupuis, *The catalyst in the CCVD of carbon nanotubes--a review.* Progress in Materials Science, 2005. **50**(8): p. 929-961.
319. S. Seraphin and D. Zhou, *Single-walled carbon nanotubes produced at high yield by mixed catalysts.* Applied Physics Letters, 1994. **64**(16): p. 2087-2089.
320. Muradyan VE Tarasov BP, Shul'ga YM, Krinichnaya EP, Kuyunko NS, Efimov ON, Obraztsova ED, Schur DV, Maehlen JP, Yartys VA, Lai HJ *Synthesis of carbon nanostructures by arc evaporation of graphite rods with Co-Ni and YNi2 catalysts* Carbon, 2003. **41**(7): p. 1357-1364.
321. Govindaraj A Rao CNR, *Carbon nanotubes from organometallic precursors* Accounts of Chemical Research, 2002. **35**(12): p. 998-1007.
322. Wal R Luo Y, V. Hall, Lee J, Scherson D A., *Preparation and Characterization of Multiwalled Carbon Nanotubes Grown Directly onto a Conducting Support.* Electrochemical and Solid-State Letters, 2003. **6**(3): p. A56-A58.
323. Su C.-H Zhu S, Lehoczky S.L,Muntele I, Ila D., *Carbon nanotube growth on carbon fibers.* Diamond and Related Materials, 2003. **12**(10): p. 1825-1828.
324. D.Z. Wang Z.P. Huang, J.G. Wen, M. Sennett, H. Gibson, Z.F. Ren *Effect of nickel, iron and cobalt on growth of aligned carbon nanotubes* Applied Physics A: Materials Science & Processing, 2002. **74**(3): p. 387-391.
325. A. A. Novakova T. Yu. Kiseleva, B. P. Tarasov, V. E. Muradyan, *Mossbauer Study of Carbon Nanostructures Obtained on Fe-Ni Catalyst* in *Hydrogen Materials Science and Chemistry of Carbon Nanomaterials*. 2005, Springer Netherlands.

Appendix A:

Tape and Electrode Specifications

1) Manufacturer: Carbonics GmbH, Germany
   Type: UVIS TR-3/2-22, Cross weave knitted fabric
   Specific weight: 770 g/m^2
   Thickness: 2 mm, 1 mm
   Filament diameter: ~ 8-10 µm
   Carbon content: 99.9%

2) Manufacturer: Carbonics GmbH, Germany
   Type: UVIS TR-3/2-22, Cross weave knitted fabric
   Specific weight: 470 g/m^2
   Thickness: 1 mm
   Filament diameter: ~ 8-10 µm
   Carbon content: 99.9%

3) Maufacturer: Sigmatex Limited, United Kingdom
   Type: 200tex 3K, Bi-directional
   Specific weight: 200 g/m^2
   Thickness: 0.8 mm
   Filament diameter: ~ 5-8 µm
   Carbon content: 99% with rest consisting of epoxy resin coating and glass fiber

4) Manufacturer: High Modulus^{TM}, New Zealand.
   Type: CCEU 610/220-150, unidirectional
   Specific weight: 610 g/m^2
   Thickness: 1.5 mm
   Filament diameter: ~10 µm
   Carbon content: 99% with rest consisting of E-glass as binder.

5) Manufacturer: National Carbon Company
   Type: L 113 SP, graphite
   Diameter: 3.0, 8.0 mm
   Impurities: ≤ 6 ppm

Appendix B:

Electrical Block diagram of the old power supply

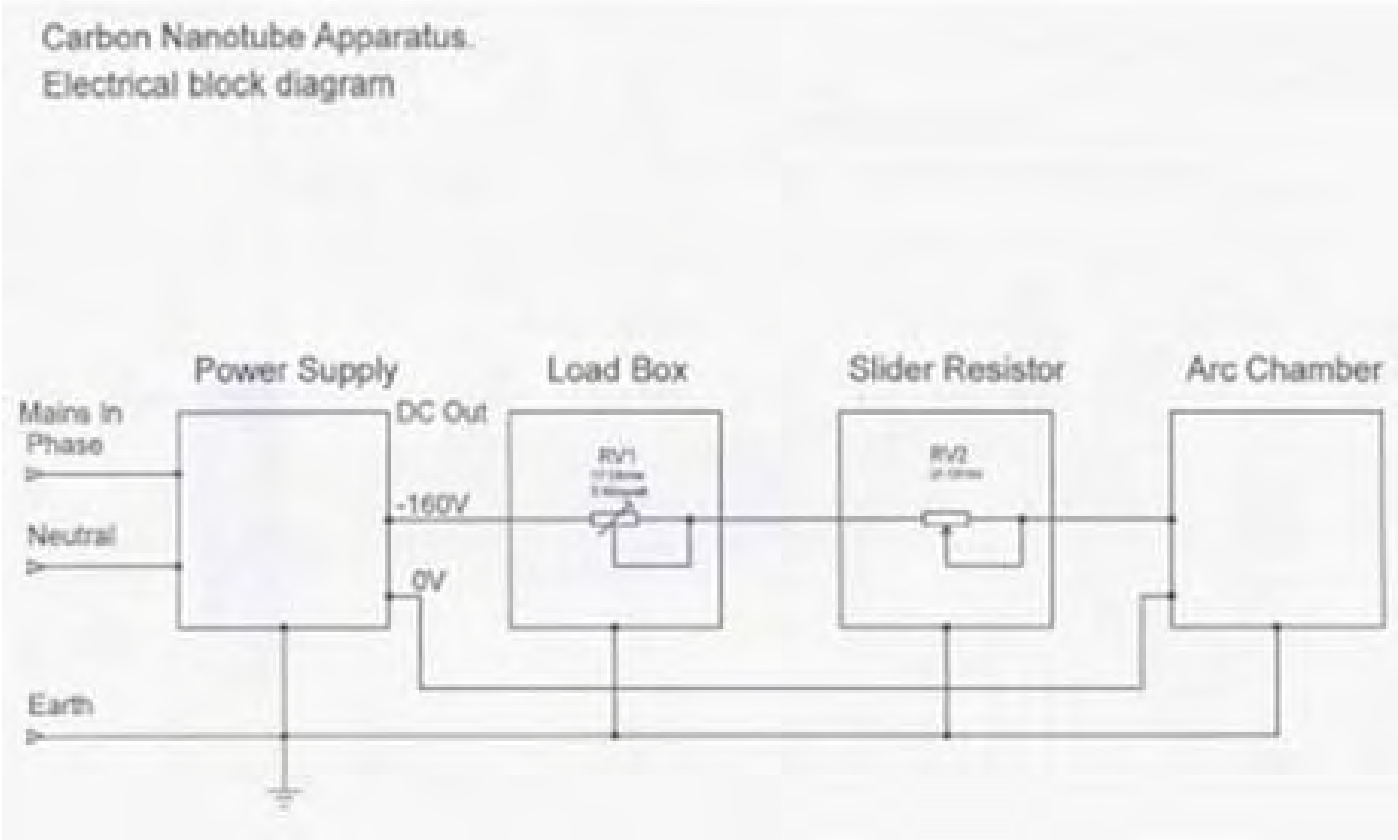

Appendix C:

Tape velocity calibration of the spool system

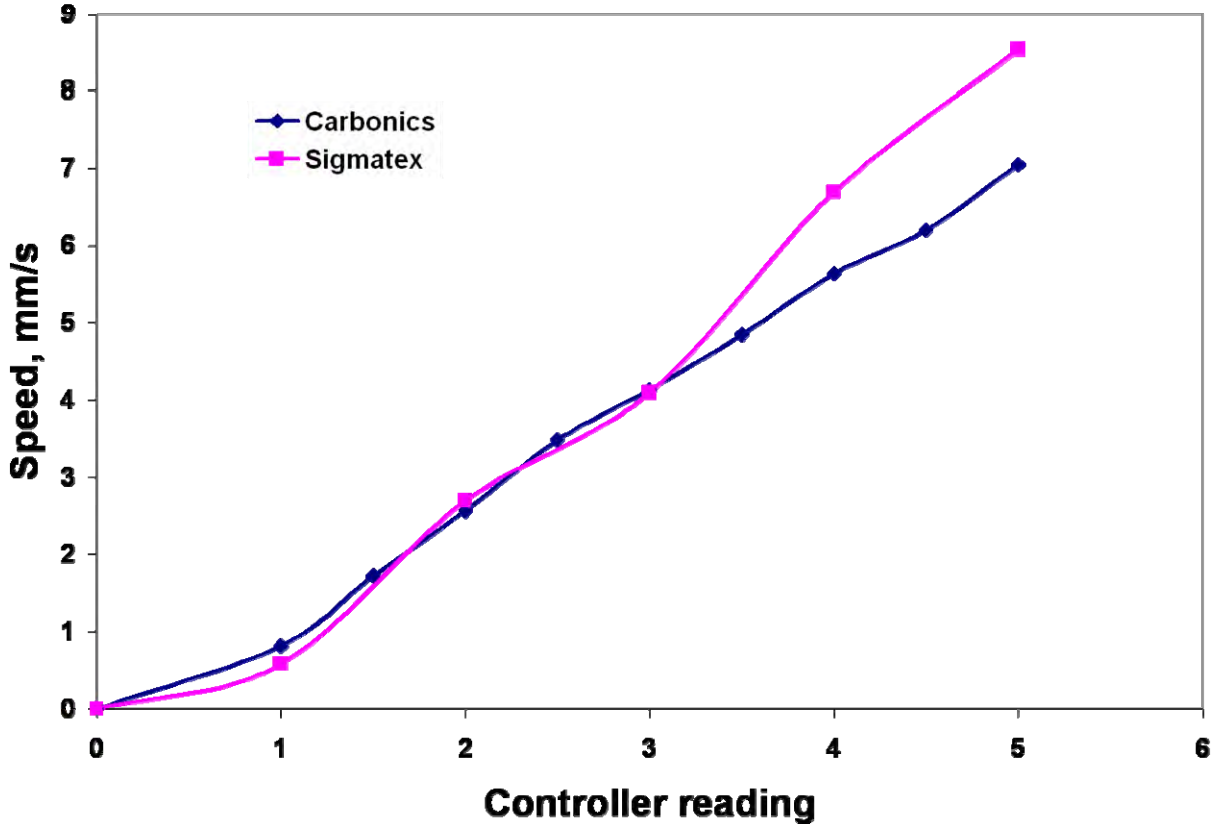

Appendix D:

SEM parameters

Make: Leica 660, JEOL, Biosciences lab
Accelerating voltage: 15 kV
Probe current: 20-50 pA
Filament current: 2.56 - 2.7 A
Working distance: 9-14 mm

Make: JEOL, JSM 6100, Mechanical Engineering
Accelerating voltage: 15 kV
Probe current: 20-50 pA
Filament current: 2.56 - 2.7 A
Working distance: 9-14 mm

All samples were coated with gold prior to its use in the SEM.

Appendix E:

Calibration curves at different pressures for Argon, Helium and Oxygen for a Nitrogen flow rate of 10 L/min

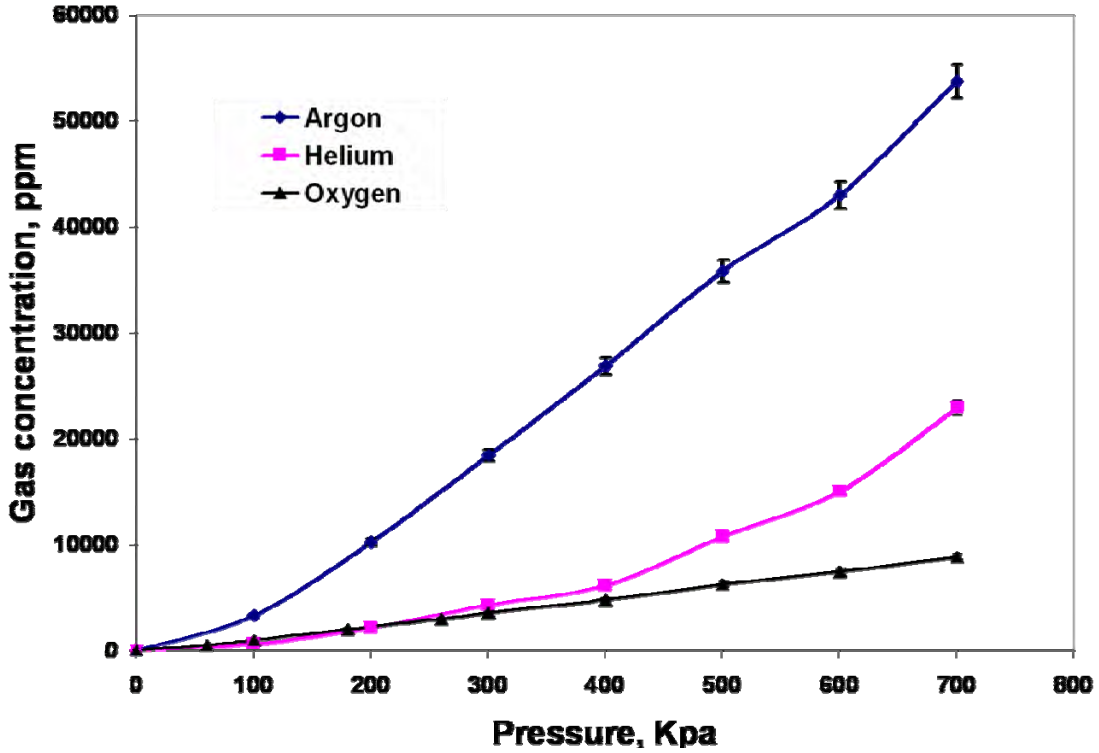

Appendix F:

Calibration curve for Anodic flushing